Virale Nanoringe für die Integration in Biohybrid-Systeme

Bioengineered viral nanorings for the insertion into bio-hybrid systems

Von der Fakultät Energie-, Verfahrens- und Biotechnik der Universität Stuttgart zur Erlangung der Würde eines Doktors der Naturwissenschaften (Dr. rer. nat.) genehmigte Abhandlung

vorgelegt von

Klara Altintoprak

aus Limmersdorf/Thurnau

Hauptberichter:	Prof. Dr. Christina Wege (apl.)
Mitberichter:	Prof. Dr. Sabine Laschat
Mitberichter:	Prof. Dr. Holger Jeske

Tag der mündlichen Prüfung: 12. April 2016

Institut für Biomaterialien und biomolekulare Systeme
Universität Stuttgart

2016

Verzeichnis

Abkürzungsverzeichnis

A	*Adenine*
Asp	*Aspartic acid*
bp	*Base pair*
C	*Cysteine*
CP	*Coat protein*
Cr-Au	Chrom-Gold
D	*Aspartic acid*
ddH_2O	*Double-distilled water*
DMDC	*Dimethyl dicarbonate*
DNA	*Desoxyribonucleic acid*
ds	*Double-stranded*
EDTA	*Ethylenediaminetetraacetic acid*
f. c.	*Final concentration*
FITC	*Fluorescein isothiocyanate*
fwd	*Forward*
H	*Histidine*
h	*Hour*
HCl	*Hydrochloric acid*
ITC-Silan (*ITC-silane*)	*3-isothiocyanatopropyltriethoxysilane*
K	*Lysine*
KOH	*Potassium hydroxide*
LPCVD	*Low pressure chemical vapour deposition*
Lys	*Lysine*
NaCl	*Sodium chloride*
NHS	*N-hydroxysuccinimide*
NKP (SPP)	Natrium-Kalium-Phosphat
nt	*Nucleotide*
OAs	*Origin of assembly*
PCR	*Polymerase chain recation*
PEG	*Polyethylene glycol*
REM (SEM)	Rasterelektronenmikroskop
rev	*Reverse*
RNA	*Ribonucleic acid*
S	*Svedberg unit*

SDS-PAGE	*Sodium dodecyl sulfate polyacrylamide gel electrophoresis*
sec	*Second*
SEM (REM)	*Scanning electron microscope*
Ser	*Serine*
Si_3N_4	*Silicon nitride*
SiO_2	*Silica, silicon dioxide*
$SM(PEG)_4$	*Succinimidyl-[(N-maleimidopropionamido)-tetraethyleneglycol] ester*
SPP (NKP)	*Sodium potassium phosphate*
SSM	*Solid-state membrane*
ss	*Single-stranded*
TAE	*Tris base, acetic acid, EDTA*
TBE	*Tris base, boric acid, EDTA*
TEM	*Transmission electron microscope*
TEOS	*Tetraethyl-orthosilicate*
TMOS	*Tetramethyl-orthosilicate*
TMV	*Tobacco mosaic virus*
Tris	*Tris-(hydroxymethyl)-aminomethane*
VLP	*Virus-like particle*
wt	*Wild type*
ZP	*ζ-potential*

Zusammenfassung

Filtereinheiten mit nanoskopischer Porengröße werden zunehmend für medizinische Anwendungen und analytische Verfahren eingesetzt. DNA-Moleküle lassen sich bereits durch Nanoporen sequenzieren, und auch für schnelle und exakte Analysen niedermolekularer Substanzen bergen sie ein hohes Potential. Besonders schwierig ist es allerdings, nanoporöse Membranen mit Millionen von identischen Poren herzustellen. Hybridmembranen könnten hier einen Ausweg bieten, indem sich selbst organisierende biologische Komponenten als "Porenadapter" in poröse anorganische Festkörpermembranen (*solid-state membranes*, SSMs) integriert werden. Die biologischen Einheiten definieren dann Durchmesser und physikochemische Eigenschaften der effektiven Poren und damit die Selektivität der Filtermembran.

Im Rahmen dieses Promotionsprojekts wurde ein neuer stabiler, aber zugleich auch genetisch und chemisch leicht manipulierbarer Porenadapter aus Pflanzenvirusbausteinen entwickelt und für die Insertion in SSM-Poren erprobt und optimiert. Er ist sowohl an seinem äußeren Rand, als auch im Innenkanal spezifisch funktionalisierbar. Als Ausgangsmaterial diente das pflanzenpathogene Tabakmosaikvirus (TMV), ein Nukleoprotein-Röhrchen, das aus einem einzelsträngige (ss)RNA-Molekül und ca. 2130 Hüllprotein-(*coat protein*, CP)-Untereinheiten besteht. Sowohl die Länge der Partikel, gesteuert über die RNA-Länge, als auch die Protein-Sequenz des CP sind leicht manipulierbar, weshalb TMV zu einem beliebten multifunktionalen Nanobaustein in Hybridmaterialien avanciert ist.

Der neuartige Porenadapter aus TMV-Komponenten wurde speziell an die Insertion in eine SSM mit konisch geformten Poren angepasst, wie sie im Labor von Projektpartnern in Ulm hergestellt wird. Aus einem kurzen RNA-Konstrukt, das über *In-vitro*-Transkription präpariert wurde, und ca. 68 CPs organisiert sich dieser Adapter selbst als eine vierwindige 10 nm lange Nukleoprotein-Helix, die angesichts ihrer lochscheibenähnlichen Form im Folgenden auch „Disk“ genannt wird. Da die „Disks“ in den SSM-Poren unter leicht alkalischen Bedingungen irreversibel fixierbar sein sollen, wurde ihre Struktur im Bereich von pH 7.2 bis 9.0 untersucht und erwies sich als stabil. Damit waren sie den natürlich vorkommenden ringförmigen RNA-freien TMV-CP-Aggregaten klar überlegen, die innerhalb dieses pH-Regimes oligomerisierten und im alkalischen Milieu zerfielen. Auf Isothiocyanat-funktionalisierten Substraten konnten die RNA-haltigen „Disks“ kovalent immobilisiert

werden, sodass alle Voraussetzungen für ihre Integration in SSM-Poren bestanden. Bereits in ersten Kombinationsversuchen ließen sich die „Disks“ mit guter Effizienz in SSM-Porenkanäle inserieren, waren aber in den Poren oft nicht richtig orientiert. Deshalb wurde im zweiten Teil des Projekts ein verfeinertes Adapter-Konstrukt mit einer stark polaren Achse konzipiert, das sich, ausgerichtet in einem elektrischen Feld, in die SSM-Poren einfädeln lässt. Es besteht aus einer Nukleoprotein-„Disk“ mit herausragender freier doppelstängiger (ds)RNA, wodurch es über eine wesentlich höhere negative Ladung als die Porenadapter der ersten Generation verfügt. Dank der spezifischen Interaktion der CPs mit ssRNA konnte ein RNA-Konstrukt, das partiell einzel- und partiell doppelsträngig ist, als Grundgerüst für solche „Disks an der Leine" dienen. In gelelektrophoretischen Analysen zeigten die Produkte tatsächlich eine höhere Mobilität als herkömmliche „Disks“.

Ziel ist schließlich eine robuste Hybridmembran, in der biologische Porenadapter irreversibel in die SSM-Kanäle implantiert und Leckströme gering sind. Dies ließe sich durch das Abscheiden von anorganischem Material zwischen SSM-Poreninnenwand und „Disk“-Rand erreichen, wenn die Lücke zwischen beiden Komponenten an der Grenzfläche ortsselektiv versiegelt werden könnte. Dafür sind im letzten Teil der Arbeit „Disks“ mit spezifisch mineralisierbarer Außenfläche entstanden, welche ihre Silikat-Ummantelung aus löslichen anorganischen Vorstufen induzieren. Verschiedene mineralisationsvermittelnde Peptide wurden chemisch an TMV-Partikel gebunden und die SiO_2-Abscheidungseffizienzen vergleichend untersucht. Besonders vielversprechend war ein Peptid mit alternierendem Lysin-Aspartat-Motiv, $(KD)_{10}C$, das auf Grundlage von Literaturdaten entworfen wurde. Es lieferte tatsächlich auch nach Konjugation an „Disk“-Außenflächen ausgezeichnete Ergebnisse: Die so mit Peptiden funktionalisierten „Disks“ bewirkten eine ringförmige Abscheidung von SiO_2, was bei unmodifizierten „Disks“ nicht beobachtet wurde.

Die neuartigen RNA-stabilisierten und leicht funktionalisierbaren „Disks“ aus TMV-Derivaten sind somit aussichtsreiche biologische Porenadapter zur lipidfreien Insertion in Festkörper-Template. Dank der großen Adaptierbarkeit dieser Nanobausteine könnten davon vielfältige Anwendungen profitieren.

Abstract

Nanoporous filters are increasingly used in various medical and analytical applications, namely for real time DNA or protein sequencing, or the characterization of molecule properties. A major challenge is the fabrication of membranes perforated with large arrays of pores of identical nanometric diameter. Additionally, an adjustment of the inner pore channels' composition or size might offer new possibilities for the separation of molecules with respect to their physical and chemical properties. Nanoporous membranes are commonly made of either inorganic or organic material. However, hybrid membranes, such as composites of porous solid-state membranes (SSM) with integrated pore adapters of biological origin, gain in importance. Such biogenic adapters may define both permeability and selectivity of the nanoporous membrane.

Hence, in this work, a novel multifunctional pore adapter was fabricated, which is stable under different buffer conditions and easily manipulated at both its outer rim and inner pore by genetic or chemical modification. The principle of self-organization of the plant-infecting tobacco mosaic virus (TMV) is essential for the new adapter type: A natural TMV particle consists of around 2130 coat protein (CP) subunits, which encapsidate a right-handed single-stranded RNA (ssRNA) helix. Due to its high stability and reproducibility, TMV has emerged as a popular biological building block in nanotechnology. Additionally, it can be manipulated with regard to its length, defined by the encapsidated RNA, as well as to the amino acid sequence of the CPs by molecular biology approaches. Suitable variants of the protein tube allow further chemical modifications *via* functional groups of appropriate amino acid residues.

A TMV-derived pore adapter was tailored in the first part of this project, by combining CPs with a short RNA of 204 nt, transcribed *in vitro* from a newly established DNA construct. The resulting virus-based four-turn helices are called “disks” in the following, due to the shape of these virus-like particles (VLPs) with an average length of 10 nm. The dimensions of the “disks” match those of conical pore channels generated in inorganic SSMs by a partner laboratory in Ulm. Hence, the new TMV-based nanoporous nucleoprotein structures were tested for their potential use as versatile pore adapters inside the SSM pores. As a covalent immobilization can be achieved at pH 9 at the functionalized inner SSM pore rim, one prerequisite for the “disks” is their stability under basic conditions. The “disks” indeed maintained their

shape in a pH range from 7.2 to 9.0, without undergoing degradation or further elongation as it would have been the case for RNA-free two-layer CP disks analyzed in parallel. The novel nucleoprotein “disks” were immobilized on a functionalized substrate as a proof of concept, demonstrating successful fixation of the biological to the inorganic material.

Already, the first attempts to implant the “disks” into SSM pores showed high insertion rates. However, inside pores they were oriented heterogeneously. Hence, in the second part an advanced adapter construct was designed to introduce a strongly polar axis, which allows improved orientation and actuation of the “disks” in an electric field. To achieve this goal, the “disks” were tethered to a double-stranded RNA-“leash”, which can serve as a guiding-strand for the migration into, and orientation inside the SSM pores. These “disks-on-a-leash” were generated by self-assembly directed by an RNA scaffold with partial self-complementarity. The products revealed higher electrophoretic mobility compared to the first-generation “disks” without protruding RNA, indicating that the novel constructs are suitable candidates for an efficient and oriented insertion into the SSM pores.

The sealing of the gap between the inner SSM pore rim and the outer “disk” edge is the key element of the last part of this project. Silica deposits accumulating in the annular gap might be a suitable “bionic glue”, since site-specific mineral formation from liquid precursor sols is possible by means of mineralization-inducing peptides. To delimit auspicious amino acid sequences, different silicification-guiding peptides were selected, chemically immobilized on the surface of TMV particles and investigated regarding their mineralization efficiencies. The most promising results were obtained with a peptide of alternating lysine and aspartic acid residues of ten repeats ($(KD)_{10}C$), designed against the background of earlier publications. To test if this peptide also induced mineralization of the “disks” selectively at their outer edges, it was conjugated to their rim. Compared to unmodified “disks”, transmission electron microscopy clearly indicated site-specific annular mineral precipitation around the peptide-equipped “disks”.

In conclusion, these novel constructs, designed for the lipid-free covalent and efficient insertion into SSM pores, have proven high stability and modifiability, and thus are appropriate for the use as variously applicable nano building blocks.

Einleitung

Ziel dieser Arbeit ist die Herstellung von Porenadaptern pflanzenviralen Ursprungs zur Integration in eine freistehende, poröse Festkörpermembran (*solid-state membrane*, SSM). Das gewünschte Endprodukt ist eine robuste Hybridmembran aus biologischen und anorganischen Komponenten, mit Millionen wohldefinierten Protein-Nanoporen. Die Entwicklung einer solchen Hybridmembran wird als Gemeinschaftsprojekt in drei naturwissenschaftlichen Disziplinen an verschiedenen Standorten durchgeführt. Beteiligt sind: (i) die Molekularbiologie und Pflanzenvirologie in Stuttgart, in der dieses Promotionsprojekt die virusbasierten Porenadapter konzipiert und analysiert, (ii) die Festkörperphysik in Ulm, wo freistehende SSMs mit einer Vielzahl konischer Porenkanäle hergestellt und auf die Adapter abgestimmt werden, und schließlich als Schnittstelle zwischen Physik und Biologie (iii) das Institut für Funktionelle Grenzflächen in Karlsruhe, das mit der chemischen Vorfixierung der Porenadapter an der Innenwand der Membranporen betraut ist. Angestrebt werden neuartige bio-anorganische Hybridmembranen mit Millionen von identischen Poren mit einem Durchmesser von 4 nm, deren Ladung und Oberflächenchemie an unterschiedliche Filtrations- und Analyse-Aufgaben angepasst werden können.

Als Ausgangsmaterial für die Porenadapter diente das Hüllprotein (*coat protein*, CP) des Tabakmosaikvirus (TMV). Ein TMV-Partikel besteht aus ca. 2130 identischen CP-Einheiten und einem einzelsträngigen Ribonukleinsäure-Molekül (*single-stranded* RNA, ssRNA), das in den helikal angeordneten CPs verpackt ist. Die ssRNA enthält innerhalb des viralen Genoms eine spezifische Sequenz, welche die Assemblierung mit den CPs auch *in vitro* induziert (Assemblierungsursprung: *origin of assembly*, OAs; Turner et al. 1988). Allerdings besitzen auch RNA-freie CPs die Fähigkeit, unter geeigneten Bedingungen zu unterschiedlichen Oligomeren zu aggregieren. Solche CP-Aggregate ohne RNA bestehen aus einem Gemisch kleiner CP-Komplexe ("A-Protein") und 20S-Aggregate, die lochscheibenartige Strukturen (20S-Disks) oder kurze Protohelices von zwei Windungen bilden und in Abhängigkeit von den Konzentrations- und Pufferbedingungen, der Ionenstärke und der Temperatur in unterschiedlichen Gleichgewichtsverhältnissen zueinander vorliegen (Raghavendra et al. 1988, Butler et al. 1992, Durham et al. 1971, Durham & Klug 1971). Die Disks und die kurzen Protohelices kommen prinzipiell als Kandidaten für Porenadapter in

Frage, da sie einen 4 nm weiten Innenkanal und 18 nm Außendurchmesser aufweisen (Butler et al. 1992). Jedoch bilden selbst unter bestmöglich eingestellten Bedingungen maximal 10 Prozent der CP-Moleküle solche lochscheibenähnlichen Formen; die übrigen finden sich entweder als kleinere Einheiten bis hin zu Monomeren, oder lagern sich zu elongierten Disk-Stapeln und heterogenen Helices zusammen (Butler et al. 1992). Um den Anteil an gewünschten CP-Aggregaten zu erhöhen, wurden deshalb TMV-CPs mit 204 Nukleotide (nt) langen ssRNA-Gerüststrängen kombiniert, welche die Sequenz des TMV OAs (Turner et al. 1988) enthalten und über geeignete cDNA-Konstrukte und *In-vitro*-Transkription zugänglich waren. Das Produkt der Assemblierung von CPs und einer solchen 204 nt-RNA ist eine vierwindige Helix mit einer Länge von 9,2 nm (**Abb. 1 a**). Der entscheidende Vorteil dieser RNA-stabilisierten „Disk“ ist, dass ihre Struktur unter verschiedenen Pufferbedingungen erhalten bleibt. Damit wäre sie eine geeignete Komponente für die geplante Hybridmembran, da sie eine bei pH 9 ablaufende Vorfixierung an der funktionalisierten Innenwand einer SSM-Pore überstehen sollte.

TMV-CPs können zudem in begrenztem Maße genetisch modifiziert werden, ohne ihre Assemblierungsfähigkeit zu verlieren (Lee et al. 2005, McCormick & Palmer 2008, Royston et al. 2008, Zhou et al. 2013, Geiger et al. 2013, Kadri et al. 2011, Ma et al. 2008). Verschiedene genetisch modifizierte CP-Varianten können gemischte Aggregate bilden und mit RNA in mischassemblierte Helices integriert werden (Eiben et al. 2014). Dies schafft die Voraussetzungen dafür, unterschiedliche funktionelle Gruppen auf den Außenseiten scheibenförmiger TMV-Derivate zu kombinieren. Ein wesentlicher Bereich dieses Projekts beschäftigt sich nämlich mit der Versiegelung der Lücken zwischen der Innenwand der anorganischen Membranporen und den Protein-Kanten der „Disks“: Nach erfolgreicher Insertion der TMV-Adapter in die konischen Porenkanäle und einer ersten chemischen Fixierung dürften diese Ringspalte noch nicht dicht geschlossen sein, was aber für einen funktionierenden Poren-Array wichtig wäre (**Abb. 1 c**). Zu diesem Zweck wurden die „Disks“ aus CP-Varianten hergestellt, die funktionelle Gruppen für chemische Konjugationsreaktionen an ihrer Außenseite präsentieren. Diese Gruppen (z.B. Amino-Gruppen) erlauben die kovalente Verknüpfung mit Peptiden, über welche lokale Mineralisationsprozesse an der „Disk“-Außenfläche induziert werden könnten. Dadurch wäre es voraussichtlich möglich, mittels eines Sol-Gel-Prozesses aus einer löslichen Vorstufe (z.B. Tetraethylorthosilikat (TEOS)) die beschriebenen Lücken

durch Abscheidung von amorphem Siliziumdioxid (SiO_2) ortsspezifisch zu schließen. SiO_2 würde dabei als "bionischer Kitt" dienen.

Da die Konstruktion der Porenadapter das Kernthema dieser Arbeit ist, soll der Aufbau des Membrantemplats hier nur kurz umrissen werden, um die Bezüge zwischen den anorganischen und biologischen Bestandteilen der geplanten Hybridmembran zu verdeutlichen. Die SSM ist aus mehreren Schichten aufgebaut: einer basalen Siliziumnitrid-Schicht (Si_3N_4), einer intermediären Siliziumdioxid-Lage (SiO_2) und einer Chrom-Gold-Deckschicht (Cr-Au). Nur im Innenbereich der konischen Porenkanäle ist die SiO_2-Lage ringförmig zugänglich und erlaubt ihre selektive Beschichtung mit Isothiocyanat-(ITC)-funktionalisierten Silanen, über welche die „Disks“ chemisch im entsprechenden Areal der SSM-Pore kovalent gebunden werden können (**Abb. 1 b**).

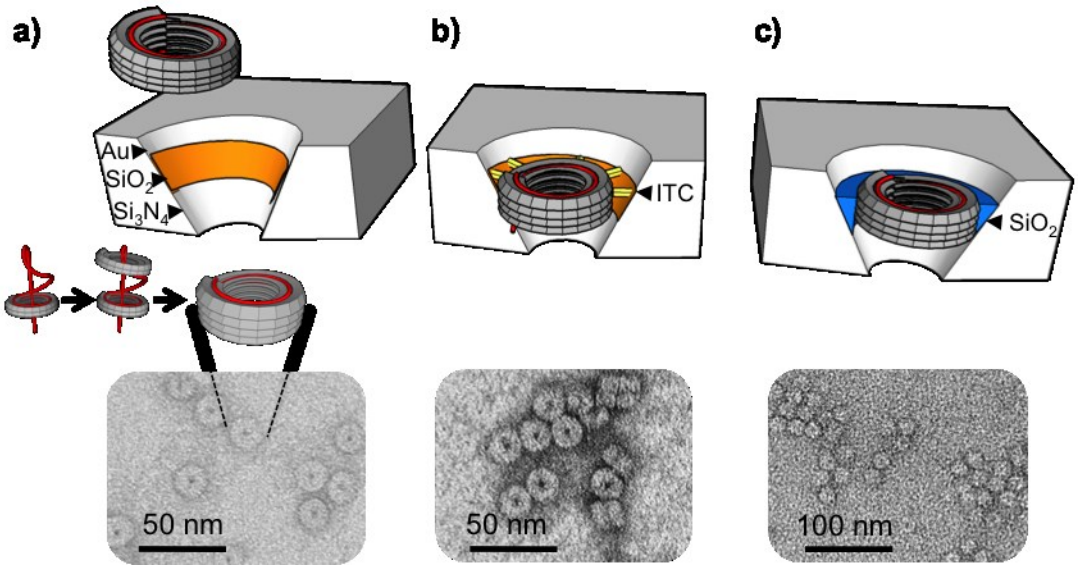

Abb. 1: Strategie zur Herstellung einer nanoporösen Hybridmembran aus biologischen Porenadaptern und einer anorganischen SSM-Pore, und elektronenmikroskopische Abbildungen korrespondierender Strukturen aus dieser Arbeit (siehe Ergebnisteil). **(a)** Assemblierung einer vierwindigen TMV-basierten RNA-Protein-Helix („Disk“) und Insertion in eine konische Pore der dreischichtigen SSM (Au: Gold, SiO_2: Siliziumdioxid, Si_3N_4: Siliziumnitrid). **(b)** Vorfixierung der „Disk“ an der ITC-funktionalisierten Porenwand bei pH 9. Die TEM-Analyse zeigt, dass die RNA-haltigen „Disks“ bei pH 9 stabil sind. **(c)** Versiegelung des Spalts zwischen Porenwand und „Disk“-Oberfläche mittels Siliziumdioxid-Präzipitation („bionischer Kitt“). Die TEM-Analyse des Primärkontrasts von Silizium, das in Gegenwart Peptid-funktionalisierter „Disks“ abgeschieden wurde, deutet auf eine ringförmige SiO_2-Kondensation selektiv an der „Disk“-Oberfläche hin.

Eine Übersicht der Arbeitsschritte zur Insertion, Vorfixierung und Versiegelung der Lücke zwischen Membranpore und Disk über ein biomimetisches Mineralisationsverfahren ist in **Abbildung 1** wiedergegeben.

Im folgenden Abschnitt werden die Bedeutung der Nanobiotechnologie, der Nanoporosität und der Viren als Nanobausteine dargelegt. Im direkten Anschluss

sind die wichtigsten Ergebnisse dieser Arbeit kurz zusammengefasst. Es folgen drei Publikationsmanuskripte, welche das Projekt im Detail erläutern und als Grundlage für zukünftige Veröffentlichungen in wissenschaftlichen Zeitschriften dienen können, sowie ein vierter bereits publizierter Artikel dazu.

Was ist Nanobiotechnologie?

Nanobiotechnologie ist ein relativ neuer Forschungszweig (Lowe 2000, Jain 2005), der Nano- und Biotechnologie verknüpft und dessen Bedeutung in Medizin (Lee et al. 2010), Materialwissenschaft (Sarikaya et al. 2003), Computertechnik (Adleman 1994) und Energiegewinnung (Lee et al. 2009) immer mehr zunimmt. Im Gegensatz zur konventionellen Nanotechnologie, die ihren Schwerpunkt in der Physik und Chemie findet und meist "destruktiv" bzw. "top-down" nanoskopische Strukturen anorganischen Ursprungs generiert (Acikgoz et al. 2011, Choi et al. 2006), bedient sich die Nanobiotechnologie im Baukasten der Natur. Dieser stellt viele verschiedene Materialien, wie Zuckerpolymere (z. B. Cellulose, Chitin; Liu et al. 2014), oligomere Proteine (α-Hämolysin, MspA; Rhee & Burns 2006, Clarke et al. 2009, Deamer 2010) und Nukleinsäuren (DNA, RNA; Gerling et al. 2015), in evolutiv optimierter Form zur Verfügung. Ein grundlegendes Prinzip zur Herstellung hierarchisch organisierter Funktionseinheiten ist in der Nanotechnologie die Selbstorganisation von mehreren Substrukturen zu einem komplexer organisierten Aggregat (De Volder & Hart 2013, Ren et al. 2013, Chiang et al. 2012, Yang et al. 2013a), das andere Eigenschaften als die einzelnen Substrukturen aufweist. Die Größenordnung von Nanostrukturen liegt im weiteren Sinne im Bereich von 0.1 nm bis 1 µm (Bittner et al. 2013), kann sich aber aufgrund der Anordnung kleiner Komposite zu größeren Einheiten auch in den Millimeter-Bereich (Membranen, Oberflächenbeschichtung, Prothesen, Zahnersatz, Gewebe; Urban et al. 2014, Banerjee et al. 2011, Studart 2013, Goudouri et al. 2014, Dvir et al. 2011) und sogar Meter-Bereich erstrecken (Spinnenseide; Hagn et al. 2011).

Was sind die besonderen Vorteile von Nanostrukturen? Von Bedeutung ist zum einen das Verhältnis von Oberfläche zu Volumen, das mit abnehmender Größe eines Objekts steigt (De Morais et al. 2014). Durch die verhältnismäßig vergrößerte Oberfläche entstehen im nanoskaligen Bereich neue chemische, physikalische und biologische Eigenschaften, die verschiedenste Anwendungen finden. Zu nennen sind hier Katalysatoren (Nam et al. 2010b, Neltner et al. 2010, Yang et al. 2013a), Biosensoren (Howes et al. 2014) oder Pharmazeutika (Kumari et al. 2010). Zum

anderen bieten nanostrukturierte Oberflächen neue Möglichkeiten für das Anwachsen von Zellen an Prothesen (Klymov et al. 2015), Bindung von Toxinen an immobilisierten „Fängerstrukturen“ (Graham et al. 2011) oder erhöhte katalytische Umsetzungsraten von Substanzen aufgrund der starken Oberflächenvergrößerung (Yang et al. 2013a, Chiang et al. 2012). Auch lassen sich neue Materialeigenschaften durch die Kombination von organischen oder biologischen mit anorganischen Materialien generieren, die sich z. B. durch erhöhte Elastizität, Bruchfestigkeit, Härte oder Reißfestigkeit auszeichnen (Harrington et al. 2010, Mirkhalaf et al. 2014). Da sich aufgrund ökonomischer und ökologischer Entwicklungen und ihrer vielfältigen Anwendungsmöglichkeiten nanoskopische Materialien immer stärker in der Biosphäre und Atmosphäre ausbreiten (Colvin 2003, Salieri et al. 2015, Tuoriniemi et al. 2012), wächst aber auch der Bedarf an Methoden zum Nachweis und zur Charakterisierung derartiger Partikel bezüglich ihrer biologischen, chemischen und physikalischen Wirkungen. Neben Massenspektroskopie, Elektronenmikroskopie und diversen anderen Analyseverfahren bieten sich insbesondere Trennverfahren wie Chromatographie und Filtration an. Da die Herstellung einer nanoporösen Hybridmembran im Fokus dieser Arbeit ist, soll im folgenden Kapitel genauer auf die Herstellung solcher Filtrationsmaterialien und deren Anwendungsfelder eingegangen werden.

Nanoporöse Membranen

Nanoporöse Materialien können für sehr verschiedene Anwendungen genutzt werden. Sie finden Einsatz als Sensoren (Venkatesan & Bashir 2011), Filtermaterial (Zavala-Rivera et al. 2012), bei der Sequenzierung von DNA (Clarke et al. 2009) und künftig voraussichtlich auch Proteinen (Nivala et al. 2013), Nachweis von DNA-Methylierung (Shim et al. 2013), beim Sortieren von Molekülen gemäß bestimmter Eigenschaften (z.B. Chiralität, Konformation; Boersma & Bayley 2012) und der Freisetzung von Substanzen aus Kapseln (Yang et al. 2010). Da eine große Vielfalt an nanoporösen Materialien existiert, werden in diesem Kapitel nur entsprechende Membranen und verschiedene Typen von Nanoporen vorgestellt.

Nanoporöse Membranen werden mittels unterschiedlicher Prozesse und aus verschiedenen Materialien hergestellt (Miles et al. 2013). Häufig verwendete Herstellungsverfahren basieren auf den Methoden der Halbleitertechnik und lassen sich in vier Arbeitsschritte untergliedern: (i) Beide Seiten einer Silizium-Membran werden mit Nitrid-reichem Silizium (SiN_x) mittels chemischer Gasphasenabscheidung

(*low pressure chemical vapour deposition*, LPCVD) beschichtet. (ii) Die Oberfläche der SiN_x-beschichteten Membran wird durch photolithographische Techniken, z.B. Aufbringen eines Fotolacks, strukturiert, was Position und Größe der Poren festgelegt. (iii) Zum lokalen Entfernen der SiN_x-Schicht wird ein reaktives Ionenätzverfahren (RIE; *reactive ion etching*) verwendet, so dass unter der Ätzmaske (Fotolack) liegende SiN_x-Bereiche erhalten bleiben. (iv) Zum Schluss wird über einen Schritt, der als Nassätzen („*wet etching*") bezeichnet wird, mittels Kaliumhydroxid (KOH) spezifisch das Silizium entfernt, wodurch die Poren entstehen (Miles et al. 2013).

Ein einfacheres Verfahren zur Herstellung von nanoporösen organischen Membranen basiert auf den selbstorganisierenden Eigenschaften von Blockcopolymeren. Diese können aufgrund von intermolekularen Wechselwirkungen Membranen mit einer hohen Anzahl an zylinderförmigen Perforationen von einheitlicher Porengröße bilden (Yang et al. 2006, Phillip et al. 2010). Der Porendurchmesser dieser Membranen ist nachträglich durch Abscheidung von Metallen wie Gold in einem Bereich von 6 nm bis 15 nm variierbar (Yang et al. 2010). Auch können Lipidmembranen mit integrierten Poren (Urban et al. 2014, Kusters et al. 2014), metallorganische Gerüstverbindungen (Oh et al. 2013) oder Graphen (Merchant et al. 2010) als nanoporöses Material verwendet werden.

Unsere Projektpartner in Ulm setzen ein kombiniertes Verfahren ein, bei dem in mehreren Teilschritten eine Si_3N_4-Membran, beschichtet mit SiO_2, mit sich selbst organisierenden Blockcopolymer-Mizellen strukturiert wird, welche eine geordnete Verteilung einer Goldnanopartikel-(AuNP)-Ätzmaske gewährleisten. Die Größe der gleichmäßig verteilten AuNP ist photochemisch veränderbar. Diese Ätzmaske lässt sich in zwei Schritten invertieren: Zuerst wird mit einem Ionenätzverfahren die SiO_2-Oberfläche strukturiert, indem die Fläche um die AuNP herum entfernt wird; infolgedessen bleiben SiO_2-Nanosäulen maskiert unter den AuNP stehen. Daran anschließend erfolgt eine Beschichtung mit Chrom und Gold. Weil die Nanosäulenspitzen maskiert sind, bleiben diese frei zugänglich und können mittels Argonionenpolitur entfernt werden. Die verbleibenden SiO_2-Nanosäulenstümpfe und die darunter liegende SiO_2- und Si_3N_4-Schicht lassen sich schließlich im anisotropen Plasma entfernen. Dieser letzte Ätzprozess trägt entscheidend zur Geometrie der Porenkanäle bei. Abhängig von der chemischen Ätzreaktion und der Isotropie des

Plasmas ist es möglich, den Winkel des Porenkanals zu steuern, wodurch konische bis zylinderförmige Perforationen in der Membran entstehen (Seidenstücker 2015).

Bei den technisch genutzten Porensystemen selbst gibt es unterschiedliche Kategorien: Die porösen Struktureinheiten und damit die Wandungen der Porenkanäle können aus anorganischen, organischen oder biologischen Materialien bestehen. Dabei kann die Porengröße entweder durch die poröse Einheit bestimmt sein (wie bei herkömmlichen Bioporen), oder durch das Herstellungsverfahren definiert und z. T. nachträglich noch verändert werden. Anorganische Poren werden häufig mit destruktiven Methoden wie fokussiertem Ionen- oder Elektronenstrahl gebohrt oder, wie zuvor erläutert, in Kombination mit Lithographie-Techniken durch Ätzlösungen in SiN_x, SiO_2 oder SiC Membranen erzeugt (Yang et al. 2011a, Storm et al. 2003, Gierak et al. 2007, Seidenstücker 2015). Um den Porendurchmesser zu verringern, können solche und Poren, die durch die Selbstassemblierung von Blockcopolymeren generiert wurden, bei Bedarf durch Abscheidung von SiO_2 oder Gold bezüglich ihrer Größe und Auskleidung modifiziert werden (Nilsson et al. 2006, Danelon et al. 2006, Yang et al. 2010).

Arrays mit mehreren Nanoporen in einer anorganischen Membran lassen sich auf unterschiedliche Weise herstellen. Fokussierte Ionen- oder Elektronenstrahlen führen in SSMs zu sehr definierten Porendurchmessern (Larkin et al. 2014). Da das Bohren der einzelnen Poren meist längere Zeit in Anspruch nimmt (ca. 10-200 ms; Gierak et al. 2007, Yang et al. 2011a), sind diese Verfahren zur Herstellung von eher geringer Porenzahl im vierstelligen Bereich geeignet. Dagegen kann mit der Kombination von einer sich selbst organisierenden Ätzmaske und nachfolgendem Ätzverfahren eine hohe Anzahl von 115 Poren pro Mikrometer erreicht werden. Bei einer Membranfläche von 500 × 500 µm entspräche das ≈30×10^6 Poren. Jedoch weisen die Porendurchmesser bei diesen Methoden eine höhere Variationsbreite auf (Seidenstücker 2015).

Bei der Herstellung von nanoporösen Membranen ist die Kontrolle über die Porengröße ein generelles Problem, insbesondere bei Einheiten, bei denen viele Poren mit identischem Durchmesser erwünscht sind (Kleefen et al. 2010). Wie von Kleefen et al. (2010) beschrieben, können Membranen mit identischen Porendurchmessern besonders effizient entstehen, indem SSM-Template mit biologischen Poren ausgestattet werden.

Biologische Poren können aus Proteinen (Deamer 2010), Nukleinsäuren (Hernandez-Ainsa & Keyser 2014) oder Lipiden (Yusko et al. 2011) bestehen. Ein entscheidender Vorteil solcher Poren ist meist eine hohe Einheitlichkeit ihrer Dimensionen und reproduzierbare Gewinnung in großer Anzahl. Häufige Verwendung findet α-Hämolysin, ein multimerer Proteinkomplex, der aus sieben Untereinheiten besteht und erstmals aus *Staphylococcus aureus* isoliert wurde (Song et al. 1996). Seine natürliche Funktion ist die Lyse von Erythrozyten (Bhakdi & Tranumjensen 1991). Es konnte jedoch gezeigt werden, dass durch diesen Porentyp auch andere Moleküle, wie ssDNA (Maglia et al. 2010) oder Proteine (Nivala et al. 2013), geschleust werden können, und dass bei geeigneter Modifizierung des Innenkanals sogar eine enantioselektive Detektion von Aminosäure-Stereoisomeren möglich ist (Boersma & Bayley 2012). Die Dimensionen des α-Hämolysin-Innenkanals (Durchmesser: ca. 1,4 - 3,6 nm; Länge des transmembranen β-Fasses: ca. 5 nm; Venkatesan & Bashir 2011) sind für die Analyse von ssDNA-Molekülen (Durchmesser: 1,2 nm) aufgrund ihres Durchmessers und anderen niedermolekularen Substanzen geeignet. Gleichzeitig jedoch ist der Spielraum für Porendurchmesser oder Kanallänge im Falle von α-Hämolysin recht begrenzt, so dass erheblich veränderte Porenweiten oder Kanal-Dimensionen bisher nicht zugänglich waren. Eine größere Formvielfalt bieten dagegen Poren aus DNA-Origami-Strukturen (Hernandez-Ainsa et al. 2014, Bell et al. 2012). Die Länge, der Durchmesser und die Form des Innenkanals können beliebig variiert werden, und auch eine Modifikation des Innenkanals durch chemische Konjugation ist potentiell möglich (Hernandez-Ainsa & Keyser 2014).

Ein Problem der biologischen Poren ist die in technischen Bauteilen fehlende Matrix, in die sie in ihrer natürlichen Umgebung eingebettet sind, um als Selektionseinheiten zu agieren. Deshalb muss in technisch anwendbaren Materialien sichergestellt sein, dass die biogenen Poren tatsächlich stabil funktionieren. Bewährt haben sich hierfür Lipidmembranen, welche das ursprüngliche Umfeld imitieren (Mayer & Yang 2013, Kleefen et al. 2010, Kusters et al. 2014), aber in manchen Fällen auch poröse anorganische SSMs (Hall et al. 2010, Bell et al. 2012, Hernandez-Ainsa et al. 2014), in die sowohl Protein-, als auch DNA-Origamiporen als Adapter inseriert werden können.

Die Insertion der biologischen Poren in die größeren Membranporen kann auf unterschiedliche Weise durchgeführt werden. Obwohl es keine statistisch

ausgewerteten Experimente zur Insertion von biologischen Poren in anorganische Template gibt, wurden vergleichende Untersuchungen zur Beladung von zylinderförmigen Poren in Lichtwellenleitern mit DNA-Polymerasen durchgeführt. Bei diffusionsvermittelter Insertion der Polymerasen in die anorganischen Zylinder fand eine erfolgreiche Integration der Biomoleküle bei einem Porendurchmesser unterhalb von 70 nm nur bei maximal 30 Prozent der Porenkanäle statt (Korlach et al. 2008). Die Beladungseffizienz der SSM-Poren mit Protein-Nukleinsäure-Komplexen konnte durch Anlegen eines elektrischen Feldes auf ca. 60 Prozent erhöht werden (Larkin et al. 2014). In diesem Beispiel wurde ein Membranarray mit acht zylinderförmigen Lichtwellenleiter-Kavitäten verwendet, die an ihrer Basis mit jeweils einer Nanopore perforiert waren (Larkin et al. 2014). Es wurde dabei demonstriert, dass Streptavidin, gekoppelt an einen 5‘-biotinylierten 1002 bp DNA-Strang, am Boden des Lichtwellenleiters platzierbar war, indem die DNA elektrophoretisch durch die Nanopore bewegt wurde und dabei Streptavidin hinter sich herzog.

Eine weitere Hürde ist die richtige Orientierung der biologischen Pore in der sie umgebenden organischen oder anorganischen Membranpore. Ein höherer Anteil richtig orientierter Bioporen, deren Kanäle parallel zu den SSM-Porenkanälen ausgerichtet waren, konnte durch Anfügen eines länglichen geladenen Moleküls an die nanoporöse Struktur ebenfalls in Kombination mit Elektrophorese-Verfahren erreicht werden: α-Hämolysin (Hall et al. 2010) und DNA-Origamiporen (Hernandez-Ainsa et al. 2014) ließen sich als Porenadapter mit „DNA-Leinen“ erfolgreich in der gewünschten Orientierung elektrophoretisch in einzelne SSM-Poren ziehen.

Als neuartige Porenadapter, die allen bisher aufgeführten Ansprüchen gerecht werden könnten, sollen in dieser Arbeit Nukleoprotein-Lochscheiben viralen Ursprungs eingeführt werden. Sie weisen einen Innenkanal von 4 nm Durchmesser auf, können mit multifunktionalen Außen- und Innenflächen ausgestattet werden und sind in unterschiedlichen pH-Bereichen stabil (**Manuskript I**). Ein weiter optimiertes Konstrukt zur zielgerichteten Integration und Orientierung der porösen Proteinscheiben in SSM-Poren wurde durch einen aus den "Disks" heraushängenden doppelsträngigen RNA-Bereich realisiert, dessen negative Ladung zu verbesserter elektrophoretischer Mobilität führte (**Manuskript II**). Im nachfolgenden Kapitel werden die dafür genutzten Viren als Bausteine in der Nanobiotechnologie - mit einem Schwerpunkt auf Tabakmosaikviren - vorgestellt.

Viren als Bausteine in nanotechnologischen Anwendungen

Viren haben sich seit einigen Jahren als vielseitige Bausteine in der Nanobiotechnologie bewährt, und zwar aufgrund ihrer geringen Größe im nanoskaligen Bereich, ihrer genetischen und chemischen Modifizierbarkeit und ihrer reproduzierbaren Struktur. In verschiedenen Zusammenhängen werden bevorzugt der M13-Phage und die Pflanzenpathogene *cowpea mosaic virus* (CPMV) und TMV verwendet. M13 und TMV sind elongierte, stäbchenförmige Viren, während CPMV ikosaedrisch organisiert ist (Soto & Ratna 2010, Love et al. 2014, Cardinale et al. 2012). Ein großer Vorteil dieser drei Viren besteht darin, dass sie für Menschen ungefährlich sind, in großen Mengen im Labor oder Gewächshaus hergestellt werden können und eine relativ hohe Stabilität aufweisen. Anwendung finden nanotechnologisch genutzte Viren insbesondere in der Medizin zur Herstellung von Vakzin-Nanopartikeln (McCormick & Palmer 2008) oder Drug-Delivery-Systemen (Bar et al. 2008), als mineralisierte (Atanasova et al. 2011) und metallisierte (Royston et al. 2008, Knez et al. 2004a, Adigun et al. 2015) Nanopartikel in der Halbleitertechnik, als Oberflächen vergrößernde Strukturelemente für Stromkollektoren (Chiang et al. 2012) oder in der Energiegewinnung als Bio-Template zur Kopplung von Lichtsammelfallen (Miller et al. 2007, Ma et al. 2008).

Der besondere Reiz der Viren geht von ihrer hohen Zahl an chemisch selektiv adressierbaren Gruppen bzw. ihrer Multivalenz aus, die von der Anzahl der CPs und ihrer zur Verfügung stehenden modifizierbaren Aminosäureresten abhängt. Diese ermöglichen hohe Besatzdichten mit Enzymen oder reaktiven Molekülen an der Virusoberfläche

TMV ist das erste entdeckte Pflanzenvirus (Beijerinck 1898), und die Mechanismen seiner Assemblierung *in vitro* sind gut untersucht und in zahlreichen Veröffentlichungen beschrieben (zusammengefasst in Butler 1999). Systematisch gehört es innerhalb der *Virgaviridae* zu den Tobamoviren (Lartey et al. 1996, Adams et al. 2012), die durch eine positive ssRNA spezifiziert sind. Es besteht aus 2130 identischen CPs und einer 6395 nt langen ssRNA (Goelet et al. 1982), in der eine Haarnadelschleifenstruktur nachgewiesen wurde, die für den Start der Assemblierung *in vitro* essentiell zu sein scheint (OAs; Turner et al. 1988). Die einzelnen CPs sind in einer rechtsgängigen Helix um die ssRNA angeordnet (Finch 1972), wobei die natürliche Partikel-Länge durchschnittlich 300 nm beträgt. Die Assemblierung erfolgt *in vitro* bidirektional, wobei davon ausgegangen wird, dass die

RNA-Verpackung in 5'-Richtung, vermittelt über CP-Disks oder Protohelices, schneller abläuft als in 3'-Richtung, in der vermutlich kleinere CP-Oligomere, die A-Protein-Aggregate, die Schlüsselkomponenten sind (Fukuda & Okada 1987). Bevorzugt dienen Nachtschattengewächse (*Solanaceae*) als Wirte, zu denen einige der agronomisch wichtigsten Pflanzenarten gehören; aber auch viele andere Pflanzenfamilien werden von TMV befallen. TMV-Partikel können in großen Mengen aus infizierten Tabakpflanzen isoliert werden (ca. 1 mg CP pro 1 g Blattmaterial; Gooding & Hebert 1967). Die isolierten Viren können wegen ihrer hohen Stabilität lange gelagert und in ihre Bestandteile (CPs und RNA) zerlegt und diese voneinander getrennt werden (Fraenkel-Conrat & Williams 1955). Die CPs sind in der Lage, auch ohne Enkapsidierung eines RNA-Moleküls zu intermediären höhermolekularen Strukturen zu aggregieren und unter geeigneten Pufferbedingungen sogar zu Stäbchen-förmigen Einheiten unterschiedlicher Länge zu assemblieren (Durham et al. 1971, Durham & Klug 1971). Bei den Intermediaten einer RNA-freien CP-Suspension handelt es sich meist um A-Proteine, die aus mindestens drei aneinandergelagerten CPs bestehen, und 20S-Aggregate, die aus 34 CPs eine Disk-förmige Struktur von zwei CP-Ringen bilden bzw. kurze Protohelices von zwei Windungen mit 16 1/3 CPs pro Windung. Diese drei Aggregationszustände liegen im Gleichgewicht zueinander vor, wobei das relative Mengenverhältnis durch Veränderung des pH-Werts, der Ionenstärke und der Temperatur reversibel verschoben werden kann (Durham & Klug 1971). Eine weitere Struktur, eine sogenannte "vierlagige Disk", entsteht bei hoher Ionenstärke und einem pH-Wert von 8,0 (Raghavendra et al. 1988). Diese sehr stabile Struktur ist aus zwei Kopf-an-Kopf aneinander gelagerten TMV-Disks zusammengesetzt. Das Gleichgewicht unter diesen Bedingungen verschiebt sich über die Zeit nahezu vollständig zugunsten der vierlagigen Disk, wodurch eine homogene Population vorhanden wäre. Bei geringfügiger Änderung des chemischen Milieus geht sie jedoch in andere Aggregationszustände über, so dass sie für technische Anwendungen kaum in Frage kommt.

Die Länge der TMV- und TMV-ähnlichen Stäbchen lässt sich *in vitro* am einfachsten und reproduzierbarsten über die Länge der verpackten RNA-Moleküle regulieren (Rego et al. 2013, Eber et al. 2013), wenn es nicht auf vollständige, Pflanzen-infektiöse Virusgenome ankommt. Auch ist es durch *In-vitro*-Assemblierung möglich, die starre, Stäbchen-förmige Struktur von CP-RNA-Partikeln zu verändern und nicht-

infektiöse TMV-ähnliche Derivate mit neuen Formen zu erzeugen. Hierzu werden mehrere TMV-Assemblierungsursprünge in eine beliebige RNA-Sequenz inseriert, welche danach durch TMV-CP bidirektional verpackt wird. So werden infolge kollidierender benachbarter Röhrchenabschnitte geknickte, Boomerang-förmige Stäbchen generiert oder, bei mehreren OAs-Sequenzen je RNA-Molekül, sogar bis zu tetrapode Arrangements (Eber et al. 2015). Ein weiteres Charakteristikum der TMV-Assemblierung ist die spezifische Verpackung von ssRNA, aber nicht ssDNA oder dsDNA oder dsRNA. Deshalb lässt sich durch Hybridisierung von komplementären RNA- oder DNA-Sequenzen an die RNA-Gerüste ihre Enkapsidierung ortsspezifisch unterbrechen, wodurch z.B. verkürzte Kapside mit heraushängendem RNA-DNA-Heteroduplex entstehen (Müller et al. 2011, Eber et al. 2013).

Für reine TMV-Proteinaggregate in Abwesenheit von RNA kann die Länge typischer Oligomere über genetische Veränderung ebenfalls beeinflusst werden, und zwar durch Austausch für die Assemblierung essentieller Aminosäuren (Lu et al. 1996, Miller et al. 2007). Beispielsweise aggregieren CPs, deren Aminosäure Glutaminsäure (E) an Position 50 gegen Glutamin (Q) ausgetauscht wurde, ohne das Beisein von RNA zu sehr langen Stäbchen (Lu et al. 1996). Eine genetische Modifikation der CPs ist ohne Verlust der Assemblierungsfähigkeit und Infektiosität der veränderten Viren für ihre Wirtspflanzen aber nur in begrenztem Rahmen möglich (Werner et al. 2006). Deshalb werden für nanotechnologische Anwendungen oft nur geringfügig modifizierte TMV-Varianten genutzt, die sich in guten Ausbeuten aus Pflanzen isolieren lassen und durch gezielten Austausch einzelner geeigneter Aminosäurereste reaktive Gruppen (Amino- oder Thiol-Gruppen) für chemische Konjugationsreaktionen bereitstellen. Solche TMV-Typen stehen für die gezielte Funktionalisierung sowohl an der Virusoberfläche als auch im Innenkanal zur Verfügung (Geiger et al. 2013, Dedeo et al. 2010). Derartige miteinander gekoppelte genetische und chemische Funktionalisierungsstrategien für TMV-Stäbchen wurden bereits in diversen Beispielen gezeigt (Yi et al. 2007, Schlick et al. 2005, Miller et al. 2007, Smith et al. 2006, Banik et al. 2015).

Ein wichtiges Anwendungsfeld natürlicher und funktionalisierter TMV-Partikel sowie anderer organischer, nanoskopischer Objekte bietet ihre Mineralisierung und Metallisierung. Sie werden dabei als Template zur Feinstrukturierung von organisch-anorganischen Hybridmaterialien benutzt (Royston et al. 2008, Yang et al. 2013a,

Chiang et al. 2012). Wie weiter unten beschrieben, konnten verschiedene Mechanismen zur Mineralbildung an Biotemplaten nachgewiesen werden, die hauptsächlich auf der Interaktion von bestimmten Aminosäureresten mit den Mineralvorläufer-Molekülen beruhen. Weil sie für die Integration TMV-basierter Nanoporenadapter in anorganische SSMs zentrale Bedeutung haben, sind im folgenden Abschnitt Mechanismen der biologisch vermittelten Mineralisierung näher beschrieben.

Mineralisierung - biomimetischer Ansatz

Biomineralisierungsprozesse sind in der Biosphäre von zentraler Bedeutung, da sie dazu beitragen, zunächst weiche biologische Bestandteile durch Anreicherung von anorganischem Material zum Schutz und als Stützstrukturen, wie Exoskelette (Fabritius et al. 2009), Muschelschalen (Marie et al. 2012) oder Knochen (Anderson 1989), zu stabilisieren. Der gravierende Unterschied zur anorganischen Mineralisierung ist die Abscheidung von Mineral unter normalen Umweltbedingungen, das heißt Normaldruck, Raumtemperatur, im neutralen pH-Bereich, bei einer geringen Konzentration der Mineralvorstufen und meist in wässrigen Lösungen an Proteinen (Cha et al. 1999) und posttranslational modifizierten Peptiden (Sumper & Brunner 2008). Die biologischen Komponenten dienen dabei als Template für die Abscheidung der Mineralien (Cha et al. 1999, Murai et al. 2013). Die dafür bekanntesten und am gründlichsten erforschten Organismen sind Muscheln (Bivalvia), Kieselalgen (Bacillariophyceae), Glasschwämme (Hexactinellida) und Säugetiere (Mammalia). Die entsprechenden Biominerale sind Perlmutt, das zu 95 % aus Calciumcarbonat und 5 % aus organischem Material zusammengesetzt ist (Song et al. 2003), Frusteln (Kröger & Poulsen 2008) und Spicula (Brutchey & Morse 2008) aus amorphem Siliziumdioxid, und Knochen beziehungsweise Zähne, die je nach Härtegrad aus Hydroxylapatit und organischen Substanzen (z.B. Kollagen oder Glykoproteine) zu verschiedenen Anteilen bestehen (Palmer et al. 2008).

Die zugrundeliegenden Mineralisierungsmechanismen haben sich evolutionsbedingt in den einzelnen taxonomischen Gruppen stark diversifiziert. So findet man bei Mollusken (Mollusca) und Nesseltieren (Cnidaria) häufig die Calciumcarbonat-Kristallstruktur Aragonit, während bei Krebstieren (Crustacea) und Ringelwürmern (Annelida) eher Calcit vorkommt (Weiner et al. 2009, Jackson et al. 2010, Murdock & Donoghue 2011). Noch prägnanter entwickelten sich die drei Klassen der

Schwämme (Porifera) auseinander. So bilden Hexactinellida und Demospongiae Skelette aus amorphem und hydratisiertem Silikat (Wang et al. 2010). Dagegen bestehen diese bei den Calcarea aus Calciumcarbonat (Uriz 2006). Da in der vorliegenden Arbeit die TMV-Oberfläche vermittelt über SiO_2-erzeugende Peptide mineralisiert werden soll, deren Ladungsübertragungseffekt bereits beschrieben wurde (Kuno et al. 2011), wird im Folgenden ausschließlich auf das Grundprinzip der Abscheidung von Siliziumdioxid eingegangen.

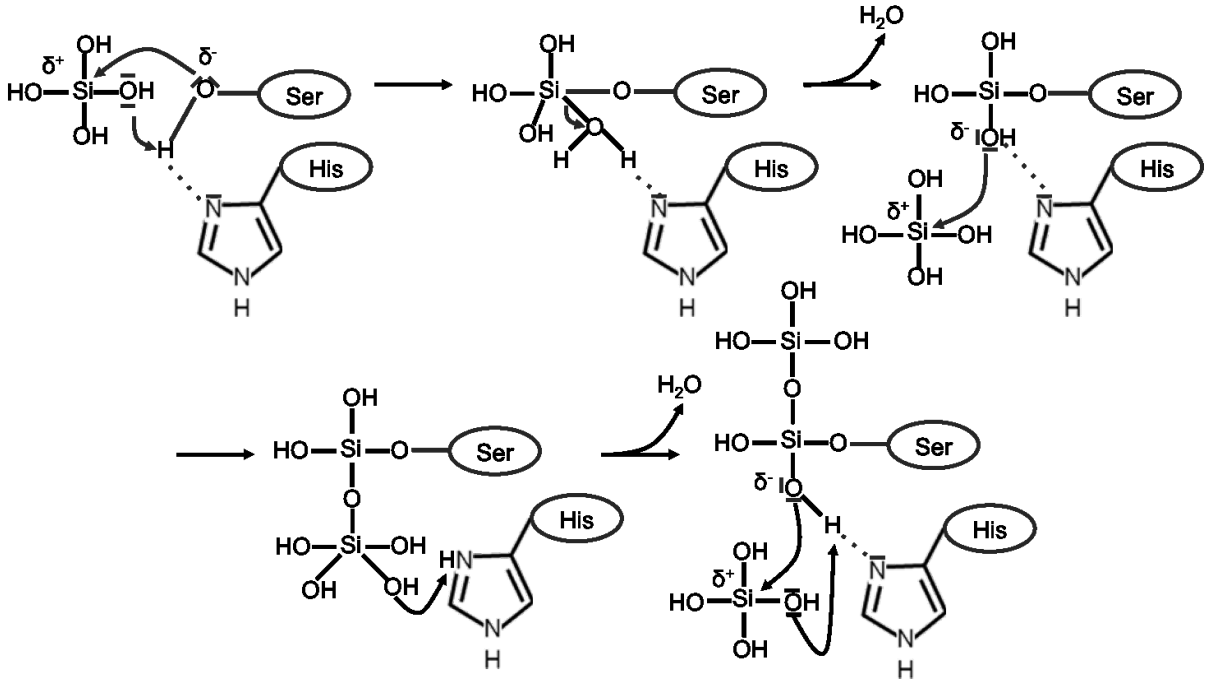

Abb. 2: Mutmaßlicher Mechanismus der SiO_2-Kondensation im aktiven Zentrum von Silicatein nach Schröder et. al. (2012). Das Modell zur Polykondensationsreaktion im enzymatisch aktiven Zentrum geht von einer nukleophilen Substitutionsreaktion aus, wobei Serin und Histidin eine Wasserstoffbrücke ausbilden, die zu einer negativen Partialladung des Serin-Sauerstoffatoms führt und dadurch einen nukleophilen Angriff auf das partiell positiv geladene Siliziumatom der Orthokieselsäure einleiten kann. Über ein Stickstoffatom im heterozyklischen Imidazol des Histidin-Rests findet ein Protonentransfer auf eine Hydroxyl-Gruppe der Kieselsäure statt, wobei ein Wassermolekül abgespalten wird und eine Siloxan-Bindung (Si-O-Si) entsteht (Schröder et al. 2012).

Die Mineralisationsmechanismen der Hexactinellida und Diatomeen sind gut charakterisiert und lassen sich in vereinfachter Weise *in vitro* mit synthetischen Templaten imitieren (Kisailus et al. 2006, Yuwono & Hartgerink 2007, Pouget et al. 2007, Altunbas et al. 2010). Dabei unterscheiden sich die Abläufe bei Glasschwämmen und Kieselalgen gravierend. Bei den Schwämmen entwickelte sich ein enzymatischer Prozess (**Abb. 2**), der auf der Kondensation von Kieselsäure-Molekülen in einem katalytisch aktiven Zentrum der Proteins Silicatein basiert (Cha et al. 1999, Schröder et al. 2012). Das aktive Zentrum besteht aus einer Triade von

Aminosäureresten, Serin (Ser, S), Histidin (His, H) und Asparagin (Asn, N; Cha et al. 1999).

Im Gegensatz dazu findet bei den Diatomeen die Polymerisation von SiO_2 an kurzen Peptiden statt, die eine komplexe Abfolge von alternierenden kationischen und anionischen Aminosäureresten aufweisen. Zusätzlich sind diese Peptide mit Polyamin-Ketten, Methylierung oder Phosphorylierung posttranslational modifiziert (Kröger et al. 1999, Sumper & Brunner 2008). Diese modifizierten Peptide wurden aus den glasartigen Zellwänden isoliert, welche die Diatomeen-Zelle umschließen. Zum einen sind es die Silaffine (Kröger et al. 1999), die hohe Anteile an phosphorylierten Serinen und methylierten oder mit Polyaminen kovalent verknüpften Lysinen enthalten, wodurch alternierend negative und positive Ladungen in unmittelbarer Nähe zueinander liegen (Sumper & Brunner 2008). Zum anderen sind Silacidine beteiligt, Peptide von saurem Charakter, die aus Aspartat, Glutamat und phosphoryliertem Serin bestehen, und vermutlich zur Vernetzung von Polyaminen beitragen (Richthammer et al. 2011). Neben den zwei funktionellen Protein- bzw. Peptid-Typen werden auch Polyaminen zwei wichtige Funktionen zugeschrieben, die zur SiO_2-Abscheidung der Kieselalgen beitragen. Im ersten Schritt findet die Stabilisierung eines Kieselsäure-Sols an den Polyaminen statt und daran anschließend die Kondensierung und Polymerisierung der Monokieselsäure in festes SiO_2. Dabei wird die Kondensationsreaktion durch Methylierung der Amine beschleunigt (Sumper & Brunner 2008).

In Anlehnung an die Silaffin-Peptide wurden in den letzten Jahren viele artifizielle Peptide mit unterschiedlicher Aminosäuresequenz generiert und die Mechanismen zur Initiation der SiO_2-Kondensation und zur Bindung an SiO_2-Oberflächen untersucht (Baio et al. 2014, Zane et al. 2014, Patwardhan et al. 2011, Kuno et al. 2011). Zur Bindung an SiO_2 konnten den Aminosäureresten unterschiedliche nicht-kovalente Wechselwirkungen zugeordnet werden, die auch für die Initiation der SiO_2-Präzipitation aus kolloidalen Intermediaten wichtig sein können (Gebauer et al. 2014, Belton et al. 2012). Die Aminosäurereste von Lysin und Arginin adsorbieren über ihre positiven Ammonium-Gruppen ($R\text{-}NH_3^+$) mittels ionischer Wechselwirkungen an negativ geladenen Silikat-Oberflächen (SiO^-), während Serin, Histidin und Asparaginsäure über Wasserstoffbrücken und polare Wechselwirkung mit Silanol-Gruppen (Si-OH) interagieren (Patwardhan et al. 2012). Da im Rahmen dieser Arbeit entsprechende mineralisationsvermittelnde Peptide erfolgreich auf TMV-Templaten

erprobt wurden, ist ihr Reaktionsmechanismus im Folgenden kurz dargestellt. Dieses vereinfachte Modell der Ladungsübertragung, die zur Dehydratisierung von Trimethylethoxysilan führte, wurde für alternierend angeordnete positiv und negativ geladene Aminosäurereste erstellt (Kuno et al. 2011). Darauf basierend wird im Zuge dieser Arbeit ein Mechanismus der Silicat-Abscheidung vorgeschlagen (**Abb 3**), der den Vorgängen im aktiven Zentrum von Silicatein mit den Aminosäureresten Histidin und Serin ähnelt (Schröder et al. 2012). Jedoch sind bei dem von Kuno et al. (2011) beschriebenen synthetischen Peptid andere Aminosäurereste an der Reaktion beteiligt, nämlich Lysin (Lys, K) und Asparaginsäure (Asp, D), die im Wechsel angeordnet sind (**Abb. 3**). Anstelle vom Imidazol-Stickstoffatom des Histidin (bei Silicatein) könnte der nukleophile Angriff im Falle des Peptids von der Hydroxyl-Gruppe der Asparaginsäure ausgehen und der Protonentransfer über die Ammonium-Gruppe des Lysins erfolgen, wodurch Kieselsäure durch Wasserabspaltung zu SiO_2 kondensiert wird (Kuno et al. 2011).

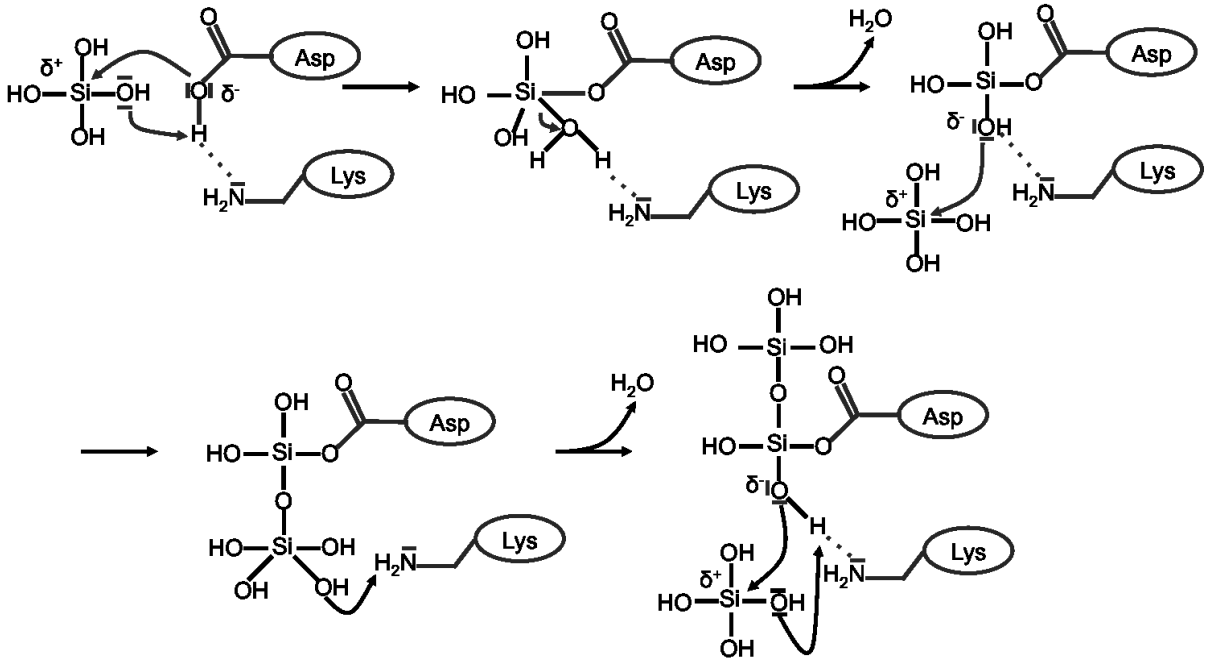

Abb. 3: Möglicher Mechanismus der SiO_2-Kondensation an einem $(KD)_x$-Motiv in Anlehnung an die Kieselsäure-Polymerisation im aktiven Zentrum von Silicatein. In dem im Zuge dieses Projekts entwickelte Modell geht der nukleophile Angriff auf das Siliziumatom der Kieselsäure vom Sauerstoffatom der Carboxylat-Gruppe von Asp aus. Dieses ist wegen der Nähe zur Ammonium-Gruppe von Lys protoniert und somit partiell negativ geladen. Das Proton der Ammonium-Gruppe geht auf die Hydroxyl-Gruppe der Kieselsäure über und wird mit dieser als Wasser-Molekül abgespalten. Die Polymerisationsreaktion geht nun von einem nukleophilen Angriff der fixierten Kieselsäure mit anschließender Wasserabspaltung aus (verändert nach Schröder et al. (2012) und Kuno et al. (2011)).

Auf diesem Aminosäure-Motiv $(KD)_x$ basierende Peptide von unterschiedlicher Länge wurden linkervermittelt chemisch an TMV-Partikel konjugiert, um die SiO_2-Präzipitation aus löslichen TEOS-Vorläufern an der funktionalisierten Virus-Oberfläche zu untersuchen (Altintoprak et al. 2015). Derart modifizierte TMV-Stäbchen wurden dabei mit solchen verglichen, die entweder andere mineralisationsvermittelnde Peptide trugen, oder aber allein Linker oder ihre freie Oberfläche exponierten. Im Vergleich zu TMV mit Histidin-haltigen Peptiden verblieben die $(KD)_x$-funktionalisierten TMV-Partikel stabil dispergiert, während die anderen getesteten Peptide die Aggregation der TMV-Stäbchen zu bündelartigen Mesostrukturen induzierten. Das im Rahmen unserer Studie entworfene Peptid $(KD)_{10}C$ erwies sich als besonders geeignet, um eine selektive, ortsspezifische und über die Reaktionsdauer gut kontrollierbare SiO_2-Kondensation an der TMV-Oberfläche zu induzieren. Eine eingehende Analyse zur möglichen Nutzung dieses Peptids als Mineralisationsvermittler in nanoporösen Hybridmembranen mit TMV-Adaptern ist in den **Manuskripten III** und **IV** dargestellt: Sie könnten entscheidend dafür sein, die virusbasierten Lochscheiben über "bionischen Kitt" fest in den anorganischen Membrantemplaten zu verankern.

Ergebnisse und Diskussion

RNA-stabilisierte „Disks“ als integraler Bestandteil von Festkörpermembranen

Wie zu Beginn dargelegt, ist das Ziel dieser Arbeit die Entwicklung von biologischen Porenadaptern für die Integration in poröse anorganische Membrantemplate (SSMs). Basierend auf ihrer Selbstorganisation und Stabilität kommen Intermediat-Strukturen der CP-Assemblierung des TMVs dafür in Frage, sogenannte Disks und Protohelices. Beide Formen ähneln Lochscheiben und erscheinen aufgrund ihrer Dimensionen als geeignete Kandidaten: Sie verfügen über einen definierten Porendurchmesser von 4 nm und einen Außendurchmesser von 18 nm. RNA-freie CPs liegen allerdings als ein Gemisch aus Disks, Protohelices, A-Proteinen und längeren Aggregaten vor. Ein besonderer Nachteil ist, dass sich stets ein Gleichgewicht zwischen den einzelnen Aggregatformen in Abhängigkeit von pH-Wert, Ionenstärke, Temperatur und CP-Konzentration einstellt (Stauffer et al. 1970, Butler et al. 1992), weshalb der Anteil an gewünschten CP-Komplexen in Lösung oft geringer ausfällt als erwartet. Um eine einheitliche Population an Disks oder Protohelices zu erhalten, wurde daher in ersten Experimenten getestet, ob sich diese Formen mittels Glutaraldehyd fixieren lassen. Danach könnten die stabilisierten Disks und Protohelices durch zonale Ultrazentrifugation von anderen Aggregationsformen abgetrennt werden. Der Fixierungsgrad der Glutaraldehyd-behandelten CPs wurde mittels denaturierender Natriumdodecylsulfat-Polyacrylamid-Gelelektrophorese (SDS-PAGE) untersucht. Dabei zeigte sich jedoch, dass die Behandlung nicht den erwünschten Effekt erzielte. Infolgedessen wurde eine alternative Disk-Struktur (vierlagige Disk, aus zwei Kopf-an-Kopf kombinierten CP-Scheiben) ins Auge gefasst, die als stabil unter hoher Ionenstärke und leicht alkalischem pH gilt (Raghavendra et al. 1988, Bhyravbhatla et al. 1998, Raghavendra et al. 1985). Auch diese Struktur schied für die weiteren Arbeiten aus, weil sie nur in einem sehr limitierten Bereich formstabil war und insbesondere bei Mischassemblierung aus unterschiedlichen CP-Varianten zu längeren gestapelten Disk-Multimeren aggregierte. Da bereits mehrere Arbeiten erfolgreich zeigen konnten, dass die Länge *in vitro* generierter TMV-Partikel über die RNA-Länge

steuerbar ist (Rego et al. 2013, Eber et al. 2013, Wu et al. 2010, Müller et al. 2011), erschienen somit kurze RNA-haltige Nukleoprotein-Strukturen aussichtsreicher.
Deshalb wurden fünf RNAs mit einer Länge von jeweils <500 nt mit Hilfe geeigneter cDNA-Konstrukte durch *In-vitro*-Transkription hergestellt und bezüglich ihrer Nukleationseffizienz und Ausbeute an Lochscheiben-Strukturen untersucht. Die besten Ergebnisse erzielte eine 204 nt lange ssRNA mit TMV OAs, die mit den CPs eine kurze vierwindige Helix bildet (**Manuskript I**). Im Vergleich wurden noch vier weitere ssRNAs von unterschiedlicher Länge getestet, von denen zwei den OAs enthielten und eine RNA eine OAs-ähnliche Sekundärstruktur, die in geringen Ausbeuten ebenfalls zu Assemblierung mit CPs führte. Der OAs der Wildtyp-TMV-RNA bildet eine Haarnadelschleife (*stem-loop*), die aus einem Nonanukleotid (*loop*, AAGAAGUUG) und 14 flankierenden invers komplementären Basenpaaren mit zwei Fehlpaarungen (*stem*) besteht (Turner et al. 1988, Zimmern 1983). Die Abfolge und Art der Basen scheint die Effizienz der Nukleation entscheidend zu beeinflussen. Während die Base Guanin (G) im Nonanukleotid in Triplet-Folge ($(NNG)_3$) eine Assemblierung von RNA-CP-Helices optimal induziert, wird die Nukleationsrate durch Austausch gegen die Base Cytosin (C, $(CCG)_3$) um das 720-fache verringert (Turner & Butler 1986). Auch eine niedrigere Anzahl der Tripletts ($(NNG)_2$) beeinträchtigt die TMV-Partikelassemblierung (Turner et al. 1988). Die Sequenz des *stems* ist irrelevant, fehlt jedoch diese Struktur, ist die Assemblierung um das 100-fache geringer (Turner et al. 1988). Die in der vorliegenden Arbeit beschriebene OAs-ähnliche Sekundärstruktur besteht aus einem Nonanukleotid (GAGCGGAUA), das ein Cytosin und viermal Guanin enthält, und benachbarten Sequenzen mit 14 invers komplementären Basenpaaren mit zwei Fehlpaarungen, führt also zu einer dem TMV-OAs strukturell vergleichbaren Haarnadelschleife. Jedoch befindet sich G im *loop* nur zweimal ($(NNG)_2$) an der dritten Position anstatt dreimal, so dass im letzten Triplett das G fehlt. Die geringe, aber doch signifikante Nukleationsrate der getesteten RNA mit OAs-ähnlicher Haarnadelschleife ist wahrscheinlich auf deren günstige Konformation und den hohen Guanin-Anteil in der *loop*-Sequenz mit zwei TMV-homologen G-Positionen zurückzuführen. Die Ergebnisse dieser Arbeit bestätigen somit vorangegangene Untersuchungen darin, dass die Nukleotidsequenz des OAs-*loops* eine wichtige Rolle bei der *in vitro* Assemblierung spielt.
Der Vergleich der mit verschiedenen RNAs erzielten Disk-ähnlichen Strukturen zeigte, dass die vierwindige Nukleoprotein-Helix mit 204 nt langer ssRNA mit OAs

aufgrund ihrer Dimensionen (Länge 10 nm, Durchmesser 18 nm) und ihrer reproduzierbaren Selbstorganisation die besten Voraussetzungen für nachfolgende Routineanwendungen mit sich brachte. Daher wurde sie weiteren Untersuchungen und Modifikationen unterzogen, um sie als Porenadapter nutzen zu können. Zur Vereinfachung werden diese kurzen helicalen RNA-CP-Strukturen im Folgenden als „Disks“ bezeichnet. Es zeigte sich, dass sie in Natrium-Kalium-Phosphat-Puffer (NKP) in einem Bereich von pH 7,2-9,0 stabil blieben und sich damit wie vollständig assemblierte, aus Pflanzen isolierte TMV-Partikel verhielten (Harrington & Schachman 1956, Pelcher & Halasa 1979). Zudem behielten die vierwindigen Helices ihre Struktur auch mehrere Tage in TAE (40 mM Tris, 20 mM Essigsäure und 1 mM EDTA, pH 8,0) oder deionisiertem H_2O (**Manuskript II und III**). Infolge dieser Stabilität unter variablen Bedingungen sind sie geeignet für verschiedenste chemische Modifikationen, wie die Konjugation von Farbstoff-Derivaten (Atto488-Maleimid, Fluorescein-Isothiocyanat (FITC)) und Peptiden, oder die Mineralisierung mit Siliziumdioxid (SiO_2). Exemplarisch wurden diese Möglichkeiten in dieser Arbeit gezeigt (**Manuskript I**), indem aus zwei genetisch modifizierten CP-Varianten mischassemblierte bifunktionale „Disks“ mit Atto488-Maleimid markiert und an ein ITC-funktionalisiertes Substrat gebunden wurden. Dieses Experiment diente auch als Machbarkeitsstudie für die chemische Immobilisierung von viralen „Disks“ in ITC-funktionalisierten konischen Poren der SSM-Template.

Die Insertion der „Disks“ in die SSM-Porenkanäle wurde mit unterschiedlichen Methoden durchgeführt, welche in erheblichen Beladungsdifferenzen resultierten. Zum einen wurden „Disks“ in Lösung auf eine poröse SSM gegeben und unter horizontaler Rotation über 14 h mit dem Membrantemplat inkubiert. Dabei wurden weniger als 1 Prozent der Poren erfolgreich mit „Disks“ beladen. Da dieses Insertionsprinzip allein auf Diffusion beruht und in einem vergleichbaren Experiment für die Integration von DNA-Polymerasen in optische Lichtwellenleiter mit einem Durchmesser unterhalb von 70 nm eine Beladung von maximal 30 Prozent erreicht werden konnte (Korlach et al. 2008), wurde geprüft, ob sich die Insertionsrate durch das Anlegen eines elektrischen Felds erhöhte. Dafür wurde die SSM zwischen zwei Elektrophorese-Kammern gespannt und eine der Kammern mit einer „Disk“-haltigen Lösung gefüllt, die andere mit Puffer (**Abb. 4 a**). Eine elektrische Spannung sollte die negativ geladenen „Disks“ elektrophoretisch in die Poren der Festkörpermembran treiben (**Abb. 4 b**). Die Insertionsrate der „Disks“ wurde nach Platin-Bedampfung der

nanoporösen Hybridmembran im Rasterelektronenmikroskop (REM) analysiert (**Abb. 4 c und d**). Im Unterschied zur diffusionsbedingten Insertion konnte für die elektrophoretisch vermittelte Implantation eine Beladung von 60-70 Prozent der Porenkanäle erreicht werden. Ähnliche Werte wurden auch für die elektrophoretische Insertion von Protein-DNA-Komplexen in nanoporöse optische Hohlleiter-Anordnungen ermittelt (Larkin et al. 2014).

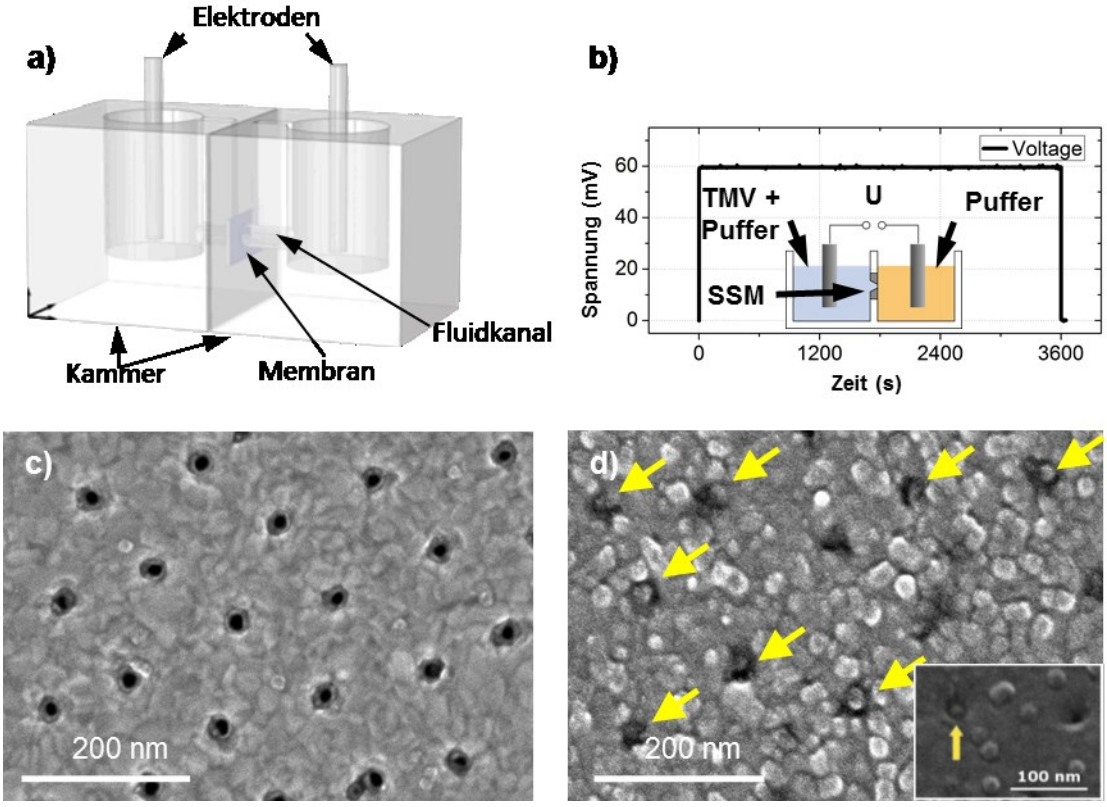

Abb. 4: Elektrophoretisch gesteuerte Insertion der „Disks" in SSM-Template mit konischen Poren. **(a)** Aufbau der Elektrophorese-Apparatur: Zwei Kammern mit Elektroden sind durch eine poröse SSM voneinander getrennt. **(b)** Potentialdifferenz zwischen einer Lösung mit und ohne „Disks" bei über zwei Elektroden angelegter Spannung. REM-Analyse einer SSM **(c)** vor und **(d)** nach der „Disk"-Insertion. Die „Disks" wurden mittels Platin-Bedampfung sichtbar gemacht und sind in einer Vielzahl der Porenkanäle erkennbar (gelbe Pfeile; Abbildungen von Axel Seidenstücker, Festkörperphysik, Universität Ulm).

Obwohl diese hohe Beladungsdichte erreicht wurde, zeigte die REM-Analyse eine zufällige Orientierung der „Disks" in den SSM-Poren, d. h. einige der „Disks" waren mit ihrem Kanal, wie erwünscht, parallel zum SSM-Poren-Kanal ausgerichtet, während andere quer dazu orientiert oder an der Poren-Wand angelagert waren. Um die Anzahl falsch orientierter „Disks" zu verringern, wurde ein neues Konstrukt entworfen und realisiert, das aus einer „Disk" mit heraushängender doppelsträngiger RNA (dsRNA) besteht. Die „Disk" wurde *de facto* an die „Leine" gelegt. Im folgenden

Abschnitt wird der Syntheseweg dieses neuartigen Nukleoprotein-Porenadapters behandelt.

Optimierung der „Disk“ für die gerichtete Insertion in nanoporöse SSMs

Die Herstellung von Hybridmembranen mit Porenadaptern, die sich in der richtigen Orientierung inserieren lassen, wurde bereits anhand von α-Hämolysin-DNA-Konjugaten und DNA-Origami-Nanoporen mit heraushängenden „DNA-Leinen“ gezeigt (Hall et al. 2010, Bell et al. 2012, Hernandez-Ainsa et al. 2014). Inspiriert von dieser Idee wurde ein entsprechendes Konstrukt aus viralem CP und partiell einzel- und doppelsträngiger RNA entworfen (**Manuskript II** und **Abb. 4 a**). Da das CP von TMV nur mit ssRNA stabil interagiert (Fraenkel-Conrat & Williams 1955), wurde über *In-vitro*-Transkription eines entsprechenden cDNA-Konstrukts eine 500 nt lange RNA-Sequenz generiert, die aus zwei Abschnitten besteht. Der 5’-Bereich mit seiner Länge von 204 nt enthält den OAs und bleibt als einzelsträngiger Abschnitt für die Assemblierung verfügbar. Diesem folgt in 3’-Richtung eine 296 nt lange Sequenz, die komplementär zum größten Teil eines 308 nt langen RNA-Moleküls ist. Nach Kombination beider RNA-Stränge unter geeigneten Bedingungen bildet sich durch molekulare Hybridisierung ein partieller RNA-Duplex, in welchem 204 verpackbare nt mit einer 296 bp langen dsRNA mit 3'-terminalem 12 nt ssRNA-Überhang verbunden sind. Der Grund dafür, dass die Hybridisierung 3’ vom OAs durchgeführt wurde, besteht im Assemblierungsmechanismus von RNA und CP *in vitro*: In 3'-Richtung verläuft die RNA-Enkapsidierung langsamer, während in 5’-Richtung eine starke Schubkraft entsteht, die hybridisierte Nukleinsäure-Moleküle abscheren kann (Eber 2012). Die beiden komplementären RNA-Stränge wurden unter Bedingungen hybridisiert, die zunächst im Rahmen dieser Arbeit optimiert wurden. Die Hybridisierungsspezifität hängt stark von der Salzkonzentration, der Hybridisierungstemperatur und der Anzahl der komplementären Basen ab (Tsuruoka et al. 1996, Okahata et al. 1998). Die Stringenz steigt dabei mit der Temperatur und mit sinkendem Salzgehalt (Meinkoth & Wahl 1984). Hierbei werden sowohl die negativ geladenen Phosphat-Gruppen des Nukleinsäure-Rückgrats, als auch die Partialladungen von Stickstoff und Sauerstoff der Nukleobasen durch Anlagerung von positiv geladenen Na^+-Ionen neutralisiert, wodurch die helikale Konformation stabilisiert und die Assoziationswahrscheinlichkeit der komplementären Nukleinsäure-Moleküle über Wasserstoffbrückenbindungen erhöht wird (Anwander et al. 1990, Nakano et al. 1999).

Die optimale Salz-Konzentration zur Bildung des dsRNA-Duplex wurde durch Zugabe unterschiedlicher Mengen an NaCl auf 80 mM eingegrenzt, bei einer RNA-Gesamtkonzentration von 0,2 µg/µl (**Abb. 5**). Das Laufverhalten des dsRNA-Duplex wurde gelelektrophoretisch im Vergleich zu den nicht hybridisierten RNA-Molekülen und einem ssRNA-Größenstandard ermittelt, dabei entsprach die elektrophoretische Mobilität des dsRNA-Duplex der von 600 bis 800 nt langer ssRNA. Die Hybridisierung wurde zudem in 75 mM NKP-Puffer durchgeführt, in dem auch die Assemblierung der CPs mit ssRNA stattfindet (siehe **Manuskript II**).

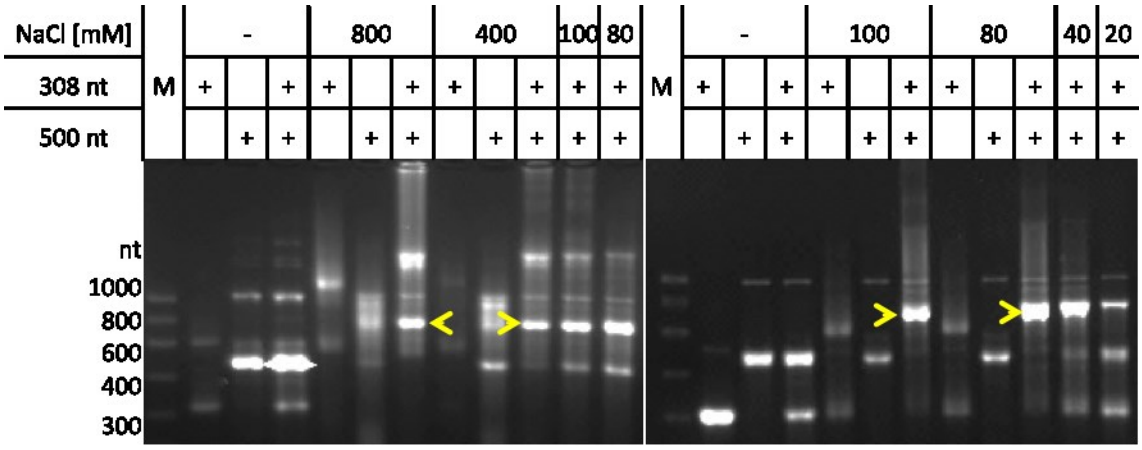

Abb. 5: Optimierung der Hybridisierungsbedingungen durch Veränderung der Salzkonzentration. Partiell zueinander komplementäre RNA-Moleküle mit Längen von 308 nt und 500 nt wurden nach Zugabe verschiedener Mengen von NaCl 10 min bei 95 °C denaturiert und durch langsames Abkühlen auf 4 °C miteinander hybridisiert. Die Hybridisierung bei einer Salzkonzentration von 80 mM NaCl weist die höchste Spezifität und die geringsten Mengen an Nebenprodukten auf (erwünschte Hybridisierungsprodukte: siehe Pfeile). Die RNA-Moleküle wurden in einem 3 % Agarosegel in 1 x TBE-Puffer getrennt und mit Ethidiumbromid gefärbt.

Die gelelektrophoretische Untersuchung zeigte sowohl ein vergleichbares Laufverhalten als auch eine entsprechende Hybridisierungseffizienz. Im Anschluss an die Bildung des dsRNA-Duplex wurde für die Fertigstellung der „Disks“ eine genetisch modifizierte CP-Variante mit exponierten Amino-Gruppen gegeben, die zur Markierung mit Atto488-NHS diente. Diese Fluoreszenz-Markierung ermöglichte es, das Migrationsverhalten der Konstrukte im nativen Agarosegel direkt zu verfolgen und erleichterte die Elektroelution der Nukleoprotein-Helices aus dem Gel. Die elektrophoretische Mobilität der „Disks“ mit und ohne RNA-„Leine“ wurde verglichen. Die „Disks“ mit RNA-„Leine“ migrierten im Gel 2,1 bis 2,4-mal schneller als gleichartige „Disks“ ohne „Leine“. Dieses beschleunigte Laufverhalten ist auf die zusätzliche negative Ladung des frei zugänglichen Phosphat-Rückgrats der dsRNA zurückzuführen. Transmissionselektronenmikroskop-(TEM)-Analysen zeigten unverkennbar die gewünschte Struktur der „Disks“ mit RNA-„Leine“, die mittels

Schräg-Bedampfung mit Platin sichtbar gemacht wurde. Diese Konstrukte wurden nachfolgend für einen ersten Test zur elektrophoretischen Insertion in die anorganische Membran genutzt (**Manuskript II**).

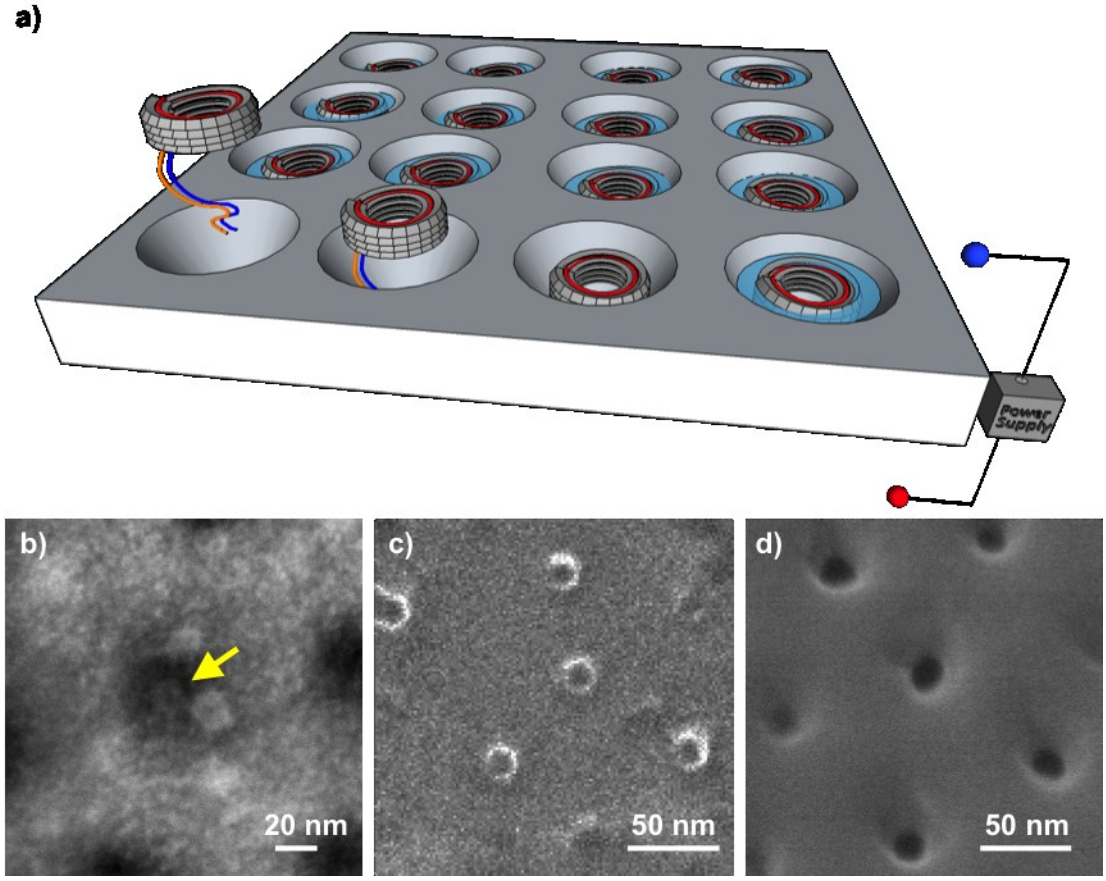

Abb. 6: Gerichtete Insertion der „Disk“ mit RNA-„Leine“ in konische Poren eines anorganischen Membrantemplats. (**a)** Schematische Darstellung der „Disks“ an der RNA-„Leine" während ihrer elektrophoretischen Implantation. **(b)** REM-Aufnahme einer korrekt orientierten „Disk“ (gelber Pfeil) mit RNA-„Leine“ (1 kV Spannung, Zeiss, Oberkochen). Helium-Ionen-Mikroskopie-Analyse **(c)** von „Disks“ auf einem Kohle-Formvar-Film und **(d)** einer nanoporösen SSM (Ruth Schwaiger, IAM-WBM, KIT, Eggenstein-Leopoldshafen).

Erste Ergebnisse der Rasterelektronenmikroskop-(REM)-Analyse unter Niedrigspannung deuten darauf hin, dass die „Disks“ mit RNA-„Leine“ tatsächlich bevorzugt in der richtigen Orientierung inseriert wurden (**Abb. 6 b**). Die Insertionsrate war bei diesem Test allerdings bei weitem geringer als bei vorangegangenen Insertionen von „Disks“ ohne RNA-Anhang, was aber auf eine 10-fach geringere "Disk"-Konzentration und eine verkürzte Elektrophoresedauer beim ersten Versuch mit elektroeluierten „Disks“ mit "Leine" zurückzuführen sein dürfte. Erhöhte Insertionsraten auch bei geringer „Disk“-Konzentration könnten dadurch erreicht werden, dass anstatt NKP alternative konduktive Medien verwendet werden. Erste Stabilitätstests deuten darauf hin, dass die „Disks“ mit RNA-„Leine“ auch in TAE-Puffer stabil sind, der verbesserte Elektrophorese-Ausbeuten erwarten lässt. Für eine

optimale Insertion des neu designten Konstrukts werden somit Puffer- und Elektrophoresbedingungen weiter optimiert.

Peptid-unterstützte Mineralisierung von „Disks“

Ein weiterer wichtiger Aspekt des Kernthemas dieser Arbeit ist die Versiegelung der Lücken zwischen SSM-Porenwandungen und den viralen „Disks“. Dieser Prozess soll, ausgehend von den inserierten „Disks“ in den Porenkanälen, über die Abscheidung von amorphem Siliziumdioxid (SiO_2) als "bionischer Kitt" ortsspezifisch ablaufen. Dass TMV-Partikel prinzipiell geeignete Biotemplate für die Präzipitation von SiO_2 aus löslichen Vorstufen sind, wurde in anderen Labors bereits bewiesen (Fowler et al. 2001, Royston et al. 2006, Royston et al. 2009), allerdings noch nie nach Ankopplung mineralisationsregulierender Peptide. Ein typischer Bestandteil der Mineralisierungsansätze mit der SiO_2-Ausgangssubstanz TEOS ist Ethanol. Da RNA-stabilisierte „Disks“ eine geringere Stabilität gegen Ethanol als ganze TMV-Partikel aufwiesen, wurden verschiedene Möglichkeiten zur möglichst schonenden Mineralisierung der äußeren Oberfläche getestet. Dafür wurde der „Disk“-Rand mit Peptiden funktionalisiert, welche die Anlagerung und Kondensation von Kieselsäure steuern (**Manuskript III**). Verwendet wurde das Peptid $(KD)_{10}C$, das in einer vorangegangen Machbarkeitsstudie – siehe nächstes Kapitel und **Manuskript IV** – reproduzierbare Ergebnisse zu einer selektiven und gut kontrollierbaren, langsamen SiO_2-Abscheidung lieferte. Die Peptid-Konjugation erfolgte über einen heterobifunktionalen Linker (*Succinimidyl-[(N-maleimidopropionamido)-tetraethyleneglycol] ester*, $SM(PEG)_4$). Die Reaktion wurde über exponierte Amino-Gruppen am „Disk“-Rand und den NHS-Ester des Linkers durchgeführt. Anschließend wurde das Peptid über die Thiol-Gruppe seines C-terminalen Cysteins *via* Michael-Addition an die freie Maleimid-Gruppe des Linkers gebunden. Diese Funktionalisierung der „Disks“ wurde über native und denaturierende Gelelektrophorese nachgewiesen. Die chemisch modifizierten CPs verhielten sich im denaturierenden Gelsystem bezüglich ihrer elektrophoretischen Mobilität umgekehrt proportional zum Molekulargewicht. Unter nativen Bedingungen war die Mobilität der „Disks“ im elektrischen Feld abhängig von ihrer Oberflächengesamtladung. Die Konjugation des negativ geladenen bifunktionalen Linkers allein erhöhte die Mobilität, während nachfolgend immobilisierte Peptide diese Ladungen wieder neutralisierten und derart modifizierte „Disks“ sich nahezu wie unmodifizierte verhielten.

Zusätzlich wurde getestet, welche der synthetischen SiO_2-Ausgangssubstanzen ((TEOS) und Tetramethylorthosilikat (TMOS)) am besten für die Bildung dünner Silikat-Schichten und somit selektive Versiegelung schmaler Spalte in den Hybridmembranen geeignet sein dürfte. Die Alkoxysilane TEOS und TMOS wurden deshalb unter sauren Bedingungen hydrolysiert und dadurch in niedermolekulare Kieselsäure-Monomeren umgewandelt. Laut Werten in der Literatur verläuft die Hydrolyse von TMOS schneller aufgrund der höheren Polarität seiner Methoxy-Gruppe (Bernards et al. 1991). Da sich an die Hydrolyse bei supersaturierten Kieselsäure-Lösungen (d. h. bei Konzentrationen über 1-2 mM Kieselsäure bei neutralem pH) eine Kondensationsreaktion der Orthokieselsäure zu Polymeren über Siloxan-Bindungen anschließt (Belton et al. 2010, Schröder et al. 2012), sollte der prä-hydrolysierte Ausgangsstoff schnellstmöglich mit dem Biotemplat in Kontakt gebracht werden, um eine unspezifische Präzipitation von SiO_2 zu vermeiden. Dies ist speziell für die effiziente Versiegelung der engen Lücke zwischen der „Disk“ und dem SSM-Porenrand entscheidend, da in der Vorläuferlösung entstehende SiO_2-Partikel mit Durchmessern über 2 nm vermutlich nicht mehr für die kontrollierte Versiegelung geeignet sind: Sie könnten nicht in den Ringspalt zwischen TMV-„Disk“ und konischer SSM-Pore eindringen. Eine weitere Analyse zur „Disk“-Mineralisierung wurde dem Einfluss des pH-Werts während der SiO_2-Präzipitationsreaktion gewidmet. Kieselsäure erhöht die Kondensationsgeschwindigkeit mit steigendem pH-Wert (Belton et al. 2012). Daher wurde untersucht, ob eine Erhöhung des pH-Werts von 5,5 auf 7,0 die Abscheidung von SiO_2 am „Disk“-Rand beschleunigt. Der Vergleich zeigte, dass bei pH 5,5 eine ortsspezifische ringförmige SiO_2-Abscheidung dort stattfand, während bei pH 7,0 tatsächlich eine erhöhte, allerdings nicht ortsspezifische, Bildung von SiO_2-Aggregaten nachgewiesen werden konnte. Weitere Untersuchungen werden bei der Fortsetzung des Projekts erforderlich sein, um eine fein-regulierte Abscheidung des Minerals an der „Disk“-Außenfläche im Inneren von konischen Membranporen zu erreichen.

Mineralisierung von Peptid-funktionalisierten TMV-Partikeln

Um ein geeignetes Peptid für die Funktionalisierung der „Disks“ als Porenadapter zu identifizieren, wurde zunächst die TMV-Oberfläche für die Abscheidung von SiO_2 optimiert, indem unterschiedliche mineralisationsvermittelnde Peptide auf vollständig assemblierten TMV-Stäbchen immobilisiert wurden. Eine eingehendere Untersuchung dieser funktionalisierten TMV-Partikel wurde als Machbarkeitsstudie

durchgeführt, um neben einer gut geeigneten Peptidsequenz auch beste Bedingungen für die kontrollierbare und ortsselektive Silizium-Präzipitation auf TMV-Derivaten einzugrenzen (**Manuskript IV**). Es wurde ein Satz von Peptiden analysiert, der sich in drei Gruppen gliedern lässt. Die erste bestand aus Peptiden mit einer sich wiederholenden Abfolge der Aminosäurereste Lysin und Aspartat $(KD)_x$ von unterschiedlicher Länge ($(KD)_5C$ und $(KD)_{10}C$). Im Vergleich zu blockartig angeordneten Aminosäureresten weisen solche alternierend angeordneten alle Voraussetzungen für eine hohe Kondensationsrate von Trimethylethoxysilan zu Hexamethylsiloxan auf (Kuno et al. 2011). Zur zweiten Gruppe mit blockartig organisierten Aminosäureresten gehörte das Peptid CA_4H_4 (Yuwono & Hartgerink 2007). Da Histidin aufgrund der hohen Affinität des Stickstoffs im Imidazolring zu SiO_2, wie im Kapitel zur Mineralisierung beschrieben, entscheidend zur Kondensation von SiO_2 beiträgt, findet sich diese Aminosäure sehr häufig in Peptid-Sequenzen, die über Phagen-Display mit SiO_2 oder Zinkoxid (ZnO) als Bindesubstrat selektiert wurden (Chen et al. 2006, Patwardhan et al. 2011). Die dritte Gruppe getesteter Peptide beinhaltete zwei ZnO-affine Peptid-Varianten, die aus einer Phagen-Display-Selektionsanalyse hervorgegangen sind (Rothenstein et al. 2012). Diese bestehen ebenso zu einem hohen Anteil aus Histidin.

Nach der Peptid-Fixierung auf TMV-Trägerstäbchen mit einem dichten Besatz an bifunktionalen Linkern wurde zunächst ein unterschiedliches Aggregationsverhalten der Produkte in wässriger Lösung beobachtet. TMV-Partikel mit Histidin-haltigen Peptiden zeigten eine starke Neigung, bündelartige Mesostrukturen auszubilden, während diejenigen mit $(KD)_x$-Motiv stabil in Lösung blieben. Die jeweilige kolloidale Stabilität wurde mittels ζ-Potential-(ZP)-Analyse bestätigt. Gewöhnlich sind anorganische Partikel mit hohem negativem oder positivem ZP kolloidal stabil (Hunter 1981). Vergleichbar zu diesen Daten wiesen $(KD)_x$-tragende TMV-Partikel tatsächlich ein stärker negatives ZP auf als die mit Histidin-haltigen Peptiden.

Im Gegensatz zu den weniger stabilen „Disks“ war es möglich, die vollständigen TMV-Partikel in einem TEOS-Ethanol-H_2O-Gemisch in einem Verhältnis 1:4:4 zu mineralisieren. Die Aggregat-Bildung spiegelte sich auch in den Mineralisierungsprodukten wider. So bildeten TMV-Partikel mit Histidin-haltigen Peptiden Aggregate im mikroskopischen Bereich aus, während die $(KD)_x$-ausgestatteten dispers als dünne Stäbchen im nanoskopischen Größenbereich nachgewiesen wurden. Nach dieser Vergleichsstudie wurde das Peptid $(KD)_{10}C$ einer

genaueren Prüfung seiner SiO_2-Präzipitationsrate über die Zeit unterzogen. Dafür wurde ein Verlaufsexperiment über 12 Tage hinweg durchgeführt, um den Zuwachs der SiO_2-Schicht zu messen. Die TEM-Analyse des Primärkontrasts der Siliziumatome zeigte, dass nach 10 Tagen die gleichmäßige SiO_2-Ablagerung zum Stillstand kam und sich unregelmäßig geformte Begleitprodukte bildeten. Innerhalb des produktiven Zeitintervalls bildet sich eine Schichtdicke von 6 nm, d. h. pro Tag durchschnittlich 0,6 nm. Verglichen mit anderen Experimenten ist diese Zuwachsrate extrem langsam (Fowler et al. 2001, Steinmetz et al. 2009, Bruckman et al. 2015). Da in diesem Ansatz ausschließlich die Aktivität der Peptide untersucht wurde ohne Beimischung von katalytisch aktiven Substanzen, wie NH_4OH oder APTES, könnte die Reaktionsgeschwindigkeit durch veränderte Milieubedingungen oder durch chemische Modifikationen der Peptid-Aminosäurereste, ähnlich wie bei den posttranslational modifizierten Silaffinen (Kröger et al. 1999), eventuell erhöht werden, wenn nötig. Andererseits stellt eine derart langsame und Biotemplat-spezifische Silikat-Abscheidung eine gute Voraussetzung dafür dar, um in bioanorganischen Hybridmembranen unerwünschte Lücken selektiv abzudichten, ohne die funktionellen Proteinporen zu verschließen.

Ausblick

Im Fokus dieser Arbeit stand die Entwicklung und Herstellung neuartiger stabiler, leicht modifizierbarer Porenadapter, welche an die direkte Insertion in poröse anorganische SSM-Template angepasst sind. Dementsprechend wurden auf Grundlage von TMV-Komponenten Nukleoprotein-Lochscheiben generiert, die exakt auf die konischen Poren entsprechender Membranen abgestimmt sind und als mischassemblierte Aggregate mit verschiedenen genetisch modifizierten CPs eine erweiterte chemische Funktionalisierung erlauben. Durch die Verwendung solcher CP-Varianten war es beispielsweise möglich, bifunktionale „Disks“ mit einem Fluoreszenz-Farbstoff zu markieren und über eine weitere funktionelle Gruppe chemisch auf ein ITC-versehenes Substrat zu koppeln. Die Fixierung von SiO_2-Präzipitation induzierenden Peptiden an den „Disk“-Außenflächen führte zur spezifischen Ausbildung einer ringförmigen Mineralschicht um die „Disks“, die für die Versiegelung der Lücke zwischen „Disk“ und SSM-Pore in der Zukunft von Bedeutung sein wird.

Wie die Daten zur Insertion von „Disks“ in die SSM-Poren zeigen, ließen sich elektrophoretisch bereits relativ hohe Beladungsraten von 60-70 Prozent erreichen.

Zur Optimierung der Insertion insbesondere im Hinblick auf eine richtige Orientierung der „Disks“ in den SSM-Poren wurden die TMV-Porenadapter weiterentwickelt und mit einer RNA-„Leine“ ausgestattet. Ihr Verhalten wird in weiterführenden Arbeiten mit verbesserten Techniken untersucht. Ein tragendes Thema wird künftig die Ausrichtung der „Disk“ mit RNA-„Leine“ im elektrischen Feld sein (**Abb. 6 a**). Hier bietet es sich an, die biologischen Strukturen nach ihrer Integration in die Porenkanäle mit REM oder Helium-Ionen-Mikroskopie (**Abb. 6 b und c**) bei niedrigen Spannungen zu analysieren, weil diese Verfahren die simultane Abbildung von organischen und anorganischen Materialien erlauben (Joens et al. 2013).

Für erfolgreich generierte bioanorganische Hybridmembranen werden Funktionsanalysen darüber entscheiden, ob und wie sie in praxistaugliche Filtereinheiten mit nanoporöser Kontrolle überführt werden können. Die einfachste Charakterisierung basiert auf Größenausschlussverfahren. Um die selektive Permeabilität zu untersuchen, könnte die Diffusionsrate von Fluoreszenz-Molekülen mit unterschiedlichen Größen und Emissionsspektren untersucht werden. Dafür würde sich das tonnenförmige grün fluoreszierende Protein (*green fluorescent protein*, GFP) mit einer Länge von 4 nm und einer Breite von 3 nm (Yang et al. 1996) anbieten, das vermutlich den 4 nm „Disk“-Innenkanal nicht passieren kann, gemischt mit relativ kleinen Farbstoffen wie den Cyaninen 3 oder 5 mit jeweils etwa 0.75 nm hydrodynamischem Durchmesser (Morgan et al. 2008), die leicht diffusibel sind. Der Molekülstrom durch die nanoporöse Hybridmembran ließe sich anhand des Fluoreszenzsignals der unterschiedlichen Emissionsspektren charakterisieren. Aber auch die Detektion und Trennung von Konformationsisomeren- oder Gasgemischen ist eine vielversprechende Anwendungsmöglichkeit. So konnte bereits gezeigt werden, dass L- und D- Aminosäuren beim Passieren einer chemisch modifizierten Proteinpore voneinander unterscheidbar sind (Boersma & Bayley 2012).

Für die Trennung von Gasgemischen haben sich sehr unterschiedliche Membrantypen etabliert, wie Graphen (Du et al. 2011), Polymere (Sanders et al. 2013, Yampolskii 2012) oder Keramikmembranen (Li 2007). Durch unterschiedliche Funktionalisierungsmethoden des TMV-Innenkanals könnte ein komplexeres Anwendungs-Niveau erreicht werden (**Abb. 7 und 8**). TMV-CP-Mutanten lassen es zu, funktionelle Gruppen wie die Thiole von Cystein oder Amino-Gruppen des Lysin für chemische Kopplungsreaktionen im Innenkanal bzw. in der „Disk“-Pore zu exponieren (Dedeo et al. 2010, Zhou et al. 2013). Folglich könnten verschiedene

Moleküle dort immobilisiert werden und die Permeabilität von kleinen Molekülen, eventuell sogar von gasförmigen Verbindungen oder auch Polymeren, beeinflussen. Vorausgesetzt, die Lücke zwischen „Disk“-Rand und SSM-Porenwand ließe sich mit Silikat stabil verschließen, wäre bei diesem bioanorganischen Hybridmembrantyp mit starr verbundenen Partnerkomponenten das Auftreten von Leckströmen unwahrscheinlich. Dies könnte ein großer Vorteil gegenüber Proteinporen sein, die in Lipidmembranen integriert mit SSM-Poren kombiniert wurden (Urban et al. 2014): Defekte der Membrandomänen führen in solchen Anordnungen stets zu Fehlfunktionen.

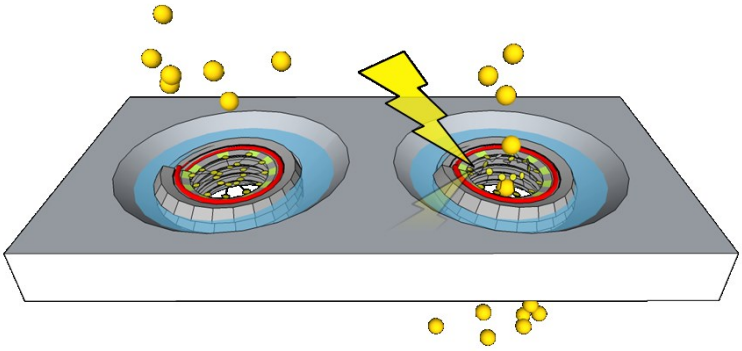

Abb. 7: Mögliche Erweiterung der Funktionalität des „Disk“-Innenkanals. Photosensitive Moleküle, immobilisiert in der Pore, könnten lichtabhängig zur gesteuerten Translokation von Molekülen verwendet werden.

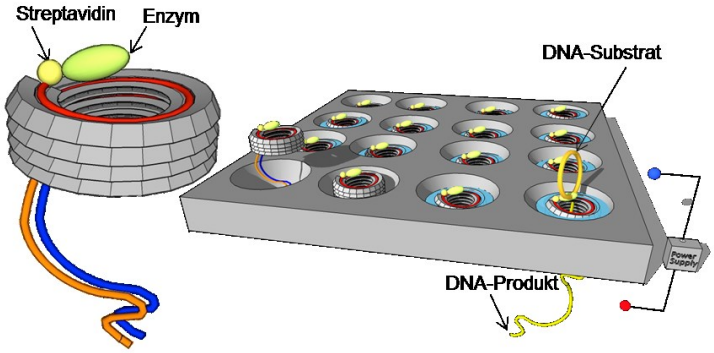

Abb. 8: Enzymatisch aktive Poren als Fernziel. Das 5’-Ende der ssRNA könnte als biotinylierter Anker für die Bindung von Streptavidin-gekoppelten Enzymen dienen. Durch die Nähe des Enzyms zur Pore würde die Trennung des Edukts vom Produkt oder dessen Analyse bei seinem Transfer begünstigt.

Abschließend sollen noch einige komplexere Entwicklungen skizziert werden, die mit solchen TMV-basierten Nanoporen in robusten Feststoff-Templaten denkbar werden. Membranen, die mit multifunktionalen Porenadaptern ausgestattet sind, wären geeignete Komponenten in Brennstoffzellen. Diese bestehen im wesentlich aus zwei porösen Elektroden, Anode und Kathode. Zwischen den Elektroden befinden sich Elektrolytlösungen oder vermehrt auch Polymermembranen (Peckham & Holdcroft 2010). Als Brennstoff wird Wasserstoff zur Anode geleitet und dort katalytisch in Elektronen und Protonen gespalten. Die Protonen diffundieren in die Elektrolytlösung, wo sie an der Kathode auf Sauerstoff-Moleküle treffen und Wasser bilden. Um die in dieser Arbeit vorgestellten Hybridmembranen in einer

Brennstoffzelle einsetzen zu können, bedürfte es noch einiger weiterer Modifikationen, damit sie zu geeigneten Bauteilen werden. Alle Teilschritte erscheinen jedoch realisierbar, einige wurden sogar bereits mit Virustemplaten optimiert: Zunächst ist es notwendig, eine Lichtsammelfalle mit einem geeigneten Katalysator zu verknüpfen, der die lichtgetriebene Wasserspaltung katalysiert. Sowohl TMV als auch M13 lassen sich mit Lichtsammelfalle (TMV: verschiedene Chromophore (Miller et al. 2007); M13: Zinkporphyrin (Nam et al. 2010b)) und den Katalysatoren Palladium (Yang et al. 2013a, Adigun et al. 2015) oder Iridiumoxid (Nam et al. 2010a) ausstatten. Lichtsammelfalle und Katalysator zusammen würden den Part der Wasserspaltung ähnlich wie im Photosystem II bei der Photosynthese übernehmen, wobei Sauer- (O_2) und Wasserstoff (H_2) entsteht (Kadereit 2014). Des Weiteren müssten die Porenkanäle so angepasst werden, dass sie spezifisch nur O_2 oder H_2 durchlassen. Wie für Graphen beschrieben, ist es möglich, darin Löcher zu erzeugen, die selektiv permeabel für H_2- oder N_2-Moleküle sind (Du et al. 2011). Zum einen basiert die Selektivität auf der Größe der Poren, zum anderen auf van der Waals-Wechselwirkungen der Gas-Moleküle mit dem Poren-Material. Dementsprechend könnte der „Disk“-Innenkanal mit Peptiden, Lipiden oder Polymeren funktionalisiert werden, sodass H_2-Moleküle an der Kanalwand haften, während O_2 hindurch diffundieren kann. Umgekehrt müsste der Porendurchmesser für die kleineren H_2-Moleküle so verringert werden, dass die Membran für Sauerstoff impermeabel ist. Die beiden selektiv permeablen Membranen könnten durch eine Protonenaustauschmembran voneinander isoliert werden (Peckham & Holdcroft 2010), so dass die Oxidation von H_2 an der O_2-durchlässigen Membran stattfindet. Dieser Aufbau einer Brennstoffzelle würde sowohl die lichtgetrieben Wasserspaltung als auch die elektrochemische Energiegewinnung miteinander verbinden und als Nebenprodukt wieder Wasser bilden, das in den Kreislauf zurückfließt.

Denkbar wäre auch die Immobilisierung von sensitiven Molekülen, die unter bestimmten Bedingungen ihre Konformation ändern, in TMV-Poren, wie es bereits für α-Hämolysin mit Azobenzol-Bipyridinium-funktionalisiertem Innenkanal gezeigt wurde (Ying et al. 2013). Ebenso ändern Retinal, das die Ionenleitfähigkeit in den Zapfen und Stäbchen der Netzhaut des Auges reguliert (Nakatani & Yau 1988), oder Anthracen (Bouas-Laurent et al. 1980) lichtabhängig ihre Konformation, wobei ersteres von 11-*cis*-Retinal in all-*trans*-Retinal übergeht; Anthracen hingegen dimerisiert.

SSMs, die mit Licht-sensitiven „Disks“ ausgestattet wären, könnten z.B. als optische Sensoren in Retina-Implantaten (Stingl et al. 2013) verwendet werden. Wie oben beschrieben, lässt sich der Innenkanal von genetisch veränderten TMV-Partikeln chemisch mit Chromophoren funktionalisieren (Miller et al. 2007). So könnten mehrere Hybridmembranen mit jeweils unterschiedlich lichtsensitiven Molekülen in „Disk“-Kanälen zu einer größeren Einheit zusammengefügt werden, die auf verschiedene Wellenlängen reagiert. Die funktionalisierten Porenkanäle würden sich darin aufgrund der Konformationsänderungen der lichtsensitiven Moleküle öffnen und schließen, wodurch ein Einstrom von Ionen oder niedermolekularen Verbindungen möglich wäre. Empfangene Lichtsingale verschiedener Wellenlängen könnten nach Ioneneinstrom als elektrische Impulse von den unterschiedlichen Hybridmembranen über Mikrochips verrechnet und über die Nervenzellen des Sehnervs weitergeleitet werden, ähnlich wie Retinal die Signaltransduktion in Zapfen oder Stäbchen G-Protein-vermittelt über Na^+-Kanäle reguliert (Heldmaier et al. 2013). Mit einem vergleichbaren Multiplexnanoporenbiochip konnten Urban et al. (2014) den Ein- und Ausstrom von Fluoreszenzmolekülen durch Tausende von Membranproteinen parallel messen.

Den Effekt der lichtabhängigen Dimerisierung von Anthracen könnte man sich zunutze machen, indem zunächst zwei Anthracen-Moleküle über ein Polymer, z. B. Polyethylenglykol (PEG), miteinander verbunden werden. Je nach Wellenlänge des eingestrahlten Lichts kann solch Anthracen-PEG-Anthracen-Dimer zirkulär oder linear vorliegen (Bouas-Laurent et al. 1980). Würden diese Konstrukte kovalent an funktionelle Gruppen im Innenkanal gebunden, könnte dieser lichtinduzierbar geöffnet oder geschlossen werden (**Abb. 7**). Da Anthracen unter UV-Bestrahlung dimerisiert (Wells et al. 2011), wäre diese Licht-gesteuerte Pore als Lichtschutzsensor einsetzbar, der zu lange Sonnenlichtexposition und damit Sonnenbrandgefahr meldet.

Neben der Modifikation des Innenkanals über reaktive Gruppen lassen sich auch die Enden der RNA mit dort fixierten Enzymen ausstatten (**Abb. 8**). Ähnlich wie die Beladung von zylinderförmigen Lichtwellenleitern (Korlach et al. 2008) oder MspA-Nanoporen (Manrao et al. 2012) mit Φ29-DNA-Polymerase wäre es möglich, diese direkt am Porenrand über Biotin-Streptavidin-Interaktion zu fixieren, um parallel tausende von ssDNA-Molekülen zu synthetisieren und in Echtzeit beim Porendurchtritt zu sequenzieren (Lieberman et al. 2010).

Das Erweiterungspotential solcher neuartigen Hybridmembranen ist also groß; daraus entwickelte Filtrationseinheiten wären vielseitig anwendbar und könnten in medizinischen, analytischen oder katalytischen Bereichen eingesetzt werden.

Eingehende Darstellung der Ergebnisse

Fachartikel-Manuskripte (I-III) und eine bereits veröffentlichte Publikation (IV)

Die Beiträge der Koautoren sind vor den einzelnen Manuskripten spezifiziert.

Manuscript I

Fabrication of bifunctional RNA-stabilized TMV "disks" as pore adapters

Klara Altintoprak[1], Axel Seidenstücker[2], Carlos Azucena[3], Holger Jeske[1], Hartmut Gliemann[3], Alfred Plettl[2], and Christina Wege[1]

[1]Department of Molecular Biology and Plant Virology, Institute of Biomaterials and Biomolecular Systems, University of Stuttgart, Pfaffenwaldring 57, 70569 Stuttgart, Germany

[2]Institute of Solid State Physics, University of Ulm, Albert-Einstein-Allee 11, 89081 Ulm, Germany

[3]Institute of Functional Interfaces (IFG), Karlsruhe Institute of Technology, Hermann-von-Helmholtz-Platz 1, 76344 Eggenstein-Leopoldshafen, Germany

Manuscript II

Viral protein nanorings on a double-stranded RNA-leash

Klara Altintoprak[1], Alfred Plettl[2], Othmar Marti[3], Hartmut Gliemann[4], Holger Jeske[1] and Christina Wege[1]

[1]Department of Molecular Biology and Plant Virology, Institute of Biomaterials and Biomolecular Systems, University of Stuttgart, Pfaffenwaldring 57, 70569 Stuttgart, Germany

[2]Institute of Solid State Physics, University of Ulm, Albert-Einstein-Allee 11, 89081 Ulm, Germany

[3]Institute for Experimental Physics, University of Ulm, Albert-Einstein-Allee 11, 89081 Ulm, Germany

[4]Institute of Functional Interfaces (IFG), Karlsruhe Institute of Technology, Hermann-von-Helmholtz-Platz 1, 76344 Eggenstein-Leopoldshafen, Germany

Manuscript III

Mineralization of peptide-equipped viral nanorings

Klara Altintoprak[1], Alfred Plettl[2], Othmar Marti[3], Hartmut Gliemann[4] and Christina Wege[1]

[1]Department of Molecular Biology and Plant Virology, Institute of Biomaterials and Biomolecular Systems, University of Stuttgart, Pfaffenwaldring 57, 70569 Stuttgart, Germany

[2]Institute of Solid State Physics, University of Ulm, Albert-Einstein-Allee 11, 89081 Ulm, Germany

[3]Institute for Experimental Physics, University of Ulm, Albert-Einstein-Allee 11, 89081 Ulm, Germany

[4]Institute of Functional Interfaces (IFG), Karlsruhe Institute of Technology, Hermann-von-Helmholtz-Platz 1, 76344 Eggenstein-Leopoldshafen, Germany

Manuscript IV (publiziert 2015)

Peptide-equipped tobacco mosaic virus templates for selective and controllable biomineral deposition

Klara Altintoprak[1], Axel Seidenstücker[2], Alexander Welle[3,4], Sabine Eiben[1], Petia Atanasova[5], Nina Stitz[5], Alfred Plettl[2], Joachim Bill[5], Hartmut Gliemann[4], Holger Jeske[1], Dirk Rothenstein[5], Fania Geiger[1], and Christina Wege[1]

[1]Department of Molecular Biology and Plant Virology, Institute of Biomaterials and Biomolecular Systems, University of Stuttgart, Pfaffenwaldring 57, 70569 Stuttgart, Germany

[2]Institute of Solid State Physics, University of Ulm, Albert-Einstein-Allee 11, 89081 Ulm, Germany

[3]Karlsruhe Nano Micro Facility (KNMF) and [4]Institute of Functional Interfaces (IFG), [3,4]Karlsruhe Institute of Technology, Hermann-von-Helmholtz-Platz 1, 76344 Eggenstein-Leopoldshafen, Germany

[5]Institute of Materials Science, University of Stuttgart, Heisenbergstraße 3, 70569 Stuttgart

Manuscript I

Altintoprak, K., Seidenstücker, S., Azucena, C., Jeske, H., Gliemann, H., Plettl, A. & Wege, C. 2015. 'Fabrication of bifunctional RNA-stabilized TMV "disks" as pore adapters.'

Authorship responsibilities

Altintoprak:

- Development of experimental strategy
- Cloning procedure, CP preparation, VLP assembly
- Native and denaturing gel electrophoresis
- TEM and fluorescence analysis
- Stability tests
- Fluorescent labeling
- Immobilization of "disks" on ITC-functionalized substrates
- Data acquisition and interpretation
- Preparation of all figures and tables
- Data discussion against the background of previous publications
- Writing and editing of the manuscript

Seidenstücker:

- Fabrication of gold-patterned ITC-functionalized substrates

Azucena:

- Preparation and optimization of ITC coating

Jeske:

- Conceptual contributions and continuous discussion

Plettl and Gliemann:

- Basic project design (jointly with Wege), advice and repeated discussion

Wege:

- Basic project design (jointly with Plettl and Gliemann), guidance and constant discussion
- Editing suggestions and proofreading

Fabrication of bifunctional RNA-stabilized TMV "disks" as pore adapters

Klara Altintoprak[1], Axel Seidenstücker[2], Carlos Azucena[3], Holger Jeske[1], Hartmut Gliemann[3], Alfred Plettl[2], and Christina Wege[1]

[1]Department of Molecular Biology and Plant Virology, Institute of Biomaterials and Biomolecular Systems, University of Stuttgart, Pfaffenwaldring 57, 70569 Stuttgart, Germany

[2]Institute of Solid State Physics, University of Ulm, Albert-Einstein-Allee 11, 89081 Ulm, Germany

[3]Institute of Functional Interfaces (IFG), Karlsruhe Institute of Technology, Hermann-von-Helmholtz-Platz 1, 76344 Eggenstein-Leopoldshafen, Germany

Abstract

The integration of nanoporous biological structures such as α-haemolysin or DNA-origami pore-shaped assemblies into single solid-state pores has received growing interest, to confine the pore diameters to a specific size and to control their surface chemistry. Taking this concept one step forth to an expedient nanoporous membrane perforated with millions of identical pores requires pore adapters of large amounts, high structure integrity and stability at various conditions. In this work a protein pore adapter of viral origin was developed with dimensions of 4 nm pore and 18 nm outer diameter, and 10 nm length. The starting material is the plant-infecting tobacco mosaic virus (TMV): a nanotube-like nucleoprotein structure with its length determined by a single-stranded RNA scaffold. RNAs of different length and with the TMV origin of assembly (OAs) were designed and encapsulated in the viral capsid protein *in vitro*, with a 204 nt RNA yielding 10 nm long four-turn helical assemblies efficiently. Their stability under variable pH conditions was explored, indicating high structural integrity in a pH range from 7.2 to 9.0. Furthermore, products containing two different genetically engineered, selectively addressable coat protein types (TMV_{Cys} and TMV_{Lys}) were generated, chemically modified with a fluorescent dye and immobilized on an isothiocyanate-(ITC)-covered substrate *via* the distinct functional groups exposed. This novel construct thus offers special opportunities as a versatile pore adapter for inorganic membranes and the fabrication of extended hybrid materials.

Introduction

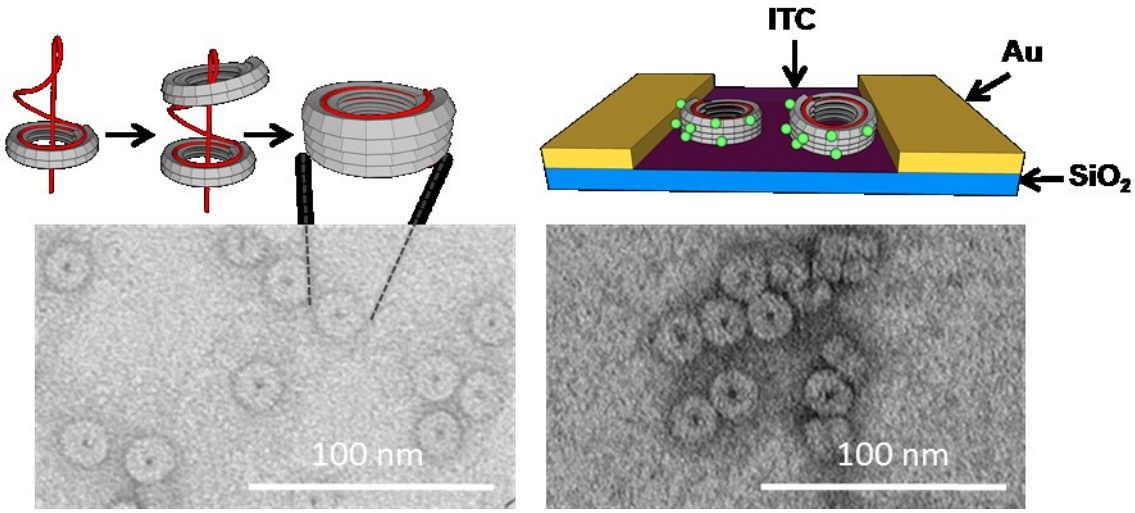

Figure 1: Scheme of TMV coat proteins (CPs) and RNA assembling into a four-turn helix ("disk"), and immobilization of bifunctional fluorescence-labeled "disks" on an ITC-covered substrate at pH 9.

The combination of biological and inorganic compounds to fabricate new hybrid materials is a growing field of research in nanotechnology science. Innovative applications such as light-driven water oxidation (Nam et al. 2010a), photoelectrochemistry in current collectors (Chiang et al. 2012), catalytic activity (Yang et al. 2013a), DNA sequencing (Eid et al. 2009), or multiplexed transport studies by help of extended nanoporous materials (Kleefen et al. 2010) were shown to enhance product transformation rates and/or quality compared to plain inorganic devices. Especially, the production of inorganic nanoporous membranes with only one pore size of a distinct diameter in the 1-5 nm range is hardly to gain by top down methods such as photolithography, focused ion beam (Danelon et al. 2006, Nilsson et al. 2006) or electron beam processes (Kleefen et al. 2010), and might therefore profit substantially from an integration of porous biogenic components.

Nano-scale building blocks of biological origin provide several advantages over inorganic materials. Compared to "top-down" processes such as inorganic etching techniques or lithography methods, "bottom-up" biomolecule assembly allows synthesis of highly reproducible structures which can be readily manipulated chemically or genetically (Bittner et al. 2005, Bittner et al. 2013). On the other hand inorganic material e.g. of solid-state membranes (Storm et al. 2003) or minerals (Royston et al. 2006, Altunbas et al. 2010) implies durability or high stability under harsh conditions. A critical point according to the fusion of biological and inorganic components to form hybrid materials is to connect such unequal compounds at their

interfaces. This challenge can be tackled by functionalization of the surfaces with reactive groups for chemical coupling, or introducing molecules, which interact by van-der-Waals, ionic or hydrophobic-hydrophilic interactions (Chiang et al. 2012, Royston et al. 2008, Patwardhan et al. 2012).

An established route of chemical coupling of biological materials onto inorganic surfaces is the application of silane interlayers equipped with reactive groups (e.g. isothiocyanate, ITC), which can be used e.g. for the functionalization of silica membranes to immobilize biomolecules on their surfaces (Azucena et al. 2012). Furthermore, site-specific functionalization of inorganic materials allows an ordered orientation of biological components on certain areas, such as a bottom-up assembly of virus-like particles (VLP) on DNA oligonucleotide-fashioned substrates generated by DNA-RNA ligation, which installed RNA scaffolds capable to guide the assembly of TMV-like nucleoprotein tubes (Müller et al. 2011).

Nanoporous solid-state membranes have already been equipped with biological protein (Hall et al. 2010) or DNA origami pores (Hernandez-Ainsa et al. 2014, Bell et al. 2012) driven into the inorganic pores by electric forces, but in no case with a fixation of the biomolecular partner at the inner pore rim so far. Comparable experiments on the loading of nanopore/optical waveguide array devices with protein-DNA complexes showed that these complexes are reversibly released (Larkin et al. 2014). Hence, for a stable integration of biological pore adapters into inorganic backbones, chemical fixation at the interfaces seems to be required.

In this present paper we therefore demonstrate the fabrication of a novel type of readily available and highly tunable biogenic pore adapters, and their selective immobilization on a functionalized substrate, to pave the way towards their future use as inlays of inorganic pores. To this aim, we have modified components derived from the plant-infecting tobacco mosaic virus (TMV), which has emerged as a favourable nanobiotechnology building block during the last decades in parallel with other plant viruses and bacteriophages, due to their structure integrity and high stability over a wide range of different conditions (Alonso et al. 2013, Bittner et al. 2013). TMV is a tube-shaped protein-nucleic acid complex assembled into a right-handed helix combined of 2130 coat proteins (CP) and one single-stranded RNA (ssRNA) molecule of 6395 nucleotides, which is encapsulated inside the CP helix in the protein capsid. A single TMV particle is 300 nm in length with a diameter of 18 nm and an inner channel of 4 nm diameter (Butler 1999). The length and structure of

TMV-like RNA-CP tubes is tunable by altering the numbers of bases (Rego et al. 2013) or origins of assemblies (OAs; Eber et al. 2015) within the ssRNA sequence. The OAs is an RNA secondary structure forming a stem-loop, which is necessary for the initiation of the nucleation reaction, starting *in vitro* assembly into rod-shaped particles (Zimmern 1977). Besides the OAs-induced assembly, CPs are able to assemble without RNA into VLPs of undefined length (Durham et al. 1971, Carpenter 1970). Further intermediate structures of CP aggregates are the “A-protein” of three to six subunits (Durham & Klug 1971), the 20 S aggregate, proposed as a mixture of polar disks of two rings with 17 subunits per ring and the proto-helices, short helices of two turns with 16 1/3 subunits per turn (Butler 1999, Butler et al. 1992), and a “bilayer disk” (Bhyravbhatla et al. 1998, Raghavendra et al. 1988), i.e. a four-layered “top-to-top” stacked disk aggregate. In principle, the 20 S aggregate, proto-helix or disk, and the stacked disk might be suitable candidates as pore adapters for hybrid membranes. However, the stability of these structures depends on the pH, temperature, ionic strength and CP concentration (Vogel 1982); i. e. an alteration of these conditions inevitably leads to changes of the nanotube length or its complete degradation. Particularly with regard to the increase of pH at low ionic strength, the CP disk or proto-helix aggregates tend to disaggregate into an A-protein fraction (Durham et al. 1971, Stauffer et al. 1970). This would not only impede reaction processes appropriate to the biopore's interconnection with the inorganic pore rim, it would also limit the use of successfully established composite membranes to a narrow range of conditions.

As shown by Rego et al (2013), short RNAs of 349 nts were able to assemble with TMV CP into virus-like nucleoprotein rings 16 nm in length, thus exceeding the length (or thickness) of a disk (4.6 nm) or a stacked disk pair (≈10 nm). In order to fabricate disk-like TMV derivatives optimally suited for an intended use as membrane pore adapters, we employed a series of three distinct RNA scaffolds between 102 and 500 nts in length, all expected to yield short ring- to barrel-shaped assemblies, and tested their efficiency in guiding product formation as well as the stability of the resulting short VLPs at various pH values. Additionally, we examined by a proof-of-concept experiment the immobilization of the most promising nucleoprotein particle type onto an ITC silane-functionalized substrate.

Materials and methods

Cloning and *in vitro* transcription of short RNA constructs

To amplify cDNA constructs allowing *in vitro* transcription of short RNAs containing the TMV core OAs (position 5442-5521 and position 5350-5531; Zimmern 1983), PCR products comprising partial TMV and plasmid sequences were synthesized with *Pfu* DNA Polymerase (#EP0571, Thermo Scientific, Darmstadt, Germany) or Q5® High-Fidelity DNA Polymerase (#M0491, NEB, Ipswich, USA) using TMV wild type sequence (p843pe35TMVr.1; Kadri et al. 2011). Amplified PCR products were equipped with an adenosine overhang at their 3'-ends by Taq DNA Polymerase (NEB Ipswich, USA). After purification (QIAquick PCR Purification Kit, QIAGEN, Hilden, Germany), the PCR products and pGEM®-T Easy vector (Promega, Mannheim, Germany) were cleaved by restriction enzyme AatII (#R0117, NEB, Ipswich, USA) and ligated with T4 DNA ligase (NEB Ipswich, USA). The designed primers ordered by Biomers (Ulm, Germany), which were used for PCR, are listed in **Table 1**. The 204^+ nt and the 102^+ nt RNA DNA templates with AatII restriction site for cloning were amplified by PCR (*Pfu* DNA Polymerase; initial denaturation at 95 °C, 3 min; 3 cycles of 95 °C, 30 sec, 32 °C, 30 sec, 72 °C, 1 min; 27 cycles of 95 °C, 30 sec, 55 °C, 30 sec, 72 °C, 1 min; final extension at 72 °C, 5 min). The ligated vector with insert (pGEM-T-Easy-102^+ and pGEM-T-Easy-204^+) as well as a religated vector (pGEM-T-Easy) without insert was transformed into chemically competent *Escherichia coli* DH5α, amplified and extracted by the use of a Plasmid Midi Kit (QIAGEN, Hilden, Germany). Sequence identity was confirmed by DNA sequencing with a CEQ™ Genetic 8000 Analysis System (Beckman Coulter, Krefeld, Germany).

The DNA templates for *in vitro* transcription of the different RNAs were synthesized by PCR using the isolated plasmids as templates and the primers listed below (**Table 1**). PCR products were separated by gel electrophoreses, the required bands were isolated from the gels with a QIAquick Gel Extraction Kit (QIAGEN, Hilden, Germany), and again amplified by PCR using the same primer combinations as before. PCR products were purified to remove residual nucleotides and DNA polymerases using a QIAquick PCR Purification Kit (QIAGEN, Hilden, Germany) and eluted in dimethyl dicarbonate-(DMDC)-treated deionized water (ddH_2O; 18.3 MΩ cm; purified by a membraPure system, Aquintus, Bodenheim, Germany). The DNA templates for 102^+ nt RNA (PCR template: pGEM-T-Easy-102^+), 204^+ nt RNA (PCR template: pGEM-T-Easy-204^+) and 90^- nt RNA (PCR template: pGEM-T-

Easy) were amplified by PCR (*Pfu* DNA polymerase; initial denaturation at 95 °C, 3 min; 30 cycles of 95 °C, 30 sec, 60 °C, 30 sec, 72 °C, 1 min; final extension at 72 °C, 5 min).

Table 1: Primers designed for cloning with AatII restriction sites (underlined letters) and RNA *in vitro* transcription (small letters indicate part of the T7 RNA polymerase promoter).

RNA product	Primer name	Primer sequence	Annealing temperature
102^+	102_AatII_fwd:	5‘-GAATTCGACGTCCGTGAGAGACGGAG-3‘	32[a], 55[b]
	102_rev:	5‘-GCCTGATCGACATAGGGAC-3‘	
	102_iv_rev	5‘-TGCCTGATCGACATAGGGACATC-3‘	60[c]
204^+	204_AatII_fwd:	5‘-GAATTCGACGTCGCGGGTTTCTGTCC-3‘	45[a], 51[b]
	204_rev:	5‘-AACTTTGCAAGCCTGATCGACA-3‘	
	204_iv_rev	5‘-TAACTTTGCAAGCCTGATCGACA AGG-3‘	60[c]
500^+	500_iv_rev	5‘-GATTCATTAATGCAGCTGGC-3‘	48[c]
90^-	102_c_iv_rev	5‘-CCATATGGTCGACCTGCAGGC-3‘	60[c]
308^-	308_fwd	5‘-CGCGCGTTGGCCGATTCATT-3‘	69[d]
	308_rev	5‘-ATCACTAGTGAATTCGCGGCC-3‘	
	308_T7_fwd	5‘-taatacgactcactatagggCGCGCGTTGG-3‘	40[e], 61[f]
	308_iv_rev	5‘-ATCACTAGTGAATTCGCGGCCGCCTG-3‘	62[c]
All except 308^-	pGEM_fwd	5‘-CGCCAGGGTTTTCCCAGTCAC-3‘	60[c]

PCR synthesis of inserts for cloning:

a. initial annealing temperature (3 cycles) to ensure hybridization
b. affiliating annealing temperature (27 cycles) for specific hybridization and PCR product amplification

PCR synthesis of DNA templates for *in vitro* transcription:

c. annealing temperature (30 cycles) for specific PCR product amplification; pGEM_fwd is used as reverse primer in all PCR reactions except with 308^- nt RNA
d. annealing temperature (30 cycles) for 308^- nt RNA DNA template amplification without T7 RNA polymerase promoter

PCR product synthesis for *in vitro* transcription of 308^- nt RNA DNA template with T7 RNA polymerase promoter

e. initial annealing temperature (3 cycles) to ensure hybridization
f. affiliating annealing temperature (27 cycles) for specific hybridization and PCR product amplification

The DNA template for 500^+ nt RNA (PCR template: pGEM-T-Easy-204^+) was amplified as above but using an annealing temperature at 48 °C, whereas the *in vitro* transcription template for 308^- nt RNA (PCR template: pGEM-T-Easy-204^+) was synthesized in three steps: in a first step the PCR product was amplified without the T7 RNA polymerase promoter (Q5® DNA Polymerase; initial denaturation at 98 °C,

30 sec; 30 cycles of 98 °C, 10 sec, 69 °C, 10 sec, 72 °C, 10 sec; final extension at 72 °C, 1 min); in a second step the PCR product - extracted from agarose gel - was fused with the T7 RNA polymerase promoter (*Pfu* DNA Polymerase; initial denaturation at 95 °C, 3 min; 3 cycles of 95 °C, 30 sec, 40 °C, 30 sec, 72 °C, 30 sec; 27 cycles of 95 °C, 30 sec, 61 °C, 30 sec, 72 °C; final extension at 72 °C, 5 min).
Finally, the PCR product was again extracted from agarose gel, amplified (Pfu DNA polymerase; initial denaturation at 95 °C, 2 min; 30 cycles of 95 °C, 30 sec, 62 °C, 30 sec, 72 °C, 30 sec; final extension at 72 °C, 5 min) and purified (QIAquick PCR Purification Kit, QIAGEN, Hilden, Germany).
The *in vitro* transcription was carried out applying a MEGAscript® T7 High Yield Transcription Kit (Ambion, Austin, USA) following the manual instructions. An amount of 100 ng DNA template was used in a reaction mix of 20 µl total volume and incubated for 6 h at 37 °C. The RNA transcript was precipitated in (final concentrations, f.c.) 1.3 M lithium chloride, 8.6 mM EDTA and 71 % (v/v) ethanol to optimize the precipitation efficiency of short RNA products over night at -20 °C. The RNA pellet was dissolved in DMDC-treated ddH_2O to an f. c. of 1 µg/µl or 3 µg/ml and stored at -80 °C. To confirm length and quality of the RNA transcripts, they were separated by native gel electrophoresis (3 % (w/v) agarose, 1xTBE) and stained with ethidium bromide.

Assembly of RNA-stabilized "disks"

Wild type TMV_{wt} (Kadri et al. 2011) and genetically modified TMV_{Cys} and TMV_{Lys} (Geiger et al. 2013) were purified according to Gooding and Hebert (1967). RNA-free CP was prepared by disaggregation of intact TMV particles in in 66.7 % (v/v) acetic acid for 20 min on ice (Fraenkel-Conrat 1957). The viral RNA was removed by centrifugation for 20 min at 20,000 x g and 4 °C. The supernatant containing the free CP was dialyzed in a dialysis tube (Spectra/Por®7 Dialysis Membrane, 8 kDa molecular weight cut-off [MWCO], Spectrum Laboratories, Rancho Dominquez, USA) against ultrapure water at 4 °C with water changes every 8 h until the isoelectric point was reached and the CP precipitated (24 to 48 h). The flocculating CP was collected by centrifugation as above and the pellet resuspended in 75 mM sodium potassium phosphate (SPP) at pH 7.2. Afterwards, the CP solution was centrifuged for 10 min at 10,000 x g and the supernatant transferred into a fresh reaction tube. The concentration of the CP solution was determined by UV spectroscopy with a NanoDrop ND-1000 spectrophotometer (PeqLab, Erlangen, Germany) at a

wavelength of 280 nm, using the extinction coefficient of TMV CP (1.3 ml mg^{-1} cm^{-1}; Raghavendra et al. 1985). For a typical assembly reaction, 10 mg/ml CP solution was incubated in 75 mM SPP (pH 7.2) for at least 48 h at 20 °C according to Butler (1972), RNA transcripts were mixed with CP in a 1:15 weight to weight ratio at a f. c. of 6 mg/ml CP and 0.4 µg/µl RNA and incubated over night at 30 °C. To investigate the initiation efficiency of nucleoprotein particle formation RNA-containing or RNA-free CP solutions were incubated for 24 h at 30 °C, 3 h at 30 °C followed by 21 h at 10 °C and 24 h at 10 °C. Nucleoprotein particle formation was analysed by native gel electrophoresis.

Native gel electrophoresis

The nucleoprotein particles were analysed by native gel electrophoresis. Samples containing 12 µg CP were supplemented with loading buffer (10 mM SPP pH 7.2, 0.1 % (w/v) bromophenol blue, 10 % glycerol) and separated in 2.5-3 % agarose gels in TBE (98 mM Tris pH 8.0, 89 mM boric acid, 2 mM EDTA). Protein bands were stained with Coomassie Brilliant Blue R250 (Serva Electrophoresis, Heidelberg, Germany). In later stages of the experiments, also VLPs equipped with fluorescent dyes were analysed by native gel electrophoresis. Such samples were first analysed under UV illumination and subsequently stained by Coomassie Brilliant Blue R250.

TEM analysis

The length of the nucleoprotein particles was assessed by transmission electron microscopy (TEM). 15 µl samples containing 50 µg/ml CP were placed on Parafilm M® (American National Can, Menasha, USA), and 400-mesh Formvar® carbon-coated copper grids (Science Service, Munich, Germany) were placed for 5 min on the droplets. Excess sample solution was removed with filter paper, grids were rinsed with 5 droplets ultrapure water and stained with 2 % (w/v) uranyl acetate solution for 90 sec. TEM analysis was carried out using a Tecnai G2 Sphera electron microscope (FEI, Hillsboro, USA) with a Tietz F214 camera (TVIPS, Gauting, Germany).

Stability tests at different pH values

The stability and structure integrity of the nucleoprotein particles at different pH values were examined by native gel electrophoresis and TEM analysis. A buffered solution (75 mM SPP pH 7.2) containing 4.3 mg/ml wild type CP was incubated with

0.3 µg/µl 204^+ nt RNA over night at 30 °C to yield four-turn helices. A control experiment with RNA-free wild type CP was carried out under the same conditions. The pH was then adjusted to 8.0, 9.0, 10.0, or 11.0 by the addition of suitable amounts of a 100 mM Na_3PO_4 stock solution. To yield acidic conditions the pH was adjusted to 6.0 by the addition of suitable amounts of a 5 % acetic acid stock solution. After 1 h at room temperature, samples were analysed on 3 % (w/v) agarose gel as above and for TEM analysis grid were prepared as describe above.

Fluorescent labeling of mixed assembled "disks" by Atto488-maleimide conjugation

Bifunctional nucleoprotein particles were generated by a mixed assembly approach (Eiben et al. 2014). CP_{Cys} and CP_{Lys} were diluted in 75 mM SPP at pH 7.2 to a f. c. each of 3 mg/ml and incubated for 24 h at 4 °C to allow the disassembly of 20S and higher aggregates into A-protein and smaller aggregates, to achieve a homogenous distribution of the different genetically modified CPs. Afterwards, the CP_{Cys}-CP_{Lys} solution was exposed for 24 h to room temperature to obtain precursor aggregates for the nucleation process of VLPs. 204^+ nt RNA to a f. c. of 0.6 µg/µl was added to the CP_{Cys}-CP_{Lys} (f. c. each 2.4 mg/ml) solution and incubated over night at 30 °C. For chemical modification of the resulting VLPs, the products were mixed with 74.6 µM Atto488-maleimide and incubated for 2.5 h under agitation (horizontal shaking at 300 rpm) at 30 °C. After the conjugation reaction, the chemically modified bifunctional nucleoprotein assemblies were purified by gel filtration using PD10 SpinTrap G-25 columns (GE Healthcare, Freiburg, Germany).

Fabrication of gold-patterned ITC-functionalized glass substrates (Axel Seidenstücker)

To obtain areas functionalized with ITC and areas without reactive groups, glass slides were spin-coated with photoresist AR-P 5350 for 40 sec at 4000 rpm and prebaked on a hotplate for 4 min at 105 °C. For patterning, the photoresist was exposed to UV-light using a lithography mask and subsequently developed in AR300-35 and immersed in a bath of ultrapure H_2O. Substrates were then metallized with a layer of 2 nm thermally evaporated chromium and afterwards with 30 nm gold. In a lift-off process, the photoresist was removed by acetone and ultrasonication.

For ITC-silane deposition, these gold-patterned substrates were treated in an oxygen plasma to activate the surface and subsequently placed together with fluid 3-

isothiocyanatopropyl-triethoxysilane (ITC-silane, ABCR, Karlsruhe, Germany) inside a desiccator and evacuated for 6 h at 100 mbar to evaporate the fluidic ITC-silane. Gold-patterned substrates with site-specific ITC-functionalization on the glass areas were removed from the desiccator and, after storage for 12 h at room temperature, rinsed with methanol to remove physisorbed ITC-silane molecules.

Immobilization on ITC-functionalized substrates

Fluorescently labeled bifunctional nucleoprotein particles were immobilized on ITC-silane-covered glass substrates patterned with sputtered gold. A volume of 40 µl fluorescently labeled bifunctional nucleoproteins (in total 4.8 mg/ml CP) was mixed with 10 µl 0.2 M Na_2HPO_4 and 20 µl 0.1 M Na_4HPO_4. For the conjugation reaction between the lysine moieties of the CP_{Lys} and the isothiocyanate groups of the ITC-silanes, the pH was adjusted to 9 by the addition of 7 to 8 µl 0.1 M Na_3PO_4. A control sample was prepared containing Atto488-maleimide without nucleoprotein particles: 40 µl 77 µM Atto488-maleimide in 75 mM SPP was mixed with 10 µl 0.2 M Na_2HPO_4 and 20 µl 0.1 M Na_4HPO_4. 30 µl fluorescence-labeled bifunctional nucleoproteins or fluorescent dye at pH 9 were dropped onto an ITC-covered glass substrate and spread by a coverslip, that was placed onto the droplet and incubated over night at room temperature in a humid chamber in the dark. The substrates were cleaned three times with 10 ml ultrapure water and air-dried. Fluorescence signals on the substrates were analysed by fluorescence microscopy with an Axiovert 200M (Zeiss, Oberkochen, Germany) using an FITC filter set.

Results and discussion

Design of OAs-containing RNA for *in vitro* assembly

We designed different RNAs with (+) and without (-) the OAs, named after their length $(nt)^{+/-}$ in the following. The OAs-containing RNAs were expected to assemble into short virus-like particles (VLPs) of different lengths and helix turn numbers (**Table 2**): 102^+ nt RNA, 204^+ nt RNA, and 500^+ nt RNA with the OAs. A 90^- nt RNA and a 308^- nt RNA both without OAs served as controls as they should not be able to induce VLP formation, since they did not contain a nucleation initiation site. Additionally, the length of the 90^- nt RNA is below that encapsulated in a typical proto-helix (Schön & Mundry 1984). For *in vitro* transcription of the five RNA constructs, DNA-templates of TMV- and pGEM®-T Easy-nucleic acid sequences fused to the T7 RNA polymerase promoter were amplified by PCR. RNAs were

synthesized by *in vitro* transcription and assembled with RNA-free TMV CPs. As described in detail below, the nucleoprotein particle assembling into a four-turn-helix was considered most suitable for technical applications because of its disk-like shape and reproducible nucleoprotein formation. This disk-like structure was therefore studied regarding its pH stability. Additionally, VLPs of bifunctional four-turn helices, an arrangement of two different genetically engineered coat proteins on the same 204^{+} nt RNA, displaying either an amino, or a thiol group on their individual outer surface, were synthesized, labeled with a fluorescent dye and tested for immobilization properties on ITC-functionalized silica substrates.

Table 2: RNA scaffolds with (+) and without (-) the OAs designed for the generation of short virus-like particles (VLPs) of different length and helix turn numbers. For RNAs without the OAs VLP formation is not expected.

Name	Expected length [nm]	Turn number	VLP formation
102^{+} nt RNA	4.6	Two	Yes
204^{+} nt RNA	9.2	Four	Yes
500^{+} nt RNA	23	Ten	Yes
90^{-} nt RNA	-	-	No
308^{-} nt RNA	-	- (Six)*	(With low efficiency)*

* For this RNA without OAs, an OAs-related secondary structure is predicted; refer to text for details.

DNA sequences of different length containing the TMV core OAs (Zimmern 1983) and at the 5'-end the T7 RNA polymerase promoter were synthesized by PCR to serve as templates for *in vitro* transcription. For amplification of 102^{+} nt RNA pGEM-T-Easy-102^{+}, and for both 204^{+} nt RNA and 500^{+} nt RNA the construct pGEM-T-Easy-204^{+} was used as DNA-template. For 90^{-} nt RNA an empty pGEM-T-Easy vector, and for the 308^{-} nt RNA pGEM-204^{+} was used. The lengths of the PCR products were judged by agarose gel electrophoresis (**Figure 2 a**). They were in agreement with the expected sizes of the DNA templates (**Table 3**). Their sequences were verified (**Table S1**). Due to the cloning strategy, the OAs-containing sequences contain segments of TMV (capital letters) and pGEM-T-Easy (small letters) origin. Sequences without OAs are pGEM-T-Easy fragments of plus (90^{-} nt RNA) or minus orientation (308^{-} nt RNA). Successful encapsulation of RNAs with a non-viral portion fused to a TMV-derived OAs-containing segment was demonstrated earlier (Turner et al. 1989), for which reason it was expected that assembly with the short RNAs is feasible. For *in vitro* assembly, RNA molecules were synthesized by *in vitro* transcription. The RNA transcripts were separated by agarose gel electrophoresis

and their lengths determined from their migration velocities in comparison to an ssRNA molecular weight standard (**Figure 2 b** and **Table 3**). They were in good agreement with the expected lengths, with only the 102^{+} nt RNA exhibiting an apparent length more than 5 % below the expected size. This might reflect incomplete denaturation of stable secondary structures of this construct increasing its electrophoretic mobility.

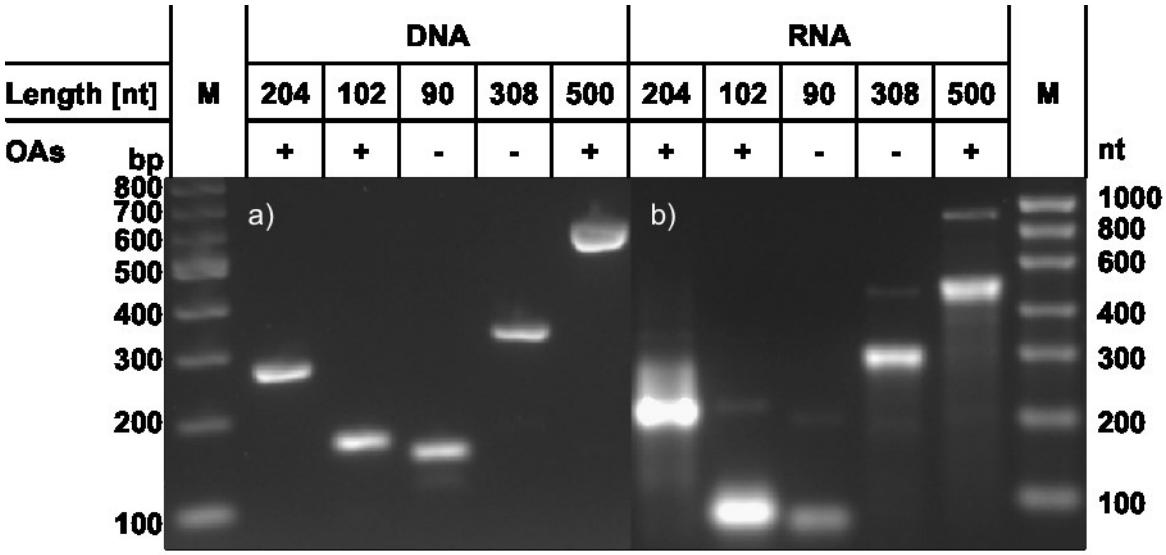

Figure 2: Native gel electrophoretic analysis. **(a)** Purified DNA templates for *in vitro* transcription of 204^{+} nt RNA , 102^{+} nt RNA, 90^{-} nt RNA , 308^{-} nt RNA and 500^{+} nt RNA constructs with OAs (+) and without OAs (-) stained with ethidium bromide. (2 % agarose in 1xTBE; M (left): 100 bp DNA ladder, NEB; bp: base pairs; OAs: origin of assembly) **(b)** RNA transcripts (3 % agarose in 1xTBE; M (right): RiboRuler Low Range RNA ladder, Life Technologies; nt: nucleotide(s)).

Table 3: DNA templates fused to the T7 polymerase promoter and *in vitro* RNA transcripts of expected (exp) size and measured (meas) length determined by gel electrophoresis.

RNA name	DNA length [bp]		Deviation [%]	RNA length [nt]		Deviation [%]
	exp	meas		exp	meas	
204+	271	258.65	4.77	204	207.58	1.73
102+	169	168.78	0.13	102	94.13	8.36
90-	157	161.37	2.71	90	88.22	2.02
500+	327	331.17	1.26	308	306.28	0.56
308-	567	587.30	3.46	500	501.28	0.26

To explore whether the OAs is necessary for nucleating assembly of VLPs *in vitro*, different transcripts with and without OAs were incubated with wild type CP for

different periods of time and at variable temperatures (**Figure 3**). All RNA templates containing the OAs induced the formation of VLP at 30 °C during a period of 3 h or 16 h, respectively, with similar efficiencies, whereas the signals of free CP in the gel declined. For the assembly reaction of 90^- nt RNA without the OAs no characteristic VLP bands were detectable. Thus, the formation of bands with higher electrophoretic mobility was due to the assembly guided by OAs-containing RNAs and not an artefact of the addition of short RNAs.

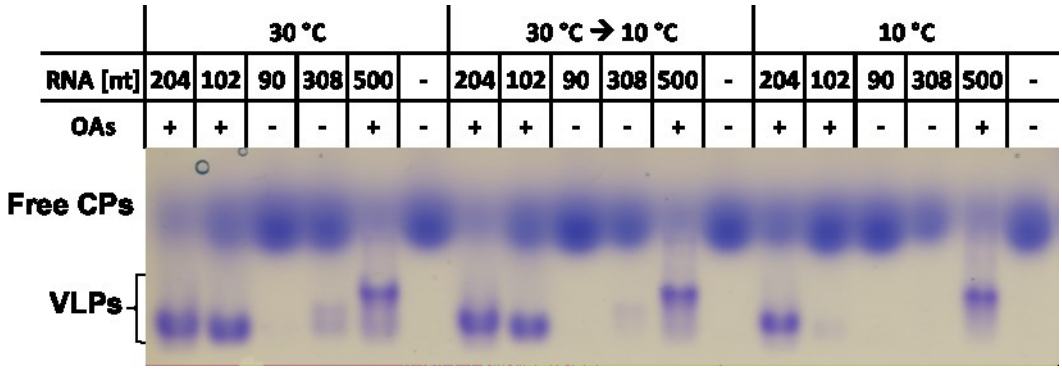

Figure 3: Native gel electrophoresis indicating the assembly efficiencies of different RNAs of 204^+ nt, 102^+ nt, and 500^+ nt all with (+) OAs, and 90^- nt and 308^- nt without (-) OAs under variable temperature conditions (24 h at 30 °C; 3 h at 30 °C and subsequently for 21 h at 10 °C; 24 h at 10 °C). The presence of an OAs increases the assembly efficiency substantially. Proteins are stained with Coomassie Brilliant Blue R250 (2.5 % agarose in 1xTBE; CP: coat protein; nt: nucleotide; OAs: origin of assembly; RNA: ribonucleic acid).

Interestingly, the second control 308^- nt RNA without an OAs sequence induced weak VLP-indicating bands when incubated at 30 °C, but not at 10 °C. In silico structure analysis of 308^- nt RNA calculated by mfold (Zuker 2003) revealed a potential secondary structure of a stem-loop similar to the OAs (**Figure 4**). The predicted loop consists of a nonanucleotide like in the TMV OAs but with a deviant sequence, and the stem of 14 base pairs with eight A-U pairs and two mismatches. The stem of the TMV OAs is also composed of 14 base pairs but with seven A-U pairs, two mismatches and two unpaired bases (Turner et al. 1988). The free energy is predicted to be ΔG = -18.30 kcal/mol for the TMV OAs and ΔG = -21.00 kcal/mol for 308^- nt RNA sequence pseudo OAs. Although the sequence differs significantly from the TMV OAs it might promote the assembly of virus-like structures to a limited extent. Previous investigations on the loop sequence extracted essential features of the base positions inside the nonanucleotide (Turner & Butler 1986, Turner et al. 1988). On the one hand triplet repeats of G residues $(NNG)_3$ are required for efficient initiation, on the other hand C has an adverse effect on nucleation induction. The sequence of the pseudo stem-loop of 308^- nt RNA contains one C residue and four

G, thus the assembly initiation activity of a non-homologous but structurally similar stem-loop of the pseudo assembly is in agreement with the previous results of Turner and co-workers. The three RNAs containing the OAs turned out to assemble with different efficiencies at 10 °C. Whereas 204^{+} nt RNA and 500^{+} nt RNA provided reliable assembly performances, nucleoprotein particle generation of 102^{+} nt RNA was extremely reduced in parallel experiments. This may be due to the fact that unfavourable secondary structures of the RNA sequence lower the nucleation efficiency, as it would be in agreement with the increased mobility of this RNA in gels (see above). An alternative explanation is the assumed instability of RNA-scaffolded two-turn helices compared to four-turn helices, since they do not undergo stabilization by the addition of a further disk (Schön & Mundry 1984). The control experiments of RNA-free CP exposed to the respective conditions revealed no typical nucleoprotein bands in the agarose gels.

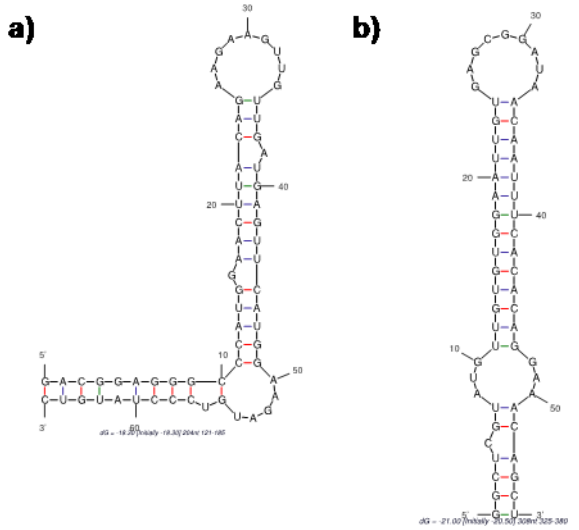

Figure 4: RNA sequence and calculated secondary structure of **(a)** the TMV OAs of assembly (ΔG = -18.30 kcal/mol) and **(b)** the similar hairpin-loop structure of the 308^{-} nt RNA (ΔG = -21.00 kcal/mol).

Taken together, we were able to generate three types of nucleoprotein particles stabilized by TMV OAs-containing RNAs, as deduced from the electrophoretic analysis. The 204^{+} nt RNA and 500^{+} nt RNA were tolerant to nucleoprotein particle formation at different temperatures. For the following experiments 204^{+} nt RNA was selected because of its dimensions (length 11.1 ± 2.5 nm, inner diameter 4 nm, N = 20) similar to commonly used biological nanopores like α-haemolysine, and due to its reliable assembly with TMV CP. In the following, we call the resulting nucleoprotein construct “disk” for simplicity, and as its shape of a four-turn-helix is related to the so-called “bilayer disk” which, however, contains two disk domains in opposite (top-to-top) orientation (Bhyravbhatla et al. 1998).

Stability test of RNA-scaffolded "disks" under variable pH conditions

To gain profound insight into the stability of the 204$^+$ nt RNA-scaffolded "disks", these short VLPs and control samples of RNA-free CP solution, containing numerous of disk aggregates, were exposed to different pH values in parallel tests for one hour and analysed by native gel electrophoresis and TEM thereafter (**Figure 5**). Electrophoretically separated samples revealed the presence of VLP-specific nucleoprotein bands after incubation in a pH range from 6.0 to 9.0. In the comparative tests, these bands had disappeared after incubation at pH values of 10.0 and above.

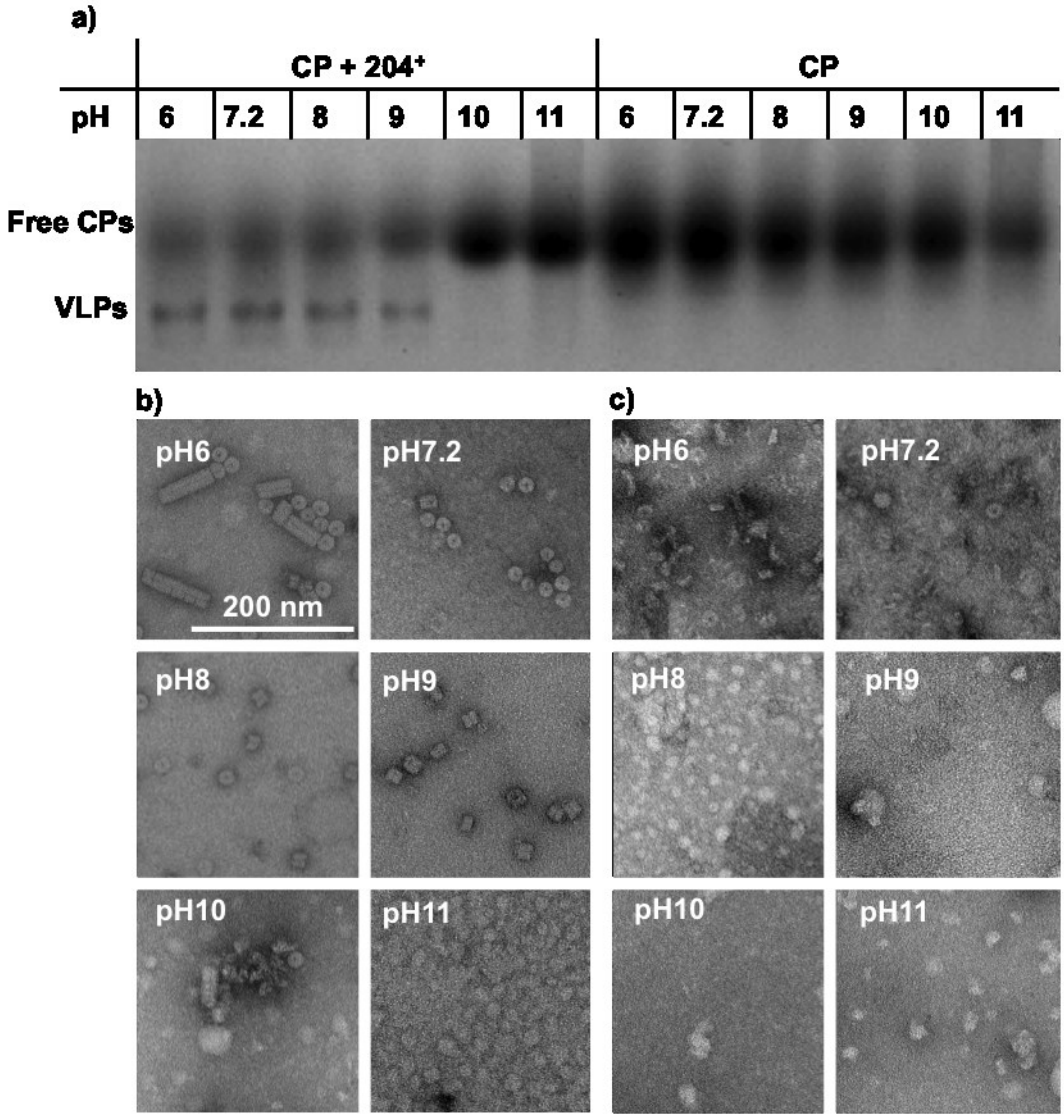

Figure 5: Stability test of 204$^+$ nt RNA-scaffolded "disks" and RNA-free CP aggregates exposed to different pH values for one hour. **(a)** Native gel electrophoretic analysis of *in vitro* assembled "disks" after parallel treatments. Proteins are stained with Coomassie Brilliant Blue R250 (2.5 % agarose in 1xTBE; CP: coat protein; 204$^+$: 204$^+$ nt RNA containing OAs). **(b,c)** TEM analysis of RNA-stabilized "disks" **(b)** and CP aggregates without RNA **(c)**. For TEM analysis, samples were stained negatively with uranyl acetate.

No such nucleoprotein “disk”-specific bands were detected for the control experiment employing RNA-free CP disk-containing preparations. The results of the TEM analysis disclosed more details and revealed that the resolution of the native electrophoretic separation of head-to-tail or top-to-top aggregates including “bilayer disks” and short continuous helices (see Introduction for details) seemed to be limited; it did obviously not allow to discriminate between separate short helices and oligomeric disk-like structures. The TEM images indicate that nucleoprotein particles exposed to pH 7.2 to 9.0 maintained their characteristic form of four-turn helices, whereas at pH 6.0 longer aggregates up to rod-shaped structures were formed. These rod-shaped structures probably represent head-to-tail aggregates of the “disks”, which are also described for whole TMV particles at acidic pH values (Niu et al. 2006). At pH 10.0 and 11.0, disaggregated clusters of CPs were detected with undefined contours. Disaggregation of whole TMV particles is also described in the literature for pH values above 9.0 (Wyckoff 1937, Perham & Wilson 1978), thus the degradation of the RNA-scaffolded “disks” in this pH range coincides with these previous studies. In contrast, TEM analysis of RNA-free CP disk-containing solution indicates that TMV disks remain der two-turn structure at pH 6.0 with low tendency to head-to-tail formation. However, they completely disaggregate at pH 8.0 and above. The comparative study of the “disk” stability at different pH values confirms the scaffolding effect of the RNAs encapsidated inside the TMV CPs. Hence, the novel “disks” are suitable for chemical reactions carried out under moderately alkaline conditions.

Fluorescent labeling of bifunctional TMV “disks”

Bifunctional “disks” displaying two types of selectively addressable coupling groups on their outer rim were generated by a mixed assembly approach (Eiben et al. 2014), combining two different types of genetically modified coat proteins in a 1:1 ratio in a single four-turn helix. Such “disks” were fabricated in order to interconnect them with two different functionalities, to serve e.g. as adapter between a fluorescent label and a chemically modified substrate as a proof-of-concept depicted in **Figure 6**. Native gel electrophoresis showed the expected deviant migration of CPs mutated at amino acid position 3 from serine to cysteine (C or CP_{Cys}), and of those mutated at amino acid position 158 from threonine to lysine (K or CP_{Lys}, **Figure 7 a**). The exchanged amino acids exposed to the outer surface of TMV particles introduce additional functional groups (thiol or amino groups, respectively) for selective coupling

chemistry (**Figure 6 a**). After combining these two protein varieties without the addition of RNA, both migrate separately (C-K) in clearly distinct bands. The two bands are disappeared as soon as RNA had been added to guide the proteins' mixed assembly into blended VLPs (C-K + 204); and a third band with a higher velocity in the electric field is detectable (**Figure 7 a**). Conjugation of the maleimide-activated fluorescent dye Atto488 to the thiol group (see also coupling scheme in **Figure 6 b**) enhances the migration velocity of the bifunctional "disks" due to the additional net charges of -1 per coupled Atto488 molecule (C-K + 204 + Atto488). Excess dye was removed by gel filtration. Hence the fluorescence signal of Atto488-maleimide on the lower part of the gel is completely reduced (C-K + 204 + Atto488 + G25, rightmost lane).

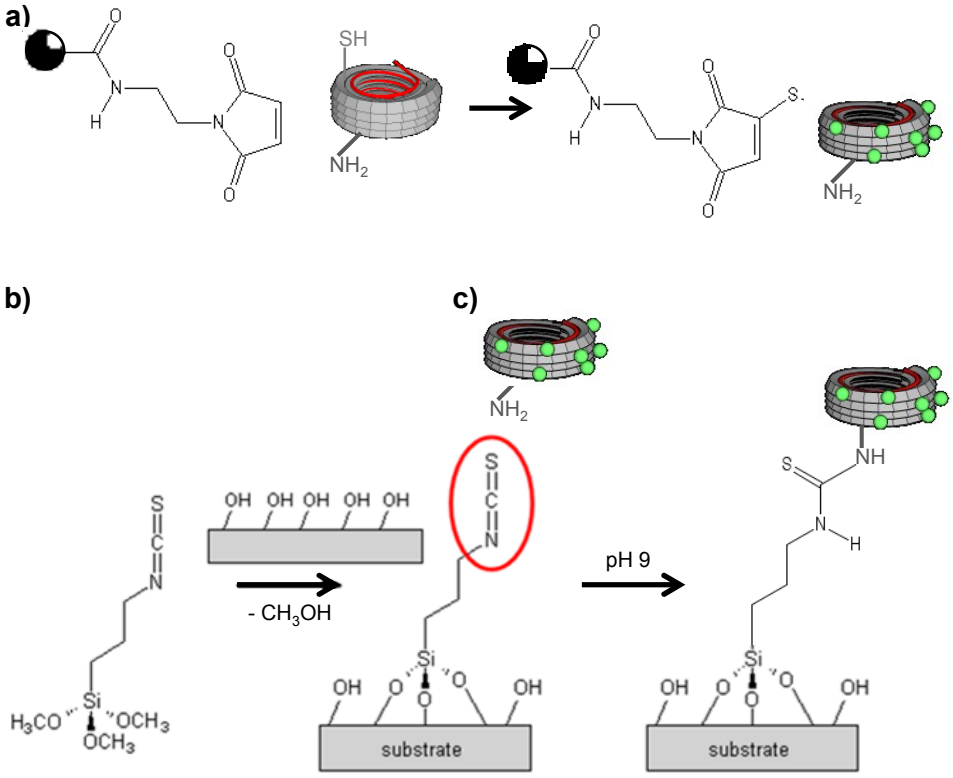

Figure 6: Fluorescent labeling of bifunctional "disks", ITC-silane functionalization of a silica substrate and "disk" immobilization of the fluorescent "disks". **(a)** Fluorescent labeling of thiol groups exposing "disks" with Atto488-maleimide. **(b)** Coupling of ITC-terminated silane to a silica surface in a gas phase reaction. **(c)** A bifunctional fluorescently labeled "disk" exposing primary amino groups on its surface forms strong thiourea-bonds *via* ITC at pH 9.

Bifunctional VLP formation and the structure integrity of the modified and purified "disks" were also confirmed by TEM analysis. TEM images indicate uniform ring-like structures before and after the chemical dye coupling and gel filtration of the bifunctional "disks" (**Figure S1 b** & **c**), whereas samples of mixed CP varieties were not able to assemble in short helices under these conditions (**Figure S1 a**). Such

chemically modified short TMV building blocks of defined length and with mutated CPs were also generated by Rego et al. (2013), but of longer dimension and of a single CP type only. Summarizing the results of native gel electrophoresis and TEM-analysis, bifunctional TMV-"disks" of specific dimensions were fabricated allowing chemical modification under moderately alkaline conditions up to at least pH 9.0, which is a considerable increase in stability compared to RNA-free ring-shaped TMV CP disk-like assemblies analysed in parallel.

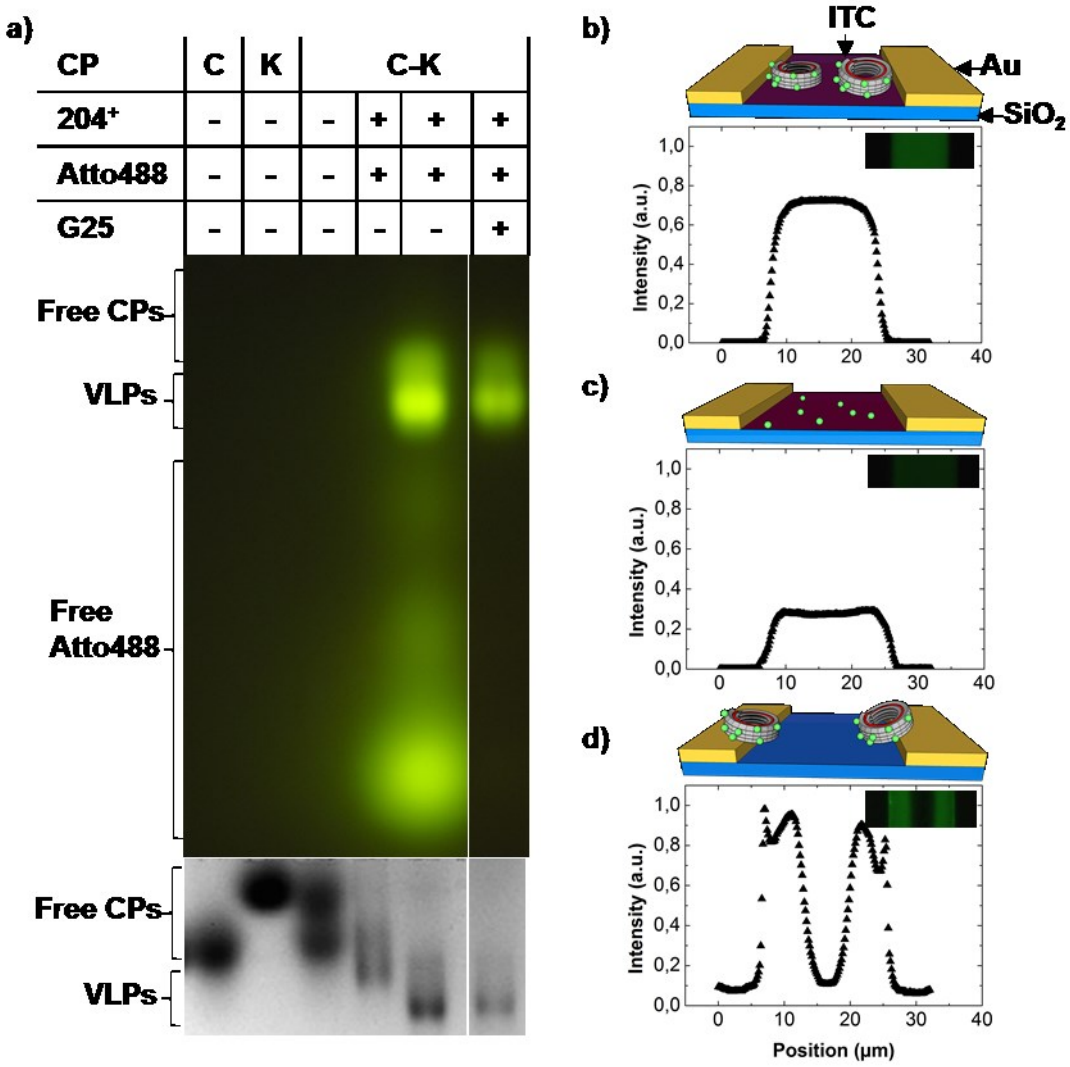

Figure 7: Immobilization of bifunctional "disks" on an ITC-functionalized solid substrate. **(a)** Agarose gel analysis of *in vitro* mixed assembled "disks" of 50 % CP_{Cys} (C) and 50 % CP_{Lys} (K) labeled with Atto488-maleimide, and 204^{+} nt RNA. Proteins are stained with Coomassie Brilliant Blue R250 (2.5 % agarose in 1xTBE). Fluorescence intensity analysis of **(b)** Atto488-labeled "disks" immobilized on an ITC-covered substrate, **(c)** Atto488-maleimide in the absence of any TMV derivative immobilized on an ITC-covered substrate and **(d)** Atto488-labeled "disks" on an ITC-free substrate. Insets in the graphs show images of fluorescence signal of the bifunctional "disks" or Atto488-maleimide immobilized on the substrates. For details, refer to the text (diagrams were prepared by Axel Seidenstücker, Univeristät Ulm).

Immobilization of bifunctional "disks" on ITC-silane-covered substrates

To fabricate a layer of "disks" on a glass substrate, bifunctional "disks", labeled with Atto488 on their CP_{Cys} and purified by gel filtration, were immobilized on ITC-silane-covered substrates. First, a gold-patterned glass slide was fabricated by lithography techniques and covered by ITC-functionalized silane (**Figure 6 b**). Next, the covalent coupling of the Atto488-equipped "disks" to the ITC *via* the primary amino groups of CP_{Lys} exposed on their outer surface was carried out at pH 9 (see scheme in **Figure 6 c**). As controls, a gold-patterned glass slide without ITC was incubated under the same conditions with bifunctional fluorescent "disks", and an ITC-silane-covered substrate was incubated with an Atto488-maleimide solution under the same conditions. The spatially resolved fluorescence signal intensities of immobilized "disks" or plain fluorescent dye molecules, respectively, were compared by microscopy. To exclude signal background from the gold patterns, the glass slides were monitored from the side opposite the immobilized components. The signal of immobilized "disks" on the ITC-silane was homogenously distributed (**Figure 7 b**). The fluorescence intensity was higher than that of the plain Atto488-maleimide-exposed ITC-silane-covered substrate (**Figure 7 c**).

For the ITC-free substrate, no fluorescence signal was expected, but a significant level of Atto488 was recorded at its edges adjacent to the gold pattern (**Figure 7 d**). Its reason may be the known interaction of gold with thiol groups: Assumedly, not all thiol-groups of CP_{Cys} were conjugated to Atto488-maleimide molecules, thus allowing interactions of residual groups with the gold pattern on the glass slide. Consequently, a strong fluorescence signal at the boundaries of the ITC-covered silica and the gold pattern is detectable, but not a homogenous coverage compared to the ITC-functionalized glass slide in **Figure 7 b**.

The structure integrity of the bifunctional "disks" in the reaction solution at pH 9 was also confirmed by TEM-analysis indicating no degradation over the extended reaction time of 16 h (**Figure S1 d**).

Conclusion

The results of this assembly and stability study put forth the advantages but also some limits of tobamoviral building blocks designed for selective interactions with synthetic components. The main benefit based on the natural viral assembly system is the highly reproducible structure formation, resulting in rings and short barrels of well-defined length tuneable by tailored RNA constructs. Since different genetically

engineered CP varieties can be combined in a single multifunctional VLP, this may provide polyvalence for chemical modifications of its outer surface; beyond this, such assemblies maintain their structure identity and uniformity over a wide pH range, allowing for convenient standard conjugation reactions with best efficiencies at mild basic pH. However, pH ranges below 7.2 or above 9 have to be viewed with caution, since in the acidic range longer biotemplate aggregates are formed, and under basic conditions disassembly occurs. Thus, it still remains important to select a suitable environment for practicing with viral building blocks, but the RNA core of our novel structures extends their use into most of the pH regime practically relevant for biochemical modification and reaction conditions.

The RNA-stabilized “disks” presented in this work might be developed further into a novel species of nanopore adapters for being implanted into inorganic nanoporous membranes. Their dimensions with an inner channel of 4 nm diameter and a length of about 10 nm seem well-suited for this use, and it is also possible to genetically modify the inner protein channel (Zhou et al. 2013, Dedeo et al. 2010). By way of an adapted coupling chemistry new physical properties may be introduced to enable molecular sorting, e.g. after installing molecules in the central pores which permit the translocation of solely hydrophobic or hydrophilic molecules, respectively. Additionally, the outer “disk” rim surface could be functionalized with peptides selectively interacting with certain material classes, or inducing mineral or metal deposition embedding the bio-adapters inside the surrounding material by a "bionic glue", as suggested recently (Altintoprak et al. 2015).

In summary, we have developed a multifunctional viral nanoring as a basic building block amenable to further modification and integration into hybrid materials.

Acknowledgments

We would like to thank Cornelia Kocher to provide protocols and technical support for the TEM analysis, Prof. Dr. S. Nussberger and PD Dr. M. Schweikert for granting access to the TEM, Gabriele Kepp for supporting fluorescence microscopy, Sigrid Kober for the preparation of TMV particles from tobacco plants, and Diether Gotthardt for taking care of the tobacco plants. We are grateful for the financial support of the DFG SPP1569 (DFG-WE-4220/2-2)

Supplementary

Table S1: DNA templates for *in vitro* transcription of RNAs with (+) and without (-) the TMV origin of assembly (OAs). Orange marked letters indicate the major loop of the OAs, capital letters DNA sequence of viral genome OAs, small letters sequence of pGEM®-T Easy origin.

RNA length [nt]	DNA-Sequence
102^{+}	gggcgaattgggcccgacgtcCGTGAGAGACGGAGGGCCCATGGAACTTA CAG*AAGAAGTTG*TTGATGAGTTCATGGAAGATGTCCCTATGTCGAT CAGGCa
204^{+}	gggcgaattgggcccgacgtcGCGGGTTTCTGTCCGCTTTCTCTGGAGTTT GTGTCGGTGTGTATTGTTTATAGAAATAATATAAAATTAGGTTTGAG AGAGAAGATTACAAACGTGAGAGACGGAGGGCCCATGGAACTTAC AG*AAGAAGTTG*TTGATGAGTTCATGGAAGATGTCCCTATGTCGATC AGGCTTGCAAAGTTa
500^{+}	gggcgaattgggcccgacgtcGCGGGTTTCTGTCCGCTTTCTCTGGAGTTT GTGTCGGTGTGTATTGTTTATAGAAATAATATAAAATTAGGTTTGAG AGAGAAGATTACAAACGTGAGAGACGGAGGGCCCATGGAACTTAC AG*AAGAAGTTG*TTGATGAGTTCATGGAAGATGTCCCTATGTCGATC AGGCTTGCAAAGTTaatcactagtgaattcgcggccgcctgcaggtcgaccatatggga gagctcccaacgcgttggatgcatagcttgagtattctatagtgtcacctaaatagcttggcgtaatc atggtcatagctgtttcctgtgtgaaattgttatccgctcacaattccacacaacatacgagccggaa gcataaagtgtaaagcctggggtgcctaatgagtgagctaactcacattaattgcgttgcgctcact gcccgctttccagtcgggaaacctgtcgtgccagctgcattaatgaatc
90^{-}	gggcgaattgggcccgacgtcgcatgctcccggccgccatggccgcgggattatcactagtgcg gccgagcctgcaggtcgaccatatgg
308^{-}	cgcgcgttggccgattcattaatgcagctggcacgacaggtttcccgactggaaagcgggcagtg agcgcaacgcaattaatgtgagttagctcactcattaggcaccccaggctttacactttatgcttccg gctcgtatgttgtgtggaattgtgagcggataacaatttcacacaggaaacagctatgaccatgatt acgccaagctatttaggtgacactatagaatactcaagctatgcatccaacgcgttgggagctctc ccatatggtcgacctgcaggcggccgcgaattcactagtgat

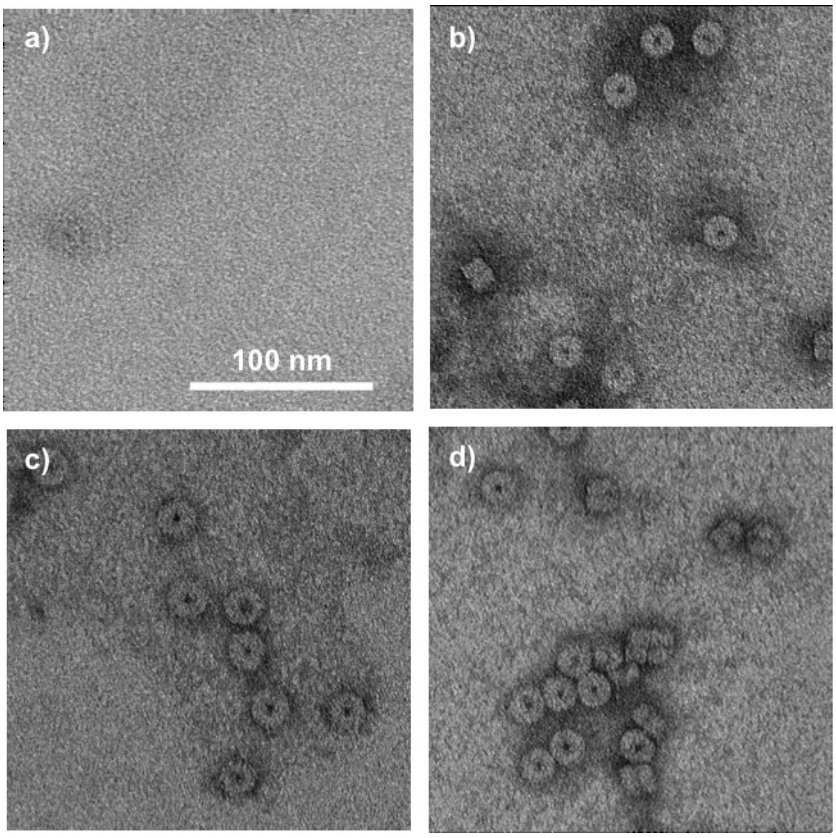

Figure S1: TEM analysis of mixed assembled TMV "disks". **(a)** 40 % CP, 30 % CP_{Cys} and 30% CP_{Lys} without RNA. **(b)** 40 % CP, 30 % CP_{Cys} and 30% CP_{Lys} with 204^{+} nt RNA. **(c)** 40 % CP, 30 % CP_{Cys} and 30% CP_{Lys} with 204^{+} nt RNA labeled with Atto488-maleimide. **(d)** 40 % CP, 30 % CP_{Cys} and 30% CP_{Lys} with 204^{+} nt RNA labeled with Atto488-maleimide after gel filtration.

References

Alonso, J. M., Gorzny, M. L. & Bittner, A. M. 2013. 'The physics of tobacco mosaic virus and virus-based devices in biotechnology.' *Trends Biotechnol,* 31, 530-538.

Altintoprak, K., Seidenstücker, A., Welle, A., Eiben, S., Atanasova, P., Stitz, N., Plettl, A., Bill, J., Gliemann, H., Jeske, H., Rothenstein, D., Geiger, F. & Wege, C. 2015. 'Peptide-equipped tobacco mosaic virus templates for selective and controllable biomineral deposition.' *Beilstein J Nanotech,* 6, 1399-1412.

Altunbas, A., Sharma, N., Lamm, M. S., Yan, C. Q., Nagarkar, R. P., Schneider, J. P. & Pochan, D. J. 2010. 'Peptide-silica hybrid networks: biomimetic control of network mechanical behavior.' *ACS Nano,* 4, 181-188.

Azucena, C., Eber, F. J., Trouillet, V., Hirtz, M., Heissler, S., Franzreb, M., Fuchs, H., Wege, C. & Gliemann, H. 2012. 'New approaches for bottom-up assembly of tobacco mosaic virus-derived nucleoprotein tubes on defined patterns on silica- and polymer-based substrates.' *Langmuir,* 28, 14867-14877.

Bell, N. A., Engst, C. R., Ablay, M., Divitini, G., Ducati, C., Liedl, T. & Keyser, U. F. 2012. 'DNA origami nanopores.' *Nano Lett,* 12, 512-517.

Bhyravbhatla, B., Watowich, S. J. & Caspar, D. L. 1998. 'Refined atomic model of the four-layer aggregate of the tobacco mosaic virus coat protein at 2.4-Å resolution.' *Biophys J,* 74, 604-615.

Bittner, A. M., Alonso, J. M., Gorzny, M. L. & Wege, C. 2013. 'Nanoscale science and technology with plant viruses and bacteriophages.' *Subcell Biochem,* 68, 667-702.

Bittner, A. M., Wu, X. C., Balci, S., Knez, M., Kadri, A. & Kern, K. 2005. 'Bottom-up synthesis and top-down organisation of semiconductor and metal clusters on surfaces.' *Eur J Inorg Chem,* 2005, 3717-3728.

Butler, P. J. 1972. 'Structures and roles of the polymorphic forms of tobacco mosaic virus protein. VI. Assembly of the nucleoprotein rods of tobacco mosaic virus from the protein disks and RNA.' *J Mol Biol,* 72, 25-35.

Butler, P. J. 1999. 'Self-assembly of tobacco mosaic virus: the role of an intermediate aggregate in generating both specificity and speed.' *Philos Trans R Soc Lond B Biol Sci,* 354, 537-550.

Butler, P. J., Bloomer, A. C. & Finch, J. T. 1992. 'Direct visualization of the structure of the "20 S" aggregate of coat protein of tobacco mosaic virus. The "disk" is the major structure at pH 7.0 and the proto-helix at lower pH.' *J Mol Biol,* 224, 381-394.

Carpenter, J. M. 1970. 'The stacked-disk structure of tobacco mosaic virus protein.' *Virology,* 41, 603-614.

Chiang, C. Y., Epstein, J., Brown, A., Munday, J. N., Culver, J. N. & Ehrman, S. 2012. 'Biological templates for antireflective current collectors for photoelectrochemical cell applications.' *Nano Lett,* 12, 6005-6011.

Danelon, C., Santschi, C., Brugger, J. & Vogel, H. 2006. 'Fabrication and functionalization of nanochannels by electron-beam-induced silicon oxide deposition.' *Langmuir,* 22, 10711-10715.

Dedeo, M. T., Duderstadt, K. E., Berger, J. M. & Francis, M. B. 2010. 'Nanoscale protein assemblies from a circular permutant of the tobacco mosaic virus.' *Nano Lett,* 10, 181-186.

Durham, A. C., Finch, J. T. & Klug, A. 1971. 'States of aggregation of tobacco mosaic virus protein.' *Nat New Biol,* 229, 37-42.

Durham, A. C. & Klug, A. 1971. 'Polymerization of tobacco mosaic virus protein and its control.' *Nat New Biol,* 229, 42-46.

Eber, F. J., Eiben, S., Jeske, H. & Wege, C. 2015. 'RNA-controlled assembly of tobacco mosaic virus-derived complex structures: from nanoboomerangs to tetrapods.' *Nanoscale,* 7, 344-355.

Eiben, S., Stitz, N., Eber, F., Wagner, J., Atanasova, P., Bill, J., Wege, C. & Jeske, H. 2014. 'Tailoring the surface properties of tobacco mosaic virions by the integration of bacterially expressed mutant coat protein.' *Virus Res,* 180, 92-96.

Eid, J., Fehr, A., Gray, J., Luong, K., Lyle, J., Otto, G., Peluso, P., Rank, D., Baybayan, P., Bettman, B., Bibillo, A., Bjornson, K., Chaudhuri, B., Christians, F., Cicero, R., Clark, S., Dalal, R., Dewinter, A., Dixon, J., Foquet, M., Gaertner, A., Hardenbol, P., Heiner, C., Hester, K., Holden, D., Kearns, G., Kong, X., Kuse, R., Lacroix, Y., Lin, S., Lundquist, P., Ma, C., Marks, P., Maxham, M., Murphy, D., Park, I., Pham, T., Phillips, M., Roy, J., Sebra, R., Shen, G., Sorenson, J., Tomaney, A., Travers, K., Trulson, M., Vieceli, J., Wegener, J., Wu, D., Yang, A., Zaccarin, D., Zhao, P., Zhong, F., Korlach, J. & Turner, S. 2009. 'Real-time DNA sequencing from single polymerase molecules.' *Science,* 323, 133-138.

Fraenkel-Conrat, H. 1957. 'Degradation of tobacco mosaic virus with acetic acid.' *Virology,* 4, 1-4.

Geiger, F. C., Eber, F. J., Eiben, S., Müller, A., Jeske, H., Spatz, J. P. & Wege, C. 2013. 'TMV nanorods with programmed longitudinal domains of differently addressable coat proteins.' *Nanoscale,* 5, 3808-3816.

Gooding, G. V., Jr. & Hebert, T. T. 1967. 'A simple technique for purification of tobacco mosaic virus in large quantities.' *Phytopathology,* 57, 1285.

Hall, A. R., Scott, A., Rotem, D., Mehta, K. K., Bayley, H. & Dekker, C. 2010. 'Hybrid pore formation by directed insertion of alpha-haemolysin into solid-state nanopores.' *Nat Nanotechnol,* 5, 874-877.

Hernandez-Ainsa, S., Misiunas, K., Thacker, V. V., Hemmig, E. A. & Keyser, U. F. 2014. 'Voltage-dependent properties of DNA origami nanopores.' *Nano Lett,* 14, 1270-1274.

Kadri, A., Maiss, E., Amsharov, N., Bittner, A. M., Balci, S., Kern, K., Jeske, H. & Wege, C. 2011. 'Engineered tobacco mosaic virus mutants with distinct physical characteristics in planta and enhanced metallization properties.' *Virus Res,* 157, 35-46.

Kleefen, A., Pedone, D., Grunwald, C., Wei, R., Firnkes, M., Abstreiter, G., Rant, U. & Tampe, R. 2010. 'Multiplexed parallel single transport recordings on nanopore arrays.' *Nano Lett,* 10, 5080-5087.

Larkin, J., Foquet, M., Turner, S. W., Korlach, J. & Wanunu, M. 2014. 'Reversible positioning of single molecules inside zero-mode waveguides.' *Nano Lett,* 14, 6023-6029.

Müller, A., Eber, F. J., Azucena, C., Petershans, A., Bittner, A. M., Gliemann, H., Jeske, H. & Wege, C. 2011. 'Inducible site-selective bottom-up assembly of virus-derived nanotube arrays on RNA-equipped wafers.' *ACS Nano,* 5, 4512-4520.

Nam, Y. S., Magyar, A. P., Lee, D., Kim, J. W., Yun, D. S., Park, H., Pollom, T. S., Jr., Weitz, D. A. & Belcher, A. M. 2010a. 'Biologically templated photocatalytic nanostructures for sustained light-driven water oxidation.' *Nat Nanotechnol,* 5, 340-344.

Nilsson, J., Lee, J. R. I., Ratto, T. V. & Letant, S. E. 2006. 'Localized functionalization of single nanopores.' *Adv Mater,* 18, 427-431.

Niu, Z., Bruckman, M., Kotakadi, V. S., He, J., Emrick, T., Russell, T. P., Yang, L. & Wang, Q. 2006. 'Study and characterization of tobacco mosaic virus head-to-tail assembly assisted by aniline polymerization.' *Chem Commun (Camb),* 28, 3019-3021.

Patwardhan, S. V., Emami, F. S., Berry, R. J., Jones, S. E., Naik, R. R., Deschaume, O., Heinz, H. & Perry, C. C. 2012. 'Chemistry of aqueous silica nanoparticle surfaces and the mechanism of selective peptide adsorption.' *J Am Chem Soc,* 134, 6244-6256.

Perham, R. N. & Wilson, T. M. A. 1978. 'Characterization of intermediates formed during disassembly of tobacco mosaic-virus at alkaline pH.' *Virology,* 84, 293-302.

Raghavendra, K., Adams, M. L. & Schuster, T. M. 1985. 'Tobacco mosaic virus protein aggregates in solution: structural comparison of 20S aggregates with those near conditions for disk crystallization.' *Biochemistry,* 24, 3298-3304.

Raghavendra, K., Kelly, J. A., Khairallah, L. & Schuster, T. M. 1988. 'Structure and function of disk aggregates of the coat protein of tobacco mosaic virus.' *Biochemistry,* 27, 7583-7588.

Rego, J. M., Lee, J. H., Lee, D. H. & Yi, H. 2013. 'Biologically inspired strategy for programmed assembly of viral building blocks with controlled dimensions.' *Biotechnol J,* 8, 237-246.

Royston, E., Ghosh, A., Kofinas, P., Harris, M. T. & Culver, J. N. 2008. 'Self-assembly of virus-structured high surface area nanomaterials and their application as battery electrodes.' *Langmuir,* 24, 906-912.

Royston, E., Lee, S. Y., Culver, J. N. & Harris, M. T. 2006. 'Characterization of silica-coated tobacco mosaic virus.' *J Colloid Interface Sci,* 298, 706-712.

Schön, A. & Mundry, K. W. 1984. 'Coordinated two-disk nucleation, growth and properties, of virus-like particles assembled from tobacco mosaic virus capsid protein with poly(A) or oligo(A) of different length.' *Eur J Biochem,* 140, 119-127.

Stauffer, H., Srinivasan, S. & Lauffer, M. A. 1970. 'Calorimetric studies on polymerization-depolymerization of tobacco mosaic virus protein.' *Biochemistry,* 9, 193-200.

Storm, A. J., Chen, J. H., Ling, X. S., Zandbergen, H. W. & Dekker, C. 2003. 'Fabrication of solid-state nanopores with single-nanometre precision.' *Nat Mater,* 2, 537-540.

Turner, D. R. & Butler, P. J. 1986. 'Essential features of the assembly origin of tobacco mosaic virus RNA as studied by directed mutagenesis.' *Nucleic Acids Res,* 14, 9229-9242.

Turner, D. R., Joyce, L. E. & Butler, P. J. 1988. 'The tobacco mosaic virus assembly origin RNA. Functional characteristics defined by directed mutagenesis.' *J Mol Biol,* 203, 531-547.

Turner, D. R., McGuigan, C. J. & Butler, P. J. 1989. 'Assembly of hybrid RNAs with tobacco mosaic virus coat protein. Evidence for incorporation of disks in 5'-elongation along the major RNA tail.' *J Mol Biol,* 209, 407-422.

Vogel, D. 1982. 'Neutral salt effects on the polymorphism of tobacco mosaic virus protein - a contribution to the understanding of its mechanism of aggregation and virus reassembly.' *Biochim Biophys Acta,* 706, 65-79.

Wyckoff, R. W. G. 1937. 'An ultracentrifugal study of the pH stability of tobacco mosaic virus protein.' *J Biol Chem,* 122, 239-247.

Yang, C., Choi, C. H., Lee, C. S. & Yi, H. 2013a. 'A facile synthesis-fabrication strategy for integration of catalytically active viral-palladium nanostructures into polymeric hydrogel microparticles *via* replica molding.' *ACS Nano,* 7, 5032-5044.

Zhou, K., Li, F., Dai, G., Meng, C. & Wang, Q. 2013. 'Disulfide bond: dramatically enhanced assembly capability and structural stability of tobacco mosaic virus nanorods.' *Biomacromolecules,* 14, 2593-2600.

Zimmern, D. 1977. 'The nucleotide sequence at the origin for assembly on tobacco mosaic virus RNA.' *Cell,* 11, 463-482.

Zimmern, D. 1983. 'An extended secondary structure model for the TMV assembly origin, and its correlation with protection studies and an assembly defective mutant.' *EMBO J,* 2, 1901-1907.

Zuker, M. 2003. 'Mfold web server for nucleic acid folding and hybridization prediction.' *Nucleic Acids Res,* 31, 3406-3415.

Manuscript II

Altintoprak, K., Plettl, A., Marti, O., Gliemann, H., Jeske, H. & Wege, C. 2015. 'Viral protein nanorings on a double-stranded RNA-leash.'

Authorship responsibilities

Altintoprak:

- Development of experimental strategy
- Cloning procedure, CP preparation, VLP assembly
- Native gel electrophoresis
- TEM analysis
- Fluorescent labeling
- Data acquisition and interpretation
- Preparation of all figures and tables
- Data discussion against background of previous publications
- Writing and editing of the manuscript

Plettl, Marti and Gliemann:

- Basic project design (jointly with Wege), advice and repeated discussion

Jeske:

- Conceptual contributions and continuous discussion

Wege:

- Basic project design (jointly with Plettl, Marti and Gliemann), guidance and constant discussion
- Editing suggestions and proofreading

Viral protein nanorings on a double-stranded RNA-leash

Klara Altintoprak[1], Alfred Plettl[2], Othmar Marti[3], Hartmut Gliemann[4], Holger Jeske[1] and Christina Wege[1]

[1]Dpt. of Molecular Biology and Plant Virology, Institute of Biomaterials and Biomolecular Systems, University of Stuttgart, Pfaffenwaldring 57, 70569 Stuttgart, Germany
[2]Institute of Solid State Physics, University of Ulm, Albert-Einstein-Allee 11, 89081 Ulm, Germany
[3]Institute for Experimental Physics, University of Ulm, Albert-Einstein-Allee 11, 89081 Ulm, Germany
[4]Institute of Functional Interfaces (IFG), Karlsruhe Institute of Technology, Hermann-von-Helmholtz-Platz 1, 76344 Eggenstein-Leopoldshafen, Germany

Abstract

The self-assembling plant-infecting tobacco mosaic virus (TMV) has emerged as a preferred biotemplate since it provides a polyvalent rigid nanotube structure with numerous options for chemical modifications, and can be manipulated by genetic engineering to yield TMV-based building blocks for various purposes. TMV is a helically organized nucleoprotein complex consisting of a single-stranded RNA (ssRNA) that is encapsulated by more than 2000 identical coat protein (CP) subunits. An outstanding feature is its tunable length that is directed by the RNA scaffold, and may be influenced by buffer conditions or mutations inside the CP amino acid sequence. In this study, inspired by nanopore adaptors equipped with nucleic acid stretches as previously reported, TMV components were modified to adopt the shape of a porous disk tethered to a protruding double-stranded (ds)RNA-leash. This “disk-on-a-leash” is stable under different buffer conditions and shows enhanced electrophoretic mobility compared to disks without the additional negative charge of a free RNA-leash. Since this construct can be fabricated in large amounts and remains stable for several days, it is considered to promote an efficient electrophoretically driven integration of biomolecular nanopores into solid-state membrane templates.

Introduction

Nanoporous devices with millions of pores with well-defined diameters below the 5 nm range are of growing interest for high-throughput analysis regarding molecule sorting (Urban et al. 2014), DNA-sequencing (McNally et al. 2010), single molecule detection (Adiga et al. 2009) or drug delivery (Yang et al. 2010). The critical point of nanoporous membrane fabrication is the generation of a vast number of identical pores inside a robust template material. Photolithography techniques and electron

beam or focused ion beam methodology can achieve high numbers of solid-state membrane (SSM) pores (Miles et al. 2013). However, they go along with significant aberrations of pore sizes below a diameter of 15 nm (Kleefen et al. 2010). To compensate this disadvantage, solid-state pores can be equipped with highly uniform biological pore proteins such as α-haemolysin (Deamer 2010), or synthetic bio-inspired DNA-nanopores (Hernandez-Ainsa & Keyser 2014).

Simultaneous fluorescence signal recording of molecules passing in parallel through several protein pores integrated in lipid bilayers was previously shown (Kleefen et al. 2010, Urban et al. 2014). However, the respective devices were only applicable for short-term assignments of 24 hours due to the instability of the lipid bilayers, which were deposited on top of a nanoporous SSM. In general, protein pore complexes are frequently embedded in a lipid environment upon hybrid membrane fabrication. This makes the products susceptible for ion or molecule leakage because of frequent lipid bilayer rupture. Additionally, the insertion frequency of protein pores seems to be diffusion-dependent as they reversibly escape from the lipid membrane (Kleefen et al. 2010).

An alternative route to insert macromolecules or supramolecular complexes into solid-state nanopores makes use of electrophoretic driving forces. The proper orientation of nanostructures transported in an electric field can be improved by increasing their polarity, e.g. by adding a protruding negatively charged DNA strand. Such nucleic acid leashes tethered to biological pore adopters indeed had the expected effects, as demonstrated for α-haemolysin (Hall et al. 2010) as well as for DNA-origami nanopores (Bell et al. 2012, Hernandez-Ainsa et al. 2014). The pore adapters connected to a DNA-leash are pulled into the solid-state pores due to the additional negative charge of the DNA phosphate backbone located on one side of the construct. Compared to diffusion-directed solid-state pore loading, the insertion rate can be significantly higher in an electric field, as evidenced recently for a nanoporous array equipped with streptavidin-DNA complexes (Larkin et al. 2014). The fabrication of tailored nanoporous units with protruding negatively charged DNA strands is most efficiently realized with biomolecular adapters accessible to genetic or chemical modification. Another major benefit of biological pores is that their inner channel can be functionalized to introduce various properties for selective molecule detection and sorting (Boersma & Bayley 2012, Bayley & Jayasinghe 2004, Mayer & Yang 2013).

In this report we demonstrate the fabrication of a synthetic nucleoprotein pore of viral origin for improved electrophoresis-directed insertion into solid-state pores and correct orientation inside the pore channels. Tobacco mosaic virus (TMV) is commonly used as a building block in nanobiotechnology due to its rigid tube-like structure of 300 nm length, a diameter of 18 nm and an inner 4 nm channel (Zaitlin & Palukaitis 2000, Butler 1999). Every TMV particle consists of a single-stranded RNA (ssRNA) embedded inside a capsid of around 2130 helically arranged coat proteins (CP) (Namba et al. 1989). CPs and ssRNA can assemble also *in vitro* into stable TMV particles (Fraenkel-Conrat & Singer 1959). The assembly process is initiated by a secondary stem-loop structure of the RNA, the origin of assembly (OAs; Zimmern 1977), that is proposed to invade the inner channel of a so-called disk, an intermediate two-layer or short helical aggregate of 34 CP subunits, thereby starting the bidirectional growth of the TMV nucleoprotein helix (Butler 1999). TMV particle length can be varied *via* the length of the encapsidated RNA scaffold (Rego et al. 2013, Eber et al. 2013, Müller et al. 2011), genetic manipulation of the CP sequence (Zhou et al. 2013, Lu et al. 1998), or altered buffer conditions that enable the CPs to assemble into virus-like particles (VLP) without RNA, but with no control over the final particle length (Durham et al. 1971). To integrate functionalities into tailored virus-like particles, TMV CPs can be manipulated genetically by amino acid insertion or exchange, which may introduce reactive groups for subsequent chemical modification (Dedeo et al. 2010, Geiger et al. 2013, Yi et al. 2005). Thereby, new properties may be displayed on the outer TMV surface or in the lumen of its inner channel. Thus, a CP disk of two turns offers 34 positions for modifications both in the inner channel and on the outer surface. In addition, to expand the functionality of TMV particles, different genetically modified CPs can be combined and arranged into the typical rod-shaped structures by *in vitro* assembly, providing multifunctionality and selective modification with different appendages (Geiger et al. 2013, Eiben et al. 2014).

As described in **manuscript I**, four-turn CP helices scaffolded by a 204^{+} nt RNA containing the core OAs (indicated by plus [+]) corresponding to position 5350 to 5531 of the TMV genome (Zimmern 1983) are stable under different buffer conditions and can be reproducibly obtained in large amounts. Furthermore, bifunctional four-turn helices, termed “disk”, were chemically modified and could be immobilized on a functionalized silica substrate by covalent conjugation. Although these short VLPs

are therefore suitable candidates as pore adaptors, their orientation inside solid-state pores is not predictable. Initial tests revealed that after simple diffusion into the inorganic templates, the central pores of numerous "disks" were not aligned with the SSM channels (see "Einleitung" of this Dissertation thesis). Hence, we designed a TMV-based four-turn CP helix derivative extended by a protruding double-stranded RNA (dsRNA), in order to achieve an unequal charge distribution along the pore adaptor axis. To this end, we made use of the selective interaction of the CPs with ssRNA but not dsRNA, by designing an RNA construct consisting of an ssRNA domain (204 nts with OAs), and a downstream portion (296 nts) yielding a dsRNA domain (**Figure 1**), with a total length of this RNA backbone of 500 nts. The RNA-duplex is realized by hybridization of the 3'-terminal 296 nt portion of the 500^{+} nt RNA to a complementary 308^{-} nt RNA without OAs (-). This generates a dsRNA domain that serves as a flexible leash, and at its end a 5'-ssRNA overhang of 12 nts that is addressable for further modifications, by hybridization of functionalized oligonucleotides as demonstrated previously (Eber et al. 2013). The complete RNA construct thus has 512 ss or ds residues.

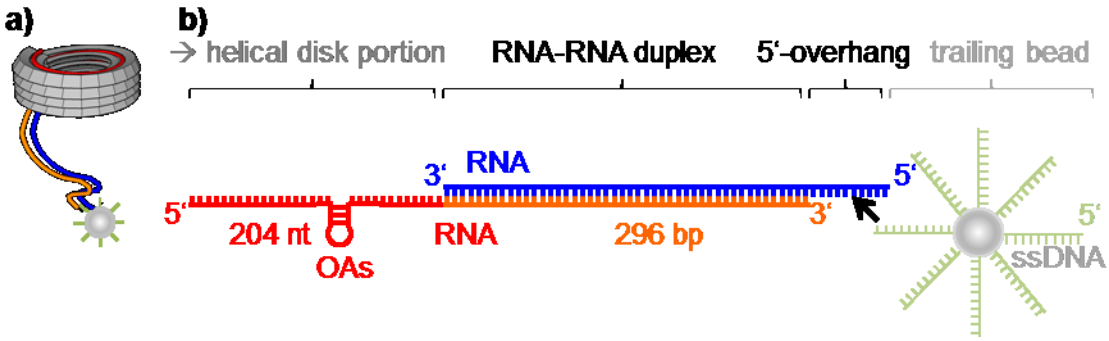

Figure 1: Outline of the disk-on-a-leash construct. **(a)** "Disk" with protruding double-stranded (ds)RNA and a putative oligonucleotide-covered trailing bead (light grey). **(b)** Detailed fabrication strategy of the dsRNA-containing construct. A 500^{+} nt RNA backbone (red and orange) containing the TMV origin of assembly (OAs) for nucleation initiation (within red ssRNA portion) is hybridized (*via* its orange 296 nt portion) with a 308^{-} nt ssRNA (blue), forming a 296 bp RNA-RNA duplex. The portion containing the OAs remains single-stranded which allows its encapsulation by TMV CP, resulting in a four-turn nucleoprotein helix with protruding dsRNA. A terminal single-stranded 12 nts 5'-overhang of the 308^{-} nt RNA (black arrow) is available for putative hybridization with single-stranded DNA-functionalized nanoparticles, to serve e.g. as a trailing bead.

In the following, this construct is called "disk-on-a-leash" to distinguish it from the "disk" without dsRNA-leash. For a detailed characterization, the disk-on-a-leash construct was subjected to native gel electrophoresis to receive insights about its electrophoretic mobility, was purified by electroelution to eliminate undesired by-products, dissolved in different buffers to test its stability and visualized by TEM-

analysis to prove its integrity and the existence of the RNA-leash. In summary, in view of the outcomes of the applied methods, we established a novel nanoporous building block with increased electrophoretic mobility in comparison to four-turn CP helices without RNA-leash, which was stable in different conductive media and accessible to chemical functionalization.

Materials and methods

DNA-template preparation for *in vitro* transcription

DNA-templates for *in vitro* transcription of 204^+ nt RNA or 500^+ nt RNA, respectively, containing the origin of assembly (OAs (+); Zimmern 1983) were amplified by PCR based on the plasmid pGEM-T-Easy-204^+ as DNA-template (see **manuscript I**), using forward primer pGEM_fwd and reverse primer 204_iv_rev (*Pfu* DNA polymerase; initial denaturation at 95 °C, 3 min; 30 cycles of 95 °C, 30 sec, 60 °C, 30 sec, 72 °C, 1 min; final extension at 72 °C, 5 min), or 500_iv_rev as above, but using an annealing temperature of 48 °C (**Table S2**). The DNA-template for *in vitro* transcription of the 308^- nt RNA without OAs (-), complementary to a segment of the 500^+ nt RNA, was synthesized in a first step with forward primers 308_fwd and 308_rev (**Table S2**), based on the reverse sequence of pGEM-T-Easy-204^+ (Q5® DNA Polymerase; initial denaturation at 98 °C, 30 sec; 30 cycles of 98 °C, 10 sec, 69 °C, 10 sec, 72 °C, 10 sec; final extension at 72 °C, 1 min). The PCR product was separated in a 2 % agarose gel and eluted using a QIAquick Gel Extraction Kit (QIAGEN, Hilden, Germany). In a second step, the PCR fragment was fused to the T7 RNA polymerase promoter (Panayotatos & Wells 1979, Rosa 1979) with forward primer 308_T7_fwd and reverse primer 308_iv_rev (*Pfu* DNA Polymerase; initial denaturation at 95 °C, 3 min; 3 cycles of 95 °C, 30 sec, 40 °C, 30 sec, 72 °C, 30 sec; 27 cycles of 95 °C, 30 sec, 61 °C, 30 sec, 72 °C; final extension at 72 °C, 5 min; **Table S2**), gel-purified and amplified again (*Pfu* DNA polymerase; initial denaturation at 95 °C, 2 min; 30 cycles of 95 °C, 30 sec, 62 °C, 30 sec, 72 °C, 30 sec; final extension at 72 °C, 5 min). Before *in vitro* transcription, the PCR products were purified using a QIAquick PCR Purification Kit (QIAGEN, Hilden, Germany) and eluted in dimethyl dicarbonate-(DMDC)-treated deionized water (ddH_2O; 18.3 MΩ cm; purified by a membraPure system, Aquintus, Bodenheim, Germany). The RNA transcripts were synthesized using the MEGAscript® T7 High Yield Transcription Kit (Ambion, Austin, USA). An amount of 100 ng of each PCR product

was used per 20 µl reaction volume and incubated for 6 h at 37 °C. The RNA transcript-containing samples were supplemented with LiCl (final concentration (f. c.) 1.3 M) and EDTA (f. c. 8.6 mM) before adding two volumes ethanol, and incubated at -20 °C over night. The precipitated transcripts were washed with 70 % (v/v) ethanol, dissolved in DMDC-treated ddH_2O (f. c. 1 µg/µl), and stored at -80 °C.

TMV CP_{Lys} preparation for *in vitro* assembly

TMV_{Lys} particles (Geiger et al. 2013) with an amino acid exchange of threonine to lysine at position 158, i.e. at the C-terminus of the CPs, were disassembled to obtain RNA-free CPs for the assembly with the novel RNA constructs. A 10 mg/ml TMV_{Lys} suspension was mixed with glacial acidic acid in a 1:3 ratio and incubated for 20 min on ice. The ssRNA was removed by centrifugation for 20 min at 20,000 x g and 4 °C. The CP-containing supernatant was transferred into a dialysis tube (Spectra/Por®7 Dialysis Membrane, 8 kDa molecular weight cut-off [MWCO], Spectrum Laboratories, Rancho Dominquez, USA) and dialyzed against precooled water (4 °C) until the CP started to flocculate with water changes every 8 h until the isoelectric point was reached and the CP precipitated (24 to 48 h at 4 °C). The flocculating CP suspension was collected in a reaction tube and harvested by centrifugation as above. The CP pellet was resuspended in 75 mM sodium potassium phosphate (SPP) buffer (pH 7.2) over night at room temperature (RT), followed by centrifugation for 10 min at 10,000 x g and RT and transmission of the supernatant into a fresh reaction tube. The concentration of the CP solution was determined by UV spectroscopy with a NanoDrop ND-1000 spectrophotometer (PeqLab, Erlangen, Germany) at a wavelength of 280 nm, using the extinction coefficient of TMV CP (1.3 ml mg^{-1} cm^{-1}; Raghavendra et al. 1985).

RNA hybridization of partially single- and double-stranded RNA scaffold

RNA hybridization was carried out in an RNase-free reaction tube. 60 µl 75 mM SPP (pH 7.2) containing 500^+ nt RNA (f. c. 0.3 µg/µl) and 308^- nt RNA (f. c. 0.3 µg/µl) were heated at 95 °C for 10 min using a thermocycler (TPersonal, Biometra, Göttingen Germany), cooled down in the cycler to 4 °C with 0.9 °C per second and kept at this temperature for 5 min. 15 µl 10 mg/ml CP_{Lys} (f. c. 2.2 mg/ml) in 75 mM SPP (f. c. pH7.2) were added to 54 µl RNA (f. c. 0.47 µg/µl) hybridization products, separated from the hybridized sample at RT to prevent disassembly of the CP_{Lys} disks. Both hybridized RNA with and without CP_{Lys} added were placed at 30 °C in a heating oven

and incubated over night for 16 h at 30 °C to allow assembly into the desired protein-RNA complexes. Additionally, "disks" without RNA-leash were generated: 60 µl 75 mM SPP (pH 7.2) containing CP_{Lys} (f. c. 2.5 mg/ml) combined with 204^{+} nt RNA (f. c. 0.17 mg/ml) were incubated as above. Subsequently, native gel electrophoresis was carried out to analyze and electroelute the resulting products (see next chapters).

Fluorescent dye labeling of viral CP_{Lys}-RNA complexes

The VLPs were labeled with the succinimidyl ester-activated fluorescent dye Atto488-NHS for tracking their migration during gel electrophoresis. Atto488-NHS (f. c. 0.35 mM, Thermo Scientific, Darmstadt, Germany) was added to 50 µl protein-RNA (f. c. 2.1 mg/ml CP) complex solution in 75 mM SPP (pH 7.2) and incubated in the dark for 2 h at 30 °C. Control experiments using "disks" with 204^{+} nt RNA devoid of protruding dsRNA-leash were carried out in parallel. For this purpose, 50 µl SPP (f. c. 75 mM, pH 7.2) with CP_{Lys} (f. c. 2.5 mg/ml) and 204^{+} nt RNA (f. c. 0.17 mg/ml) were labeled with Atto488-NHS as above.

Native gel electrophoresis

Both types of fluorescent VLPs were separated electrophoretically in agarose gels comparing two different buffer systems. All buffers were filtered through FP 30/0.2 CA-S syringe filter units (GE Healthcare, Freiburg, Germany) and diluted with DMDC-treated ddH_2O to exclude RNase contamination. For electrophoresis and electroelution, 2 % agarose gels were either prepared with 1 x TBE (89 mM Tris base, 89 boric acid, 2 mM EDTA) or 1 x TAE (20 mM Tris acetate, 1 mM EDTA). For electroelution from preparative gels, 35 µl Atto488-labeled protein-RNA (2.1 mg/ml CP_{Lys} in 75 mM SPP, pH 7.2) complexes were mixed with 15 µl particle loading dye (20 mM SPP pH 7.2, 0.2 % (w/v) bromophenol blue, 50 % glycerol) and loaded onto the gel. In parallel, control gels were started. The samples for the control gels were prepared as follows: 10 µl ddH_2O containing either 500^{+} nt RNA (f. c. 0.1 mg/ml) or 308^{-} nt RNA (f. c. 0.1 mg/ml) or both combined together were heated for 10 min at 95 °C and cooled down to 4 °C with 0.9 °C per second. For hybridization controls, 10 µl 75 mM SPP (pH 7.2) containing either 500^{+} nt RNA (f. c. 0.1 mg/ml) or 308^{-} nt RNA (f. c. 0.1 mg/ml) were heated for 10 min at 95 °C, cooled down to 4 °C with 0.9 °C per second and mixed with 3 µl particle loading dye (as above). To estimate the RNA lengths, 2 µl RiboRuler Low Range RNA Ladder (Thermo Fisher Scientific,

Darmstadt, Germany) were mixed with 2 µl RNA loading dye (95 % formamide, 0.025 % SDS, 0.025 % bromophenol blue, 0.025 % xylene cyanol FF, 0.025 % ethidium bromide, 0.5 mM EDTA), heated at 70 °C for 10 min and cooled down to 4 °C. 10 µl VLP solution (2.1 mg/ml CP_{Lys} in 75 mM SPP, pH 7.2) were mixed with 5 µl particle loading dye. Gel electrophoresis was carried out at RT. A constant voltage of 5.2 V/cm was applied for 3 h. After electrophoresis, agarose gels were stained with ethidium bromide and expose to UV light to visualize the RNA. After imaging of the ethidium bromide stained RNA using a Canon PowerShot G6 7.1MP, the proteins in the gels were fixed (10 % acetic acid and 40 % ethanol) for 15 min and stained with Coomassie Brilliant Blue R250 (Serva Electrophoresis, Heidelberg, Germany).

Electroelution of fluorescently labeled VLPs

The migration of the fluorescently labeled VLPs during electrophoretic separation was monitored under UV light. The electrophoresis was stopped as soon as the particles were sufficiently resolved. The conductive medium was removed until the upper surface of the gel was 1 mm above the liquid phase surface. In front of each band, a 2 x 8 mm trough was cut out. To prevent sample translocation into the gel on the downstream side of the trough, it was covered with a piece of dialysis membrane (8 kDa [MWCO]). Subsequently, the gel run was resumed to collect the VLPs inside the trough. The VLPs eluted from the gels prepared with 1 x TBE were directly transferred onto PD10 SpinTrap G-25 columns (GE Healthcare, Freiburg, Germany) equilibrated with 75 mM SPP (pH 7.2) for buffer exchange.

The VLPs eluted from gels prepared with 1 x TAE were transferred from the trough either into a fresh RNase-free reaction tube, or supplemented with KCl (f. c. 37 mM KCl and 0.9 x TAE) or directly onto PD10 SpinTrap G-25 columns (GE Healthcare, Freiburg, Germany) for buffer exchange into 75 mM SPP (pH 7.2). The VLPs were stored for two days at 10 °C and again separated by native gel electrophoresis using 1 x TAE as conductive media. After electrophoresis, agarose gels were stained as above.

TMV CP_{Lys} concentration estimation by SDS-PAGE analysis

The protein concentration of the electroeluted VLPs was estimated by denaturing sodium dodecyl sulphate polyacrylamide gel electrophoresis (SDS-PAGE) according to Laemmli et al. (1970). A standard series of known CP_{Lys} amounts (1 µg, 0,5 µg,

0,25 µg, 0,125 µg and 0,0625 µg) was separated on a 15 % acrylamide gel simultaneously with 10 µl electroeluted VLP samples of unknown concentration. Before loading, the samples were heated for 5 min at 95 °C in sample buffer (f. c.: 50 mM Tris-HCl (Tris(hydroxymethyl)aminomethane hydrochloric acid) pH 6.8, 2 % (w/v) SDS, 0.1 % (w/v) bromophenol blue, 10 % glycerol, 100 mM dithiothreitol). Protein bands, fixed (10 % acetic acid and 40 % ethanol) in polyacrylamide gels for 15 min, were stained with Coomassie Brilliant Blue R250 (Serva Electrophoresis, Heidelberg, Germany). After destaining (10 % acetic acid and 40 % ethanol) the gels were digitalized. The mean grey value of each band was determined by means of ImageJ (Schneider et al. 2012) and a calibration curve was created plotting the mean grey values against known CP concentrations. The unknown concentrations of electroeluted VLPs were calculated using the calibration curve.

TEM analysis

The structure of the electroeluted VLPs was investigated by TEM analysis. For preparation of TEM grids, a 15 µl droplet of electroeluted VLP solution (0.04 to 0.1 mg/ml with regard to CP_{Lys} in 75 mM SSP (pH 7.2), 1 x TAE or 1 x TAE plus 37 mM KCl) was placed on Parafilm M® (American National Can, Menasha, USA). A 400-mesh Formvar® carbon-covered copper grid was incubated for 5 min on top of the droplet, followed by washing with three droplets of ddH_2O and negative staining with 15 µl 2 % (w/v) uranyl acetate.

To visualize the RNA protruding from electroeluted VLPs, 6 µl spreading solution (f. c.: 30 % (v/v) formamide, 0.001 % cytochrome c, 2 mM Tris (pH 8), 0.2 mM EDTA) was prepared and mixed with 4 µl electroeluted VLPs (f. c. 0.02 to 0.04 mg/ml CP_{Lys} in 1 x TAE plus 37 mM KCl). The solution was instantly dropped onto a 200 µl ddH_2O droplet (hypophase) placed on Parafilm M®. The hyperphase was adsorbed onto a 400-mesh Parlodion®-covered copper grid. As a control, 1.4 ng/µl 500^+ nt RNA was heated in 85 % (v/v) formamide for 1 min at 65 °C and chilled on ice. The denatured RNA was supplemented with cytochrome c and TE buffer (f .c.: 0.1 ng/µl RNA, 60 % (v/v) formamide, 0.0025 % cytochrome c, 2 mM Tris (pH 8), 0.2 mM EDTA) and was dropped onto the hypophase and adsorbed to the grids as above. Grids were shadowed with 1.1 nm platinum at an angle of 7.5° and subsequently with 4 nm carbon at an angle of 90°. All samples were analyzed with a Zeiss EM-10A TEM (CARL ZEISS, Oberkochen, Germany) at 60 kV and with a Tecnai G2 Sphera

electron microscope (FEI, Hillsboro, USA) at 120 kV using a 16 megapixel camera TemCam F416 (TVIPS, Gauting, Germany).

Results and discussion

Fabrication of a double-stranded RNA-leash

For the generation of a partly single- and partly double-stranded RNA (ssRNA and dsRNA) construct, a 500^+ nt RNA backbone was designed with a 5'-terminal 204 nts TMV sequence portion containing the OAs (position 5350-5531; Zimmern 1983), flanked by segments of pGEM-T® Easy up- and downstream (**Figure 1** and **Table S1**). This RNA portion remains single-stranded to be encapsidated by CP. The 3'-terminal portion from nucleotides 205 to 500 is dedicated to the hybridization to a complementary RNA of 308 nt, to yield a dsRNA stretch which cannot be packaged into TMV CP. This 308^- nt RNA is designed in such a way that it leaves a terminal 5'-overhang of 12 nucleotides for putative hybridization to a ssDNA or ssRNA oligonucleotide which may introduce further functions. As double strand formation of nucleic acids is preferred in the presence of mono- or bivalent cations (Anwander et al. 1990), RNA-RNA duplex formation was investigated and compared to the single RNA strands. For this purpose, 500^+ nt RNA and 308^- nt RNA were synthesized by *in vitro* transcription, subjected to hybridization in the absence or presence of monovalent cations and the partner RNA, and the products compared with respect to their mobility in native agarose gels. The RNA-RNA duplex of 500^+ nt RNA and 308^- nt RNA is termed "RNAs 500-308" in the following (**Figure 2 a**, lanes lacking CP_{Lys} [-]). RNAs dissolved in ddH_2O could be separated by native gel electrophoresis into defined bands migrating at the expected apparent sizes in comparison to ssRNA marker fragments (**Figure 2 a**). For 500^+ nt RNA a faint second band is visible at an apparent size of around 700 nt. This phenomenon is frequently observed during separation of RNAs in native gels, since RNAs tend to form secondary structures, resulting in several bands in a single lane (Buchmueller & Weeks 2004, Lehrach et al. 1977). If combined in ddH_2O prior to electrophoresis, a mixture of the two RNAs 308^- nt and 500^+ nt yielded the same bands as present in the samples with single RNAs. In contrast, if 308^- nt RNA and 500^+ nt RNA had been subjected to intermolecular hybridization in buffer, an additional band migrating at an apparent size of about 580 nt appeared, indicating successful generation of the partial dsRNA hybrid (RNA 500-308, see asterisk in **Figure 2 a**). The band of the individual

precursor RNAs disappeared completely, which proves the efficiency of the reaction. The single RNAs of 500^{+} nt or 308^{-} nt, respectively, behaved differently after incubation in SPP under conditions promoting hybridization.

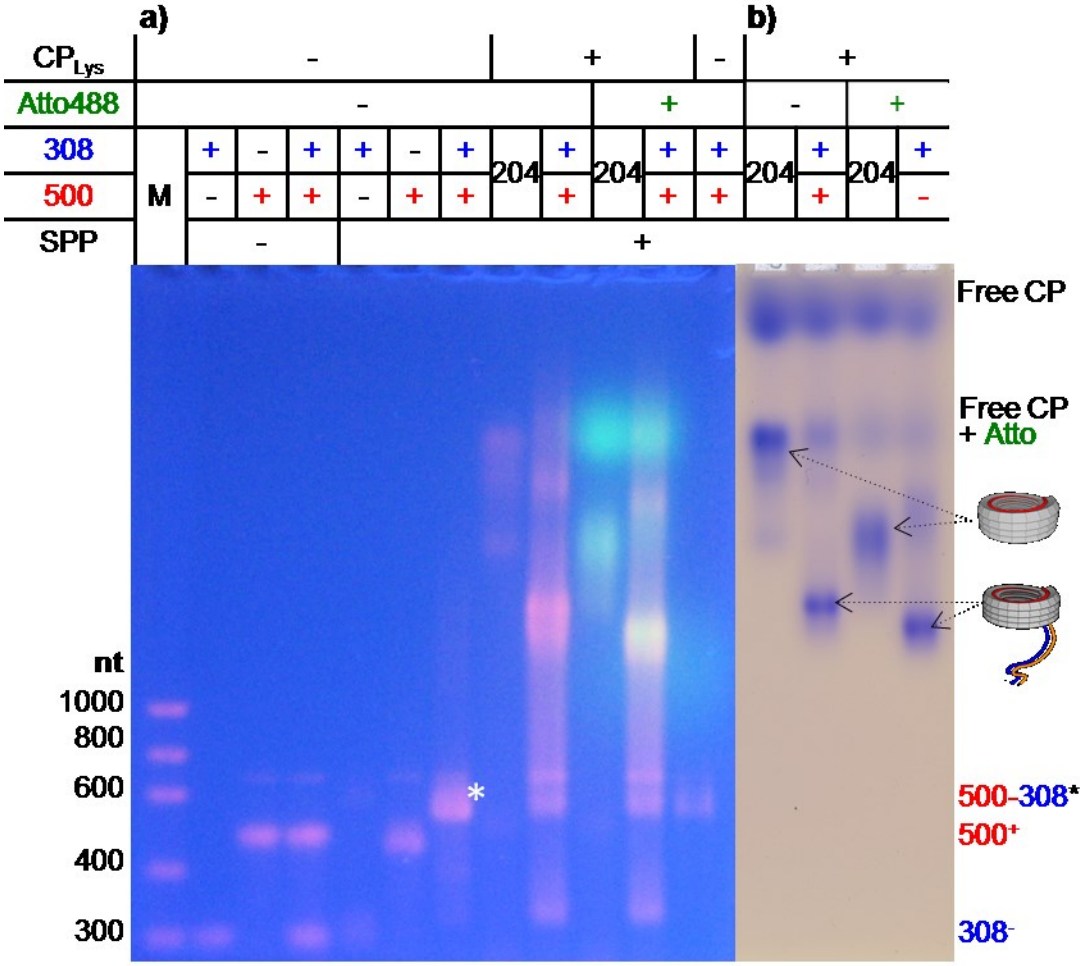

Figure 2: Analysis of RNA-RNA hybridization, formation of disk-on-a-leash compared to "disk" constructs lacking a protruding dsRNA, and the velocities of the distinct building blocks by native gel electrophoresis. **(a)** Left: RNA educts in ddH_2O (-) and hybridization products formed in SPP (+) in different molecule combinations, asterisk indicates RNA hybrid 500-308; right: *in vitro* assembled "disks" (204: made with 204^{+} nt RNA) and disk-on-a-leash constructs (both RNAs present: +), compared with respect to their electrophoretic mobilities. Nucleic acid is stained with ethidium bromide (magenta), green fluorescence indicates Atto488-labeled proteins or protein complexes. **(b)** The same gel after protein-specific staining with Coomassie Brilliant Blue R250 (2 % agarose in 1xTBE; CP_{Lys}: coat protein; M: RNA ladder; nt: nucleotide; RNA: ribonucleic acid; compounds combined to form supramolecular complexes as indicated above).

While 500^{+} nt RNA remained unaffected, a weak additional band with an apparent size of about 600 nt was detected with 308^{-} nt RNA alone. This might reflect a minor extent of hybridization of 308^{-} nt RNA also with itself. However, its interaction with the intended 500^{+} nt partner RNA is substantially more favourable, as demonstrated by the strong corresponding signal.

Establishment of TMV CP disks-on-a-leash with enhanced velocity in electric fields

To generate nanoporous disk-on-a-leash constructs intended to serve as efficiently implantable pore adapters, the partial dsRNA duplexes (i.e. RNAs 500-308) were mixed with TMV CP_{Lys} in the same buffer (75 mM SPP pH 7.2), to encapsidate the ssRNA part of 204 nt that contains the OAs, expected to result in a four-turn nucleoprotein helix structure with a protruding 296 bp dsRNA with terminal 12 nts ssRNA overhang ("leash"). An accelerated migration velocity during electrophoresis was anticipated due to the additional negative charge of the accessible dsRNA phosphate backbone, for which reason the mobility of the products was compared to that of “disks” in native gel electrophoresis. After the assembly reaction, both disks-on-a-leash and control “disks” without protruding RNA were labeled with a fluorescent dye (Atto488) to allow tracing of the protein components. To visualize the RNA simultaneously with the fluorescent proteins, gels were stained with ethidium bromide after electrophoretic separation. **Figure 2 a** (right half) and b shows the results, indicating successful RNA-directed self-organization of disk-on-a-leash constructs by means of the novel RNA scaffold. Without Atto488-label, they can be seen as a bright magenta-colored band (**Figure 2 a**), due to the intercalation of ethidium bromide (EtBr) into the free dsRNA portion. The EtBr signal intensity of the “disk” without RNA-leash (left-hand lane "204") is considerably lower, since the 204^{+} nt RNA is encapsulated inside the protein shell (see protein stain in **Figure 2 b**) and, furthermore, single-stranded, impeding the intercalation of EtBr. For the fluorescently labeled particles, magenta EtBr-signals are reduced and superimposed by the green CP_{Lys}-specific signals of the four-turn helices, resulting in a yellow fluorescence signal of the disk-on-a-leash constructs. The merge of the magenta RNA and the green protein signal into yellow verifies the presence of proteins and RNA at the same position. This is substantiated by the co-localized protein stain (**see Figure 2 b**).

As intended and expected, disk-on-a-leash constructs exhibited a higher electrophoretic mobility than “disks” without RNA-leash (**Figure 2**). In addition to the negative charge introduced by the dsRNA phosphate backbone, Atto488 fluorescence labeling accelerated the migration slightly further, compared to unlabeled particles, since the net electrical charge per conjugated Atto488 molecule increases by -1. Compared to the non-encapsulated bare RNA scaffold, the VLPs

migrate remarkably slower due to the low negative charge of the CP_{Lys} shielding that of the RNA, in combination with the large particle weight.

To confirm the identity of the protein-RNA complexes, the proteins were stained with a protein-specific dye and became visible at the same positions of the ethidium bromide and the fluorescence signals (**Figure 2 b**). This further scrutinized that the CPs indeed interacted with the partly single- and double-stranded RNA. In addition to the distinct bands, there is also a weak background smear spread along the whole lane which is likely to represent assembly intermediates and/or secondary products of free RNA and viral CPs.

In subsequent stages of the study, native gels comparable to these shown in **Figure 2** were therefore applied to purify the desired nucleoprotein complexes from by-products (see below). For this purpose, fluorescently labeled VLPs were monitored during gel electrophoresis by UV irradiation and eluted from the agarose gel.

Structural analysis of disks-on-a-leash by RNA spreading and TEM

In order to visualize the structure of the novel TMV-based nucleoprotein pore adaptor constructs, assembly products eluted from the agarose gels were subjected to electron microscopy after spreading the dsRNA strands and metal shadowing. As the diameter of dsRNA molecules is around 2 nm only, proving the existence of the dsRNA-leash connected to the “disk” by TEM analysis is more elaborate than imaging nucleoprotein “disks” lacking any free nucleic acid portion. In first experiments we attempted to spread the dsRNA protruding from the TMV “disks” by nucleic acid preparation techniques for electron microscopy which are usually applied for dsDNA and dsRNA spreading (Coggins 1987). However, these techniques did not reveal distinguishable, efficiently spread dsRNA-leashes (data not shown). Therefore, the spreading solution was supplemented with a limited amount of formamide, which is commonly used in higher concentrations for the spreading of ssDNA or ssRNA. Upon their preparation for TEM, nucleic acid strands are typically spread at an air-water interface by forming a mixed film with a basic protein such as cytochrome c, binding to the nucleic acid from a hypophase. To fully expand ssDNA or ssRNA strands or partially single-stranded constructs, these are frequently subjected to treatment with formamide and heated (53 °C to 80 °C) to denature base-paired regions and remove secondary structures. The hyperphase including the stretched nucleic acid is subsequently adsorbed to a Parlodion®-covered copper grid (Kleinschmidt et al. 1962, Evenson et al. 1978, Glass & Wertz 1980, Vollenweider et

al. 1975). The adsorbed molecules are contrasted by rotary shadowing at a small angle of about 4 ° to 7 ° with a thin layer of platinum and thereafter with carbon at an angle of 90 ° (Riou & Delain 1969, Griffith & Christiansen 1978). Formamide, however, is known to induce disassembly of TMV VLPs at a concentration of ≥67 % (Yuan-Jen et al. 1964, Yuan-Jen & Yun-Shang 1964) and as mentioned above to disrupt hydrogen bonds between complementary nucleic acid strands. Hence, it was added to the spreading solution employed with pore adapters in a lower concentration than with plain ssRNA (30 % versus 60 % formamide, respectively). Although the major portion of the "leash" was designed to consist of dsRNA which would not need the presence of formamide upon spreading at all, this intended to ensure similar stretching of the disk-on-a-leash construct analyzed in parallel to the 500^{+} nt ssRNA backbone. Additionally, the cytochrome c concentration (0.0010 % versus 0.0025 % cytochrome c, respectively) in the spreading solution of disk-on-a-leash constructs was decreased to reduce the background of cytochrome c film on the Parlodion®-covered grids. TEM analysis demonstrates that disk-on-a-leash constructs became well distinguishable from plain RNA without undergoing disassembly to an extended degree under these conditions (**Figure 3**). Disk-like structures of about 20 nm diameter were in many cases connected to the ends of flexuous nucleic acid strands, thus solidifying the evidence for the structural integrity of the constructs. Compared to disk-on-a-leash constructs spread without formamide (data not shown), the dsRNA-leash was stretched out from the disks. Presumably, the phosphates of the dsRNA-leash adhered to the CPs of the "disks" *via* hydrogen bonds which were disrupted in the presence of formamide. Such protein-RNA interactions are mainly between basic amino acid residues, e.g. arginine (Arg) and lysine (Lys), and the oxygen atoms of the RNA phosphate groups (Draper 1999). In case of the mutant TMV_{Lys} three basic amino acid residues (Arg61, Arg141 and Lys158) are exposed at the outer circumference of the viral capsid. Both arginine residues form salt bridges with acidic amino acid residues (Glu145 with Arg61 and Asp64 with Arg141) or hydrogen bonds with each other (Namba et al. 1989, Bloomer et al. 1978). Furthermore, the genetically inserted Lys158 is accessible at the outer rim which was shown by chemical coupling (Geiger et al. 2013). Hence, these three amino acid residues might form hydrogen bonds with the phosphate of the RNA backbone and, consequently, impair the spreading of the dsRNA-leash in the absence of formamide. The length measured for the RNA-leashes (72.2 nm) is

shorter than that determined for the 500^+ nt RNA (125.6 nm), with a ratio of 500^+ nt RNA to RNA-leash length (125.6 nm : 72.2 nm) of 1.7, confirming the encapsidation of the ssRNA portion of the hybrid RNA 500-308 into CP. The length of the protruding dsRNA with 12 nt ssRNA overhang as well as that of the 500^+ nt ssRNA scaffold estimated by TEM analysis after spreading (**Table 1**) were shorter than calculated for 269 bp elongated by 12 nt ssRNA (for 296 bp × 0.27 nm nt^{-1} + 12 nt × 0.29 nm nt^{-1} = 83.4 nm) and 500 nt (for 500 nt × 0.29 nm nt^{-1} = 145.0 nm), respectively, in relation to the rise of one dsRNA base pair of 0.27 nm determined by transient electric birefringence measurements (Kebbekus et al. 1995) and ssRNA with a rise of 0.29 nm per base determined by NMR (Broido & Kearns 1982). This is in agreement with numerous studies on the spreading of nucleic acids for microscopic analyses (see above), all of which revealed that the contour lengths of the expanded molecules differed significantly dependent on the conditions applied, and remained below the values obtained *via* high-resolution techniques for structure determination such as NMR or electric birefringence.

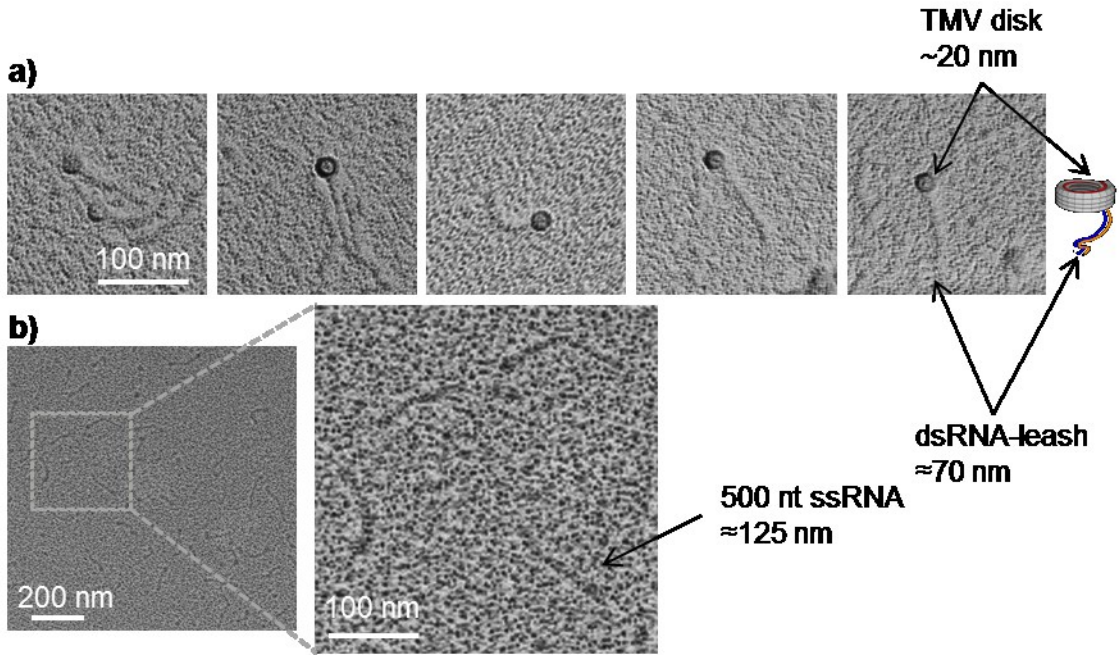

Figure 3: TEM analysis of disk-on-a-leash complexes electroeluted from native agarose gels. dsRNA-leash and ssRNA (500^+ nt RNA) is visualized by spreading in the presence of cytochrome c and formamide and shadowing with platinum and carbon. **(A)** Disk-on-a-leash constructs in 1 x TAE at pH 8.4. **(B)** Plain 500^+ nt RNA without proteins visualized with the same technique like the disk-on-a-leash, but with higher formamide and cytochrome c concentrations. For details, refer to text.

However, the ratio of the 500^+ nt RNA to the 308^- nt RNA of 1.7, as determined from TEM-images, is equal to the expected ratio for 500^+ nt to the dsRNA-leash of 269 bp elongated by 12 nt ssRNA (145.0 nm : 83.4 nm) of 1.7. The deviance of calculated

compared to measured RNA contour length from TEM images is presumably due to the bending of the RNA upon spreading, comparable to flexible DNA (Cognet et al. 1999). The contour length of the ssRNA measured in the present study was 4000 bases per µm for the 500^+ nt RNA and 4266 bases per µm for the dsRNA-leash with the 12 nt 5'-overhang. These measurements are in full agreement with the contour length of spread ssRNA denatured in 80 % formamide with 4200 to 4800 bases per µm determined by TEM analysis (Glass & Wertz 1980).

Despite the use of cytochrome c, the width of dsRNA found in this study is around 4.6-5.6 nm, which is similar to double-stranded T7 DNA spread without cytochrome c (2 to 6 nm; Vollenweider et al. 1975). In contrast, the width of about 11.6 nm determined for ssRNA exceeds that of ssDNA associated with cytochrome c (8 nm; Vollenweider et al. 1975).

Table 1: Length determination of RNA scaffolds and leashes determined after spreading, and diameter of interconnected disk-like structures. Lengths were determined for dsRNA protruding from disk-on-a-leash assemblies, or plain 500^+ nt ssRNA without proteins (results from one TEM image); "disk" diameters results from N examples from two different TEM images. The expected RNA length after complete spreading is larger than the measured length by a factor of about 1.2 (exp: expected, meas: measured).

Sample	Expected RNA length [nm|	Measured RNA length [nm]	RNA diameter [nm]	"Disk" diameter [nm]	Ratio RNA length exp:meas
Disk-on-a-leash	83.4[a,b]	72.2 ± 11.0 (N=28)	5.1 ± 1.4(N=32)	19.9 ± 2.4 (N=36)	1.2
500^+ nt ssRNA	145[b]	125.6 ± 20.1 (N=19)	11.6 ± 2.4 (N=19)	-	1.2

[a] Related to the length of dsRNA length of 0.27 nm per base pair determined by transient electric birefringence measurements (Kebbekus et al. 1995).
[b] Related to the length of ssRNA length of 0.29 nm per base determined by NMR (Broido & Kearns 1982).

The differences in the measured widths of the dsRNA and ssRNA, in relation to earlier findings, might be due to the different concentrations of cytochrome c used for the spreading procedure. The dsRNA was spread in the presence of 0.001 % cytochrome c, whereas ssRNA was spread with 0.0025 % cytochrome c. Hence, more cytochrome c is presumably associated with the ssRNA because of a higher concentration in the spreading solution. The increased apparent diameter of the disk-like structure of 20 nm, compared to 18 nm of negatively stained TMV particles (Namba et al. 1989), is caused by the platinum deposition of 1.1 nm layer thickness which extends the typical shape by around 2 nm in total.

The results of TEM imaging of the disk-on-a-leash nanopore adapter, after RNA spreading clearly show that CPs solely encapsulated the single-stranded part of the RNA partial hybrid, leaving free the dsRNA portion. The contour length and width of the dsRNA and ssRNA portions are in good agreement with results described in the literature, thus confirming successful preparation of the envisaged nucleoprotein assembly.

Determination of disk-on-a-leash stability in different buffers to optimize gel purification and implantation into SSM templates

The disk-like VLPs ("disks" with and without dsRNA-leash) were separated in preparative agarose gels in two different conductive media (TBE or TAE) and electroeluted; first, to remove unwanted by-products which are detectable as a smear spread along the lane (**Figure 2**, $I1^{*}$, $I2^{*}$, $r1^{*}$and $r2^{*}$) and second, to find a suitable solvent in which the disk-on-a-leash construct remains intact. This was intended to delimit appropriate conditions for their efficient insertion into inorganic SSM templates. As it was demonstrated in **manuscript I**, the "disks" without dsRNA-leash remained stable during native gel electrophoresis when they were separated in the conductive medium TBE. Hence, to separate and electroelute the VLPs, TBE was tested initially. However, the VLPs emerged as instable or structurally affected in TBE buffer (**Figure S1**). After electroelution and storage in TBE over night at 10 °C, the VLPs disassembled, which was detectable by the released RNA (**Figure S1**, $I1^{a}$ and $I2^{a}$). Consequently, the integrity of them was investigated comparing the conductive media TBE and TAE: The VLPs were separated in two different gels with either TBE or TAE, respectively, and afterwards electroeluted (for details see experimental section). Subsequently, the conductive media containing the electroeluted VLPs were exchanged to 75 mM SPP pH 7.2 by gel filtration and stored in this buffer over night at 10 °C, before being separated electrophoretically in the corresponding buffer again (e.g. TBE, if prior separation was carried out in TBE) to confirm their structure integrity (**Figure 4**). Characteristic signals at the position of the "disk" with and without the RNA-leash were detectable in both conductive media (**Figure 4**, $I1^{a}$, $I1^{b}$, $r1^{a}$ and $r1^{b}$). However, for VLPs with an RNA-leash an RNA smear was obvious below the disk-on-a-leash band (**Figure 4 b**, $r1^{a}$ and $r1^{b}$), if separated in TBE but not in TAE. This result indicates that the disk-on-a-leash construct was more stable and remained structurally intact if separated in gels prepared with TAE, in comparison to gels with TBE. As no smear below the disk-on-a-leash band occurred

when separated in TAE (**Figure 4 a**, $I1^a$ and $I1^b$), it was explored whether this construct remained intact when it was stored in TAE alone, or in TAE supplemented with 37 mM KCl (TAE-KCl), or in 75 mM SPP (pH 7.2; with buffer exchange *via* gel filtration) after electroelution from native TAE agarose gels.

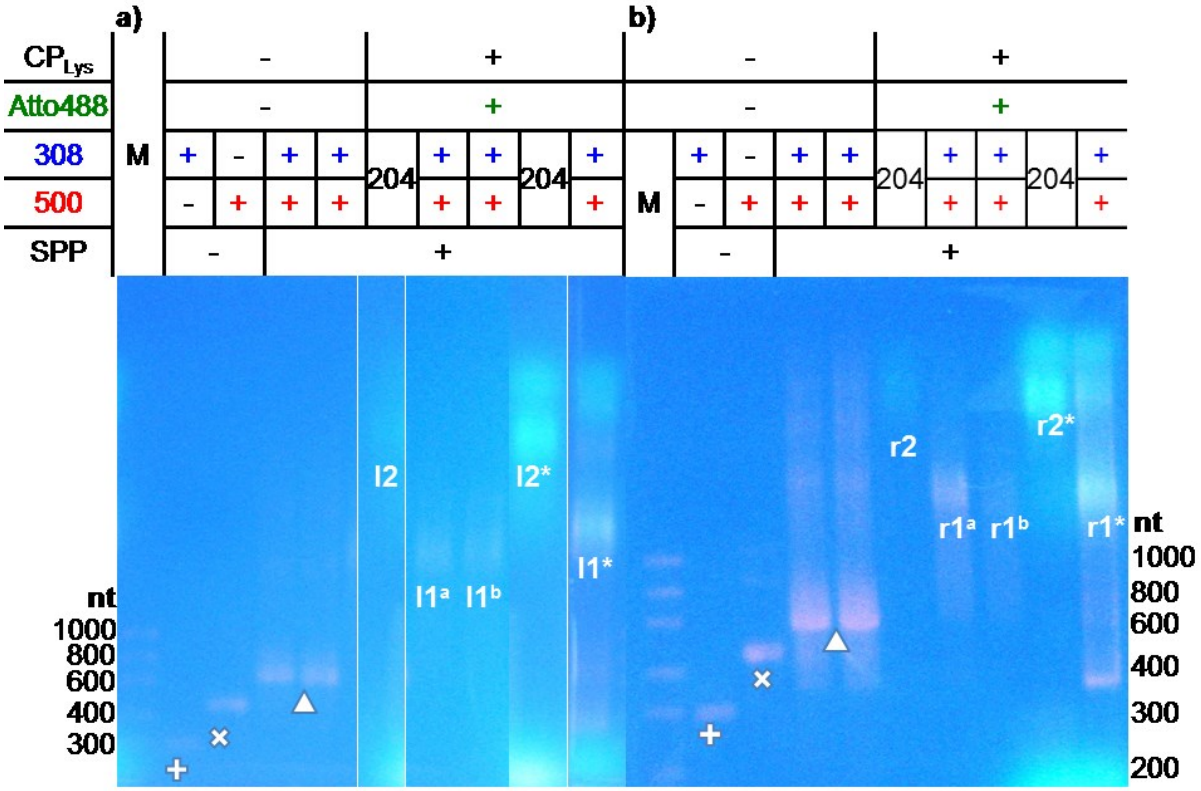

Figure 4: Comparison of the integrity of electroeluted protein-RNA complexes in two distinct conductive media during native agarose gel electrophoresis. **(a)** 1 x TAE-buffered gels used for the separation of RNAs without SPP (+ and ×) and after hybridization (Δ) in SPP, of *in vitro* assembled disk-on-a-leash constructs (I1*, $I1^a$ and $I1^b$), and of TMV "disks" (I2 and I2*) and **(b)** 1 x TBE-gels used in parallel with RNAs without SPP (+ and ×) and after hybridization (Δ) in SPP, *in vitro* assembled disk-on-a-leash constructs (r1*, $r1^a$ and $r1^b$) and TMV disks (r2 and r2*). "Disks" and disks-on-a-leash before* (number indicated with asterisk (*)) and after (number without star) electroelution; I indicates bands at the left gel and r at the right one; 1^a and 1^b indicate two independent replica of *in vitro* assembled disk-on-a-leash constructs. Nucleic acid was stained with ethidium bromide (magenta), green fluorescence indicates Atto488-labeled proteins as in **Figure 2**. (2 % agarose; M: RNA ladder; nt: nucleotide; RNA: ribonucleic acid, SPP: sodium potassium phosphate (pH 7.2); 308: 308^- nt RNA; 500: 500^+ nt RNA).

The VLPs were stored for two days at 10 °C and analyzed by electrophoresis using again TAE as conductive medium (**Figure 5**). Contrary to the results obtained for VLPs stored in TBE, typical signals of disk-on-a-leash constructs were detectable after storage for two days at 10 °C in SPP, TAE or TAE-KCl, respectively, with a VLP concentration of about 0.1 mg/ml (**Figure 5**). This suggests that boric acid was the component affecting the VLPs when they were freely dispersed in TBE buffer. The structure integrity of the disk-on-a-leash constructs stored in different buffers for two

days at 10 °C was additionally investigated by TEM analysis after negative staining (**Figure 6**).

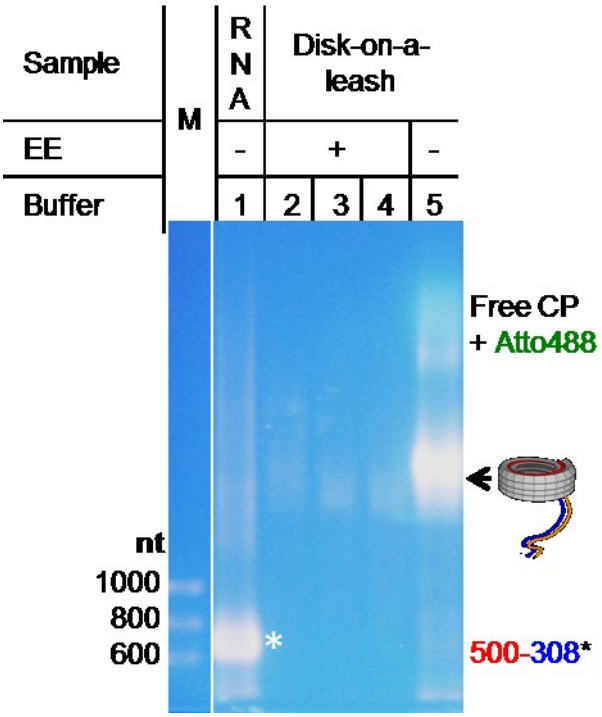

Figure 5: Analysis of storage stability of disks-on-a-leash in TAE or SPP buffer, respectively, after initial purification in TAE gels and electroelution. Native gel electrophoretic analysis of 500-308 RNA hybrid scaffold (1 and *) established in 75 mM SPP at pH 7.2, and *in vitro* assembled disk-on-a-leash constructs stored in 75 mM SPP at pH 7.2 (2), in 1 x TAE with 37 mM KCl at pH 8.4 (3) and in 1 x TAE at pH 8.4 (4) for two days at 10 °C after electroelution (EE, [+]). Non-electroeluted (EE [-]) disk-on-a-leash constructs in 75 mM SPP (pH 7.2) stored as above (5). Nucleic acid is stained with ethidium bromide (magenta), green fluorescence indicates Atto488-labeled proteins. (Analysis here in 2 % agarose; running buffer 1 x TAE; EE: electroelution; further abbreviations see **Figure 4**).

Disk-like structures were present following storage under each examined condition. The stability of the dsRNA-leashes was not verifiable by this method, but was successfully proven as well: They were detected after spreading by use of a protein film of cytochrome c, as visualized above in **Figure 3**, which shows constructs after elution from TAE gels and storage in 1 x TAE pH 8.4.

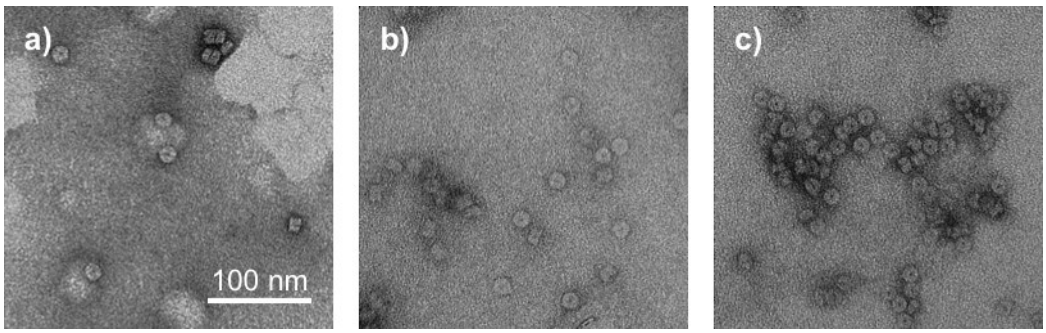

Figure 6: TEM analysis of electroeluted disks-on-a-leash stored for two days in different buffers at 10 °C. Storage buffers were **(a)** 75 mM SPP pH 7.2, **(b)** 1 x TAE pH 8.4 with 37 mM KCl, and **(c)** 1 x TAE pH 8.4. Proteins were negatively stained with uranyl acetate prior to TEM.

Although TMV “disks” lacking a leash were stable in a weakly alkaline pH range (pH 7.2 to 9.0; see **manuscript I Figure 3**), they were structurally affected after extended storage in borate containing buffer (TBE), similar to the disk-on-a-leash constructs (**Figure S1**). In contrast to these short ring-shaped artificial VLPs, whole TMV

particles were stable in 50 mM borate buffer at pH 8.5 (Oldenbourg et al. 1988). Other investigations demonstrated that TMV particles degraded at pH values above 9 (Harrington & Schachman 1956, Pelcher & Halasa 1979). This was assigned to alkaline disassembly since the portion of degraded TMV particles rose with increasing pH. As the VLPs remained stable in TAE at pH 8.4, the exploration of the disk-on-a-leash construct in this work indicates that the instability of the VLPs in TBE (**Figure S1**) may arise from interactions of the borate ions with nucleic acid. The putatively underlying depolymerization mechanism induced by boric acid is not clear. According to the literature, borate ions interact with amino groups of the nucleic acid bases and oxygen groups of the phosphate (Stellwagen et al. 2000). Equally, the interplay of the RNA and the TMV CP RNA-binding site – each CP subunit interacts with three nucleotides of the RNA *via* repeated arginine (interaction *via* phosphates of the RNA backbone) and aspartic acid or glutamine (interaction *via* N of the bases) residues (Namba et al. 1989, Ge & Zhou 2011) – might be destabilized when the VLPs are freely dissolved in TBE. In contrast, the VLPs might be more stable during agarose gel electrophoresis in TBE, as borate ions preferably interact with the carbohydrate matrix of the polysaccharides in comparison to the nucleic acid (Stellwagen et al. 2000), with less degradation than freely dispersed in buffer due to the protective gel matrix. Thus, for the storage of the disk-like structures presented in this work, the buffer should be devoid of borate ions to prevent the degradation of the VLPs.

Conclusively, appropriate conditions for the storage and electrophoretic migration of the disk-on-a-leash were found, allowing the electrophoretically driven insertion of the novel construct into SSM pores.

Quantification of gel-purified pore adapters available for integration into SSM templates

To examine the yield of the electroeluted disk-shaped VLPs with or without dsRNA-leash, the concentrations and numbers of constituent CP subunits were estimated by SDS-PAGE, Coomassie staining of CP bands (**Figure 7 a**) and software-aided analysis of band mean gray values in comparison with a known CP concentration test series. The mean grey value of every calibration band was determined by ImageJ (Schneider et al. 2012) and plotted versus the respective CP amount to create a calibration line (**Figure 7 b**). This served as reference for the eluted “disk” samples shown in **Figure 7 a** and revealed concentrations of the electroeluted VLPs

between 0.04 and 0.1 g/l, with a volume of around 250 µl eluted per sample and thus total yields of 10 up to 25 µg per assembly reaction (**Figure 7 c**). For a typical electrophoretic insertion setup to equip an SSM template with biological pore adapters, a volume of 1 ml is necessary in an appropriate chamber. The total numbers of disk-on-a-leash constructs were determined under the assumption that one RNA-scaffolded particle contains 68 CPs with a total molecular weight of 1,165,000 g/mol. This means that after dilution in a volume of 1 ml, a concentration of 0.01 g/l disk-on-a-leash adapters can be achieved with the fabrication and purification strategy developed in this study.

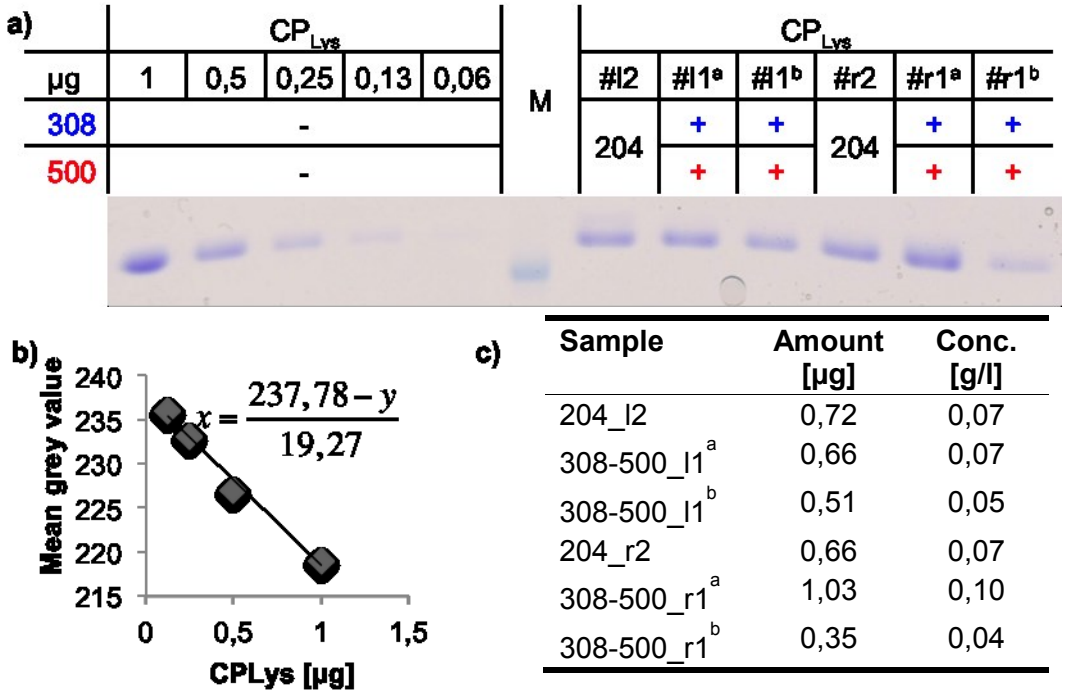

c)

Sample	Amount [µg]	Conc. [g/l]
204_l2	0,72	0,07
308-500_l1[a]	0,66	0,07
308-500_l1[b]	0,51	0,05
204_r2	0,66	0,07
308-500_r1[a]	1,03	0,10
308-500_r1[b]	0,35	0,04

Figure 7: Protein concentration estimation by SDS-PAGE analysis. **(a)** A dilution series of known CP_{Lys} quantities separated in a 15 % polyacrylamide gel simultaneously with electroeluted "disks" and disks-on-a-leash (#1 to #2: samples specified in c; samples #l1[a], #l1[b], #r1[a] and #r1[b] were loaded from different CP-disk-on-a-leash preparations). **(b)** The mean grey values ("sum of the grey value of all the pixels in the selection divided by the number of pixels", ImageJ User Guide, 2012/10/02) of Coomassie brilliant blue R250-stained bands of known CP amounts were determined by image evaluation software ImageJ (Schneider et al. 2012). Mean grey values are plotted against the corresponding CP amount to create a calibration line. **(c)** Protein concentrations of electroeluted "disk" assemblies determined from the calibration series (for sample details see **Figure 4**).

In that case, around 5.3×10^{12} particles are dissolved, with a molarity of 8.8 nM of the supramolecular complexes. From initial insertion experiments and REM analysis of the resulting hybrid structures (see German Introduction/Outlook, **Abb. 4**), it may be estimated that a 50-fold excess of nanopore adapters would suffice to achieve efficient electrophoretic implantation of a single adapter into every SSM pore channel (with the surplus disks sputtered on the SSM surface between the pore cavities).

Therefore, the yield per eluted band would allow to equip 1×10^{11} inorganic pores with TMV-derived disk-on-a-leash pore adapters, which corresponds to 44 ng RNA scaffold in combination with 192 ng CP as starting material. The free-standing SSM templates fabricated in our partner lab in Ulm typically contain 3×10^{7} inorganic pores in an area of 500 mm^2, a size which meets the dimensions of flow-channels in lab-on-a-chip devices (Dittrich & Manz 2006).

Conclusion

Inspired by previous work on DNA or haemolysin nanopores (Bell et al. 2012, Hernandez-Ainsa et al. 2014, Hall et al. 2010), we fabricated a novel nucleoprotein complex destined to serve as a pore adaptor for the insertion into nanoporous membranes, to obtain thousands of identical protein pores below 4 nm diameter. Based on plant viral components, the natural mechanism of self-organization was manipulated by genetic and biochemical engineering to generate a synthetic nanopore inlay by combining modified viral capsid proteins with a dsRNA-leash. The negatively charged dsRNA-leash connected to the nanoporous nucleoprotein "disk" was designed to allow threading the pore adapters through the inorganic pore channels, while simultaneously promoting their desired orientation in an electric field. The dsRNA-leash was designed with a comparably short length of 83.4 nm, since efficient threading is impeded with increasing DNA stretches (Larkin et al. 2014). The additional negative charge of the RNA phosphate backbone enhances its electrophoretic mobility, raising the likelihood of a fast and complete occupation of the solid-state pores.

In a recent study, a loading efficiency of around 60 % was reported for biotinylated DNA complexed with streptavidin, if drawn eletrophoretically into 35 nm wide wells with 3-5 nm inorganic pores at their bottoms; since no covalent fixation was applied, the insertion was reversible (Larkin et al. 2014). In our work, the disk-on-a-leash construct used for targeting conical SSM channels with a central diameter of about 20 nm exposed reactive groups on its modifyable outer protein "disk" surface; hence it can be chemically conjugated to a functionalized inner pore rim to prevent ejection. The nucleoprotein ring could also be equipped with peptides promoting correct targeting and immobilization. These might include peptides with high affinity to the inner pore material as well as mineralization-directing peptide sequences, which may enable sealing of the annular gaps between protein and SSM by converting dissolved precursor molecules into solid "glue".

Considering the constructs' stability in different conductive media, the conditions for disk-on-a-leash insertion into the porous solid-state membranes can be adapted to meet the requirements of the electrophoresis chambers applied, or the chemical coupling reactions; with the exception of borate-containing buffers. As demonstrated previously for α-haemolysin with 30 to 40 % protein insertion (Hall et al. 2010) and DNA-origami pore adaptors (Hernandez-Ainsa et al. 2014, Bell et al. 2012), we expect high integration performance for our disk-on-a-leash construct because of the additional negative charge of the RNA-leash phosphate backbone.

For future applications, modifications of the disks' inner protein channel are expected to enable the filtration of molecules according to their chemical and physical properties. Different TMV mutants with genetically exchanged CP amino acids in their inner channel have been described (Zhou et al. 2013, Dedeo et al. 2010), which may facilitate the conjugation of small molecules to enhance the selectivity for molecules passing the channel. This novel disk-on-a-leash construct thus paves the way for further modifications of both the inner channel and the outer surface of its nanoporous "disk" portion, to expand the field of nano-hybrid materials. In particular, nanoporous hybrid membranes for molecule sorting or characterization of chemical and physical properties of pharmaceutical or medical compounds may profit from the new layout, which is likely to increase the fabrication efficiencies of large and robust bionanopore arrays.

Acknowledgments

We like to thank Cornelia Kocher to provide protocols and technical support for the TEM analysis, Prof. Dr. Stephan Nussberger and PD Dr. Michael Schweikert for granting access to the TEM, Sigrid Kober for the preparation of TMV particles from tobacco plants, and Diether Gotthardt for taking care of the plants. We are grateful for the financial support of the DFG SPP1569 (DFG-WE-4220/2-1 and -2).

Supplementary information

Table S1: DNA templates for *in vitro* transcription of RNAs with (+) and without (-) the origin of assembly (OAs). The position of the OAs loop is highlighted orange, capital letters indicate DNA sequence of viral genome origin, small letters DNA sequence of pGEM®-T Easy origin, grey letters the complementary sequence for RNA-RNA hybridization; the 12 nts 5'-overhang of the 308⁻ nt RNA is marked green.

RNA length [nt]	DNA-Sequence
204⁺	gggcgaattgggcccgacgtcGCGGGTTTCTGTCCGCTTTCTCTGGAGTTT GTGTCGGTGTGTATTGTTTATAGAAATAATATAAAATTAGGTTTGAG AGAGAAGATTACAAACGTGAGAGACGGAGGGCCCATGGAACTTAC AGAAGAAGTCGTTGATGAGTTCATGGAAGATGTCCCTATGTCGAT CAGGCTTGCAAAGTTa
500⁺	gggcgaattgggcccgacgtcGCGGGTTTCTGTCCGCTTTCTCTGGAGTTT GTGTCGGTGTGTATTGTTTATAGAAATAATATAAAATTAGGTTTGAG AGAGAAGATTACAAACGTGAGAGACGGAGGGCCCATGGAACTTAC AGAAGAAGTCGTTGATGAGTTCATGGAAGATGTCCCTATGTCGAT CAGGCTTGCAAAGTTaatcactagtgaattcgcggccgcctgcaggtcgaccatatggg agagctcccaacgcgttggatgcatagcttgagtattctatagtgtcacctaaatagcttggcgtaat catggtcatagctgtttcctgtgtgaaattgttatccgctcacaattccacacaacatacgagccgga agcataaagtgtaaagcctggggtgcctaatgagtgagctaactcacattaattgcgttgcgctca ctgcccgctttccagtcgggaaacctgtcgtgccagctgcattaatgaatc
308⁻	cgcgcgttggccgattcattaatgcagctggcacgacaggtttcccgactggaaagcgggcagtg agcgcaacgcaattaatgtgagttagctcactcattaggcaccccaggctttacactttatgcttccg gctcgtatgttgtgtggaattgtgagcggataacaatttcacacaggaaacagctatgaccatgatt acgccaagctatttaggtgacactatagaatactcaagctatgcatccaacgcgttgggagctctc ccatatggtcgacctgcaggcggccgcgaattcactagtgat

Table S1: Primers designed for PCR amplification of the DNA templates for RNA *in vitro* transcription specified in **Table S1** (small letters: T7 RNA polymerase promoter).

RNA product	Primer name	Sequence
204⁺ nt	204_iv_rev	5'-TAACTTTGCAAGCCTGATCGACAAGG-3'
500⁺ nt	500_iv_rev	5'-GATTCATTAATGCAGCTGGC-3'
308⁻ nt	308_fwd	5'-ATCACTAGTGAATTCGCGGCC-3'
	308_rev	5'-CGCGCGTTGGCCGATTCATT-3'
	308_T7_fwd	5'-taatacgactcactatagggCGCGCGTTGG-3'
	308_iv_rev	5'-ATCACTAGTGAATTCGCGGCCGCCTG-3'
204⁺ nt & 500⁺ nt	pGEM fwd	5'-CGCCAGGGTTTTCCCAGTCAC-3'

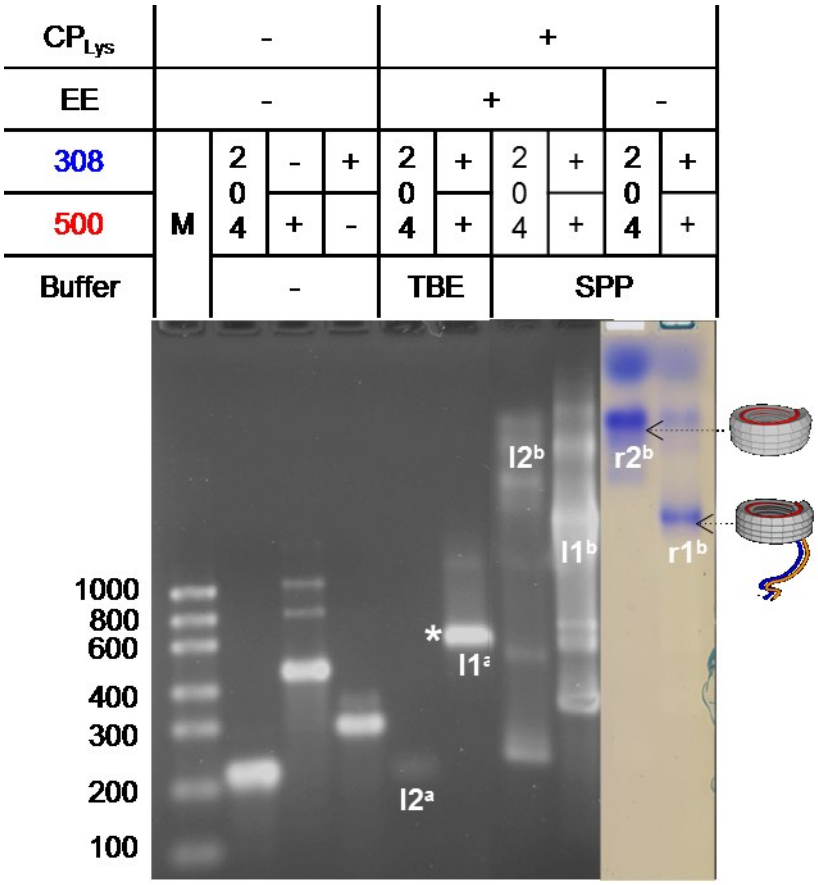

Figure S1: Native gel electrophoresis analysis of the electroeluted protein-RNA complexes stored in TBE for 16 h at 10 °C. 1 x TBE-buffered gels used for the separation of RNAs without SPP (-), of *in vitro* assembled disk-on-a-leash constructs ($I1^a$ and $I1^b$), and of TMV "disks" ($I2^a$ and $I2^b$). Disks-on-a-leash and "disks" electroeluted (EE [+]) from native agarose gels (conductive medium: TBE) were separated after storage in TBE buffer ($I1^a$ and $I2^a$) and compared to non-electroeluted (EE [-]) VLPs ($I/r1^b$ and $I/r2^b$). The apparent size of the RNAs ($I1^a$ [580 nts] and $I2^a$ [204 nts]) indicates their release from TMV CPs probably due to disassembly. Nucleic acid in the left (I) image was stained with ethidium bromide. Proteins in the same gel (right image: r1 and r2) were stained with Coomassie Brilliant Blue R250 (2 % agarose prepared with 1 x TBE; M: RNA ladder; nt: nucleotide; RNA: ribonucleic acid, SPP: sodium potassium phosphate (pH 7.2); 204: 204^+ nt RNA; 308: 308^- nt RNA; 500: 500^+ nt RNA; 500-308*: RNA 500-308, asterisk [*] indicates the RNA signal in the gel).

References

Adiga, S. P., Jin, C., Curtiss, L. A., Monteiro-Riviere, N. A. & Narayan, R. J. 2009. 'Nanoporous membranes for medical and biological applications.' *Wiley Interdiscip Rev Nanomed Nanobiotechnol,* 1, 568-581.

Anwander, E. H., Probst, M. M. & Rode, B. M. 1990. 'The influence of Li^+, Na^+, Mg^{2+}, Ca^{2+}, and Zn^{2+} ions on the hydrogen bonds of the Watson-Crick base pairs.' *Biopolymers,* 29, 757-769.

Bayley, H. & Jayasinghe, L. 2004. 'Functional engineered channels and pores (Review).' *Mol Membr Biol,* 21, 209-220.

Bell, N. A., Engst, C. R., Ablay, M., Divitini, G., Ducati, C., Liedl, T. & Keyser, U. F. 2012. 'DNA origami nanopores.' *Nano Lett,* 12, 512-517.

Bloomer, A. C., Champness, J. N., Bricogne, G., Staden, R. & Klug, A. 1978. 'Protein disk of tobacco mosaic virus at 2.8 Å resolution showing the interactions within and between subunits.' *Nature,* 276, 362-368.

Boersma, A. J. & Bayley, H. 2012. 'Continuous stochastic detection of amino acid enantiomers with a protein nanopore.' *Angew Chem Int Ed Engl,* 51, 9606-9609.

Broido, M. S. & Kearns, D. R. 1982. '^{1}H NMR evidence for a left-handed helical structure of poly(ribocytidylic acid) in neutral solution.' *J Am Chem Soc,* 104, 5207-5216.

Buchmueller, K. L. & Weeks, K. M. 2004. 'Tris-borate is a poor counterion for RNA: a cautionary tale for RNA folding studies.' *Nucleic Acids Res,* 32, 1-6.

Butler, P. J. 1999. 'Self-assembly of tobacco mosaic virus: the role of an intermediate aggregate in generating both specificity and speed.' *Philos Trans R Soc Lond B Biol Sci,* 354, 537-550.

Coggins, L. W. 1987. 'Preparation of nucleic acids for electron microscope.' In J. Sommerville & U. Scheer (Eds.) *Electron microscopy in molecular biology: a practical approach:* 1-29. Oxford: IRL Press.

Cognet, J. A. H., Pakleza, C., Cherny, D., Delain, E. & Le Cam, E. 1999. 'Static curvature and flexibility measurements of DNA with microscopy. A simple renormalization method, its assessment by experiment and simulation.' *J Mol Biol,* 285, 997-1009.

Deamer, D. 2010. 'Nanopore analysis of nucleic acids bound to exonucleases and polymerases.' *Annu Rev Biophys,* 39, 79-90.

Dedeo, M. T., Duderstadt, K. E., Berger, J. M. & Francis, M. B. 2010. 'Nanoscale protein assemblies from a circular permutant of the tobacco mosaic virus.' *Nano Lett,* 10, 181-186.

Dittrich, P. S. & Manz, A. 2006. 'Lab-on-a-chip: microfluidics in drug discovery.' *Nat Rev Drug Discov,* 5, 210-218.

Draper, D. E. 1999. 'Themes in RNA-protein recognition.' *J Mol Biol,* 293, 255-270.

Durham, A. C., Finch, J. T. & Klug, A. 1971. 'States of aggregation of tobacco mosaic virus protein.' *Nat New Biol,* 229, 37-42.

Eber, F. J., Eiben, S., Jeske, H. & Wege, C. 2013. 'Bottom-up-assembled nanostar colloids of gold cores and tubes derived from tobacco mosaic virus.' *Angew Chem Int Ed Engl,* 52, 7203-7207.

Eiben, S., Stitz, N., Eber, F., Wagner, J., Atanasova, P., Bill, J., Wege, C. & Jeske, H. 2014. 'Tailoring the surface properties of tobacco mosaic virions by the integration of bacterially expressed mutant coat protein.' *Virus Res,* 180, 92-96.

Evenson, D. P., Scotto, A., Pla, D. & de Harven, E. 1978. 'The sizes of RNA subunits isolated from high and low leukaemogenic Friend virus.' *J Gen Virol,* 39, 475-486.

Fraenkel-Conrat, H. & Singer, B. 1959. 'Reconstitution of tobacco mosaic virus. III. Improved methods and the use of mixed nucleic acids.' *Biochim Biophys Acta,* 33, 359-370.

Ge, P. & Zhou, Z. H. 2011. 'Hydrogen-bonding networks and RNA bases revealed by cryo electron microscopy suggest a triggering mechanism for calcium switches.' *Proc Natl Acad Sci U S A,* 108, 9637-9642.

Geiger, F. C., Eber, F. J., Eiben, S., Müller, A., Jeske, H., Spatz, J. P. & Wege, C. 2013. 'TMV nanorods with programmed longitudinal domains of differently addressable coat proteins.' *Nanoscale,* 5, 3808-3816.

Glass, J. & Wertz, G. W. 1980. 'Different base per unit length ratios exist in single-stranded RNA and single-stranded DNA.' *Nucleic Acids Res,* 8, 5739-5751.

Griffith, J. D. & Christiansen, G. 1978. 'Electron microscope visualization of chromatin and other DNA-protein complexes.' *Annu Rev Biophys Bio,* 7, 19-35.

Hall, A. R., Scott, A., Rotem, D., Mehta, K. K., Bayley, H. & Dekker, C. 2010. 'Hybrid pore formation by directed insertion of alpha-haemolysin into solid-state nanopores.' *Nat Nanotechnol,* 5, 874-877.

Harrington, W. F. & Schachman, H. K. 1956. 'Studies on the alkaline degradation of tobacco mosaic virus. I. Ultracentrifugal analysis.' *Arch Biochem Biophys,* 65, 278-295.

Hernandez-Ainsa, S. & Keyser, U. F. 2014. 'DNA origami nanopores: developments, challenges and perspectives.' *Nanoscale,* 6, 14121-14132.

Hernandez-Ainsa, S., Misiunas, K., Thacker, V. V., Hemmig, E. A. & Keyser, U. F. 2014. 'Voltage-dependent properties of DNA origami nanopores.' *Nano Lett,* 14, 1270-1274.

Kebbekus, P., Draper, D. E. & Hagerman, P. 1995. 'Persistence length of RNA.' *Biochemistry,* 34, 4354-4357.

Kleefen, A., Pedone, D., Grunwald, C., Wei, R., Firnkes, M., Abstreiter, G., Rant, U. & Tampe, R. 2010. 'Multiplexed parallel single transport recordings on nanopore arrays.' *Nano Lett,* 10, 5080-5087.

Kleinschmidt, A. K., Lang, D., Jacherts, D. & Zahn, R. K. 1962. 'Preparation and length measurements of the total desoxyribonucleic acid content of T2 bacteriophages.' *Biochim Biophys Acta,* 61, 857-864.

Laemmli, U. K. 1970. 'Cleavage of structural proteins during the assembly of the head of bacteriophage T4.' *Nature,* 227, 680-685.

Larkin, J., Foquet, M., Turner, S. W., Korlach, J. & Wanunu, M. 2014. 'Reversible positioning of single molecules inside zero-mode waveguides.' *Nano Lett,* 14, 6023-6029.

Lehrach, H., Diamond, D., Wozney, J. M. & Boedtker, H. 1977. 'RNA molecular weight determinations by gel electrophoresis under denaturing conditions, a critical re-examination.' *Biochemistry,* 16, 4743-4751.

Lu, B., Stubbs, G. & Culver, J. N. 1998. 'Coat protein interactions involved in tobacco mosaic tobamovirus cross-protection.' *Virology,* 248, 188-198.

Mayer, M. & Yang, J. 2013. 'Engineered ion channels as emerging tools for chemical biology.' *Acc Chem Res,* 46, 2998-3008.

McNally, B., Singer, A., Yu, Z., Sun, Y., Weng, Z. & Meller, A. 2010. 'Optical recognition of converted DNA nucleotides for single-molecule DNA sequencing using nanopore arrays.' *Nano Lett,* 10, 2237-2244.

Miles, B. N., Ivanov, A. P., Wilson, K. A., Dogan, F., Japrung, D. & Edel, J. B. 2013. 'Single molecule sensing with solid-state nanopores: novel materials, methods, and applications.' *Chem Soc Rev,* 42, 15-28.

Müller, A., Eber, F. J., Azucena, C., Petershans, A., Bittner, A. M., Gliemann, H., Jeske, H. & Wege, C. 2011. 'Inducible site-selective bottom-up assembly of virus-derived nanotube arrays on RNA-equipped wafers.' *ACS Nano,* 5, 4512-4520.

Namba, K., Pattanayek, R. & Stubbs, G. 1989. 'Visualization of protein-nucleic acid interactions in a virus. Refined structure of intact tobacco mosaic virus at 2.9 Å resolution by x-ray fiber diffraction.' *J Mol Biol,* 208, 307-325.

Oldenbourg, R., Wen, X., Meyer, R. B. & Caspar, D. L. 1988. 'Orientational distribution function in nematic tobacco-mosaic-virus liquid crystals measured by x-ray diffraction.' *Phys Rev Lett,* 61, 1851-1854.

Panayotatos, N. & Wells, R. D. 1979. 'Recognition and initiation site for four late promoters of phage T7 is a 22-base pair DNA sequence.' *Nature,* 280, 35-39.

Pelcher, L. E. & Halasa, M. C. 1979. 'Factors influencing the production of intermediate particles during alkaline degradation of tobacco mosaic virus: time, pH, salt concentration, and temperature.' *J Virol,* 29, 431-437.

Raghavendra, K., Adams, M. L. & Schuster, T. M. 1985. 'Tobacco mosaic virus protein aggregates in solution: structural comparison of 20S aggregates with those near conditions for disk crystallization.' *Biochemistry,* 24, 3298-3304.

Rego, J. M., Lee, J. H., Lee, D. H. & Yi, H. 2013. 'Biologically inspired strategy for programmed assembly of viral building blocks with controlled dimensions.' *Biotechnol J,* 8, 237-246.

Riou, G. & Delain, E. 1969. 'Electron microscopy of the circular kinetoplastic DNA from *Trypanosoma cruzi*: ocurrence of catenated forms ' *Proc Natl Acad Sci U S A,* 62, 210-217.

Rosa, M. D. 1979. 'Four T7 RNA polymerase promoters contain an identical 23 bp sequence.' *Cell,* 16, 815-825.

Schneider, C. A., Rasband, W. S. & Eliceiri, K. W. 2012. 'NIH Image to ImageJ: 25 years of image analysis.' *Nat Methods,* 9, 671-675.

Stellwagen, N. C., Gelfi, C. & Righetti, P. G. 2000. 'DNA and buffers: the hidden danger of complex formation.' *Biopolymers,* 54, 137-142.

Urban, M., Kleefen, A., Mukherjee, N., Seelheim, P., Windschiegl, B., Vor der Bruggen, M., Kocer, A. & Tampe, R. 2014. 'Highly parallel transport recordings on a membrane-on-nanopore chip at single molecule resolution.' *Nano Lett,* 14, 1674-1680.

Vollenweider, H. J., Sogo, J. M. & Koller, T. 1975. 'A routine method for protein-free spreading of double- and single-stranded nucleic acid molecules.' *Proc Natl Acad Sci U S A,* 72, 83-87.

Yang, S. Y., Yang, J. A., Kim, E. S., Jeon, G., Oh, E. J., Choi, K. Y., Hahn, S. K. & Kim, J. K. 2010. 'Single-file diffusion of protein drugs through cylindrical nanochannels.' *ACS Nano,* 4, 3817-3822.

Yi, H., Nisar, S., Lee, S. Y., Powers, M. A., Bentley, W. E., Payne, G. F., Ghodssi, R., Rubloff, G. W., Harris, M. T. & Culver, J. N. 2005. 'Patterned assembly of genetically modified viral nanotemplates *via* nucleic acid hybridization.' *Nano Lett,* 5, 1931-1936.

Yuan-Jen, C. & Yun-Shang, C. 1964. 'Polymerization and depolymerization of virus protein II. Kinetic study of the depolymerization action of formamide and sodium dodecyl sulfate on tobacco mosaic virus.' *Acta Biochim Biophys Sin (Shanghai),* 4, 645-651.

Yuan-Jen, C., Yun-Shang, C. & Tien-Chin, T. 1964. 'The polymerization and depolymerization of virus protein I. The depolymerization of TMV protein and the conformational changes of its subunits.' *Acta Biochim Biophys Sin (Shanghai),* 4, 610-621.

Zaitlin, M. & Palukaitis, P. 2000. 'Advances in understanding plant viruses and virus diseases.' *Annu Rev Phytopathol,* 38, 117-143.

Zhou, K., Li, F., Dai, G., Meng, C. & Wang, Q. 2013. 'Disulfide bond: dramatically enhanced assembly capability and structural stability of tobacco mosaic virus nanorods.' *Biomacromolecules,* 14, 2593-2600.

Zimmern, D. 1977. 'The nucleotide sequence at the origin for assembly on tobacco mosaic virus RNA.' *Cell,* 11, 463-482.

Zimmern, D. 1983. 'An extended secondary structure model for the TMV assembly origin, and its correlation with protection studies and an assembly defective mutant.' *EMBO J,* 2, 1901-1907.

Manuscript III

Altintoprak, K., Plettl, A., Marti, O., Gliemann, H. & Wege, C. 2015. 'Mineralization of peptide-equipped viral nanorings.'

Authorship responsibilities

Altintoprak:

- Development of experimental strategy
- CP preparation, VLP assembly
- Native and denaturing gel electrophoresis
- TEM analysis
- Chemical modification of VLPs
- Mineralization procedure
- Data acquisition and interpretation
- Preparation of all figures and tables
- Data discussion against background of previous publications
- Writing and editing of the manuscript

Plettl, Marti and Gliemann:

- Basic project design (jointly with Wege), advice and repeated discussion

Wege:

- Basic project design (jointly with Plettl, Marti and Gliemann), guidance and constant discussion
- Editing suggestions and proofreading

Mineralization of peptide-equipped viral nanorings

Klara Altintoprak[1], Alfred Plettl[2], Othmar Marti[3], Hartmut Gliemann[4] and Christina Wege[1]

[1]Dpartment of Molecular Biology and Plant Virology, Institute of Biomaterials and Biomolecular Systems, University of Stuttgart, Pfaffenwaldring 57, 70569 Stuttgart, Germany
[2]Institute of Solid State Physics, University of Ulm, Albert-Einstein-Allee 11, 89081 Ulm, Germany
[3]Institute for Experimental Physics, University of Ulm, Albert-Einstein-Allee 11, 89081 Ulm, Germany
[4]Institute of Functional Interfaces (IFG), Karlsruhe Institute of Technology, Hermann-von-Helmholtz-Platz 1, 76344 Eggenstein-Leopoldshafen, Germany

Abstract

The fabrication of well-defined mineralized nanoscale structures is still a challenging task, though interesting for numerous applications. The selective and controllable precipitation of minerals is especially difficult to achieve at the interface of biological and synthetic materials, since the biogenic components require mild conditions. Since natural components may offer precise shapes attractive for being used as templates for the deposition of inorganic shells, however, compatible methods for mineral precipitation are a matter of continuous research. In this work, nano-building blocks were generated based on the self-organization process of plant viral coat proteins (CP) and single-stranded (ss)RNA strands, assembling into short four-turn nucleoprotein helices of a disk-like structure. To investigate the mineral deposition at the outer surface of these particles, they were functionalized with silica precipitation-inducing peptides and subjected to silicification in aqueous precursor solutions under different conditions (pH 4.0, 5.5 and 7.0). The peptides applied, consisting of alternating lysine and aspartic acid (KD) residues, were previously proven to induce well-controllable silica precipitation in the presence of the precursor tetraethyl-orthosilicate (TEOS) and ethanol. Due to an inherent instability of the viral “disks” in ethanol-containing liquids, this study delimited novel protocols enabling the use of the respective peptides to obtain evenly precipitated silica shells around the “disks”. Two different silica precursors (TEOS and tetramethyl-orthosilicate [TMOS]) were examined in the absence of ethanol. Best results of highly site-specific silica formation at the peptide-equipped outer “disk” rim were obtained with TMOS at low pH (5.5) and low ionic strength.

Introduction

Bio-inspired mineralization of functionalized carrier materials is subject of intense research due to a growing interest in externally controlled tooth and bone regeneration (Kirkham et al. 2007, Semino 2008, Martins-Junior et al. 2013, Tenenbaum & Heersche 1982, Bhattacharya et al. 2011, Chung et al. 2011), surface nano-patterning e.g. for array applications (Coffman et al. 2004, Lee et al. 2011), the production of nano-electronic devices (Yamashita 2008, Kisailus et al. 2006) and drug-delivery systems (Tang et al. 2012), or the generation of self-healing materials (van der Zwaag et al. 2009). Immobilization of mineralization-inducing peptides on synthetic nanoscale scaffolds or bio-templates, such as carbon nanotubes (CNT) or viruses, respectively, was demonstrated to yield efficiently mineralized nanoparticles (Aljabali et al. 2011b). This strategy provides the opportunity to characterize the mineralization-guiding effects of different peptides conjugated to defined structures, e.g. bio-templates or CNTs, without exorbitant efforts. Bio-templates such as viruses allow the structuration of surfaces, enhancing the total surface area of nanoscopic devices (Royston et al. 2008, Müller et al. 2011, Chiang et al. 2012). Such scaffolds equipped with mineralization-inducing peptides are putatively applicable for the sealing of gaps between the interfaces of different material types, similar to self-healing materials (Müller et al. 2013). The major advantage of naturally occurring mineralization-inducing mechanisms deduced from mineral-precipitating organisms such as diatoms (Kröger 2007, Richthammer et al. 2011) or glass sponges (Cha et al. 1999) is that silica condensation occurs at low temperature, near neutral pH and ambient pressure. The key elements of the mineralization in these organisms are proteins. The most prominent examples are the lysine-rich silaffin proteins of the diatoms (Kröger et al. 1999) and the enzyme silicatein of the glass sponges (Cha et al. 1999). Based on the mineral precipitation mechanisms promoted in the presence of these proteins, a variety of different peptides and biomimetic approaches were designed to accomplish and investigate mineral formation under various conditions (Baio et al. 2014, Zane et al. 2014, Kuno et al. 2011, Lechner & Becker 2013, Yildirim et al. 2011, Kisailus et al. 2005, Kisailus et al. 2006, Polini et al. 2012). These pioneer works provide insight into, and the prediction of peptide mineralization performance in solution or after immobilization onto a scaffold surface, allowing the formation of well-defined structures like spheres, networks or tubes. Biomineralization-directing peptides and protein domains from diatoms are mainly

based on the basic amino acid lysine alternating with rather negatively charged or polar amino acid residues (aspartic acid, glutamic acid or serine). These silaffins are post-translationally modified, whereby lysine residues are methylated (R-N-CH_3) or covalently bound to polyamines and serine residues are phosphorylated (R-O-PO_3H^-; Sumper & Brunner 2008). Deduced from this principle of alternating positively and negatively charged amino acid residues, Kuno et al. (2011) validated a charge relay effect for a peptide composed of five repetitively arranged lysine-aspartic acid $(KD)_5$ motifs. Compared to block-wise-arranged lysine-aspartic acid residues, the alternating order of the amino acids induces silica precursor (TEOS) conversion in a sol-gel process with high efficiency, resulting in silica spheres of around 500 nm diameter if used in the absence of immobilization template (Kuno et al. 2011). Because of this convincing silica precipitation performance, we previously investigated the mineralization-directing efficiency of such peptides, containing different repeats of the KD motif ($(KD)_5$ and $(KD)_{10}$), after immobilization on a structuring template. The peptides were coupled by chemical conjugation to the plant-infecting pathogen tobacco mosaic virus (TMV), and site-specific silica deposition was achieved on the resulting peptide-equipped TMV particles, contrary to plain viruses such as wild type TMV (TMV_{wt}) and the mutated variant serving as peptide carrier (Altintoprak et al. 2015).

Similar to previously generated artificial viral building blocks of metallized disk-like structures (Zahr & Blum 2012), we have recently tailored both length and surface of TMV to obtain biomolecular nanorings (see **Manuscript I**). They represent a species of highly uniform building blocks apt to various technical applications, including uses as nanoporous compounds after immobilization in suitable devices. Such integration into distinct materials is envisaged by help of an annular silica shell serving as a glue, which might be spatially directed to the outer nanoring rim by mineralization-inducing peptides. A typical TMV particle is composed of 2130 identical coat proteins (CP), encapsidating a single-stranded RNA (ssRNA) molecule, which is the viral genome. Generally, the TMV particle length is 300 nm with a diameter of 18 nm and an inner channel of 4 nm width (Butler 1999, Zaitlin & Palukaitis 2000). Purified CPs assemble under appropriate conditions (ionic strength, pH, temperature and CP concentration) into an intermediate ring-like protein aggregate of 34 CP subunits, which is commonly known as “20S” aggregate and does not contain any RNA. In the early beginning of self-assembly research it was demonstrated that this aggregate together

with ssRNA was necessary for the TMV particle assembly process *in vitro* under the conditions tested (Fraenkel-Conrat & Williams 1955). The nucleation of the corresponding assembly reaction is initiated by a specific secondary RNA structure, a stem-loop, termed the origin of assembly (OAs; Turner et al. 1988). The length of TMV particles can be defined by that of the RNA (Rego et al. 2013, Eber et al. 2013). RNAs of different length containing the OAs were shown to assemble into rod-shaped structures (Rego et al. 2013, Müller et al. 2011, Eber et al. 2013). In principle, it is possible to receive ring-shaped CP disks devoid of RNA under properly adjusted conditions (pH, ionic strength or temperature), or upon use of adapted, genetically modified CPs (Durham et al. 1971, Durham & Klug 1971, Zhou et al. 2013, Butler et al. 1992, Miller et al. 2007). For the production of versatile nanorings for applications in robust biohybrid devices, however, we opted for the RNA-guided strategy since minor alterations of buffer conditions and temperature affect the aggregation of the CP intermediates and thus may degrade plain CP complexes (Schlick et al. 2005). Consequently, CPs (proto-helices or disks) were stabilized by short RNAs of 204 nucleotides (nt), inducing the assembly into four-turn helices (see **manuscript I**), which are termed “disks” or short virus-like particles (VLPs) hereafter.

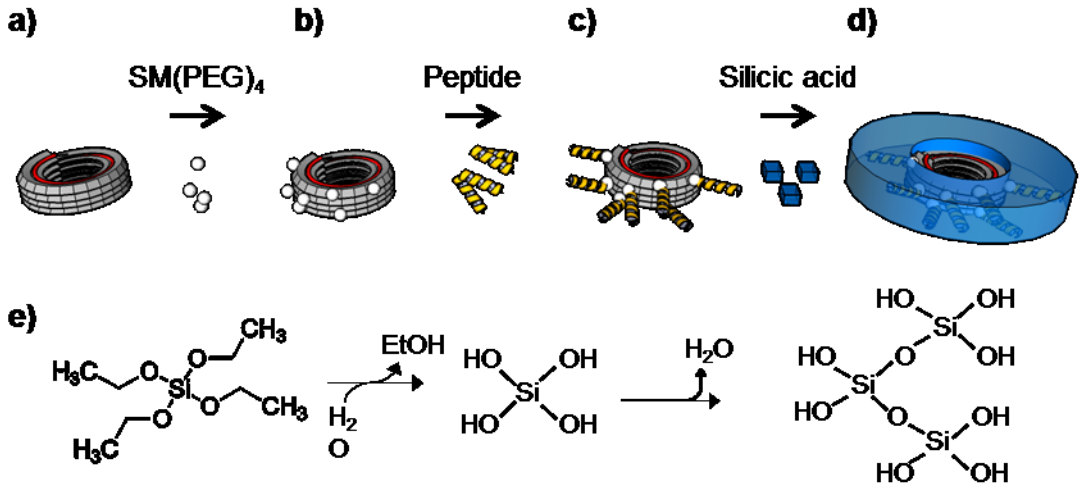

Figure 1: Outline of chemical modification strategy and silicification of “disks”. **(a)** Four-turn helix of a short virus-like particle termed “disk” consisting of a short RNA containing the TMV origin of assembly (OAs) and about 68 genetically engineered coat proteins (CP_{Lys}), each exposing an amino group allowing coupling chemistry at the outer particle surface. **(b)** Conjugation of hetero-bifunctional crosslinker molecules (succinimidyl-[(N-maleimidopropionamido)-tetraethyleneglycol] ester ($SM(PEG)_4$) and **(c)** subsequent coupling of silica-deposition inducing peptides $(KD)_{10}C$. **(d)** Incubation with tetraethyl-orthosilicate (TEOS) hydrolyzed into a silicic acid precursor results in condensation of a silica shell around the peptide-equipped “disk”. **(e)** Alkoxysilane (e.g. TEOS) hydrolysis and silica condensation reaction.

Additionally, the CP can be genetically engineered to a certain extent, introducing functional groups for chemical coupling or selective material accumulation (Geiger et al. 2013, Jung & Yi 2014, Ma et al. 2008, Dedeo et al. 2010, Eiben et al. 2014, Lee et al. 2005, Kadri et al. 2011). For the functionalization of the four-turn helices, a mutated coat protein (CP_{Lys}), which is genetically modified by the amino acid exchange T158K (Geiger et al. 2013), was used for assembly, providing amino groups for chemical coupling of succinimidyl (NHS) ester-activated molecules (**Figure 1**). In **Figure 1** the coupling strategy applied in this work and the subsequent mineralization process is outlined as explained in detail in **manuscript IV** or Altintoprak et al. (2015).

According to Altintoprak et al. (2015), the $(KD)_{10}C$ peptides identified as modification enabling a controllable silification of TMV rods were expected to improve silica precipitation also at the chemically identical “disk” surface, in comparison to plain “disks”. As described above, the induction of silica precipitation was attributed to a charge relay mechanism of the KD motif (Kuno et al. 2011), which probably guides the polymerization of silicic acid resulting in silica deposition. Both silica precipitation reactions performed either with plain peptides $(KD)_5$ (Kuno et al. 2011) or with $(KD)_{10}C$ immobilized at TMV rods (Altintoprak et al. 2015) were carried out in an aqueous solution supplemented with 40 % ethanol. Usually, biogenic components, e.g. TMV, are prone to denature in organic solvents such as alcohols (Lee et al. 2008). Alternatively, organic solvent free reaction conditions can be used to mimic biological silica forming mechanisms (Kröger et al. 1999, Haase et al. 2011, Zane et al. 2014, Pouget & Grelet 2013). For silica condensation (see Figure 1 e) devoid of alcohols, commonly used precursors like alkoxysilanes (tetraethyl-orthosilicate [TEOS] or tetramethyl-orthosilicate [TMOS]) are hydrolyzed under acidic conditions (HCl) or in pure water into silicic acid molecules which undergo condensation in the presence of bio-templates, e.g. mineralization-inducing peptides, resulting in silica precipitates (Kröger et al. 1999, Baio et al. 2014, Zane et al. 2014, Pouget & Grelet 2013).

The hydrolysis-condensation process of the alkoxysilanes is affected by different parameters such as pH value, temperature, ionic strength (Belton et al. 2010) and polarity of the alkoxy groups (Bernards et al. 1991). With increasing pH, the size of the resulting silica particles increases (Belton et al. 2012), potentially impairing homogenous silica shell formation along the bio-template surfaces applied. With

increasing temperature, the activation energy of the condensation-hydrolysis reaction gets reduced, enhancing the probability of effective molecule collision during the reaction process and thus accelerated silica formation (Belton et al. 2010). Hence, it is not excluded that an increase in temperature is combined with unspecific condensation in the aqueous environment. Furthermore, silica oligomerization is also enhanced at high ionic strength, in neutral pH range and supersaturated monomeric silica solution (Icopini et al. 2005). Finally, the reaction velocity of alkoxysilane hydrolysis into silicic acid is dependent on the polarity of the alkoxy groups; the lower the polarity, the higher the hydrolysis rate (Bernards et al. 1991).

To obtain evenly covered bio-template surfaces without unspecific condensation, all these factors have to be taken into account for achieving a site-directed silica enrichment at the "disk" rim. Thus, after testing the original TMV mineralization protocol employing an ethanolic TEOS precursor solution, hydrolysates of two different alkoxysilanes (TEOS- and TMOS-derived silicic acids) were compared with respect to a specific mineral shell formation around the "disks". Additionally, because a higher condensation rate is expected at neutral pH (Icopini et al. 2005), the silicification performance was examined not only at pH 5.5, according to the reaction conditions of whole TMV particles (Altintoprak et al. 2015), but also at pH 7.0. Silica shell formation was analyzed by monitoring the primary contrast of the electron deflection of pure silica upon transmission electron microscopy (TEM) of "disks" without additional negative contrasting.

Materials and methods

Fabrication of RNA-stabilized TMV "disks"

TMV CP disks or proto-helices were stabilized with short RNAs of 204 nucleotides (nt) length containing the TMV OAs. For cloning and synthesis procedures see **manuscript I**. Basically, the 204^{+} nt RNA was synthesized by *in vitro* transcription by means of a MEGAscript® T7 High Yield Transcription Kit (Ambion, Austin, USA). A short TMV genome fragment, containing the TMV core OAs (position 5350-5531; Zimmern 1983), fused to the T7 RNA polymerase promoter sequence (Rosa 1979, Panayotatos & Wells 1979) was applied as *in vitro* transcription template (**Table S1**, **manuscript I**). In a 20 µl volume, 100 µg DNA-template was incubated for 6 h at 37 °C during the *in vitro* transcription reaction. The DNA-template was degraded by DNaseI treatment for 15 min at 37 °C. The synthesized RNA was precipitated by the

addition of lithium chloride (final concentration (f. c.) 1.3 M), EDTA (f. c. 8.6 mM) and ethanol (f. c. 71 % (v/v) over night at -20 °C. After centrifugation according to the supplier's information, the pellet was washed with 1 ml 70 % (v/v) ethanol and dissolved in DMDC-(dimethyl dicarbonate)-treated deionized water (ddH_2O; 18.3 MΩ cm; purified by a membraPure system, Aquintus, Bodenheim, Germany) to a final concentration of 3 µg/µl and stored at -80 °C.

RNA-free CP was prepared by acidic degradation of whole TMV particles (Fraenkel-Conrat & Williams 1955). For "disk" assembly, a genetically engineered TMV mutant, TMV_{Lys}, was used (Geiger et al. 2013). A 10 mg/ml TMV_{Lys} solution was mixed in a 1:3 ratio (v/v) with glacial acetitc acid and incubated for 20 min on ice. Released RNA was removed by centrifugation for 20 min at 20,000 x g and 4 °C. The CP-containing supernatant was dialyzed against ddH_2O in a dialysis tube (Spectra/Por®7 Dialysis Membrane, 8 kDa molecular weight cut-off [MWCO], Spectrum Laboratories, Rancho Dominquez, USA) with water changes every 8 h at 4 °C. As soon as the proteins started to flocculate (after 24 to 48 h), the dialysate was centrifuged as above. The resulting CP pellet was dissolved in 75 mM sodium potassium phosphate buffer (SPP) pH 7.2 and centrifuged for 10 min at 10,000 x g to remove aggregated CP_{Lys}. The supernatant was transferred to a new reaction tube. The CP concentration was determined by a NanoDrop ND-1000 spectrophotometer (PeqLab, Erlangen, Germany) at a wavelength of 280 nm, using the extinction coefficient of TMV CP (1.3 ml mg^{-1} cm^{-1}; Raghavendra et al. 1985), adjusted to 10 mg/ml and incubated for at least 48 h at room temperature to allow disk formation according to Butler (1972).

For a typical assembly reaction, 66 µg RNA were incubated with 1000 µg CP_{Lys} with an f. c. of 0.9 µg/µl RNA and 6.8 mg/ml CP_{Lys} in 75 mM SPP (pH 7.2) for 16 h at 30 °C. Nucleoprotein assemblies in 75 mM SPP (pH 7.2) were stored at 10 °C without any further purification.

Functionalization of "disks" with mineralization-inducing peptides

RNA-stabilized "disks" were functionalized *via* the amino groups of the genetically modified CP_{Lys}, which are exposed at the outer "disk" rim, with a heterobifunctional crosslinker.

In a volume of 120 µl RNA-stabilized "disks" (f. c. 5.1 mg/ml with regard to CP_{Lys} amount) in SPP (f. c. 75 mM, pH 7.2) were incubated with the bifunctional linker $SM(PEG)_4$ (f. c. in the reacation 1.2 mM, succinimidyl-[(N-maleimidopropionamido)-tetraethyleneglycol] ester (Thermo Scientific, Karlsruhe, Germany) stored in dimethyl

sulfoxide (f. c. in the reaction 0.001 %) at -20 °C) for 2 h under agitation (horizontal shaking at 500 rpm) at 30 °C. Excess crosslinker was removed by gel filtration using PD10 SpinTrap G-25 columns (GE Healthcare, Freiburg, Germany) which were equilibrated with 75 mM SPP at pH 7.2. This step was repeated twice. Subsequently, the purified crosslinker-functionalized "disks" (f. c. of 3.4 mg/ml), providing maleimide groups for chemical conjugation, were incubated in a total volume of 105 µl with 0.3 mg/ml (f. c.) $(KD)_{10}C$ (dissolved in dimethylformamide, f. c. in coupling reaction 0.05 %) in SPP (f. c. 75 mM, pH 7.2) to couple the peptides *via* their thiol group at the C-terminal cysteine residue. The total volume of peptide functionalized "disks" was purified by gel filtration as above. Immediately before mineralization, 75 mM SPP buffer (pH 7.2), containing functionalized or unmodified "disks" (in a volume of 105 µl with a f. c. of 2 mg/ml relating to the CP_{Lys} amount), was exchanged by gel filtration as above, however, using PD10 SpinTrap G-25 columns equilibrated with ddH_2O.

Characterization of functionalized "disks"

The ratio of chemically modified to unmodified CP_{Lys} subunits per "disk" was determined by denaturing SDS-PAGE (sodium dodecyl sulphate polyacrylamide gel electrophoresis) according to Laemmli et al. (1970). An amount of 3 µg "disks" was heated for 5 min at 95 °C in sample buffer (f. c.: 50 mM Tris-HCl (tris-(hydroxymethyl)-aminomethane hydrochloric acid) pH 6.8, 2 % (w/v) SDS, 0.1 % (w/v) bromophenol blue, 10 % glycerol, 100 mM dithiothreitol) and separated on a 15 % polyacrylamide gel. Proteins were fixed in the gels (10 % acetic acid, 40 % ethanol) for 15 min and stained with Coomassie Brilliant Blue R250 (Serva Electrophoresis, Heidelberg, Germany).

The electrophoretic mobility of whole "disks" after chemical modification was compared to non-modified "disks" by native gel electrophoresis. An amount of 12 µg "disks" were combined with sample buffer (f. c.: 10 mM SPP pH 7.2, 0.1 % (w/v) bromophenol blue, 10 % glycerol) and separated on a 2.7 % agarose gel (Biozym Sieve 3:1 Agarose, Biozym, Hessisch Oldendorf, Germany) in 1 x TBE (89 mM Tris base, 89 mM boric acid, 2 mM EDTA). Proteins in the agarose gel were fixed and stained just as in the SDS-PAGE gels.

The structural integrity of the functionalized and unmodified "disks" stored in ddH_2O for three days at 10 °C was determined by TEM analysis. A volume of 15 µl "disk" solution was dropped on Parafilm M® (American National Can, Menasha, USA) with a concentration of 0.05 mg/ml CP_{Lys}. A carbon/Formvar®-covered 400-mesh copper

grid (Science Service, Munich, Germany) was placed onto the droplet for 5 min. Excess solution was removed from the grids with filter paper, which were washed with three droplets of ddH_2O. Samples on the grid were stained with 15 µl 2 % (w/v) uranyl acetate for 3 min. After removing residual uranyl acetate with a filter paper, the grids were air-dried and analyzed with a Tecnai G2 Sphera electron microscope (FEI, Hillsboro, USA) at 120 kV using a 16 megapixel camera TemCam F416 (TVIPS, Gauting, Germany).

Mineralization of functionalized "disks"

Chemically modified or plain "disks" were treated with 10 % TEOS in 40 % ethanol in initial experiments according to Altintoprak et al. (2015), or TEOS or TMOS using protocols established in this study on the basis of different references (Pouget & Grelet 2013, Kröger et al. 1999, Zane et al. 2014, Haase et al. 2011). From TEOS, a silicic acid precursor solution was prepared by hydrolyzing 22.4 µl TEOS in 77.6 µl 1 mM HCl (with a f. c. of 1 M TEOS and 0.78 mM HCl) for 10 min at room temperature (modified from Pouget & Grelet 2013). A volume of 11.2 µl of the resulting silicic acid solution was added to 22.5 µl 2 mg/ml "disks" (to a f. c. of 0.26 mM HCl with an ionic strength of 1.3 10^{-7} M and 1.3 mg/ml "disks"; silicic acid of unidentified concentration) and incubated for 24 h or four days under agitation (500 rpm in a horizontal shaker) at 15 °C. The pH value was measured in the beginning of the mineralization reaction and after 24 h and 4 days with a pH meter (SevenCompact™ pH/Ion, Mettle-Toledo, Giessen, Germany) equipped with a special electrode (InLab® Micro, Mettle-Toledo, Giessen, Germany). To remove excess silicic acid, the silicification solution containing "disks" was dialyzed three times against 200 ml ddH_2O at 4 °C with ddH_2O changes every 1 h, using Slide-A-Lyzer™ MINI Dialysis Devices (10K MWCO, Thermo Fischer Scientific, Darmstadt, Germany). Silica accumulation on the "disks" was analyzed by TEM as above, however, without uranyl acetate staining.

For silicification with the starting compound TMOS, a silicic acid precursor solution was prepared (modified from Kröger et al. 1999, Haase et al. 2011, Zane et al. 2014) by hydrolyzing 15 µl TMOS in 85 µl 1 mM HCl for 5 min at room temperature to obtain a 1 M silicic acid solution (final concentration of 0.85 mM HCl). To investigate the influence of the pH value two different reaction mixtures at pH 5.5 or 7.0 were prepared. For mineralization at pH 5.5, functionalized or unmodified "disks" (f. c. 1.3 mg/ml) in ddH_2O were mixed with silicification solution to a f. c. of 20 mM

hydrolyzed TMOS and 0.017 mM HCl with an ionic strength of $8.5\ 10^{-9}$ M and incubated for 30 min under agitation at 23 °C. For the silicification reaction at pH 7.0, the same mixture was prepared, however, in the presence of 20 mM Tris-HCl pH 7.0 and incubated for 30 min as above. The pH was measured in the beginning of the mineralization and after 30 min as above. Excess silicic acid was removed by dialysis against three times 500 ml ddH_2O at 4 °C with ddH_2O changes every 1 h, using Slide-A-Lyzer™ MINI Dialysis Devices (10K MWCO, Thermo Fischer Scientific, Darmstadt, Germany).

Silica accumulation on the "disks" was analyzed by TEM analysis as above, however, without uranyl acetate staining.

Results and discussion

Viral "disks" functionalized with mineralization-inducing peptides

Based on the natural self-organization process of plant infecting TMV, a short 204^+ nt RNA, containing the core OAs (Zimmern 1983: plus (+) indicates the presence of the OAs, for details see **manuscript I**), was used to generate four-turn helical structures, termed "disks" in the following. These short VLPs consist of genetically modified coat proteins (CP_{Lys}), which expose per CP_{Lys} subunit one additional amino group (Geiger et al. 2013). "Disk" aggregates composed of CP_{Lys} are indicated as "disk"-Lys in the following. Their functional groups allow chemical modification by succinimidyl ester-activated molecules at the outer "disk" rim. As described previously, mineralization specificity and efficiency can be improved by the immobilization of mineralization-inducing peptides on plant virus templates (Aljabali et al. 2011b, Altintoprak et al. 2015). For TMV_{Lys} particles equipped with such peptides a well-controllable slow and site-directed silica precipitation occurred, in comparison to the peptide-free plain or linker-coated TMV_{Lys} scaffold, as well as to TMV_{wt} particles lacking exposed amino groups. Since there was no detectable silica precipitate forming around TMV_{wt} nanotubes, "disks" consisting of CPwt were not investigated in this study. The "disk"-Lys was chemically modified with mineralization-guiding peptides as follows: In a first step, the "disk"-Lys rim was functionalized with a hetero-bifunctional crosslinker, $SM(PEG)_4$, which was conjugated *via* its reactive NHS ester to the amino groups of the genetically optimized CP_{Lys}, resulting in crosslinker-functionalized "disk"-PEG. Subsequently, mineralization-inducing peptides ($(KD)_{10}C$; Kuno et al. 2011, Altintoprak et al. 2015) were conjugated *via* their C-terminal cysteine thiol groups to

the maleimide of the crosslinker exposed on the “disk”-PEG surface. In the following, these peptide-equipped “disks” are named “disk”-KD10.

The ratio of chemically modified and unmodified CP_{Lys} subunits was determined by SDS-PAGE analysis (**Figure 2 a**). After reaction with $SM(PEG)_4$, more than 50 % of the ≈68 CP_{Lys} subunits per "disk" were functionalized with the hetero-bifunctional crosslinker, which then could be conjugated to peptides with nearly 100 % efficiency. This means that one “disk”-KD10 provides a heterogeneous surface of roughly 50 % unmodified and 50 % peptide-equipped CP_{Lys}.

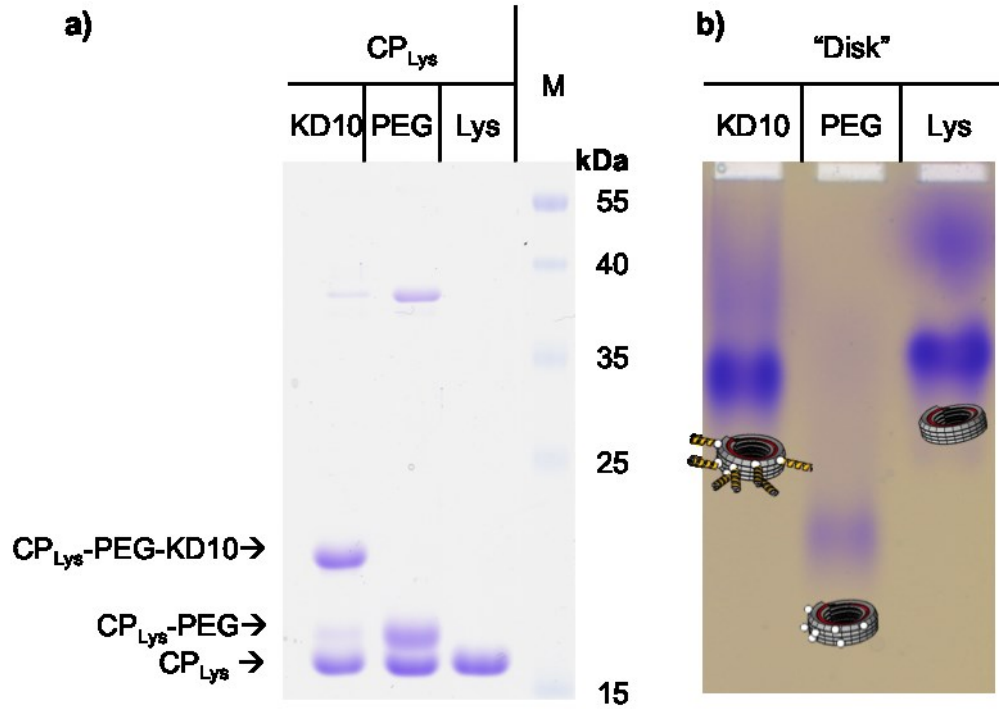

Figure 2: Electrophoretic analysis of chemically modified “disks”. **(a)** TMV CP_{Lys} characterized by denaturing SDS-PAGE analysis. After conjugation of the heterobifunctional crosslinker $SM(PEG)_4$ (CP_{Lys}-PEG), a second band of reduced electrophoretic mobility compared to non-modified CP_{Lys} (Lys) subunits appears. Conjugation of peptide $(KD)_{10}C$ (KD10) introduces a further band shift due to increased molecular weight (15 % acrylamide stained with Coomassie Brilliant Blue R250). **(b)** Native gel electrophoresis of whole “disks” shows differences in electrophoretic mobility after chemical modification. The heterobifunctional crosslinker (PEG) increases the migration velocity due to an enhanced overall negative charge on the particles’ surface, while addition of the peptide $(KD)_{10}C$ (KD10) neutralizes the charge of the crosslinker (2.7 % agarose gel stained with Coomassie Brilliant Blue R250) resulting in a lower particle mobility.

Additionally, the electrophoretic mobility of chemically modified “disk”-PEG and -KD10 was compared to non-modified “disk”-Lys by native agarose gel electrophoresis (**Figure 2 b**). “Disk”-PEG functionalized with $SM(PEG)_4$ migrated with increased mobility compared to non-modified and peptide-coupled “disks”, as the peptides almost reconstituted the initial total surface charge of the plain “disk”-Lys. Corresponding alterations of the electrophoretic mobilities, caused by the distinct

chemical modifications, was observed for whole TMV particles as well (Altintoprak et al. 2015).

For first tests on the mineralization reaction, “disks” were diluted in ddH_2O of pH 5.5. This low pH is due to the dissolved carbonic acid which is in equilibrium with atmospheric CO_2 at pH 5.5 (Hunter 1981). Concerning the assembly behavior of TMV, it is described in the literature that aggregation into long rods is expected at acidic pH values (Durham et al. 1971). Hence, the structural integrity and dispersion of four-turn helices in ddH_2O was determined by TEM (**Figure 3**). The TEM images indicate that “disks” stored at pH 5.5 for three days at 10 °C maintained their initial structure of four-turn helices without forming head-to-tail aggregates, as they usually occur under acidic conditions (Niu et al. 2006). The integrity of the “disk” preparations at pH 5.5 is presumably due to the absence of salt, since head-to-tail formation is not induced at low ionic strength (Durham et al. 1971). Thus, the identified aqueous conditions which were previously established for silica precipitation on TMV particles equipped with silica-directing peptides (Altintoprak et al. 2015) seemed to be also applicable for “disk” mineralization.

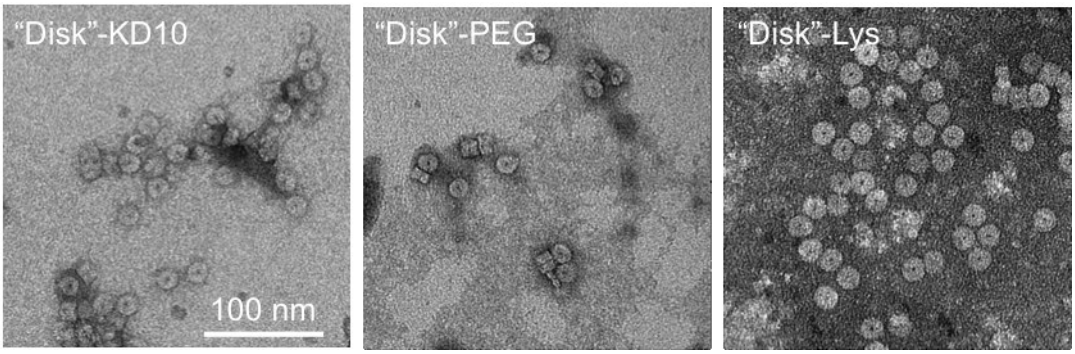

Figure 3: “Disks” stored for three days in ddH_2O (pH 5.5) at 10 °C retain their typical structure without assembling into head-to-tail aggregates (as indicated). TEM analysis of uranyl acetate negatively stained “disks”.

Peptide-directed silica precipitation around “disks”

As shown previously, the thickness of silica layers precipitating at the surface of peptide-equipped TMV rods can be controlled by the incubation time in a sol-gel process in a TEOS-ethanol-water (1:4:4) mixture (Altintoprak et al. 2015). Following this strategy, “disks” were subjected to the same conditions. However, different from intact TMV, the short disk-like structures investigated in this study proved to be instable in a 40 % (v/v) ethanol solution. As demonstrated by Bernards et al. (1991), the hydrolysis and condensation reaction of an alkoxysilane-alcohol mixture decreased with decreasing water content, which allowed to slow down mineral

deposition by means of the ethanol amount added. This fact was specifically important for obtaining kinetic control over the silica shell thickness on TMV rods. In turn, since the initial investigations indicated that the “disks” were degraded in the presence of ethanol, the conditions used for the peptide-equipped TMV particles could not be applied for guiding silicification on the outer "disk" rim. Consequently, an alternative mineralization process was selected, which proceeds under mild conditions without ethanol. “Disks” functionalized with mineralization-inducing peptide $(KD)_{10}C$ or with $SM(PEG)_4$ only, or unmodified VLPs were subjected to mineralization processes, comparing two different silica-forming precursors, hydrolyzed silicic acids generated from TEOS or TMOS, respectively. The TEOS and TMOS hydrolysates were investigated in terms of their silicification capacity in aqueous solution, according to previous bio-inspired mineralization experiments conducted with various silica precipitation-inducing peptides (Kröger et al. 1999, Zane et al. 2014, Haase et al. 2011) or virus templates (Pouget & Grelet 2013). The two different silica precursors were pre-hydrolyzed in HCl solution to convert them into silicic acids of different oligomerization state. In comparison to the decomposition reaction with TMOS, the TEOS/HCl solution remained separated in two phases even after 15 min of shaking, while TMOS converted into silicic acid within 5 min, as apparent from the vanished phase boundary. According to the literature, the different hydrolysis efficiencies are due to the different polarities of the substrates' alkoxy groups, as it was shown that decreasing polarity of these groups results in a decline of the alkoxysilanes' hydrolysis (Bernards et al. 1991). On account of the incomplete conversion of TEOS, solely the aqueous phase containing an unknown silicic acid concentration was used as precursor for silicification of the “disks”, while the TMOS-derived products were applied as prepared. To get a rough idea of the silicic acid content during silicification, we estimated its concentration from published data. The aqueous phase of hydrolyzed TEOS contains around 1 mM silicic acid at pH 6 (Shimada & Tarutani 1979), which is sufficient to mineralize hydrophilic PEGylated M13 bacteriophages, displaying reasonable silica shell formation as described previously (Pouget & Grelet 2013). Referred to these data, the final concentration of silicic acid in the “disk” mineralization reaction employing TEOS-derived precursors was estimated to be around 0.3 mM, whereas those in TMOS-derived preparations was about 20 mM (see experimental section). Consequently, the silicic acid concentration was below supersaturated conditions. Supersaturation of silicic acid in

aqueous solution (around 1-2 mM) results in polymerization into silica (Krauskopf 1956). The silica shell formation from TEOS-derived silicic acid precursors was monitored by TEM-analysis after 24 hours (**Figure 4 a**) and four days (**Figure 4 b**), respectively. The reaction was carried out at a pH of 4.0 in ddH_2O combined with TEOS-derived silicic acid precursors and HCl at 15 °C to reduce the velocity of silica condensation (Belton et al. 2010) and, furthermore, to minimize unspecific polymerization of the silicic acid. The mineralized "disk"-KD10, functionalized with the peptides, clearly shows a spatially specific accumulation of silica around its protein rim, whereas unspecific precipitation of silica is detectable for the peptide-free bio-templates, "disk"-Lys and "disk"-PEG, respectively (**Figure 4 a**).

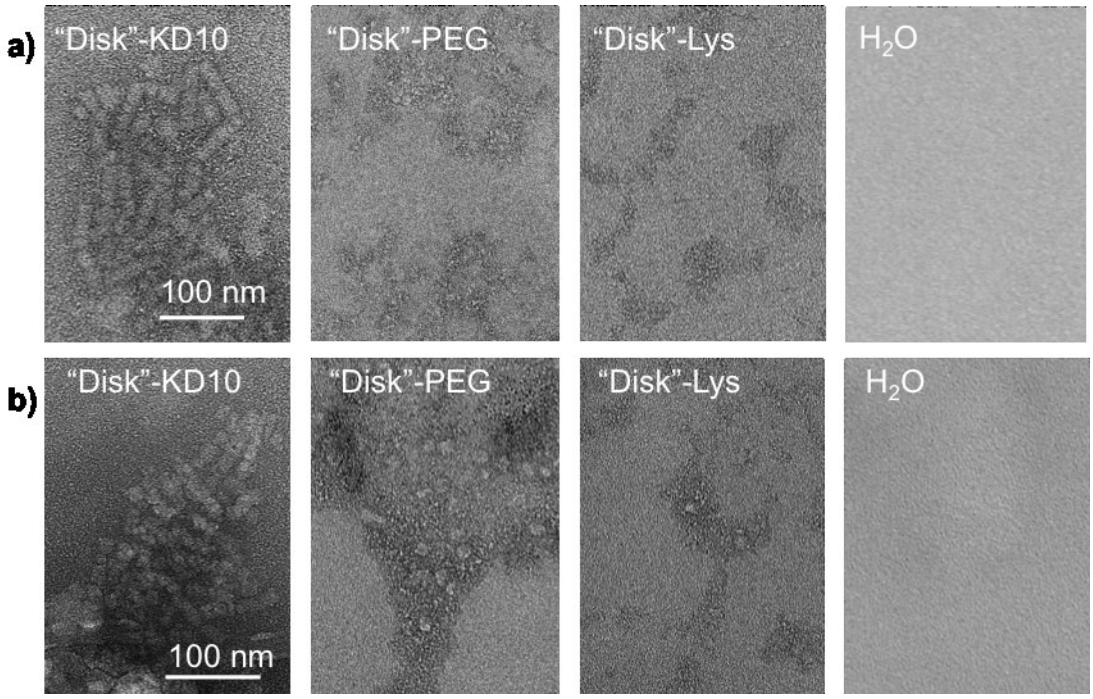

Figure 4: TEM-analysis of silicified "disks" with hydrolyzed TEOS of undefined silicic acid concentration **(a)** after 24 h at 15 °C (inset scale bar: 50 nm), and **(b)** after 4 days at pH 4.0 15 °C (as indicated). "H_2O": control lacking a bio-template (template replaced by water in the reaction mixture). For details, refer to text.

Longer reaction time induced higher contour contrast due to a higher degree of silica precipitation at the "disk"-KD10 rims (**Figure 4 b**), whereas the appearance of both "disk"-Lys and -PEG remained unaffected after the longer exposure to silicic acid. In the course of the ongoing silica precipitation, also an increase in unspecific mineralization for the "disk"-KD10 sample was observed, with electron-dense deposits covering the entire analyzed area of the copper grid after four days (**Figure 4 b**). Since silica formation was not observed for the control reaction with all educts but ddH_2O replacing the bio-templates, the "disks" were assumed to be responsible for the induction of polycondensation and silica precipitation. Based on the above

calculated silicic acid concentration (0.3 mM), the results of “disk” mineralization indicate that the VLPs induced the silica precipitation in an undersaturated silicic acid solution.

Although the silica-forming precursor TEOS thus exhibited appropriate performance, the exact concentration of the silicic acid educt is unknown, restricting concentration-dependent investigations of mineral precipitation. Additionally, under the conditions applied, “disk”-KD10 particles assembled into head-to-tail aggregates (**Figure 4**). This was presumably induced by the HCl added into the reaction mixture, decreasing the pH from 5.5 to 4.0, and increasing the ionic strength from zero to 1.3 10^{-7} M. Head-to-tail aggregation of TMV particles is known to be induced at low pH (Shenton et al. 1999, Lu et al. 1996). Furthermore, increasing ionic strength also enhances the polymerization of TMV CP independent from RNA templates (Paglini & Lauffer 1968, Stauffer et al. 1970). As a result, the short four-turn helices apparently were influenced in their aggregation behavior and assembled into particles of higher aspect ratio (**Figure 4 a** and **4 b**). Furthermore, it was observed that silicified “disks”-KD10 accumulated to small networks of several head-to-tail aggregates stuck together. Such 3D networks are commonly observed in the presence of salt, amines or basic amino acids at neutral and alkaline pH values (Belton et al. 2012). In contrast, “disks” devoid of peptides remained unaffected under these conditions. Such “disks” were scarcely detected by TEM analysis, and were surrounded by unspecific silica precipitates, which might have impeded head-to-tail aggregation or accumulation.

Due to the inefficient hydrolysis of TEOS in HCl and thus uncertain silicic acid concentration, the silicification efficiency at two different pH values was examined using hydrolyzed TMOS as precursor. According to the literature, silicic acid condensates faster at neutral or alkaline pH and forms particles with increased diameter in comparison to low pH values (Belton et al. 2012). To obtain clearly distinguishable effects, a slightly acidic pH at 5.5 in carbon dioxide-saturated ddH_2O, and neutral conditions at pH 7.0 in 20 mM Tris-HCl buffer were selected. Furthermore, the temperature was increased to enhance the silica precipitation velocity (Belton et al. 2010), and the reaction time was reduced to prevent the accumulation of unspecific large silica particles. The silicification reaction was executed for 30 min at 23 °C and the mineral precipitation on the “disk” rims was studied by TEM analysis (**Figure 5 a**). At pH 5.5, the precipitation of a thin electron-

dense layer of silica around the “disk”-KD10 rim was induced. The controls “disk”-Lys and “disk”-PEG were scarcely detectable *via* electron density contrast (**Figure 5 a**), indicating that the peptide improved and guided the silica precipitation under these conditions.

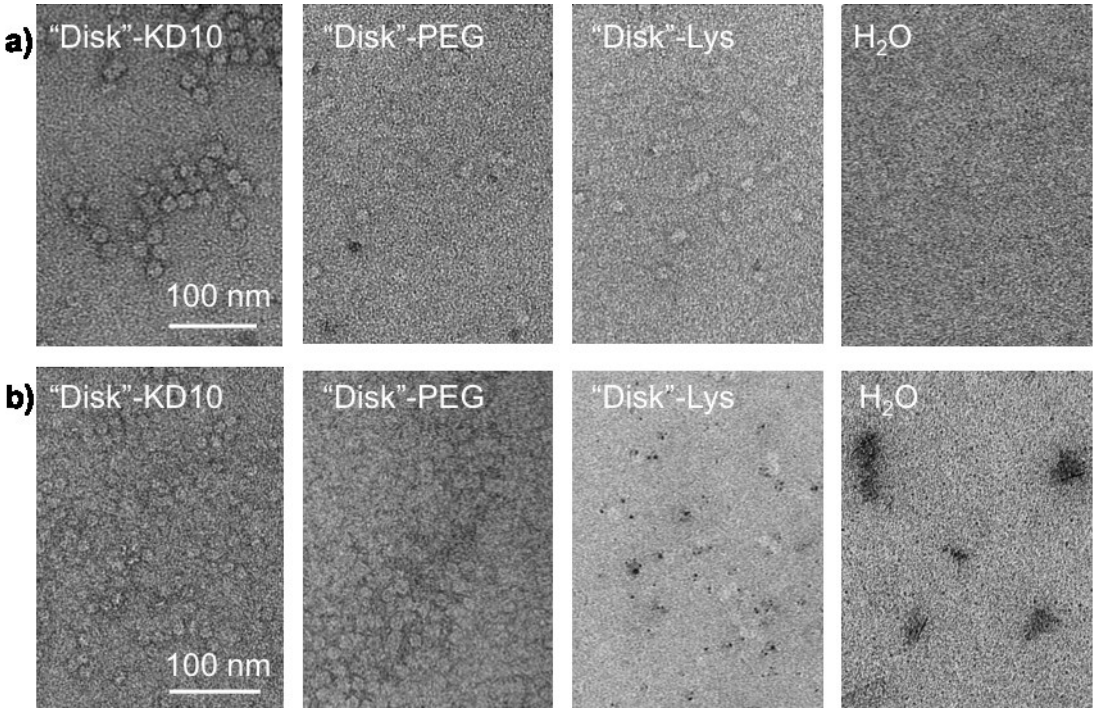

Figure 5: TEM analysis of “disks” silicified with hydrolyzed TMOS. “Disks” were combined with 20 mM silicic acid in an aqueous solution for 30 min at 23 °C **(a)** in ddH_2O at pH 5.5 and **(b)** in 20 mM Tris-HCl at pH 7.0. "H_2O": control lacking a bio-template (template replaced by water in the reaction mixture). For details, refer to text.

Similar to the agglomeration of “disk”-KD10 particles upon incubation with prehydrolyzed TEOS (**Figure 4**), the VLPs silicified from hydrolyzed TMOS at pH 5.5 accumulated locally and attached side-by-side in a monolayer covering the carbon film. However, compared to “disk” mineralization reactions with TEOS-derived silicic acids, no head-to-tail aggregation was detectable. As described above, decreasing pH and increasing ionic strength induce the polymerization of the TMV CP. Because of the different HCl concentrations in the reaction mixtures, the ionic strength (in relation to Cl^- ions) as well as the pH value of the silicification solution differed: 1.3 10^{-7} M at pH 4.0 (TEOS) and 8.5 10^{-9} M at pH 5.5 (TMOS), respectively. Thus, the calculated ionic strength of the reaction with hydrolyzed TMOS was by a factor of 15.3 smaller than with hydrolyzed TEOS, which favored the dispersion of the nucleoprotein "disks". These findings resemble those of earlier systematic analyses on TMV CP or nanotube polymerization: a 10-fold decrease in ionic strength induced depolymerization of TMV CP aggregates at pH 7.5 (Stauffer et al. 1970), whereas at

pH 6.5, head-to-tail aggregation of TMV tubes occurred after increasing the salt concentration (ammonium persulfate) of a TMV-aniline solution (Niu et al. 2006). To our knowledge, for the assembly and disassembly at pH 5.5, comparable data are not available in literature. Conclusively and in fundamental agreement with previous studies, RNA-stabilized four-turn helices retained their structure at low pH in the absence of salt, without undergoing head-to-tail aggregation during silica sheathing from hydrolyzed TMOS precursors. After mineralization reactions at neutral pH 7.0, however, the TEM analysis of silica precipitation from hydrolyzed TMOS indicated mainly unspecific condensation for both “disk”-KD10 and “disk”-Lys templates, resulting in a silica layer that covered the carbon film, or granular structures, respectively (**Figure 5 b**). Although with increasing pH a higher silica condensation rate is expected, and has also been observed in this study (see e.g. “disk”-Lys and H_2O in **Figure 5 b**), silica formation at pH 7.0 was not site-specifically directed to the outer functionalized “disk” rim if compared to the results of “disk”-KD10 at pH 4.0 or 5.5, using prehydrolyzed TEOS or TMOS, respectively (**Figure 4 a** and **5 a**).

Taken together, the silicification experiments carried out with the peptide $(KD)_{10}C$ and hydrolyzed TMOS at different pH values (5.5 and 7.0) in the presence of equal amounts of silicic acid (20 mM), indicate that spatially specific silica accumulation was favored at low pH. This is different from poly-lysine induced silica condensation, which shows optimal polymerization in a pH range of 7.2 to 9.2 promoting the interaction of poly-lysine with the negatively charged silicic acid, and also different from the effect of poly-aspartate which exhibits a slight catalytic activity at pH 4.9, where neutral silicic acid is the predominant form (Coradin & Livage 2001). As silicic acid is supposed to exist in its protonated form at low pH, its interaction possibility with positively charged amino acid residues is generally reduced under acidic conditions (Belton et al. 2010). For the peptide $(KD)_{10}C$, a positive net charge (0.7) is calculated for pH 5.5, and a slightly negative charge (-0.1) at pH 7.0 (Putnam accessed 2015). Hence, at pH 5.5 more than half of the peptides' amino acids are protonated. Thus, the site-specific mineralization of “disk”-KD10 at pH 5.5 could be induced by different mechanisms. According to the literature, negatively charged silica surfaces interact weakly with polar amino acid residues such as serine or histidine as well as with the acidic aspartic acid, forming hydrogen bonds, whereas they interact strongly with protonated lysine (Patwardhan et al. 2012). As the isoelectric point of silicic acid is around pH 2 (El Shafei 2000), silicate molecules are

partially deprotonated at higher pH values. Thus, silicic acid might be attracted by aspartic acid as well as by lysine due to polar and ionic interactions, respectively. Hence, it seems to be favorable to select conditions causing an overall rather positive net charge at the "disk" rim, which induces silica precipitation around the "disks". Alternatively, the spatially selective silica precipitation, which proceeds under unfavorable conditions at pH 5.5 around the "disk"-KD10 rim, might be induced by a so-called charge relay mechanism. This effect was proposed for such peptides with alternating amino and carboxyl groups (Kuno et al. 2011).

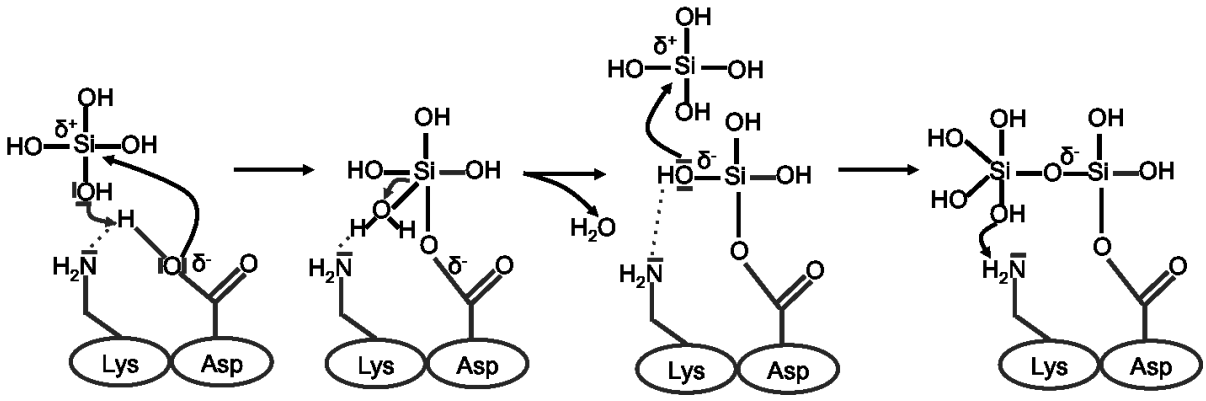

Figure 6: Proposed charge relay effect possible on a "disk"-KD10 rim, as deduced from the mechanism of silicatein-catalyzed orthosilicic acid condensation according to Schröder et al. (2012), and details on the putative charge relay functionality of repetitive KD_x sequences according to Kuno et al. (2011: for details see text).

From this point of view, the mineralization process of the peptide $(KD)_{10}C$ at pH 5.5 might be related to the enzymatically governed silica condensation at the active site of silicatein (Schröder et al. 2012), and thus biological catalysis. Due to the close proximity of protonated amino and negatively charged carboxyl groups under acidic conditions (**Figure 6**), intramolecular hydrogen bond formation between these side chains might be possible, resulting in positive or negative partial charges, respectively. In this model, similar to the interplay between histidine and serine of the silicatein active site, the Si atom of silicic acid can be immobilized by nucleophilic attack of the partially negatively charged oxygen atom of the aspartic acid carboxyl group, in combination with a proton transfer from the lysine amino group and a subsequent water molecule release. Thereafter, polymerization is induced by a nucleophilic attack of the OH group of the covalently bound silicic acid at a second orthosilicic acid molecule. The main advantage of such a charge relay mechanism for spatially selective mineral formation is a reduced unspecific condensation of silica precursors, which possibly occurs under neutral and basic pH or in the presence of catalysts like NH_4OH (Yuwono & Hartgerink 2007). In summary, the charge relay

effect is stronger pronounced under acidic than neutral conditions, presumably due to the proton transfer of the slightly positive peptides, driving the condensation reaction of the silicic acid into silica.

Conclusion

Based on the extensive prior investigations of TMV particles functionalized with several distinct silica precipitation-directing peptides (Altintoprak et al. 2015), the peptide $(KD)_{10}C$ was selected for the functionalization of short TMV-derived helices of about 68 viral CPs stabilized by a ssRNA. These disk-like structures revealed most promising annular silica precipitation at their outer rim.

The in-depth exploration of silica deposition on tailored nano-building blocks of viral origin provides insight in the versatile possibilities such structures offer for new materials fabrication. Under optimized conditions, silicified nanorings of defined shape in the 20 nm range were generated. As a critical point to maintain structural integrity, especially to prevent head-to-tail formation of the “disks” at low pH values, it was found that the salt concentration had to be kept at a minimum level. The different hydrolyzed silica precursors (silicic acids from TEOS and TMOS) precipitated at the peptide-equipped “disk” rim formed a thin annular-shaped shell at pH 5.5 (TMOS) or 4.0 (TEOS), whereas unspecific silica particle formation occurred at neutral pH. A time-resolved analysis of silica precipitation to eventually fine-tune silica shell formation, as carried out previously in a time course experiment over ten days (Altintoprak et al. 2015), was not possible due to the fast condensation of silicic acid in aqueous solutions.

The usage of hydrolyzed TMOS (20 mM) has proven to be more practical than that of TEOS (estimated: 0.3 mM) due to the easier control over the silicic acid concentration during the silicification reaction. To fine-tune the shell thickness, investigations of the silicic acid concentration below supersaturation might enable to optimize silica condensation directed exclusively to the “disk” rim further, and to prevent unspecific polymerization of inorganic silica precursors in solution.

The peptide-equipped nanorings presented in this study are usable for the fabrication of hybrid materials, especially as biological pore adapters similar to α-haemolysin for the insertion into porous solid-state membrane (SSM) templates (Hall et al. 2010). The optimized silicification strategy allows the generation of nucleoprotein nanorings with annular silica shells. Thus, the functionalized “disks” may be able to direct sealing gaps between the nanoporous inorganic SSMs and the protein pore adapters

after insertion *in situ*. The resulting bio-inorganic filter-devices with tightly fastened nanorings of defined protein pore size could be valuable tools to improve molecule sorting routines. The bionic silica "glue" might reduce current or molecule leakage with improved efficiency if compared to hybrid membranes with protein pores embedded in more fragile lipid bilayers (Urban et al. 2014).

However, the "disks" were mineralized dispersed in solution in the current work. Possibly, the mineralization in a narrow gap of around 2 nm width will be a special challenge. As silica deposition at bio-templates is discussed controversially, two different mechanisms have to be considered: First, homogeneous silica aggregation which would start with the condensation of monomeric orthosilicic acid molecules, forming pre-nucleation clusters followed by phase separation and nanoparticle precipitation (Gebauer et al. 2014). These pre-nucleation clusters of around 1 to 3 nm diameter are supposed to interact with bio-templates by electrostatic or ionic interactions (Evans 2013), prior to their transformation into a closed silica shell. Second, heterogeneous silica formation might take place, which is supposed to initiate on the surface of a template which directs the condensation reaction (e.g. biological templates like silicatein; Kisailus et al. 2006). As it is expected that particles larger than 2 nm are incapable to diffuse into the gap between SSM pore and "disk" rim, the respective future investigations could provide insight into the predominant mineralization mechanism occurring in the gap: It might be possible to discriminate between hetero- or homogeneous mineralization, since the first reaction type would probably be more efficient under spatially confined conditions.

Acknowledgments

We like to thank Prof. Dr. Nils Kröger, Prof. Dr. Joachim Bill and Prof. Dr. Helmut Cölfen for the discussion of the mineralization procedure, Prof. Dr. Holger Jeske for continuous support and discussion of the project, Cornelia Kocher to provide protocols and technical support for the TEM analysis, Prof. Dr. Stephan Nussberger and PD Dr. Michael Schweikert for granting access to the TEM, Sigrid Kober for the preparation of TMV particles from tobacco plants, and Diether Gotthardt for taking care of the plants. We are grateful for the financial support of the DFG SPP1569 (DFG-WE-4220/2-1 and -2).

References

Aljabali, A. A. A., Shah, S. N., Evans-Gowing, R., Lomonossoff, G. P. & Evans, D. J. 2011b. 'Chemically-coupled-peptide-promoted virus nanoparticle templated mineralization.' *Integr Biol,* 3, 119-125.

Altintoprak, K., Seidenstücker, A., Welle, A., Eiben, S., Atanasova, P., Stitz, N., Plettl, A., Bill, J., Gliemann, H., Jeske, H., Rothenstein, D., Geiger, F. & Wege, C. 2015. 'Peptide-equipped tobacco mosaic virus templates for selective and controllable biomineral deposition.' *Beilstein J Nanotech,* 6, 1399-1412.

Baio, J. E., Zane, A., Jaeger, V., Roehrich, A. M., Lutz, H., Pfaendtner, J., Drobny, G. P. & Weidner, T. 2014. 'Diatom mimics: directing the formation of biosilica nanoparticles by controlled folding of lysine-leucine peptides.' *J Am Chem Soc,* 136, 15134-15137.

Belton, D. J., Deschaume, O., Patwardhan, S. V. & Perry, C. C. 2010. 'A solution study of silica condensation and speciation with relevance to *in vitro* investigations of biosilicification.' *J Phys Chem B,* 114, 9947-9955.

Belton, D. J., Deschaume, O. & Perry, C. C. 2012. 'An overview of the fundamentals of the chemistry of silica with relevance to biosilicification and technological advances.' *FEBS J,* 279, 1710-1720.

Bernards, T. N. M., Vanbommel, M. J. & Boonstra, A. H. 1991. 'Hydrolysis - condensation processes of the tetra-alkoxysilanes TPOS, TEOS and TMOS in some alcoholic solvents.' *J Non-Cryst Solids,* 134, 1-13.

Bhattacharya, M., Wutticharoenmongkol-Thitiwongsawet, P., Hamamoto, D. T., Lee, D., Cui, T., Prasad, H. S. & Ahmad, M. 2011. 'Bone formation on carbon nanotube composite.' *J Biomed Mater Res A,* 96, 75-82.

Butler, P. J. 1972. 'Structures and roles of the polymorphic forms of tobacco mosaic virus protein. VI. Assembly of the nucleoprotein rods of tobacco mosaic virus from the protein disks and RNA.' *J Mol Biol,* 72, 25-35.

Butler, P. J. 1999. 'Self-assembly of tobacco mosaic virus: the role of an intermediate aggregate in generating both specificity and speed.' *Philos Trans R Soc Lond B Biol Sci,* 354, 537-550.

Butler, P. J., Bloomer, A. C. & Finch, J. T. 1992. 'Direct visualization of the structure of the "20 S" aggregate of coat protein of tobacco mosaic virus. The "disk" is the major structure at pH 7.0 and the proto-helix at lower pH.' *J Mol Biol,* 224, 381-394.

Cha, J. N., Shimizu, K., Zhou, Y., Christiansen, S. C., Chmelka, B. F., Stucky, G. D. & Morse, D. E. 1999. 'Silicatein filaments and subunits from a marine sponge direct the polymerization of silica and silicones *in vitro*.' *Proc Natl Acad Sci U S A,* 96, 361-365.

Chiang, C. Y., Epstein, J., Brown, A., Munday, J. N., Culver, J. N. & Ehrman, S. 2012. 'Biological templates for antireflective current collectors for photoelectrochemical cell applications.' *Nano Lett,* 12, 6005-6011.

Chung, W. J., Kwon, K. Y., Song, J. & Lee, S. W. 2011. 'Evolutionary screening of collagen-like peptides that nucleate hydroxyapatite crystals.' *Langmuir,* 27, 7620-7628.

Coffman, E. A., Melechko, A. V., Allison, D. P., Simpson, M. L. & Doktycz, M. J. 2004. 'Surface patterning of silica nanostructures using bio-inspired templates and directed synthesis.' *Langmuir,* 20, 8431-8436.

Coradin, T. & Livage, J. 2001. 'Effect of some amino acids and peptides on silicic acid polymerization.' *Colloid Surface B,* 21, 329-336.

Dedeo, M. T., Duderstadt, K. E., Berger, J. M. & Francis, M. B. 2010. 'Nanoscale protein assemblies from a circular permutant of the tobacco mosaic virus.' *Nano Lett,* 10, 181-186.

Durham, A. C., Finch, J. T. & Klug, A. 1971. 'States of aggregation of tobacco mosaic virus protein.' *Nat New Biol,* 229, 37-42.

Durham, A. C. & Klug, A. 1971. 'Polymerization of tobacco mosaic virus protein and its control.' *Nat New Biol,* 229, 42-46.

Eber, F. J., Eiben, S., Jeske, H. & Wege, C. 2013. 'Bottom-up-assembled nanostar colloids of gold cores and tubes derived from tobacco mosaic virus.' *Angew Chem Int Ed Engl,* 52, 7203-7207.

Eiben, S., Stitz, N., Eber, F., Wagner, J., Atanasova, P., Bill, J., Wege, C. & Jeske, H. 2014. 'Tailoring the surface properties of tobacco mosaic virions by the integration of bacterially expressed mutant coat protein.' *Virus Res,* 180, 92-96.

El Shafei, G. M. S. 2000. 'Silica surface chemical properties.' In E. Papirer (Ed.) *Adsorption on silica surfaces:* 35-62. New York: Marcel Dekker Inc.

Evans, J. S. 2013. '"Liquid-like" biomineralization protein assemblies: a key to the regulation of non-classical nucleation.' *Crystengcomm,* 15, 8388-8394.

Fraenkel-Conrat, H. & Williams, R. C. 1955. 'Reconstitution of active tobacco mosaic virus from its inactive protein and nucleic acid components.' *Proc Natl Acad Sci U S A,* 41, 690-698.

Gebauer, D., Kellermeier, M., Gale, J. D., Bergstrom, L. & Colfen, H. 2014. 'Pre-nucleation clusters as solute precursors in crystallisation.' *Chem Soc Rev,* 43, 2348-2371.

Geiger, F. C., Eber, F. J., Eiben, S., Müller, A., Jeske, H., Spatz, J. P. & Wege, C. 2013. 'TMV nanorods with programmed longitudinal domains of differently addressable coat proteins.' *Nanoscale,* 5, 3808-3816.

Haase, N. R., Shian, S., Sandhage, K. H. & Kröger, N. 2011. 'Biocatalytic nanoscale coatings through biomimetic layer-by-layer mineralization.' *Adv Funct Mater,* 21, 4243-4251.

Hall, A. R., Scott, A., Rotem, D., Mehta, K. K., Bayley, H. & Dekker, C. 2010. 'Hybrid pore formation by directed insertion of alpha-haemolysin into solid-state nanopores.' *Nat Nanotechnol,* 5, 874-877.

Hunter, R. J. 1981. *Zeta potential in colloid science: principles and applications.* London, San Diego, New York, Berkeley, Boston, Sydney, Tokoy, Toronto: Academic Press.

Icopini, G. A., Brantley, S. L. & Heaney, P. J. 2005. 'Kinetics of silica oligomerization and nanocolloid formation as a function of pH and ionic strength at 25 °C.' *Geochim Cosmochim Ac,* 69, 293-303.

Jung, S. & Yi, H. 2014. 'An integrated approach for enhanced protein conjugation and capture with viral nanotemplates and hydrogel microparticle platforms *via* rapid bioorthogonal reactions.' *Langmuir,* 30, 7762-7770.

Kadri, A., Maiss, E., Amsharov, N., Bittner, A. M., Balci, S., Kern, K., Jeske, H. & Wege, C. 2011. 'Engineered tobacco mosaic virus mutants with distinct physical characteristics in planta and enhanced metallization properties.' *Virus Res,* 157, 35-46.

Kirkham, J., Firth, A., Vernals, D., Boden, N., Robinson, C., Shore, R. C., Brookes, S. J. & Aggeli, A. 2007. 'Self-assembling peptide scaffolds promote enamel remineralization.' *J Dent Res,* 86, 426-430.

Kisailus, D., Najarian, M., Weaver, J. C. & Morse, D. E. 2005. 'Functionalized gold nanoparticles mimic catalytic activity of a polysiloxane-synthesizing enzyme.' *Adv Mater,* 17, 1234-1239.

Kisailus, D., Truong, Q., Amemiya, Y., Weaver, J. C. & Morse, D. E. 2006. 'Self-assembled bifunctional surface mimics an enzymatic and templating protein for the synthesis of a metal oxide semiconductor.' *Proc Natl Acad Sci U S A,* 103, 5652-5657.

Krauskopf, K. B. 1956. 'Dissolution and precipitation of silica at low temperatures.' *Geochim Cosmochim Ac,* 10, 1-26.

Kröger, N. 2007. 'Prescribing diatom morphology: toward genetic engineering of biological nanomaterials.' *Curr Opin Chem Biol,* 11, 662-669.

Kröger, N., Deutzmann, R. & Sumper, M. 1999. 'Polycationic peptides from diatom biosilica that direct silica nanosphere formation.' *Science,* 286, 1129-1132.

Kuno, T., Nonoyama, T., Hirao, K. & Kato, K. 2011. 'Influence of the charge relay effect on the silanol condensation reaction as a model for silica biomineralization.' *Langmuir,* 27, 13154-13158.

Laemmli, U. K. 1970. 'Cleavage of structural proteins during the assembly of the head of bacteriophage T4.' *Nature,* 227, 680-685.

Lechner, C. C. & Becker, C. F. 2013. 'Modified silaffin R5 peptides enable encapsulation and release of cargo molecules from biomimetic silica particles.' *Bioorg Med Chem,* 21, 3533-3541.

Lee, S. Y., Lim, J. S., Culver, J. N. & Harris, M. T. 2008. 'Coagulation of tobacco mosaic virus in alcohol-water-LiCl solutions.' *J Colloid Interface Sci,* 324, 92-98.

Lee, S. Y., Royston, E., Culver, J. N. & Harris, M. T. 2005. 'Improved metal cluster deposition on a genetically engineered tobacco mosaic virus template.' *Nanotechnology,* 16, S435-S441.

Lee, W. J., Lee, D. H., Han, T. H., Lee, S. H., Moon, H. S., Lee, J. A. & Kim, S. O. 2011. 'Biomimetic mineralization of vertical N-doped carbon nanotubes.' *Chem Commun (Camb),* 47, 535-537.

Lu, B., Stubbs, G. & Culver, J. N. 1996. 'Carboxylate interactions involved in the disassembly of tobacco mosaic tobamovirus.' *Virology,* 225, 11-20.

Ma, Y. Z., Miller, R. A., Fleming, G. R. & Francis, M. B. 2008. 'Energy transfer dynamics in light-harvesting assemblies templated by the tobacco mosaic virus coat protein.' *J Phys Chem B,* 112, 6887-6892.

Martins-Junior, P. A., Alcantara, C. E., Resende, R. R. & Ferreira, A. J. 2013. 'Carbon nanotubes: directions and perspectives in oral regenerative medicine.' *J Dent Res,* 92, 575-583.

Miller, R. A., Presley, A. D. & Francis, M. B. 2007. 'Self-assembling light-harvesting systems from synthetically modified tobacco mosaic virus coat proteins.' *J Am Chem Soc,* 129, 3104-3109.

Müller, A., Eber, F. J., Azucena, C., Petershans, A., Bittner, A. M., Gliemann, H., Jeske, H. & Wege, C. 2011. 'Inducible site-selective bottom-up assembly of virus-derived nanotube arrays on RNA-equipped wafers.' *ACS Nano,* 5, 4512-4520.

Müller, W. E. G., Wang, X. H., Jochum, K. P. & Schröder, H. C. 2013. 'Self-healing, an intrinsic property of biomineralization processes.' *IUBMB Life,* 65, 382-396.

Niu, Z., Bruckman, M., Kotakadi, V. S., He, J., Emrick, T., Russell, T. P., Yang, L. & Wang, Q. 2006. 'Study and characterization of tobacco mosaic virus head-to-tail assembly assisted by aniline polymerization.' *Chem Commun (Camb),* 28, 3019-3021.

Paglini, S. & Lauffer, M. A. 1968. 'Polymerization-depolymerization of tobacco mosaic virus protein. XI. Osmotic pressure studies of solutions in water and in deuterium.' *Biochemistry,* 7, 1827-1835.

Panayotatos, N. & Wells, R. D. 1979. 'Recognition and initiation site for four late promoters of phage T7 is a 22-base pair DNA sequence.' *Nature,* 280, 35-39.

Patwardhan, S. V., Emami, F. S., Berry, R. J., Jones, S. E., Naik, R. R., Deschaume, O., Heinz, H. & Perry, C. C. 2012. 'Chemistry of aqueous silica nanoparticle surfaces and the mechanism of selective peptide adsorption.' *J Am Chem Soc,* 134, 6244-6256.

Polini, A., Pagliara, S., Camposeo, A., Cingolani, R., Wang, X., Schröder, H. C., Müller, W. E. & Pisignano, D. 2012. 'Optical properties of *in vitro* biomineralised silica.' *Sci Rep,* 2, 607.

Pouget, E. & Grelet, E. 2013. 'Dispersions of monodisperse hybrid rod-like particles by mineralization of filamentous viruses.' *Langmuir,* 29, 8010-8016.

Putnam, C. accessed 2015. 'Protein Calculator v3.4 ' *The Scripps Research Institute, La Jolla, California, U.S.A.,* http://protcalc.sourceforge.net.

Raghavendra, K., Adams, M. L. & Schuster, T. M. 1985. 'Tobacco mosaic virus protein aggregates in solution: structural comparison of 20S aggregates with those near conditions for disk crystallization.' *Biochemistry,* 24, 3298-3304.

Rego, J. M., Lee, J. H., Lee, D. H. & Yi, H. 2013. 'Biologically inspired strategy for programmed assembly of viral building blocks with controlled dimensions.' *Biotechnol J,* 8, 237-246.

Richthammer, P., Bormel, M., Brunner, E. & van Pee, K. H. 2011. 'Biomineralization in diatoms: the role of silacidins.' *Chembiochem,* 12, 1362-1366.

Rosa, M. D. 1979. 'Four T7 RNA polymerase promoters contain an identical 23 bp sequence.' *Cell,* 16, 815-825.

Royston, E., Ghosh, A., Kofinas, P., Harris, M. T. & Culver, J. N. 2008. 'Self-assembly of virus-structured high surface area nanomaterials and their application as battery electrodes.' *Langmuir,* 24, 906-912.

Schlick, T. L., Ding, Z., Kovacs, E. W. & Francis, M. B. 2005. 'Dual-surface modification of the tobacco mosaic virus.' *J Am Chem Soc,* 127, 3718-3723.

Schröder, H. C., Wiens, M., Schlossmacher, U., Brandt, D. & Müller, W. E. G. 2012. 'Silicatein-mediated polycondensation of orthosilicic acid: modeling of a catalytic mechanism involving ring formation.' *Silicon-Neth,* 4, 33-38.

Semino, C. E. 2008. 'Self-assembling peptides: from bio-inspired materials to bone regeneration.' *J Dent Res,* 87, 606-616.

Shenton, W., Douglas, T., Young, M., Stubbs, G. & Mann, S. 1999. 'Inorganic-organic nanotube composites from template mineralization of tobacco mosaic virus.' *Adv Mater,* 11, 253-256.

Shimada, K. & Tarutani, T. 1979. 'Gel chromatographic study of the polymerization of silicic acid.' *J Chromatogr,* 168, 401-406.

Stauffer, H., Srinivasan, S. & Lauffer, M. A. 1970. 'Calorimetric studies on polymerization-depolymerization of tobacco mosaic virus protein.' *Biochemistry,* 9, 193-200.

Sumper, M. & Brunner, E. 2008. 'Silica biomineralization in diatoms: the model organism *Thalassiosira pseudonana*.' *Chembiochem,* 9, 1187-1194.

Tang, F., Li, L. & Chen, D. 2012. 'Mesoporous silica nanoparticles: synthesis, biocompatibility and drug delivery.' *Adv Mater,* 24, 1504-1534.

Tenenbaum, H. C. & Heersche, J. N. 1982. 'Differentiation of osteoblasts and formation of mineralized bone *in vitro*.' *Calcif Tissue Int,* 34, 76-79.

Turner, D. R., Joyce, L. E. & Butler, P. J. 1988. 'The tobacco mosaic virus assembly origin RNA. Functional characteristics defined by directed mutagenesis.' *J Mol Biol,* 203, 531-547.

Urban, M., Kleefen, A., Mukherjee, N., Seelheim, P., Windschiegl, B., Vor der Bruggen, M., Kocer, A. & Tampe, R. 2014. 'Highly parallel transport recordings on a membrane-on-nanopore chip at single molecule resolution.' *Nano Lett,* 14, 1674-1680.

van der Zwaag, S., van Dijk, N. H., Jonkers, H. M., Mookhoek, S. D. & Sloof, W. G. 2009. 'Self-healing behaviour in man-made engineering materials: bioinspired but taking into account their intrinsic character.' *Philos Trans A Math Phys Eng Sci,* 367, 1689-1704.

Yamashita, I. 2008. 'Biosupramolecules for nano-devices: biomineralization of nanoparticles and their applications.' *J Mater Chem,* 18, 3813-3820.

Yildirim, A., Acar, H., Erkal, T. S., Bayindir, M. & Guler, M. O. 2011. 'Template-directed synthesis of silica nanotubes for explosive detection.' *ACS Appl Mater Interfaces,* 3, 4159-4164.

Yuwono, V. M. & Hartgerink, J. D. 2007. 'Peptide amphiphile nanofibers template and catalyze silica nanotube formation.' *Langmuir,* 23, 5033-5038.

Zahr, O. K. & Blum, A. S. 2012. 'Solution phase gold nanorings on a viral protein template.' *Nano Lett,* 12, 629-633.

Zaitlin, M. & Palukaitis, P. 2000. 'Advances in understanding plant viruses and virus diseases.' *Annu Rev Phytopathol,* 38, 117-143.

Zane, A. C., Michelet, C., Roehrich, A., Emani, P. S. & Drobny, G. P. 2014. 'Silica morphogenesis by lysine-leucine peptides with hydrophobic periodicity.' *Langmuir,* 30, 7152-7161.

Zhou, K., Li, F., Dai, G., Meng, C. & Wang, Q. 2013. 'Disulfide bond: dramatically enhanced assembly capability and structural stability of tobacco mosaic virus nanorods.' *Biomacromolecules,* 14, 2593-2600.

Zimmern, D. 1983. 'An extended secondary structure model for the TMV assembly origin, and its correlation with protection studies and an assembly defective mutant.' *EMBO J,* 2, 1901-1907.

Manuscript IV

Altintoprak, K., Seidenstücker, A., Welle, A., Eiben, S., Atanasova, P., Stitz, N., Plettl, A., Bill, J., Gliemann, H., Jeske, H., Rothenstein, D., Geiger, F. & Wege, C. 2015. 'Peptide-equipped tobacco mosaic virus templates for selective and controllable biomineral deposition.' *Beilstein J Nanotechnol,* 6, 1399-1412.

Authorship responsibilities

Altintoprak:

- Development of experimental strategy
- Chemical modification of TMV particles: conjugation of heterbifunctional cross linker and peptides
- Native and denaturing gel electrophoresis, ImageJ analysis
- Optimization of SiO_2 mineralization protocol
- TEM analysis
- REM analysis (introduced by Axel Seidenstücker)
- Data acquisition and interpretation
- Preparation of **Table 1** and **2** and **Figure 1**, **2**, **4** and **5**
- Data discussion against the background of previous publications
- Writing and editing of the manuscript

Seidenstücker:

- Si wafer preparation for REM and ToF-SIMS analysis

Welle:

- ToF-SIMS analysis
- Writing and editing of the manuscript
- Preparation of **Table 3** and **Figure 6**

Eiben:

- Zeta potential measurement
- Preparation of **Figure 3**
- Editing suggestions and proofreading

Atanasova:

- XRD analysis (data not shown)

Stitz:

- AFM analysis (data not shown)

Rothenstein:

- Supply of peptide 44C and 31C
- ZnO mineralization (data not shown)
- Data discussion against the background of previous publications
- Editing suggestions and proofreading

Bill and Jeske:

- Conceptual contributions and continuous discussion

Plettl and Gliemann:

- Basic project design (jointly with Wege), advice and repeated discussion

Geiger:

- Editing suggestions and proofreading

Wege:

- Basic project design (jointly with Plettl and Gliemann), guidance and constant discussion
- Editing suggestions and proofreading

Peptide-equipped tobacco mosaic virus templates for selective and controllable biomineral deposition

Klara Altintoprak[1], Axel Seidenstücker[2], Alexander Welle[3,4], Sabine Eiben[1], Petia Atanasova[5], Nina Stitz[5], Alfred Plettl[2], Joachim Bill[5], Hartmut Gliemann[4], Holger Jeske[1], Dirk Rothenstein[5], Fania Geiger[1], and Christina Wege[1]*

[1]Department of Molecular Biology and Plant Virology, Institute of Biomaterials and Biomolecular Systems, University of Stuttgart, Pfaffenwaldring 57, 70569 Stuttgart, Germany
[2]Institute of Solid State Physics, University of Ulm, Albert-Einstein-Allee 11, 89081 Ulm, Germany
[3]Karlsruhe Nano Micro Facility (KNMF) and [4]Institute of Functional Interfaces (IFG), [3,4]Karlsruhe Institute of Technology, Hermann-von-Helmholtz-Platz 1, 76344 Eggenstein-Leopoldshafen, Germany
[5]Institute of Materials Science, University of Stuttgart, Heisenbergstraße 3, 70569 Stuttgart

Email: Christina Wege - christina.wege@bio.uni-stuttgart.de

* Corresponding author

Abstract

The coating of regular-shaped, readily available nanorod biotemplates with inorganic compounds has attracted increasing interest during recent years. The goal is an effective, bioinspired fabrication of fiber-reinforced composites and robust miniaturized technical devices. Major challenges in the synthesis of applicable mineralized nanorods lie in selectivity and adjustability of the inorganic materials' deposition on the biological rod-shaped backbones, with respect to thickness and surface profile of the resulting coating as well as the avoidance of aggregation into extended superstructures. Nanotubular tobacco mosaic virus (TMV) templates have proved particularly suitable towards this goal: Their multivalent protein coat can be modified by high surface-density conjugation of peptides, inducing and governing silica deposition from precursor solutions *in vitro*. In this study, TMV has been equipped with mineralization-directing peptides designed to yield silica coatings in a reliable and predictable manner, *via* precipitation from tetraethoxysilane (TEOS) precursors. Three peptide groups were compared regarding their influence on silica polymerization. (i) Two peptide variants with alternating basic and acidic residues, i.e. lysine-aspartic acid $(KD)_x$ motifs expected to act as charge relay systems promoting TEOS hydrolysis and silica polymerization; (ii) a tetrahistidine-exposing polypeptide (CA_4H_4) known to induce silicification due to the positive charge of its clustered

imidazole side-chains; and (iii) two peptides with high ZnO binding affinity. Differential effects on the mineralization of the TMV surface were demonstrated, with a $(KD)_x$ charge relay peptide designed in this study leading to the most reproducible and selective silica deposition. A homogenous coating of the biotemplate and tight control of shell thickness were achieved.

Keywords

Biomineralization; charge relay system; peptide; silica; tobacco mosaic virus (TMV)

Introduction

Amorphous silica (SiO_2) precipitated from silicate precursor sols comprises a wide range of versatile materials applied in various technological approaches, e.g. as structural modifier or filler in rubber (Leblanc 2002), food (Stark et al. 2015, Bouwmeester et al. 2014) or healthcare products (Henstock et al. 2015), bioceramics for medical purposes (Vallet-Regi & Ruiz-Hernandez 2011), mesoporous nanoparticulate or -tubular drug delivery systems (reviewed by Tang et al. 2012), sensor surfaces (Yildirim et al. 2011), or biocatalytic formulations (reviewed by Yang et al. 2011b). An important focus of research and industry lies on the development of nanoshaped materials enabling the further miniaturization of devices and effector units, in addition to a reduced consumption of resources. In the field of functional mineral synthesis, significant progress has been made in using nanodimensional biological templates, allowing specific coating with inorganic materials to yield hybrid particles of pre-determined structure and composition (Mann 2009, Paris et al. 2010, Zollfrank et al. 2014). The surfaces of optimal templates nucleate and direct the formation of inorganic materials from suitable precursors, resembling a natural matrix-mediated mineral deposition in living organisms known also as “biologically controlled mineralization” (Mann 1983, Weiner & Dove 2003). Such bio-inspired mineralization approaches can accomplish precise coating processes and offer several benefits such as environmentally friendly fabrication routes and reaction parameters compatible with biological structures, namely low synthesis temperatures and aqueous deposition media. In this context, tube- or rod-like templates of high aspect ratio are of particular interest, since they enable the fabrication of elongated nanostructures which are otherwise difficult to obtain, because chemical synthesis or technical approaches applied at mild conditions commonly generate spherical structures (Wu et al. 2006). Mineral nanofibers of predetermined sizes are of major

importance for the preparation of functional films and extended three-dimensional materials. Hence, anisotropic scaffolds such as high molecular weight-polymers (Cademartiri et al. 2009), carbon nanotubes (Aljabali et al. 2011b), peptide nanotubes (Yuwono & Hartgerink 2007), certain plant viruses (Bittner et al. 2013, Mao et al. 2009, Lomonossoff & Evans 2014, Shenton et al. 1999), filamentous bacteriophages (Yang et al. 2013b, Pouget & Grelet 2013), and bacterial flagellae (Li et al. 2012) have been evaluated for their applicability on a technical scale. To achieve control over mineral precipitation, the templates' modification by chemical conjugation of peptides (Aljabali et al. 2011b), polyethylene glycol (PEG; Pouget & Grelet 2013), aniline (Niu et al. 2007, Royston et al. 2009), or succinamate (Aljabali et al. 2011a) has been reported.

Virus-based templates have gained especially important roles in the synthesis of organic-inorganic hybrid nanostructures. They combine several advantages, namely high availability, robustness and an exact multiplication of the particle shape and dimensions, which are genetically determined and result in a narrow size distribution. Different species such as the fibrous bacteriophage M13, icosahedral cowpea mosaic virus (CPMV), or tubular tobacco mosaic virus (TMV) were used as templates for the coating with inorganic materials including Pt, Au (Rothenstein et al. 2013), Ag (Evans 2009, Dujardin et al. 2003), Pd (Yang et al. 2013a, Knez et al. 2004b), TiO_2 (Fujikawa & Kunitake 2003), SiO_2 (Royston et al. 2006), NiO (Chiang et al. 2012), CdS (Shenton et al. 1999), CoPt, FePt, ZnS (Mao et al. 2004, Aljabali et al. 2011a) and ZnO (Atanasova et al. 2011, Atanasova et al. 2015, Balci et al. 2009). Among the virus-based templates, plant viruses are especially suitable nanostructured scaffolds because of their biological safety for humans, animals, and their commensal bacteria. TMV is a widespread plant-infecting pathogen, which can be isolated in large amounts from susceptible plants (Adams et al. 2012). TMV particles are highly-ordered supramolecular complexes consisting of a single-stranded helical RNA and ≈2130 identical coat protein (CP) subunits arranged around the RNA molecule, which is completely buried inside the protein shell (Culver 2002, Butler 1999, Namba et al. 1989, Ge & Zhou 2011, Sachse et al. 2007, Clare & Orlova 2010). The viral particle has an average length of 300 nm and an outer and inner (channel) diameter of 18 nm and 4 nm, respectively. TMV has become a powerful building block in bionanotechnology due to its tube-like structure, high stability under a wide range of different conditions (e.g. pH, temperature, solvent), low production

costs and multivalent CP surface (see e.g. Alonso et al. 2013, Bittner et al. 2013, Culver et al. 2015).

The CP subunits of TMV can be genetically or chemically modified for the presentation of effector molecules (e.g. Schlick et al. 2005, Smith et al. 2006, Chiang et al. 2012, Eiben et al. 2014, Shukla et al. 2015). Modified TMV templates maintain their 3D structure along with preserved particle stability, which is a prerequisite for the subsequent mineralization of inorganic materials. Furthermore, length and also overall shape of TMV-derived particles can be altered by means of engineered, non-natural RNA molecules, supporting the assembly of artificial, non-infectious TMV-like nucleoprotein tube systems. This technology was refined to even allow the production of kinked boomerang, branched tetrapod and multi-armed nanostar structures (Eber et al. 2013, Eber et al. 2015), or into particles fashioned evenly with mixtures of two or more functional groups at pre-defined ratios (Eiben et al. 2014).

To vary and control the deposition of inorganic minerals on TMV templates, extensive modifications of the surface amino acids are desirable. They enable defined alterations of the outer TMV CP surface charge and the introduction of specific amino acid motifs guiding the nucleation and growth of mineral coatings around the TMV core. This is in analogy to natural biomineralization-directing protein domains identified for various organisms (Baio et al. 2014, Zane et al. 2014, Cha et al. 1999, Kröger et al. 1999, Poulsen & Kröger 2004). Direct genetic modification of the TMV CP sequence is, however, limited in view of the extent of alteration tolerated by virus particles upon their multiplication in plants, regarding number and composition of exchanged or inserted amino acids. In addition, high-throughput screening of different surface-expressed peptides is restricted upon TMV “farming” due to a need of 10-14 days for TMV mutant accumulation. Bacterially expressed CP can be engineered to a much higher extent and integrated into TMV-like particles reconstituted *in vitro* in substantial amounts (Eiben et al. 2014). However, purification of such protein types from the bacteria cultures is much less efficient compared to CP isolation from intact TMV particles from leaf tissues.

Therefore, we have followed a third strategy and made use of plant-enriched moderately engineered TMV templates exposing selectively addressable reactive surface groups. These were subjected to chemical conjugation of synthetic peptides meant to regulate subsequent coating with silica (workflow indicated in Fig. 1). This procedure is insensitive to both size and sequence of the peptides of choice, and the

generation of various types of decorated TMV rods is fast. The amino acid sequences employed had been delimited by phage display to affect mineralization previously in our labs (Rothenstein et al. 2012) or by other researchers (Yuwono & Hartgerink 2007), or were predicted to influence silica deposition based on the literature (Kuno et al. 2011). Control experiments were carried out with bare TMV treated equally in parallel, to assess its capacity of silica nucleation in the absence of additional peptide domains.

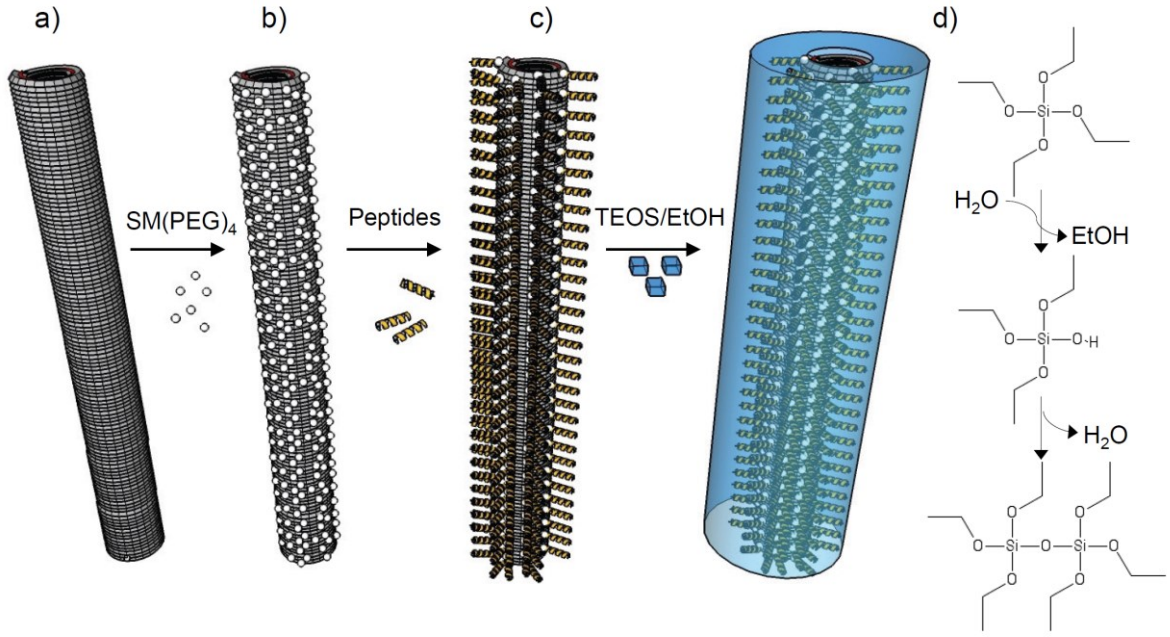

Figure 1: Schematic representation of the chemical modification and mineralization of tobacco mosaic virus (TMV) nucleoprotein nanotubes. a) Genetically engineered virus particles with thousands of surface-exposed amino groups of lysine residues (TMV_{Lys}) served as biotemplates for chemical conjugation reactions. b) Hetero-bifunctional linker molecules (succinimidyl-[(N-maleimidopropionamido)-tetraethyleneglycol] ester, $SM(PEG)_4$) were coupled to TMV_{Lys} *via* N-hydroxysuccinimide (NHS) ester-mediated crosslinking with lysine primary amines yielding amide bonds. c) Mineralization-affecting peptides were conjugated to the maleimide-activated $SM(PEG)_4$ linker portion *via* the sulfhydryl groups of their terminal cysteine residues yielding stable thioether linkages. The resulting functionalized TMV templates fashioned with a dense peptide coating were d) subjected to silica mineralization *via* hydrolysis and condensation of a tetraethoxysilane (TEOS) precursor in solution (mechanism indicated).

Generally, it still remains a challenge to predictably, selectively and uniformly coat individual nanotemplate particles with silica, for which sol-gel condensation from precursors in alcoholic solutions seems most viable according to conditions established by Stöber et al. (1968) for the fabrication of plain silica spheres. Reaction parameters such as time, temperature, pH, solvent composition and precursor as well as catalyst concentration affect the thickness of the mineral coating, in

interdependence with chemistry and charge distribution of the surface of the core (Kim et al. 2013, Royston et al. 2009, Aljabali et al. 2011a, Fowler et al. 2001, Pouget & Grelet 2013). During the mineralization process, great effort is needed to avoid non-templated by-products as well as aggregation, re-organization and precipitation of the templates into extended superstructures of amorphous silica-template composites.

Several earlier studies have demonstrated that native TMV capsids are effective biological nucleation cores for the deposition of mineral layers from silicate sols on their surfaces. This is typically carried out *via* hydrolysis and condensation of tetraethoxysilane (also known as tetraethyl-orthosilicate, TEOS) in alcohol-containing media (see Fig. 1 for a mechanistic scheme). Obviously, the viral coat that exhibits patches of both positively and negatively charged amino acids in nanometric vicinity to each other is prone to silica deposition by itself. Concomitant with silicification reactions, however, TMV particles came out to undergo extensive re-arrangement into head-to-tail structures (Royston et al. 2006, Royston et al. 2009), laterally aligned or even star-shaped (Fowler et al. 2001) three-dimensional arrays in many of the studies, reflecting and expanding the well-known capacities of these bio-nanorods to form various aggregates up to liquid-crystalline phases. In contrast, protocols resulting in nanoparticulate TMV-silica composites devoid of inorganic background granules and, moreover, with closed shells of well-adjustable thickness are a matter of intense investigation. Such methods would enable the manufacture of novel TMV derivatives, further expanding their application potential as it is currently being explored in miniaturized arrays and devices (Müller et al. 2011, Chen et al. 2011, Li & Wang 2014) and “smart” functional materials (Yang et al. 2013a, Luckanagul et al. 2012) for numerous purposes. TMV-inorganic hybrids will likely yield rigid and durable (Wu et al. 2010) technical components compatible also with biological molecules and activities (Luckanagul et al. 2015).

To fabricate thick continuous silica coatings (e.g. on immobilized TMV rods), polyaniline interlayers were employed to shield both charges and hydrophobic patches of the viral protein coat before subjecting it to TEOS-mediated mineralization (Royston et al. 2009). A more refined and tighter control of silica mineralization can be achieved by ordered repetitive arrangements of differently charged protein domains and specific functional groups therein, as demonstrated *in vitro* by help of various mineralization-inducing peptides (Kuno et al. 2011, Patwardhan et al. 2012,

Baio et al. 2014, Zane et al. 2014). Positively charged amino acid residues (Lys, Arg) in such peptides interact electrostatically with siloxane groups, while Ser, His and Asp may undergo hydrogen bonding or polar interactions with solute or nanosized colloidal mineral precursors (Kim et al. 2013, Steinmetz et al. 2009, Yildirim et al. 2011, Rothenstein et al. 2012, Patwardhan et al. 2012, Gebauer et al. 2014). Additionally present negatively charged amino acids are supposed to have enhancing effects on TEOS hydrolysis, especially if closely adjacent to positive charges, where such combinations may act as charge relay systems (Kuno et al. 2011, Almora-Barrios et al. 2009). Effective peptides may resemble motifs found in natural silica biomineralization-directing proteins, in both their amino acid composition and sequence (Kröger et al. 1999), but may also comprise randomly assembled sequences resulting from mere *in vitro* library screening.

Since a growing body of experience with relatively diverse silicification-guiding peptides is available, we decided to install a number of distinct amino acid sequence types on structure-directing TMV nanorods. This allows for the systematical investigation of their influence on silica coating reactions *via* ethanol-containing TEOS on this viral backbone for the first time.

Table 1: Mineralization-affecting peptides installed on TMV templates to compare their influence on silica deposition from TEOS. Amino acid sequence and total number (aa) are indicated for each peptide. Molecular weight (M_W), isoelectric point (pI), and net charge at pH 8.0 and 5.5 were calculated with Protein Calculator v3.4 (Putnam accessed 2015).

Name	Abbre-viation	Sequence	aa	M_W [g/mol]	pI	Net charge *at pH*	
						8.0	*5.5*
$(KD)_5C$	KD5	KDKDKDKDKDC	11	1337.5	6.25	-0.8	0.4
$(KD)_{10}C$	KD10	$(KDKDKDKDKD)_2C$	21	2553.8	6.62	-0.8	0.7
CA_4H_4	AH	CAAAAHHHH	9	945.0	7.52	-0.6	3.6
44C	44C	HSSHHQPKGTNPC	13	1429.5	8.31	0.3	3.7
31C	31C	HHGHSPTSPQVRC	13	1442.6	8.31	0.4	3.7

Genetically modified TMV particles (TMV_{Lys}) with an accessible amino group on every CP subunit (Geiger et al. 2013) were chemically equipped with a dense peptide coating *via* succinimidyl ester-activated bifunctional PEG-based linkers, and their subsequent maleimide-mediated conjugation to thiol groups of terminal cysteine residues present in every peptide. Five different peptide sequences were selected (see **Table 1**): (i) $(KD)_5C$ and $(KD)_{10}C$ with alternating amino and carboxyl

functionalities (sequences KDKDKDKDKDC and KDKDKDKDKDKDKDKDKDKDC, respectively) on the basis of Kuno *et al*. (2011); (ii) CA_4H_4 (sequence CAAAAHHHH) according to Yuwono and Hartgerink (2007), with two stretches of different amino acid residues arranged blockwise to expose a cluster of imidazole side chains; (iii) 44C (HSSHHQPKGTNPC) and 31C (HHGHSPTSPQVRC), two ZnO-binding peptides isolated by phage display (Rothenstein et al. 2012). The distinct peptide-fashioned TMV_{Lys} templates were incubated in TEOS precursor solution in parallel with linker-coated and plain TMV_{Lys} controls (and in some tests wildtype TMV_{wt}) under equal conditions. The products were analyzed and compared to determine favorable TMV template-peptide combinations for specific silica mineralization.

Materials and methods

Materials

Peptides $(KD)_5C$, $(KD)_{10}C$, and CA_4H_4 of 90 % purity were provided by GeneCust (Dudelange, Luxembourg). Peptides 31 C and 44C were purchased from EMC microcollections (Tübingen, Germany).

TMV functionalization with bifunctional linker molecules and peptides

Wild type TMV_{wt} and genetically modified TMV_{Lys} (Geiger et al. 2013: also named TMV-Lys here to underscore the functional amino groups exposed by its lysine side chains) were purified according to Gooding and Hebert (1967). Peptide conjugation onto the virus surface followed a protocol established on the basis of literature data (Bruckman & Steinmetz 2014, Bruckman et al. 2014) and a lab instruction kindly provided by Sourabh Shukla and Nicole Steinmetz, Case Western Reserve University, Cleveland, Ohio, U.S.A.. 1200 µl TMV-Lys particles (5 mg/ml) in 10 mM sodium potassium phosphate (SPP) pH 7.2 were mixed with 9 µl of 1 M heterobifunctional crosslinker $SM(PEG)_4$ (succinimidyl-[(N-maleimidopropionamido)-tetraethyleneglycol] ester (Thermo Scientific, Karlsruhe, Germany)) dissolved in dimethyl sulfoxide and incubated at 37 °C for 2 h under agitation (horizontal shaking at 500 rpm). TMV particles were sedimented for 1.5 h at 90,500 g and 4 °C in an Optima L-90K ultracentrifuge (Beckman Coulter, Krefeld, Germany). The resulting pellet of linker-equipped TMV (named TMV-PEG) was resuspended in 600 µl 10 mM SPP pH 7.2. An amount of 100 µl TMV-PEG solution was mixed with 800 µl 10 mM SPP pH 7.2 and 40 µl peptides (3.3 mg/ml) dissolved in dimethylformamide and incubated at 30 °C for 2 h and subsequently at 4 °C overnight under agitation as

above. TMV particles with conjugated peptides were sedimented by ultracentrifugation as above. Pellets were washed with 1 ml ultrapure water (ddH_2O; 18.3 MΩ cm; purified by a membraPure system, Aquintus, Bodenheim, Germany) and resuspended in 100 µl ddH_2O. TMV_{wt} and TMV-Lys concentrations were determined by UV spectroscopy with a NanoDrop ND-1000 spectrophotometer (PeqLab, Erlangen, Germany) at a wavelength of 260 nm, using the extinction coefficient of TMV particles (3 ml mg^{-1} cm^{-1}; Zaitlin 2000). For estimating concentrations of the different biotemplate rods, band intensities of modified CPs and unmodified CP_{Lys} after SDS-PAGE separation and Comassie Blue staining were compared (see below).

Electrophoretic analysis

The modified CPs were analyzed by denaturing SDS-PAGE (Laemmli 1970). Samples containing 0.2 µg protein were heated for 5 min at 95 °C in sample buffer (50 mM Tris-HCl (tris-(hydroxymethyl)-aminomethan hydrochloride acid) pH 6.8, 2 % (w/v) SDS, 0.1 % (w/v) bromophenol blue, 10 % glycerol, 100 mM dithiothreitol) and separated on 15 % PA gels. Fixed gels were stained with Coomassie Brilliant Blue R250 (Serva Electrophoresis, Heidelberg, Germany) according to standard procedures (Green & Sambrook 2012).

Modified and unmodified TMV-Lys templates were separated as intact particles in native 0.9 % agarose gels in 98 mM Tris pH 8.0, 89 mM boric acid, 2 mM EDTA. 12 µg of total protein in sample buffer (10 mM SPP pH 7.2, 0.1 % (w/v) bromophenol blue, 10 % glycerol) were applied per lane. TMV bands were stained with Coomassie Brilliant Blue R250.

Zeta potential determination and charge calculation

Zeta potentials were measured using a Malvern Zetasizer Nano ZS (Malvern Instruments, Worcestershire, UK) using disposable folded cuvettes. The Smoluchowski approximation was used according to instrument settings, to convert the electrophoretic mobility to a zeta potential. Experiments consisted of 30 runs per measurement and all experiments were carried out in triplicates. The zeta potential was measured for each sample with a concentration of 0.5 mg/ml TMV particles solution in ddH_2O (pH 5.5) as well as in 30 mM Tris-HCl at pH 8.0.

TMV particle mineralization

Peptide-functionalized TMV templates resuspended in water (see above) were kept for one to two days at 4 °C to allow their complete dispersion after ultracentrifugation. For the mineralization of particles with and without linkers and conjugated peptides, 40 µl TMV template solution (10 mg/ml) was mixed with 50 µl 20 % (v/v) TEOS (Sigma Aldrich, München, Germany) in ethanol (99.8 % p.a.), resulting in final concentrations in the mineralization reaction mixture of 4.4 mg/ml TMV, 11.1 % (v/v) TEOS, and 44.4 % (v/v) ethanol in an aqueous solution of pH 5.5-5.6. It was crucial to mix TEOS and ethanol before combining it with TMV particles, to preserve their structural integrity. Mineralization reactions were incubated for 1, 2, 5, 7, 10 or 12 days under agitation (horizontal shaking at 500 rpm) at 25 °C. The reaction mix was precipitated in a table centrifuge for 15 min at 20,000 g and 18 °C, the supernatant was discarded and the pellet washed twice with 200 µl 50 % (v/v) ethanol to remove residual unconverted TEOS. The pellet was resuspended in 50 µl ddH_2O, centrifuged for 30 min at 10,000 g. The resulting pellet was dissolved in 50 µl ultrapure water.

Characterization of mineralized TMV particles

The surface of mineralized TMV particles was characterized by SEM analysis. 20 µl of 1:250 diluted mineralized TMV solutions in ultrapure water (mineralized TMV particle solution preparation see TMV particle mineralization) were pipetted on n-Si wafer substrates and air-dried. Samples were analyzed in an S-5200 ultra-high resolution Field-Emission SEM (FE-SEM; Hitachi Ltd., Tokyo, Japan) at 30 kV.

TEM analysis was carried out to determine the silica shell thickness of TMV-KD10 particles after different reaction times. 3 µl of mineralized TMV particles in solution were incubated on a 400-mesh Formvar® carbon-covered copper grid for 5 min. The droplet was removed with five droplets of ultrapure water and air-dried. Samples were analyzed under a Zeiss EM-10A TEM (CARL ZEISS, Oberkochen, Germany) at 60 kV.

For ToF-SIMS analysis, Si chips (5x10 mm) were cut from n-Si wafers (CrysTec, Berlin, Germany) and used as supporting substrates. They were coated with a 4 nm thick chromium layer for adhesion and a 30 nm thick gold layer by physical vapour deposition (PVD; Varian NRC 836, Palo Alto, California, U.S.A.). All samples used for mineralization analysis were found to be free of Si and silicon oil contaminations potentially interfering with the analysis.

10 µl of 1:250 diluted solution of mineralized TMV or control preparations in ultrapure water (see TMV particle mineralization) were pipetted on a gold-covered n-Si wafer and air-dried. ToF-SIMS was performed on a TOF.SIMS5 instrument (ION-TOF GmbH, Münster, Germany). This spectrometer is equipped with a Bi cluster primary ion source and a reflectron type time-of-flight analyzer. UHV base pressure was $< 5\times10^{-9}$ mbar. For high mass resolution the Bi source was operated in the "high current bunched" mode providing short Bi_1^+ primary ion pulses at 25 keV energy and a lateral resolution of approx. 4 µm. The short pulse length of 0.6 to 1.0 ns allowed for high mass resolution. The primary ion beam was rastered across a 500×500 μm^2 field of view on the sample, and 128×128 data points were recorded. Primary ion doses were kept below 10^{11} ions/cm^2 (static SIMS limit). Spectra were calibrated on the omnipresent C^-, CH^-, CH_2^-, and Au^-, or on the C^+, CH^+, CH_2^+, and CH_3^+ peaks, respectively. Based on these datasets the chemical assignments for characteristic fragments were determined.

Results and discussion

Surface functionalization of TMV_{Lys} templates by conjugation of mineralization-promoting peptides

To nucleate and govern the deposition of silica shells, functionalized plant viral nanorod templates were generated by linker-assisted chemical conjugation of mineralization-active peptides to the outer surface of genetically modified TMV_{Lys} particles from plants. Every CP_{Lys} subunit provided a primary amine group of a lysine residue close to the protein's C terminus, resulting in ≈2130 sites selectively accessible to NHS ester-mediated coupling reactions per rod (Geiger et al. 2013). These were equipped with heterobifunctional crosslinker molecules (succinimidyl-[(N-maleimidopropionamido)-tetraethyleneglycol] ester [$SM(PEG)_4$]) serving as spacers and adapters for mineralization-affecting peptides, which were installed via maleimide-mediated conjugation of the cysteine sulfhydryl groups of the peptides. The resulting five distinct types of TMV_{Lys}-PEG-peptide particles with their different CP derivatives are listed in **Table 2**, as well as the linker-fashioned and plain TMV_{Lys} templates used as references. The abbreviation scheme used in the following: abbreviations underscore the relevant functionalities or amino acids exposed; therefore TMV_{Lys} is named TMV-Lys from now on. Covalent conjugation of peptides

was confirmed for both single CPs and intact TMV particles by denaturing and native gel electrophoresis, respectively.

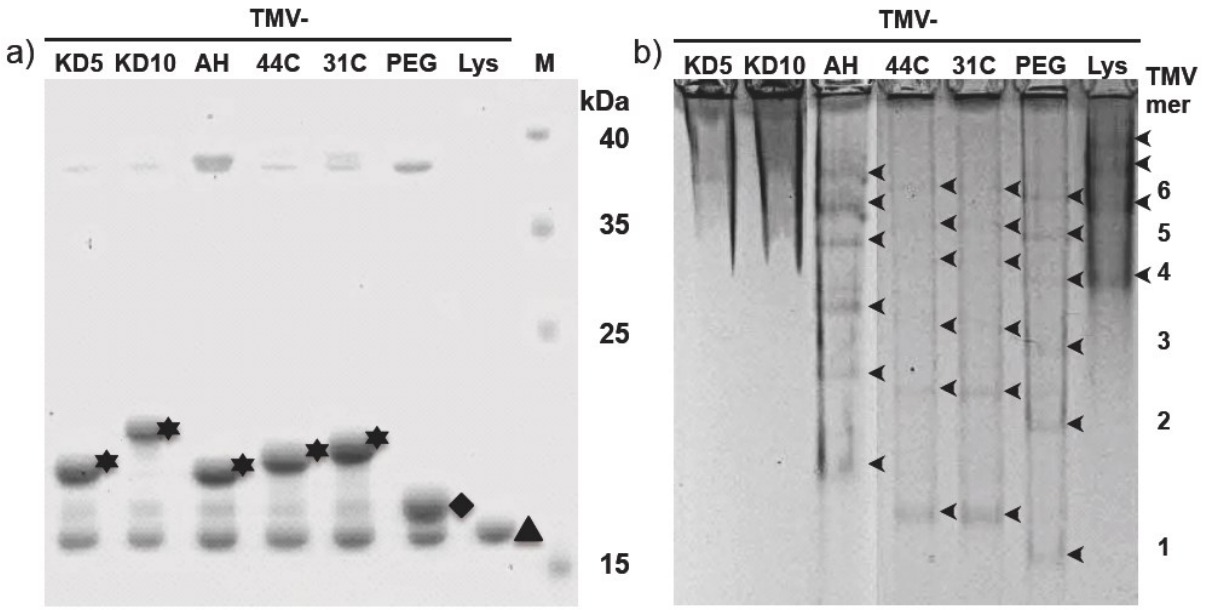

Figure 2: Gel electrophoretic analysis of chemically modified TMV-Lys particles. a) SDS-PAGE shows retarded bands of CPs modified with the linker $SM(PEG)_4$ (diamond, PEG), or after coupling $SM(PEG)_4$ and different peptides (stars, peptides as indicated above), compared to unmodified CP_{Lys} (triangle, Lys). b) Peptide-equipped TMV-Lys particles exhibiting different separation patterns during native agarose gel electrophoresis, indicating various states of head-to-tail aggregation in combination with distinct negative overall charges. Moieties exposed on the TMV templates are indicated (abbreviations as in **Table 2**). Numbers on the right: approximate numbers of TMV particles in head-to-tail aggregates (in relation to lane 'TMV-PEG').

Table 2: Composition of TMV derivatives used in this study. Calculated and measured* molecular weight (M_W) of modified CP species were in good agreement.

Name of TMV derivate	Abbreviation (TMV-)	Composition of TMV derivate			Calculated M_W of CP conjugate [kDa]	Measured M_W of CP conjugate* [kDa]
		TMV_{Lys}	$SM(PEG)_4$	Peptide		
TMV_{Lys}-PEG-$(KD)_5C$	KD5	+	+	$(KD)_5C$	19.5	19.9
TMV_{Lys}-PEG-$(KD)_{10}C$	KD10	+	+	$(KD)_{10}C$	20.7	21.9
TMV_{Lys}-PEG-CA_4H_4	AH	+	+	CA_4H_4	19.1	20.2
TMV_{Lys}-PEG-44C	44C	+	+	44C	19.6	20.4
TMV_{Lys}-PEG-31C	31C	+	+	31C	19.6	20.9
TMV_{Lys}-PEG	PEG	+	+	-	18.1	18.2
TMV_{Lys}	Lys	+	-	-	17.6	17.4

*Measured M_W values are derived from SDS-PAGE band analyses *via* retardation factor values determined by ImageJ software (Schneider et al. 2012) and calibration curves obtained from M_W standards separated on the same gel.

Peptide modification of CPs resulted in a band shift according to their increased molecular weight, as compared to non-modified CP in denaturing sodium dodecyl sulphate-polyacrylamide gel electrophoresis (SDS-PAGE; **Figure 2 a**).

The efficiency of peptide conjugation was determined by the ratio of band intensities of modified and non-modified CPs after Coomassie Blue staining. The binding efficiencies to individual CP subunits were ≈60 % for all investigated peptides, corresponding to about 1250 peptides exposed on every 300 nm rod. The molecular weights of the differently modified CPs were in good agreement with the values calculated for the distinct conjugates (**Table 2**).

The intact TMV particles were analyzed by native gel electrophoresis (0.9 % agarose in TBE buffer, pH 8.0; **Figure 2b**). The linker coating of the control derivative TMV_{Lys}-PEG (TMV-PEG) increased its negative net charge in comparison to TMV-Lys, resulting in a higher electrophoretic mobility. This effect was reduced by the conjugation of mineralization-affecting peptides: TMV_{Lys}-PEG-CA_4H_4 (TMV-AH), TMV_{Lys}-PEG-44C (TMV-44C) and TMV_{Lys}-PEG-31C (TMV-31C) exhibited retarded bands, which indicated the linkage of the peptides to the TMV-PEG template. TMV derivatives TMV_{Lys}-PEG-$(KD)_5$C (TMV-KD5) and TMV_{Lys}-PEG-$(KD)_{10}$C (TMV-KD10) could not be separated under the conditions applied: both samples did not migrate into the gel phase to a sufficient extent.

Zeta potential measurement

The zeta potentials (ZPs) of TMV-Lys nanorods and their derivatives were determined by a Malvern NanoSizer at a virus particle concentration of 0.5 mg/ml in ultrapure water (ddH_2O) and in 30 mM Tris-HCl buffer, pH 8.0, respectively (**Figure 3**). The ZPs measured in ddH_2O were in general more negative (-28 mV to -78 mV) compared to those determined in buffer (-10 mV to -25 mV), owing to the lower pH of ≈5.5 of ultrapure water with CO_2 dissolved in equilibrium with that in the air (Hong et al. 2010). In addition, the increased electrolyte concentrations in the buffer lead to an enrichment of counter ions in the proximity of the TMV nanorods and thus a steeper decrease of the potential within a shorter distance from their surface (decrease of the Debye length). Therefore, ZP values measured in ddH_2O are closer to the electric surface (Stern) potential of the particles (Hunter 1981).

The ZPs of the TMV derivatives (**Figure 3**) were correlated with the calculated isoelectric points (pIs) of the conjugated peptides (see **Table 1**), and in most cases with the effective particle charges affecting their relative mobility in native agarose gel

electrophoresis (see **Figure 2 b**). Peptides 44C and 31C both are predicted to exhibit moderate positive charges (of about 0.3 or 0.4, respectively) at pH 8.0, while peptides AH (-0.6), KD5 and KD10 (both -0.8) are supposed to be negative. As coating of the TMV particles with maleimide-reactive $SM(PEG)_4$ linker molecules devoid of peptides (TMV-PEG) introduced the most negative net charge (**Figure 2 b**), all peptide-fashioned TMV derivatives had less negative ZPs compared to the linker-modified control (with about -80 mV in water and about -25 mV in buffer). While the ZP values of four products were largely in line with the peptides' calculated charges (with TMV-44C and TMV-31C shifted to significantly less negative ZP values compared to those of TMV-KD5 and -KD10), the absolute ZP determined for TMV-AH was shifted most extensively to more positive values, due to the contribution of the uncharged alanines (**Figure 3**). This reflects the sheath of tetrahistidine clusters exposed by the C-termini of peptide AH. Bare TMV-Lys templates with their plain protein coat exhibited ZP values close to those of TMV-KD5.

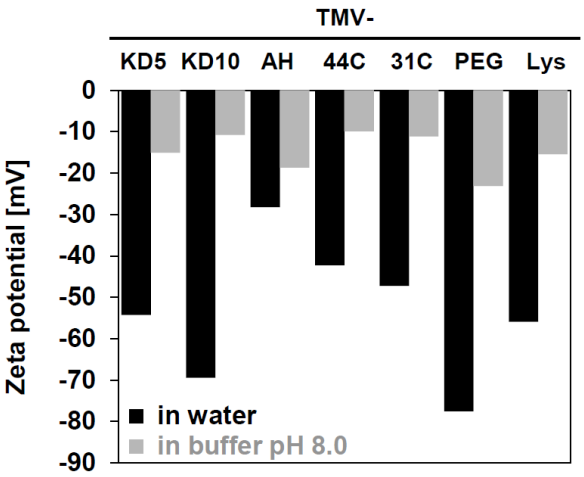

Figure 3: Zeta potential of bare and chemically modified TMV-Lys particles in ddH_2O or 30 mM Tris-HCl pH 8.0, respectively (modifications of TMV rods indicated above).

At high concentrations, TMV-AH aggregated into bundle-like structures in water but not in buffer. Such agglomerates could be separated by ultrasound; however, re-aggregation occurred after short time. 44C- or 31C-functionalized TMV formed raft-like aggregates in both water and buffer (as detected also after their mineralization, see SEM analysis below). For inorganic particles, the physical stability of dispersions increases with the magnitude of the ZP. That is, highly negative or highly positive ZP typically both result in stable suspensions (Reed 1995, Müller & Hildebrand 1996) by Coulomb repulsion. The organic TMV template structures thus behaved analogously, with the agglomerating species TMV-AH, -44C, and -31C exhibiting the lowest ZP magnitudes in water. TMV-Lys with an absolute ZP value above 55 did not show aggregation at all.

Mineralization of functionalized TMV templates

The different TMV templates were subjected to silica deposition by dispersion in buffer-free deposition solution of ≈11 % (f.c. v/v) TEOS precursor solution in ≈45 % (f.c. v/v) ethanol in ultrapure water (resulting in a pH of ≈5.5) under agitation (500 rpm) at 25°C for up to twelve days in parallel experiments (see Experimental section). These conditions were adapted with respect to the ethanol concentration from an earlier comparative study on the mineralization capacities of distinct kinds of peptides (Kuno et al. 2011). The method was established in initial tests to achieve improved control over mineralization kinetics and product characteristics with peptide-equipped TMV templates. This is in comparison to protocols used for the TEOS-mediated silicification of bare (Fowler et al. 2001, Shenton et al. 1999, Royston et al. 2006, Rong et al. 2009, Niu et al. 2009) or aniline-coated (Royston et al. 2009) TMV. Those all employed reaction mixes of either alkaline or significantly lower pH, in most cases in buffer-free solutions, in variable ethanol concentrations and in one study supplemented by (3-aminopropyl)triethoxysilane (APTES; Fowler et al. 2001).

All TMV templates with absolute ZP magnitudes above 50 mV showed a good dispersion in the mineralization solution, while TMV-AH, -44C and -31C did not form stable suspensions. At different reaction times, products were collected by centrifugation. After seven days of incubation, inorganic material could be sedimented from all reaction mixes, regardless of the presence or absence of TMV templates (**Figure 4 a**). The precipitates were transparent in the presence of TMV-KD5, -PEG, and -Lys, as well as for the reference sample without template, whereas the sediments of TMV-KD10, -AH, -44C and -31C appeared milky white. In the absence of TMV, the reaction solution had solidified completely, while all suspensions containing TMV templates remained liquid during the course of silica condensation (**Figure 4 a**). The morphology of TMV hybrid products subjected to mineralization for ten days was analyzed by transmission electron microscopy (TEM; see below and data not shown), and high resolution scanning electron microscopy (HRSEM; **Figure 4 b**). A clear difference in the mineralization of functionalized and non-functionalized TMV templates was observed: Only nanorods presenting the silica-binding peptides KD5 or KD10 showed continuous inorganic surface coatings on every single particle, with no significant agglomeration of the virus hybrids.

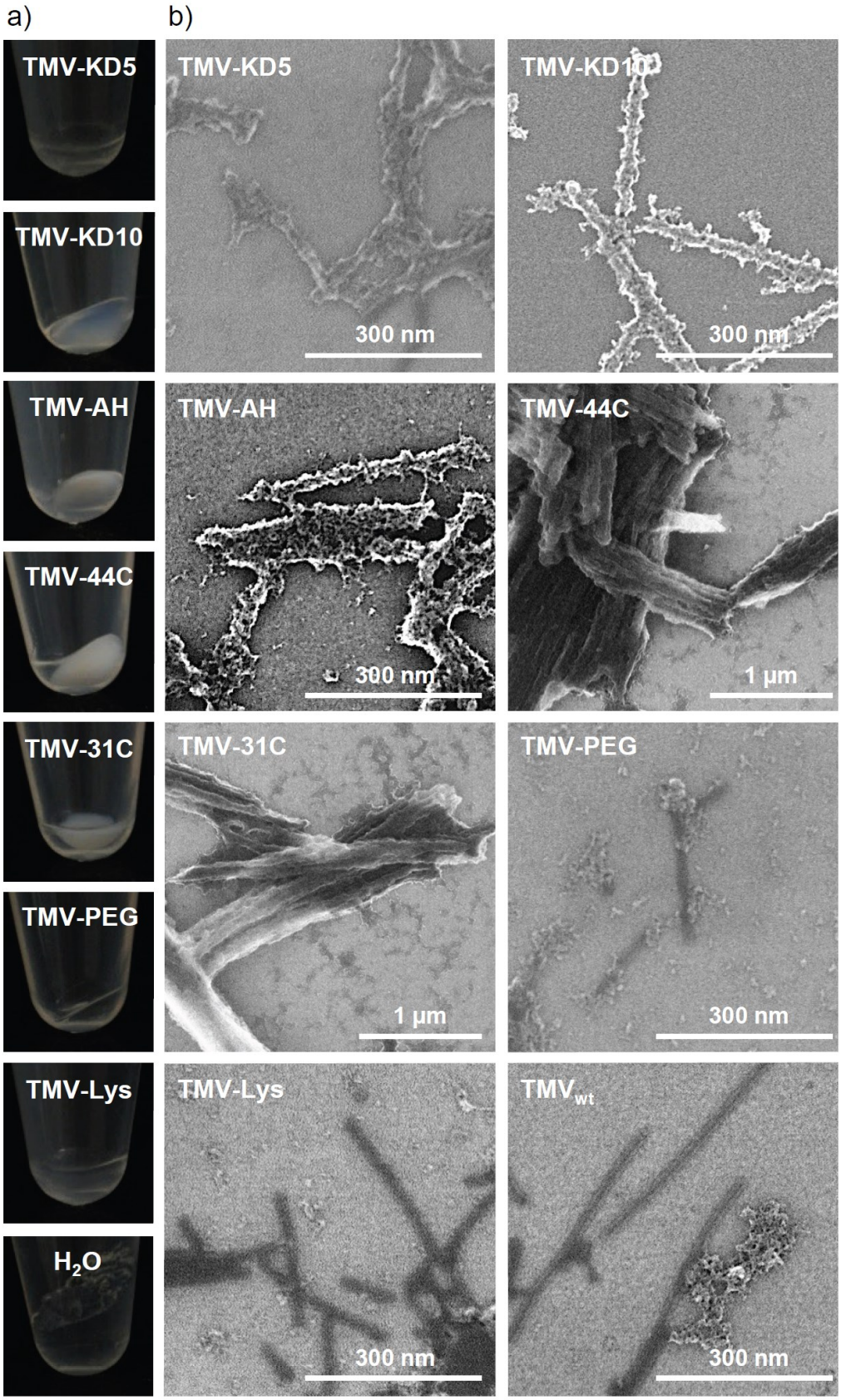

Figure 4: SiO_2 deposition reactions using functionalized and non-modified TMV templates, as indicated. a) Images of sedimented products, and b) corresponding SEM analysis. TMV-Lys-template (or water control) solutions were mixed with $EtOH_{abs}$ (99.9 %) and TEOS in a 4:4:1 volume ratio. Reaction products were sedimented by centrifugation [after 7 days incubation in (a) or 10 days in (b)], resuspended in ddH_2O and prepared for SEM (for details, refer to text).

Furthermore, deposition on these templates was highly specific; only a low amount of non-bound silica particles had formed (**Figure 4 b**). The templates TMV-AH, -31C, and -44C induced silica deposition as well, but in contrast to TMV-KD5 and -KD10, the resulting composites did not contain separate rods anymore, but formed extended aggregates and bundles up to the µm size regime, especially pronounced for -31C and -44C. TMV templates lacking specific effector peptides (i.e. TMV-PEG, -Lys, TMV_{wt}) did not show any substantial inorganic coating at all; instead, some unspecific silica precipitation was observed (**Figure 4 b**). It is known for *in vitro* systems that an alternating arrangement of lysine and aspartic acid residues, as in peptides KD5 and KD10, enhances dehydration of the TEOS precursor in the mineralization solution, in direct comparison to blockwise arrangements of the same amino acids, by offering an increased number of active sites for charge relay effects (Kuno et al. 2011). The results of our comparative tests showing superior capacities of KD5 and KD10 to induce local silicification are in line with these earlier observations, pointing at the beneficial effect of amino acid-based charge relay on a spatially directed TEOS conversion. Silica precipitation by sol-gel reactions from precursor solutions is likely to involve a gradual growth of individual silica nucleation cores rather than single or few specific phase transformations (Gebauer et al. 2014). Hence, high surface densities of cooperating starter sites (such as repetitive KD pairs) may provide best chances for an even growth of mineral shells, which are induced simultaneously at numerous closely adjacent sites.

The other peptides explored in this study, AH, 31C and 44C, all contain histidine residues as potential mineralization effectors: Their imidazole rings can catalyze hydrolysis of the TEOS precursor resulting in deprotonated, negatively charged silicic acid, which then accumulates in the vicinity of the positively charged amino acids to facilitate silica mineralization (Yuwono & Hartgerink 2007). The good efficiency of AH in promoting silica sheath formation from TEOS in the context of amphiphilic peptide fibers has been demonstrated (Yuwono & Hartgerink 2007). 31C and 44C had not been tested with TEOS before, as they were originally identified due to their ZnO binding properties (Rothenstein et al. 2012: and data not shown). The agglomeration and bundle formation we found for all three respective mineralized TMV templates might be due to their aggregation before the mineralization process, as it is known for histidine-presenting TMV particles (Eiben et al. 2014, Bruckman et al. 2011, Kadri et

al. 2011). This is also indicated by their absolute ZP values below 50 mV measured in this study.

Most of the silicification-active peptides that convey the dehydration of precursor molecules such as TEOS (Steinmetz et al. 2009, Baio et al. 2014, Zane et al. 2014, Altunbas et al. 2010, Acar et al. 2011) contain disproportionate amounts of positively charged amino acid residues (lysine, arginine or histidine). This reflects the design of silaffin, a natural silica-mineralizing protein rich in lysine and arginine residues (Kröger et al. 1999, Sumper & Kröger 2004). Therefore, we speculated that bare TMV-Lys templates could support the formation of silica shells in TEOS solution. The effect could be greater since the viral CPs are known to be N-terminally acetylated (Filner & Marcus 1974) and thereby might act as repetitive charge relay systems on the viral surface. However, we could not detect any silica coating on TMV-Lys templates under the conditions applied. This may be due to the surrounding amino acids in the CP environment, which might slow down or even inhibit putative mineralization-supporting activity of the lysine moieties of the CPs.

TMV_{wt} was also not mineralized in this experimental setup to an electron-optically detectable extent. This is in contrast to the strong and much faster mineralization of TMV_{wt} particles from TEOS solution in alkaline or more acidic pH regimes, as performed in other labs and described above.

TEM analyses of the mineralized products confirmed the findings for the distinct TMV templates (not shown), with TMV-KD10-silica composites showing the strongest and most homogeneous contrast of otherwise non-stained samples. This template was therefore selected for a twelve day time course experiment to investigate the growth kinetics of its mineral shells, and if the thickness of the silica coating might be controlled *via* the TEOS incubation time. Total widths of randomly selected low-contrast TMV-KD10 cores surrounded by electron-dense sheaths were measured on digital TEM images by help of image processing software from the fifth day onwards, which revealed an increase of layer thickness with progressing time (**Figure 5**). After ten days reaction time, the TMV-silica hybrids exhibited average diameters of about 29 ±2 nm, which did not further increase upon extended incubation. At the same time, granular SiO_2 deposits began to differentiate on the nanotube surfaces, rendering them less smooth than during earlier stages. The overall diameter, that is the height of TMV-KD10-templated hybrid rods after ten days mineralization was additionally measured by AFM (data not shown). For this purpose, mineralized

viruses were deposited on a silicon substrate. The average of the resulting mean values of the virus height was in good agreement with the TEM data and revealed a typical particle diameter of 30 nm, corresponding to a ≈6 nm linker-peptide-silica coating of the 18 nm TMV core. Different from non-modified viral rods immobilized on a silicon substrate, where reduction of the virus height due to attraction to the substrate surface is observed (Knez et al. 2004b), the adhesion of mineralized viruses from suspensions to the wafer substrates did not reduce the objects' height. This indicated the formation of a rigid composite not radially compressed upon its surface adsorption.

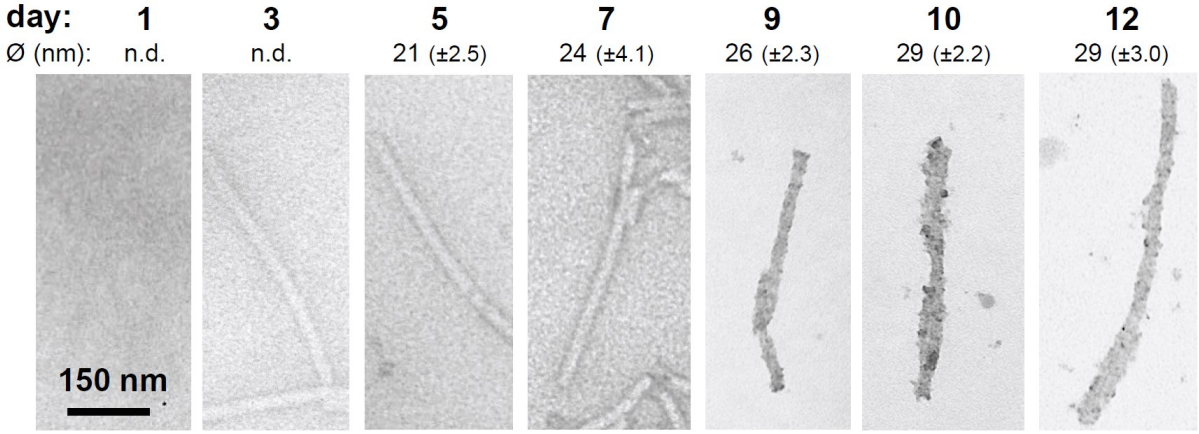

Figure 5: Time-resolved monitoring of silica shell growth on TMV-KD10 templates: TEM analysis of non-stained specimens, after the reaction times indicated above. Total average diameters (Ø; ± standard deviations) of mineralized TMV-KD10-hybrids were determined from 11-15 randomly selected nanorod products collected in-between one and twelve days incubation times.

ToF-SIMS analysis of the deposited material

An analysis of the deposited materials with time-of-flight secondary ion mass spectrometry (ToF-SIMS; Belu et al. 2003) was performed on air-dried drop cast suspensions of TMV_{wt} or TMV-KD10 particles (both with and without 10 days of exposure to TEOS). Positive and negative secondary ion spectra were recorded from random positions of the TMV deposits. The peak assignment is based on high mass resolution data and isotope patterns for Si. As shown in **Figure 6**, the intensity of Si^+ signals decreases substantially from TMV-KD10 particles incubated with TEOS (blue) to the TMV_{wt} control with TEOS (red) to both negative controls not incubated in TEOS solutions (green and purple). Analyzing $SiOH^+$ and several fragments characteristic for silica in negative polarity spectra (SiO_2^-, SiO_3^-,SiO_3H^-) indicated the same trend. Since the sample preparation method did not yield fully TMV-covered samples, the recorded mass spectra averaged over a field of view of 500×500 μm^2

show individual levels of Au^- stemming from the underlying substrate. In order to correct for this dispersion or area effect, the raw intensities of Si^+ and $SiOH^+$ were normalized according to the gold signals of each analyzed spot. Semi-quantitative silicification levels obtained thereof are presented in **Table 3**. As shown in **Table 3**, normalized intensities of two silica-derived fragments obtained with SIMS allow for a rough but reasonable quantification of the conversion of TEOS to silica induced by bare and KD10-functionalized TMV particles.

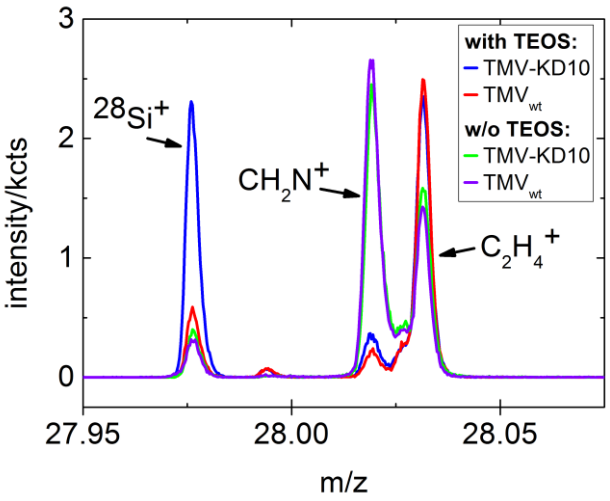

Figure 6: ToF-SIMS analysis for determination of silica deposition. TMV-KD10 with TEOS (blue) and without TEOS (green), TMV_{wt} with TEOS (red) and without TEOS (purple) after ten days incubation. The peak at m/z 27.97 indicates Si, the peak at m/z 28.02 CH_2N^+, and the peak at m/z 28.03 $C_2H_4^+$. For TMV-KD10 with TEOS and TMV_{wt} with TEOS the decrease of the CH_2N^+ peak, indicating peptide/protein components, is an indirect effect of the mineralization shielding the soft-matter surface of biotemplate particles.

Table 3: Relative silicification levels determined from normalized Si^+ and $SiOH^+$ intensities in SIMS. TEOS exposure 10 days, if applicable. For details see text.

Construct	Normalized Si^+	Normalized $SiOH^+$
TMV-KD10 with TEOS	100%	100%
TMV_{wt} with TEOS	18%	17%
TMV-KD10 w/o TEOS	1%	1%
TMV_{wt} w/o TEOS	<1%	<1%

While all negative controls not exposed to TEOS show negligible levels of Si^+ and $SiOH^+$, both TMV-KD10 and TMV_{wt} exposed to TEOS did form insoluble silica to considerably different extents. This resulted in about five times higher amounts of mineral on the peptide-modified virus. This finding is in agreement with our microscopic observations, which were not sufficient to resolve the deposition of silica on the wild type viral template. The ToF-SIMS analysis therefore revealed either a spontaneous hydrolysis of TEOS also occurring in the absence of effector peptides, or a low but specific mineralization-promoting activity of the bare viral CP surface not detectable by electron-optical imaging. The low SIMS Si^+ and $SiOH^+$ signal intensities, and necessary high mass resolution for unambiguous fragment

assignments precluded SIMS imaging with high lateral resolution. Hence, the obtained SIMS data cannot visualize mineralized individual TMV particles or distinguish between silica bound to virus particles and silica deposited by self-hydrolysis.

Conclusion

A systematic comparison of TMV-based nanobiotemplates chemically functionalized with different types of mineralization-affecting peptides revealed superior capacities of repetitive alternating KD sequences in guiding the deposition of silica sheaths from TEOS precursor solutions around the viral soft-matter cores. The peptide KD10 designed in this study on the basis of earlier tests (Kuno et al. 2011) allowed for the most selective and controllable silicification by sol-gel condensation. This was likely due to its charge relay activity, in comparison to different histidine-containing effector peptides and the bare or linker-coated viral scaffold surface. To our knowledge, this is the first evaluation of peptide-equipped TMV templates with regard to the generation of silica nanostructures of adjustable diameter. The previous studies of other researchers, all of which employed natural or aniline-modified TMV to nucleate silica deposition (as specified above), yielded either nanometric coatings of individual particles, or differently organized bio-inorganic mesostructures, but did not focus on fine-tuning the growth of the silica shells on the one-to-ten nm range. This was intended here and best achieved by the KD10-exposing TMV variant, for which a convincing correlation between silicification time and mineral layer thickness could be demonstrated.

The KD10-fashioned plant viruses thus enable the one-pot manufacture of freely suspended silica nanorods with soft-matter core, devoid of significant amounts of by-products. It would be interesting to characterize the mechanical properties of these composites in comparison to synthetically synthesized silica nanorods. This could potentially lead to fundamentally novel types of fiber-reinforced biohybrid materials. Furthermore, the method may also give rise to an efficient fabrication of rigid ultrasmall components of unusual shapes, on the basis of different non-linear kinked and branched TMV-based architectures generated recently in our lab (Eber et al. 2015).

Finally, peptides spatially immobilized in a selective manner on certain target sites of biotemplates might also be a clue to the use of silica deposition as a “bionic glue”. On appropriate TMV variants, specific coupling groups of amino acids are confined to

outer, inner or end surfaces of the nucleoprotein tubes, respectively. Serial *in vitro* assembly of different genetically engineered CP types on RNA scaffolds can even generate nanorod subdomains, offering unique coupling functionality (Geiger et al. 2013). Addressing such sites for a selective conjugation of mineralization-guiding peptides such as KD10 might pave future routes towards a firm and controlled integration of TMV-based nanostructures into miniaturized devices, where they might act e.g. as adaptor templates enabling an ultradense presentation of functional molecules on the non-mineralized regions of their multivalent protein surfaces.

Taken together, extended composite bio-hybrid materials and complex miniaturized systems both might profit from the precise shapes, high availabilities and immense *in vitro* tuning potential of plant viral templates, and their peptide-controlled transformation into mineralized nanostructured composites adapted to specific future applications.

Acknowledgments

The authors are grateful to Diether Gotthardt and Sigi Kober for gardening and technical assistance at the University of Stuttgart, and to Sourabh Shukla and Nicole Steinmetz, Case Western Reserve University, Cleveland, Ohio, U.S.A., for sharing lab instructions with us. Many thanks go to the DFG (SPP1569 and PAK415) for funding, and the Carl-Zeiss-Stiftung for additional financial support via the Projekthaus NanoBioMater at the University of Stuttgart.

References

Acar, H., Garifullin, R. & Guler, M. O. 2011. 'Self-assembled template-directed synthesis of one-dimensional silica and titania nanostructures.' *Langmuir,* 27, 1079-1084.

Adams, M. J., Heinze, C., Jackson, A. O., Kreuze, J. F., MacFarlane, S. A. & Torrance, L. 2012. 'Virus taxonomy: ninth report of the international committee on taxonomy of viruses.' In A. M. Q. King, M. J. Adams, E. B. Carstens & E. J. Lefkowitz (Eds.) *Family Virgaviridae:* 1139-1162. San Diego, CA, U.S.A.: Elsevier.

Aljabali, A. A. A., Barclay, J. E., Cespedes, O., Rashid, A., Staniland, S. S., Lomonossoff, G. P. & Evans, D. J. 2011a. 'Charge modified cowpea mosaic virus particles for templated mineralization.' *Adv Funct Mater,* 21, 4137-4142.

Aljabali, A. A. A., Shah, S. N., Evans-Gowing, R., Lomonossoff, G. P. & Evans, D. J. 2011b. 'Chemically-coupled-peptide-promoted virus nanoparticle templated mineralization.' *Integr Biol,* 3, 119-125.

Almora-Barrios, N., Austen, K. F. & de Leeuw, N. H. 2009. 'Density functional theory study of the binding of glycine, proline, and hydroxyproline to the hydroxyapatite (0001) and (0110) surfaces.' *Langmuir,* 25, 5018-5025.

Alonso, J. M., Gorzny, M. L. & Bittner, A. M. 2013. 'The physics of tobacco mosaic virus and virus-based devices in biotechnology.' *Trends Biotechnol,* 31, 530-538.

Altunbas, A., Sharma, N., Lamm, M. S., Yan, C. Q., Nagarkar, R. P., Schneider, J. P. & Pochan, D. J. 2010. 'Peptide-silica hybrid networks: biomimetic control of network mechanical behavior.' *ACS Nano,* 4, 181-188.

Atanasova, P., Rothenstein, D., Schneider, J. J., Hoffmann, R. C., Dilfer, S., Eiben, S., Wege, C., Jeske, H. & Bill, J. 2011. 'Virus-templated synthesis of ZnO nanostructures and formation of field-effect transistors.' *Adv Mater,* 23, 4918-4922.

Atanasova, P., Stitz, N., Sanctis, S., Maurer, J. H., Hoffmann, R. C., Eiben, S., Jeske, H., Schneider, J. J. & Bill, J. 2015. 'Genetically improved monolayer-forming tobacco mosaic viruses to generate nanostructured semiconducting bio/inorganic hybrids.' *Langmuir,* 31, 3897-3903.

Baio, J. E., Zane, A., Jaeger, V., Roehrich, A. M., Lutz, H., Pfaendtner, J., Drobny, G. P. & Weidner, T. 2014. 'Diatom mimics: directing the formation of biosilica nanoparticles by controlled folding of lysine-leucine peptides.' *J Am Chem Soc,* 136, 15134-15137.

Balci, S., Bittner, A. M., Schirra, M., Thonke, K., Sauer, R., Hahn, K., Kadri, A., Wege, C., Jeske, H. & Kern, K. 2009. 'Catalytic coating of virus particles with zinc oxide.' *Electrochim Acta,* 54, 5149-5154.

Belu, A. M., Graham, D. J. & Castner, D. G. 2003. 'Time-of-flight secondary ion mass spectrometry: techniques and applications for the characterization of biomaterial surfaces.' *Biomaterials,* 24, 3635-3653.

Bittner, A. M., Alonso, J. M., Gorzny, M. L. & Wege, C. 2013. 'Nanoscale science and technology with plant viruses and bacteriophages.' *Subcell Biochem,* 68, 667-702.

Bouwmeester, H., Brandhoff, P., Marvin, H. J. P., Weigel, S. & Peters, R. J. B. 2014. 'State of the safety assessment and current use of nanomaterials in food and food production.' *Trends Food Sci Tech,* 40, 200-210.

Bruckman, M. & Steinmetz, N. 2014. 'Chemical modification of the inner and outer surfaces of tobacco mosaic virus (TMV).' In B. Lin & B. Ratna (Eds.) *Virus hybrids as nanomaterials:* 173-185. New York: Humana Press.

Bruckman, M. A., Jiang, K., Simpson, E. J., Randolph, L. N., Luyt, L. G., Yu, X. & Steinmetz, N. F. 2014. 'Dual-modal magnetic resonance and fluorescence imaging of atherosclerotic plaques *in vivo* using VCAM-1 targeted tobacco mosaic virus.' *Nano Lett,* 14, 1551-1558.

Bruckman, M. A., Soto, C. M., McDowell, H., Liu, J. L., Ratna, B. R., Korpany, K. V., Zahr, O. K. & Blum, A. S. 2011. 'Role of hexahistidine in directed nanoassemblies of tobacco mosaic virus coat protein.' *ACS Nano,* 5, 1606-1616.

Butler, P. J. 1999. 'Self-assembly of tobacco mosaic virus: the role of an intermediate aggregate in generating both specificity and speed.' *Philos Trans R Soc Lond B Biol Sci,* 354, 537-550.

Cademartiri, R., Brook, M. A., Pelton, R. & Brennan, J. D. 2009. 'Macroporous silica using a "sticky" Stober process.' *J Mater Chem,* 19, 1583-1592.

Cha, J. N., Shimizu, K., Zhou, Y., Christiansen, S. C., Chmelka, B. F., Stucky, G. D. & Morse, D. E. 1999. 'Silicatein filaments and subunits from a marine sponge direct the polymerization of silica and silicones *in vitro*.' *Proc Natl Acad Sci U S A,* 96, 361-365.

Chen, X. L., Gerasopoulos, K., Guo, J. C., Brown, A., Ghodssi, R., Culver, J. N. & Wang, C. S. 2011. 'High rate performance of virus enabled 3D n-type Si anodes for lithium-ion batteries.' *Electrochim Acta,* 56, 5210-5213.

Chiang, C. Y., Epstein, J., Brown, A., Munday, J. N., Culver, J. N. & Ehrman, S. 2012. 'Biological templates for antireflective current collectors for photoelectrochemical cell applications.' *Nano Lett,* 12, 6005-6011.

Clare, D. K. & Orlova, E. V. 2010. '4.6 Å Cryo-EM reconstruction of tobacco mosaic virus from images recorded at 300 keV on a 4k x 4k CCD camera.' *J Struct Biol,* 171, 303-308.

Culver, J. N. 2002. 'Tobacco mosaic virus assembly and disassembly: determinants in pathogenicity and resistance.' *Annu Rev Phytopathol,* 40, 287-308.

Culver, J. N., Brown, A. D., Zang, F., Gnerlich, M., Gerasopoulos, K. & Ghodssi, R. 2015. 'Plant virus directed fabrication of nanoscale materials and devices.' *Virology,* 479-480, 200-212.

Dujardin, E., Peet, C., Stubbs, G., Culver, J. N. & Mann, S. 2003. 'Organization of metallic nanoparticles using tobacco mosaic virus templates.' *Nano Lett,* 3, 413-417.

Eber, F. J., Eiben, S., Jeske, H. & Wege, C. 2013. 'Bottom-up-assembled nanostar colloids of gold cores and tubes derived from tobacco mosaic virus.' *Angew Chem Int Ed Engl,* 52, 7203-7207.

Eber, F. J., Eiben, S., Jeske, H. & Wege, C. 2015. 'RNA-controlled assembly of tobacco mosaic virus-derived complex structures: from nanoboomerangs to tetrapods.' *Nanoscale,* 7, 344-355.

Eiben, S., Stitz, N., Eber, F., Wagner, J., Atanasova, P., Bill, J., Wege, C. & Jeske, H. 2014. 'Tailoring the surface properties of tobacco mosaic virions by the integration of bacterially expressed mutant coat protein.' *Virus Res,* 180, 92-96.

Evans, D. J. 2009. 'Exploitation of plant and archaeal viruses in bionanotechnology.' *Biochem Soc Trans,* 37, 665-670.

Filner, B. & Marcus, A. 1974. 'TMV coat protein synthesis *in vivo*: analysis of the N-terminal acetylation.' *Virology,* 61, 537-546.

Fowler, C. E., Shenton, W., Stubbs, G. & Mann, S. 2001. 'Tobacco mosaic virus liquid crystals as templates for the interior design of silica mesophases and nanoparticles.' *Adv Mater,* 13, 1266-1269.

Fujikawa, S. & Kunitake, T. 2003. 'Surface fabrication of hollow nanoarchitectures of ultrathin titania layers from assembled latex particles and tobacco mosaic viruses as templates.' *Langmuir,* 19, 6545-6552.

Ge, P. & Zhou, Z. H. 2011. 'Hydrogen-bonding networks and RNA bases revealed by cryo electron microscopy suggest a triggering mechanism for calcium switches.' *Proc Natl Acad Sci U S A,* 108, 9637-9642.

Gebauer, D., Kellermeier, M., Gale, J. D., Bergstrom, L. & Colfen, H. 2014. 'Pre-nucleation clusters as solute precursors in crystallisation.' *Chem Soc Rev,* 43, 2348-2371.

Geiger, F. C., Eber, F. J., Eiben, S., Müller, A., Jeske, H., Spatz, J. P. & Wege, C. 2013. 'TMV nanorods with programmed longitudinal domains of differently addressable coat proteins.' *Nanoscale,* 5, 3808-3816.

Gooding, G. V., Jr. & Hebert, T. T. 1967. 'A simple technique for purification of tobacco mosaic virus in large quantities.' *Phytopathology,* 57, 1285.

Green, M. R. & Sambrook, J. 2012. *Molecular cloning: a laboratory manual.* New York, NY, U.S.A.: Cold Spring Harbor Laboratory Press.

Henstock, J. R., Canham, L. T. & Anderson, S. I. 2015. 'Silicon: the evolution of its use in biomaterials.' *Acta Biomater,* 11, 17-26.

Hong, J. H., Duncan, S. E. & Dietrich, A. M. 2010. 'Effect of copper speciation at different pH on temporal sensory attributes of copper.' *Food Qual Prefer,* 21, 132-139.

Hunter, R. J. 1981. *Zeta potential in colloid science: principles and applications.* London, San Diego, New York, Berkeley, Boston, Sydney, Tokoy, Toronto: Academic Press.

Kadri, A., Maiss, E., Amsharov, N., Bittner, A. M., Balci, S., Kern, K., Jeske, H. & Wege, C. 2011. 'Engineered tobacco mosaic virus mutants with distinct physical characteristics in planta and enhanced metallization properties.' *Virus Res,* 157, 35-46.

Kim, Y. J., Hwang, K. H., Park, S. J., Jeon, D. Y., Nam, C. H. & Kim, G. T. 2013. 'Fabrication of a silica nanocable using hydroxyl-group core-engineered filamentous virus.' *J Nanosci Nanotechnol,* 13, 6203-6207.

Knez, M., Sumser, M. P., Bittner, A. M., Wege, C., Jeske, H., Hoffmann, D. M. P., Kuhnke, K. & Kern, K. 2004b. 'Binding the tobacco mosaic virus to inorganic surfaces.' *Langmuir,* 20, 441-447.

Kröger, N., Deutzmann, R. & Sumper, M. 1999. 'Polycationic peptides from diatom biosilica that direct silica nanosphere formation.' *Science,* 286, 1129-1132.

Kuno, T., Nonoyama, T., Hirao, K. & Kato, K. 2011. 'Influence of the charge relay effect on the silanol condensation reaction as a model for silica biomineralization.' *Langmuir,* 27, 13154-13158.

Laemmli, U. K. 1970. 'Cleavage of structural proteins during the assembly of the head of bacteriophage T4.' *Nature,* 227, 680-685.

Leblanc, J. L. 2002. 'Rubber-filler interactions and rheological properties in filled compounds.' *Prog Polym Sci,* 27, 627-687.

Li, D., Qu, X., Newton, S. M., Klebba, P. E. & Mao, C. 2012. 'Morphology-controlled synthesis of silica nanotubes through pH- and sequence-responsive morphological change of bacterial flagellar biotemplates.' *J Mater Chem,* 22, 15702-15709.

Li, F. & Wang, Q. B. 2014. 'Fabrication of nanoarchitectures templated by virus-based nanoparticles: strategies and applications.' *Small,* 10, 230-245.

Lomonossoff, G. & Evans, D. 2014. 'Applications of plant viruses in bionanotechnology.' In K. Palmer & Y. Gleba (Eds.) *Plant viral vectors:* 61-87. Berlin, Heidelberg: Springer-Verlag.

Luckanagul, J., Lee, L. A., Nguyen, Q. L., Sitasuwan, P., Yang, X. M., Shazly, T. & Wang, Q. 2012. 'Porous alginate hydrogel functionalized with virus as three-dimensional scaffolds for bone differentiation.' *Biomacromolecules,* 13, 3949-3958.

Luckanagul, J. A., Lee, L. A., You, S. J., Yang, X. M. & Wang, Q. 2015. 'Plant virus incorporated hydrogels as scaffolds for tissue engineering possess low immunogenicity *in vivo*.' *J Biomed Mater Res A,* 103, 887-895.

Mann, S. 1983. 'Mineralization in biological systems.' *Struct Bond,* 54, 125-174.

Mann, S. 2009. 'Self-assembly and transformation of hybrid nano-objects and nanostructures under equilibrium and non-equilibrium conditions.' *Nat Mater,* 8, 781-792.

Mao, C., Liu, A. & Cao, B. 2009. 'Virus-based chemical and biological sensing.' *Angew Chem Int Ed Engl,* 48, 6790-6810.

Mao, C. B., Solis, D. J., Reiss, B. D., Kottmann, S. T., Sweeney, R. Y., Hayhurst, A., Georgiou, G., Iverson, B. & Belcher, A. M. 2004. 'Virus-based toolkit for the directed synthesis of magnetic and semiconducting nanowires.' *Science,* 303, 213-217.

Müller, A., Eber, F. J., Azucena, C., Petershans, A., Bittner, A. M., Gliemann, H., Jeske, H. & Wege, C. 2011. 'Inducible site-selective bottom-up assembly of virus-derived nanotube arrays on RNA-equipped wafers.' *ACS Nano,* 5, 4512-4520.

Müller, R. H. & Hildebrand, G. E. 1996. *Zetapotential und Partikelladung in der Laborpraxis: Einführung in die Theorie - praktische Messdurchführung - Dateninterpretation; Colloidal drug carriers (cdc) 1st expert meeting Berlin 15. - 17. 6. 1995.* Stuttgart: Wissenschaftliche Verlagsgesellschaft.

Namba, K., Pattanayek, R. & Stubbs, G. 1989. 'Visualization of protein-nucleic acid interactions in a virus. Refined structure of intact tobacco mosaic virus at 2.9 Å resolution by x-ray fiber diffraction.' *J Mol Biol,* 208, 307-325.

Niu, Z., Kabisatpathy, S., He, J., Lee, L. A., Rong, J., Yang, L., Sikha, G., Popov, B., Emrick, T., Russell, T. & Wang, Q. 2009. 'Synthesis and characterization of bionanoparticle—Silica composites and mesoporous silica with large pores.' *Nano Res,* 2, 474-483.

Niu, Z., Liu, J., Lee, L. A., Bruckman, M. A., Zhao, D., Koley, G. & Wang, Q. 2007. 'Biological templated synthesis of water-soluble conductive polymeric nanowires.' *Nano Lett,* 7, 3729-3733.

Paris, O., Burgert, I. & Fratzl, P. 2010. 'Biomimetics and biotemplating of natural materials.' *Mrs Bulletin,* 35, 219-225.

Patwardhan, S. V., Emami, F. S., Berry, R. J., Jones, S. E., Naik, R. R., Deschaume, O., Heinz, H. & Perry, C. C. 2012. 'Chemistry of aqueous silica nanoparticle surfaces and the mechanism of selective peptide adsorption.' *J Am Chem Soc,* 134, 6244-6256.

Pouget, E. & Grelet, E. 2013. 'Dispersions of monodisperse hybrid rod-like particles by mineralization of filamentous viruses.' *Langmuir,* 29, 8010-8016.

Poulsen, N. & Kröger, N. 2004. 'Silica morphogenesis by alternative processing of silaffins in the diatom *Thalassiosira pseudonana*.' *J Biol Chem,* 279, 42993-42999.

Putnam, C. accessed 2015. 'Protein Calculator v3.4 ' *The Scripps Research Institute, La Jolla, California, U.S.A.,* http://protcalc.sourceforge.net.

Reed, J. S. 1995. *Principles of ceramics processing.* New York, NY, U.S.A.: John Wiley & Sons, Inc.

Rong, J. H., Oberbeck, F., Wang, X. N., Li, X. D., Oxsher, J., Niu, Z. W. & Wang, Q. 2009. 'Tobacco mosaic virus templated synthesis of one dimensional inorganic-polymer hybrid fibres.' *J Mater Chem,* 19, 2841-2845.

Rothenstein, D., Claasen, B., Omiecienski, B., Lammel, P. & Bill, J. 2012. 'Isolation of ZnO-binding 12-mer peptides and determination of their binding epitopes by NMR spectroscopy.' *J Am Chem Soc,* 134, 12547-12556.

Rothenstein, D., Facey, S. J., Ploss, M., Hans, P., Melcher, M., Srot, V., van Aken, P. A., Hauer, B. & Bill, J. 2013. 'Mineralization of gold nanoparticles using tailored M13 phages.' *Bioinspir Biomim Nan,* 2, 173-185.

Royston, E., Lee, S. Y., Culver, J. N. & Harris, M. T. 2006. 'Characterization of silica-coated tobacco mosaic virus.' *J Colloid Interface Sci,* 298, 706-712.

Royston, E. S., Brown, A. D., Harris, M. T. & Culver, J. N. 2009. 'Preparation of silica stabilized tobacco mosaic virus templates for the production of metal and layered nanoparticles.' *J Colloid Interface Sci,* 332, 402-407.

Sachse, C., Chen, J. Z., Coureux, P. D., Stroupe, M. E., Fandrich, M. & Grigorieff, N. 2007. 'High-resolution electron microscopy of helical specimens: a fresh look at tobacco mosaic virus.' *J Mol Biol,* 371, 812-835.

Schlick, T. L., Ding, Z., Kovacs, E. W. & Francis, M. B. 2005. 'Dual-surface modification of the tobacco mosaic virus.' *J Am Chem Soc,* 127, 3718-3723.

Schneider, C. A., Rasband, W. S. & Eliceiri, K. W. 2012. 'NIH Image to ImageJ: 25 years of image analysis.' *Nat Methods,* 9, 671-675.

Shenton, W., Douglas, T., Young, M., Stubbs, G. & Mann, S. 1999. 'Inorganic-organic nanotube composites from template mineralization of tobacco mosaic virus.' *Adv Mater,* 11, 253-256.

Shukla, S., Eber, F. J., Nagarajan, A. S., DiFranco, N. A., Schmidt, N., Wen, A. M., Eiben, S., Twyman, R. M., Wege, C. & Steinmetz, N. F. 2015. 'The impact of aspect ratio on the biodistribution and tumor homing of rigid soft-matter nanorods.' *Adv Healthc Mater,* 4, 874-882.

Smith, M. L., Lindbo, J. A., Dillard-Telm, S., Brosio, P. M., Lasnik, A. B., McCormick, A. A., Nguyen, L. V. & Palmer, K. E. 2006. 'Modified tobacco mosaic virus particles as scaffolds for display of protein antigens for vaccine applications.' *Virology,* 348, 475-488.

Stark, W. J., Stoessel, P. R., Wohlleben, W. & Hafner, A. 2015. 'Industrial applications of nanoparticles.' *Chem Soc Rev,* 44, 5793-5805.

Steinmetz, N. F., Shah, S. N., Barclay, J. E., Rallapalli, G., Lomonossoff, G. P. & Evans, D. J. 2009. 'Virus-templated silica nanoparticles.' *Small,* 5, 813-816.

Stöber, W., Fink, A. & Bohn, E. 1968. 'Controlled growth of monodisperse silica spheres in micron size range.' *J Colloid Interface Sci,* 26, 62-69.

Sumper, M. & Kröger, N. 2004. 'Silica formation in diatoms: the function of long-chain polyamines and silaffins.' *J Mater Chem,* 14, 2059-2065.

Tang, F., Li, L. & Chen, D. 2012. 'Mesoporous silica nanoparticles: synthesis, biocompatibility and drug delivery.' *Adv Mater,* 24, 1504-1534.

Vallet-Regi, M. & Ruiz-Hernandez, E. 2011. 'Bioceramics: from bone regeneration to cancer nanomedicine.' *Adv Mater,* 23, 5177-5218.

Weiner, S. & Dove, P. M. 2003. 'An overview of biomineralization processes and the problem of the vital effect.' *Rev Mineral Geochem,* 54, 1-29.

Wu, Z., Müller, A., Degenhard, S., Ruff, S. E., Geiger, F., Bittner, A. M., Wege, C. & Krill, C. E., 3rd 2010. 'Enhancing the magnetoviscosity of ferrofluids by the addition of biological nanotubes.' *ACS Nano,* 4, 4531-4538.

Wu, Z., Xiang, H., Kim, T., Chun, M. S. & Lee, K. 2006. 'Surface properties of submicrometer silica spheres modified with aminopropyltriethoxysilane and phenyltriethoxysilane.' *J Colloid Interface Sci,* 304, 119-124.

Yang, C., Choi, C. H., Lee, C. S. & Yi, H. 2013a. 'A facile synthesis-fabrication strategy for integration of catalytically active viral-palladium nanostructures into polymeric hydrogel microparticles *via* replica molding.' *ACS Nano,* 7, 5032-5044.

Yang, S. H., Chung, W. J., McFarland, S. & Lee, S. W. 2013b. 'Assembly of bacteriophage into functional materials.' *Chem Rec,* 13, 43-59.

Yang, X., Tang, H., Cao, K., Song, H., Sheng, W. & Wu, Q. 2011b. 'Templated-assisted one-dimensional silica nanotubes: synthesis and applications.' *J Mater Chem,* 21, 6122-6135.

Yildirim, A., Acar, H., Erkal, T. S., Bayindir, M. & Guler, M. O. 2011. 'Template-directed synthesis of silica nanotubes for explosive detection.' *ACS Appl Mater Interfaces,* 3, 4159-4164.

Yuwono, V. M. & Hartgerink, J. D. 2007. 'Peptide amphiphile nanofibers template and catalyze silica nanotube formation.' *Langmuir,* 23, 5033-5038.

Zaitlin, M. 2000. 'Tobacco mosaic virus.' *AAB Descr. Plant Viruses,* 370, 1-13.

Zane, A. C., Michelet, C., Roehrich, A., Emani, P. S. & Drobny, G. P. 2014. 'Silica morphogenesis by lysine-leucine peptides with hydrophobic periodicity.' *Langmuir,* 30, 7152-7161.

Zollfrank, C., Scheibel, T., Seitz, H. & Travitzky, N. 2014. 'Bioinspired materials engineering.' *Ullmann's Encyclopedia of Industrial Chemistry*. Wiley-VCH Verlag GmbH & Co. KGaA.

Bibliographie

Acar, H., Garifullin, R. & Guler, M. O. 2011. 'Self-assembled template-directed synthesis of one-dimensional silica and titania nanostructures.' *Langmuir,* 27, 1079-1084.

Acikgoz, C., Hempenius, M. A., Huskens, J. & Vancso, G. J. 2011. 'Polymers in conventional and alternative lithography for the fabrication of nanostructures.' *Eur Polym J,* 47, 2033-2052.

Adams, M. J., Heinze, C., Jackson, A. O., Kreuze, J. F., MacFarlane, S. A. & Torrance, L. 2012. 'Virus taxonomy: ninth report of the international committee on taxonomy of viruses.' In A. M. Q. King, M. J. Adams, E. B. Carstens & E. J. Lefkowitz (Eds.) *Family Virgaviridae:* 1139-1162. San Diego, CA, U.S.A.: Elsevier.

Adiga, S. P., Jin, C., Curtiss, L. A., Monteiro-Riviere, N. A. & Narayan, R. J. 2009. 'Nanoporous membranes for medical and biological applications.' *Wiley Interdiscip Rev Nanomed Nanobiotechnol,* 1, 568-581.

Adigun, O. O., Freer, A. S., Miller, J. T., Loesch-Fries, L. S., Kim, B. S. & Harris, M. T. 2015. 'Mechanistic study of the hydrothermal reduction of palladium on the tobacco mosaic virus.' *J Colloid Interface Sci,* 450, 1-6.

Adleman, L. M. 1994. 'Molecular computation of solutions to combinatorial problems.' *Science,* 266, 1021-1024.

Aljabali, A. A. A., Barclay, J. E., Cespedes, O., Rashid, A., Staniland, S. S., Lomonossoff, G. P. & Evans, D. J. 2011a. 'Charge modified cowpea mosaic virus particles for templated mineralization.' *Adv Funct Mater,* 21, 4137-4142.

Aljabali, A. A. A., Shah, S. N., Evans-Gowing, R., Lomonossoff, G. P. & Evans, D. J. 2011b. 'Chemically-coupled-peptide-promoted virus nanoparticle templated mineralization.' *Integr Biol,* 3, 119-125.

Almora-Barrios, N., Austen, K. F. & de Leeuw, N. H. 2009. 'Density functional theory study of the binding of glycine, proline, and hydroxyproline to the hydroxyapatite (0001) and (0110) surfaces.' *Langmuir,* 25, 5018-5025.

Alonso, J. M., Gorzny, M. L. & Bittner, A. M. 2013. 'The physics of tobacco mosaic virus and virus-based devices in biotechnology.' *Trends Biotechnol,* 31, 530-538.

Altintoprak, K., Seidenstücker, A., Welle, A., Eiben, S., Atanasova, P., Stitz, N., Plettl, A., Bill, J., Gliemann, H., Jeske, H., Rothenstein, D., Geiger, F. & Wege, C. 2015. 'Peptide-equipped tobacco mosaic virus templates for selective and controllable biomineral deposition.' *Beilstein J Nanotech,* 6, 1399-1412.

Altunbas, A., Sharma, N., Lamm, M. S., Yan, C. Q., Nagarkar, R. P., Schneider, J. P. & Pochan, D. J. 2010. 'Peptide-silica hybrid networks: biomimetic control of network mechanical behavior.' *ACS Nano,* 4, 181-188.

Anderson, H. 1989. 'Mechanism of mineral formation in bone.' *Lab Invest,* 60, 320-330.

Anwander, E. H., Probst, M. M. & Rode, B. M. 1990. 'The influence of Li^+, Na^+, Mg^{2+}, Ca^{2+}, and Zn^{2+} ions on the hydrogen bonds of the Watson-Crick base pairs.' *Biopolymers,* 29, 757-769.

Atanasova, P., Rothenstein, D., Schneider, J. J., Hoffmann, R. C., Dilfer, S., Eiben, S., Wege, C., Jeske, H. & Bill, J. 2011. 'Virus-templated synthesis of ZnO nanostructures and formation of field-effect transistors.' *Adv Mater,* 23, 4918-4922.

Atanasova, P., Stitz, N., Sanctis, S., Maurer, J. H., Hoffmann, R. C., Eiben, S., Jeske, H., Schneider, J. J. & Bill, J. 2015. 'Genetically improved monolayer-forming tobacco mosaic viruses to generate nanostructured semiconducting bio/inorganic hybrids.' *Langmuir,* 31, 3897-3903.

Azucena, C., Eber, F. J., Trouillet, V., Hirtz, M., Heissler, S., Franzreb, M., Fuchs, H., Wege, C. & Gliemann, H. 2012. 'New approaches for bottom-up assembly of tobacco mosaic virus-derived nucleoprotein tubes on defined patterns on silica- and polymer-based substrates.' *Langmuir,* 28, 14867-14877.

Baio, J. E., Zane, A., Jaeger, V., Roehrich, A. M., Lutz, H., Pfaendtner, J., Drobny, G. P. & Weidner, T. 2014. 'Diatom mimics: directing the formation of biosilica nanoparticles by controlled folding of lysine-leucine peptides.' *J Am Chem Soc,* 136, 15134-15137.

Balci, S., Bittner, A. M., Schirra, M., Thonke, K., Sauer, R., Hahn, K., Kadri, A., Wege, C., Jeske, H. & Kern, K. 2009. 'Catalytic coating of virus particles with zinc oxide.' *Electrochim Acta,* 54, 5149-5154.

Banerjee, I., Pangule, R. C. & Kane, R. S. 2011. 'Antifouling coatings: recent developments in the design of surfaces that prevent fouling by proteins, bacteria, and marine organisms.' *Adv Mater,* 23, 690-718.

Banik, S., Mansour, A. A., Suresh, R. V., Wykoff-Clary, S., Malik, M., McCormick, A. A. & Bakshi, C. S. 2015. 'Development of a multivalent subunit vaccine against tularemia using tobacco mosaic virus (TMV) based delivery system.' *PLoS One,* 10, e0130858.

Bar, H., Yacoby, I. & Benhar, I. 2008. 'Killing cancer cells by targeted drug-carrying phage nanomedicines.' *BMC Biotechnol,* 8, 1-14.

Bayley, H. & Jayasinghe, L. 2004. 'Functional engineered channels and pores (Review).' *Mol Membr Biol,* 21, 209-220.

Beijerinck, M. 1898. 'Concerning a *contagium vivum fluidum* as cause of the spot disease of tobacco leaves.' *Phytopathological Classics,* 7, 33-52.

Bell, N. A., Engst, C. R., Ablay, M., Divitini, G., Ducati, C., Liedl, T. & Keyser, U. F. 2012. 'DNA origami nanopores.' *Nano Lett,* 12, 512-517.

Belton, D. J., Deschaume, O., Patwardhan, S. V. & Perry, C. C. 2010. 'A solution study of silica condensation and speciation with relevance to *in vitro* investigations of biosilicification.' *J Phys Chem B,* 114, 9947-9955.

Belton, D. J., Deschaume, O. & Perry, C. C. 2012. 'An overview of the fundamentals of the chemistry of silica with relevance to biosilicification and technological advances.' *FEBS J,* 279, 1710-1720.

Belu, A. M., Graham, D. J. & Castner, D. G. 2003. 'Time-of-flight secondary ion mass spectrometry: techniques and applications for the characterization of biomaterial surfaces.' *Biomaterials,* 24, 3635-3653.

Bernards, T. N. M., Vanbommel, M. J. & Boonstra, A. H. 1991. 'Hydrolysis - condensation processes of the tetra-alkoxysilanes TPOS, TEOS and TMOS in some alcoholic solvents.' *J Non-Cryst Solids,* 134, 1-13.

Bhakdi, S. & Tranumjensen, J. 1991. 'Alpha-toxin of *Staphylococcus aureus*.' *Microbiol Rev,* 55, 733-751.

Bhattacharya, M., Wutticharoenmongkol-Thitiwongsawet, P., Hamamoto, D. T., Lee, D., Cui, T., Prasad, H. S. & Ahmad, M. 2011. 'Bone formation on carbon nanotube composite.' *J Biomed Mater Res A,* 96, 75-82.

Bhyravbhatla, B., Watowich, S. J. & Caspar, D. L. 1998. 'Refined atomic model of the four-layer aggregate of the tobacco mosaic virus coat protein at 2.4-Å resolution.' *Biophys J,* 74, 604-615.

Bittner, A. M., Alonso, J. M., Gorzny, M. L. & Wege, C. 2013. 'Nanoscale science and technology with plant viruses and bacteriophages.' *Subcell Biochem,* 68, 667-702.

Bittner, A. M., Wu, X. C., Balci, S., Knez, M., Kadri, A. & Kern, K. 2005. 'Bottom-up synthesis and top-down organisation of semiconductor and metal clusters on surfaces.' *Eur J Inorg Chem,* 2005, 3717-3728.

Bloomer, A. C., Champness, J. N., Bricogne, G., Staden, R. & Klug, A. 1978. 'Protein disk of tobacco mosaic virus at 2.8 Å resolution showing the interactions within and between subunits.' *Nature,* 276, 362-368.

Boersma, A. J. & Bayley, H. 2012. 'Continuous stochastic detection of amino acid enantiomers with a protein nanopore.' *Angew Chem Int Ed Engl,* 51, 9606-9609.

Bouas-Laurent, H., Castellan, A. & Desvergne, J.-P. 1980. 'From anthracene photodimerization to jaw photochromic materials and photocrowns.' *Pure Appl Chem,* 52, 2633-2648.

Bouwmeester, H., Brandhoff, P., Marvin, H. J. P., Weigel, S. & Peters, R. J. B. 2014. 'State of the safety assessment and current use of nanomaterials in food and food production.' *Trends Food Sci Tech,* 40, 200-210.

Broido, M. S. & Kearns, D. R. 1982. '^{1}H NMR evidence for a left-handed helical structure of poly(ribocytidylic acid) in neutral solution.' *J Am Chem Soc,* 104, 5207-5216.

Bruckman, M. & Steinmetz, N. 2014. 'Chemical modification of the inner and outer surfaces of tobacco mosaic virus (TMV).' In B. Lin & B. Ratna (Eds.) *Virus hybrids as nanomaterials:* 173-185. New York: Humana Press.

Bruckman, M. A., Jiang, K., Simpson, E. J., Randolph, L. N., Luyt, L. G., Yu, X. & Steinmetz, N. F. 2014. 'Dual-modal magnetic resonance and fluorescence imaging of atherosclerotic plaques *in vivo* using VCAM-1 targeted tobacco mosaic virus.' *Nano Lett,* 14, 1551-1558.

Bruckman, M. A., Randolph, L. N., Gulati, N. M., Stewart, P. L. & Steinmetz, N. F. 2015. 'Silica-coated Gd(DOTA)-loaded protein nanoparticles enable magnetic resonance imaging of macrophages.' *J Mater Chem B,* 3, 7503-7510.

Bruckman, M. A., Soto, C. M., McDowell, H., Liu, J. L., Ratna, B. R., Korpany, K. V., Zahr, O. K. & Blum, A. S. 2011. 'Role of hexahistidine in directed nanoassemblies of tobacco mosaic virus coat protein.' *ACS Nano,* 5, 1606-1616.

Brutchey, R. L. & Morse, D. E. 2008. 'Silicatein and the translation of its molecular mechanism of biosilicification into low temperature nanomaterial synthesis.' *Chem Rev,* 108, 4915-4934.

Buchmueller, K. L. & Weeks, K. M. 2004. 'Tris-borate is a poor counterion for RNA: a cautionary tale for RNA folding studies.' *Nucleic Acids Res,* 32, 1-6.

Butler, P. J. 1972. 'Structures and roles of the polymorphic forms of tobacco mosaic virus protein. VI. Assembly of the nucleoprotein rods of tobacco mosaic virus from the protein disks and RNA.' *J Mol Biol,* 72, 25-35.

Butler, P. J. 1999. 'Self-assembly of tobacco mosaic virus: the role of an intermediate aggregate in generating both specificity and speed.' *Philos Trans R Soc Lond B Biol Sci,* 354, 537-550.

Butler, P. J., Bloomer, A. C. & Finch, J. T. 1992. 'Direct visualization of the structure of the "20 S" aggregate of coat protein of tobacco mosaic virus. The "disk" is the major structure at pH 7.0 and the proto-helix at lower pH.' *J Mol Biol,* 224, 381-394.

Cademartiri, R., Brook, M. A., Pelton, R. & Brennan, J. D. 2009. 'Macroporous silica using a "sticky" Stober process.' *J Mater Chem,* 19, 1583-1592.

Cardinale, D., Carette, N. & Michon, T. 2012. 'Virus scaffolds as enzyme nano-carriers.' *Trends Biotechnol,* 30, 369-376.

Carpenter, J. M. 1970. 'The stacked-disk structure of tobacco mosaic virus protein.' *Virology,* 41, 603-614.

Cha, J. N., Shimizu, K., Zhou, Y., Christiansen, S. C., Chmelka, B. F., Stucky, G. D. & Morse, D. E. 1999. 'Silicatein filaments and subunits from a marine sponge

direct the polymerization of silica and silicones *in vitro*.' *Proc Natl Acad Sci U S A,* 96, 361-365.

Chen, H. B., Su, X. D., Neoh, K. G. & Choe, W. S. 2006. 'QCM-D analysis of binding mechanism of phage particles displaying a constrained heptapeptide with specific affinity to SiO_2 and TiO_2.' *Anal Chem,* 78, 4872-4879.

Chen, X. L., Gerasopoulos, K., Guo, J. C., Brown, A., Ghodssi, R., Culver, J. N. & Wang, C. S. 2011. 'High rate performance of virus enabled 3D n-type Si anodes for lithium-ion batteries.' *Electrochim Acta,* 56, 5210-5213.

Chiang, C. Y., Epstein, J., Brown, A., Munday, J. N., Culver, J. N. & Ehrman, S. 2012. 'Biological templates for antireflective current collectors for photoelectrochemical cell applications.' *Nano Lett,* 12, 6005-6011.

Choi, Y., Baker, L. A., Hillebrenner, H. & Martin, C. R. 2006. 'Biosensing with conically shaped nanopores and nanotubes (vol 8, pg 8, 2006).' *Phys Chem Chem Phys,* 8, 5131-5131.

Chung, W. J., Kwon, K. Y., Song, J. & Lee, S. W. 2011. 'Evolutionary screening of collagen-like peptides that nucleate hydroxyapatite crystals.' *Langmuir,* 27, 7620-7628.

Clare, D. K. & Orlova, E. V. 2010. '4.6 Å Cryo-EM reconstruction of tobacco mosaic virus from images recorded at 300 keV on a 4k x 4k CCD camera.' *J Struct Biol,* 171, 303-308.

Clarke, J., Wu, H. C., Jayasinghe, L., Patel, A., Reid, S. & Bayley, H. 2009. 'Continuous base identification for single-molecule nanopore DNA sequencing.' *Nat Nanotechnol,* 4, 265-270.

Coffman, E. A., Melechko, A. V., Allison, D. P., Simpson, M. L. & Doktycz, M. J. 2004. 'Surface patterning of silica nanostructures using bio-inspired templates and directed synthesis.' *Langmuir,* 20, 8431-8436.

Coggins, L. W. 1987. 'Preparation of nucleic acids for electron microscope.' In J. Sommerville & U. Scheer (Eds.) *Electron microscopy in molecular biology: a practical approach:* 1-29. Oxford: IRL Press.

Cognet, J. A. H., Pakleza, C., Cherny, D., Delain, E. & Le Cam, E. 1999. 'Static curvature and flexibility measurements of DNA with microscopy. A simple renormalization method, its assessment by experiment and simulation.' *J Mol Biol,* 285, 997-1009.

Colvin, V. L. 2003. 'The potential environmental impact of engineered nanomaterials.' *Nat Biotechnol,* 21, 1166-1170.

Coradin, T. & Livage, J. 2001. 'Effect of some amino acids and peptides on silicic acid polymerization.' *Colloid Surface B,* 21, 329-336.

Culver, J. N. 2002. 'Tobacco mosaic virus assembly and disassembly: determinants in pathogenicity and resistance.' *Annu Rev Phytopathol,* 40, 287-308.

Culver, J. N., Brown, A. D., Zang, F., Gnerlich, M., Gerasopoulos, K. & Ghodssi, R. 2015. 'Plant virus directed fabrication of nanoscale materials and devices.' *Virology,* 479-480, 200-212.

Danelon, C., Santschi, C., Brugger, J. & Vogel, H. 2006. 'Fabrication and functionalization of nanochannels by electron-beam-induced silicon oxide deposition.' *Langmuir,* 22, 10711-10715.

De Morais, M. G., Martins, V. G., Steffens, D., Pranke, P. & da Costa, J. A. 2014. 'Biological applications of nanobiotechnology.' *J Nanosci Nanotechnol,* 14, 1007-1017.

De Volder, M. & Hart, A. J. 2013. 'Engineering hierarchical nanostructures by elastocapillary self-assembly.' *Angew Chem Int Edit,* 52, 2412-2425.

Deamer, D. 2010. 'Nanopore analysis of nucleic acids bound to exonucleases and polymerases.' *Annu Rev Biophys,* 39, 79-90.

Dedeo, M. T., Duderstadt, K. E., Berger, J. M. & Francis, M. B. 2010. 'Nanoscale protein assemblies from a circular permutant of the tobacco mosaic virus.' *Nano Lett,* 10, 181-186.

Dittrich, P. S. & Manz, A. 2006. 'Lab-on-a-chip: microfluidics in drug discovery.' *Nat Rev Drug Discov,* 5, 210-218.

Draper, D. E. 1999. 'Themes in RNA-protein recognition.' *J Mol Biol,* 293, 255-270.

Du, H. L., Li, J. Y., Zhang, J., Su, G., Li, X. Y. & Zhao, Y. L. 2011. 'Separation of Hydrogen and Nitrogen Gases with Porous Graphene Membrane.' *J Phys Chem C,* 115, 23261-23266.

Dujardin, E., Peet, C., Stubbs, G., Culver, J. N. & Mann, S. 2003. 'Organization of metallic nanoparticles using tobacco mosaic virus templates.' *Nano Lett,* 3, 413-417.

Durham, A. C., Finch, J. T. & Klug, A. 1971. 'States of aggregation of tobacco mosaic virus protein.' *Nat New Biol,* 229, 37-42.

Durham, A. C. & Klug, A. 1971. 'Polymerization of tobacco mosaic virus protein and its control.' *Nat New Biol,* 229, 42-46.

Dvir, T., Timko, B. P., Kohane, D. S. & Langer, R. 2011. 'Nanotechnological strategies for engineering complex tissues.' *Nat Nanotechnol,* 6, 13-22.

Eber, F. J. 2012. 'RNA-directed formation of nanostructures: self-assembly of novel nuceloprotein architectures using plant viral building blocks.' *Fakultät 4: Energie-, Verfahrens- und Biotechnik:* 151. Universität Stuttgart.

Eber, F. J., Eiben, S., Jeske, H. & Wege, C. 2013. 'Bottom-up-assembled nanostar colloids of gold cores and tubes derived from tobacco mosaic virus.' *Angew Chem Int Ed Engl,* 52, 7203-7207.

Eber, F. J., Eiben, S., Jeske, H. & Wege, C. 2015. 'RNA-controlled assembly of tobacco mosaic virus-derived complex structures: from nanoboomerangs to tetrapods.' *Nanoscale,* 7, 344-355.

Eiben, S., Stitz, N., Eber, F., Wagner, J., Atanasova, P., Bill, J., Wege, C. & Jeske, H. 2014. 'Tailoring the surface properties of tobacco mosaic virions by the integration of bacterially expressed mutant coat protein.' *Virus Res,* 180, 92-96.

Eid, J., Fehr, A., Gray, J., Luong, K., Lyle, J., Otto, G., Peluso, P., Rank, D., Baybayan, P., Bettman, B., Bibillo, A., Bjornson, K., Chaudhuri, B., Christians, F., Cicero, R., Clark, S., Dalal, R., Dewinter, A., Dixon, J., Foquet, M., Gaertner, A., Hardenbol, P., Heiner, C., Hester, K., Holden, D., Kearns, G., Kong, X., Kuse, R., Lacroix, Y., Lin, S., Lundquist, P., Ma, C., Marks, P., Maxham, M., Murphy, D., Park, I., Pham, T., Phillips, M., Roy, J., Sebra, R., Shen, G., Sorenson, J., Tomaney, A., Travers, K., Trulson, M., Vieceli, J., Wegener, J., Wu, D., Yang, A., Zaccarin, D., Zhao, P., Zhong, F., Korlach, J. & Turner, S. 2009. 'Real-time DNA sequencing from single polymerase molecules.' *Science,* 323, 133-138.

El Shafei, G. M. S. 2000. 'Silica surface chemical properties.' In E. Papirer (Ed.) *Adsorption on silica surfaces:* 35-62. New York: Marcel Dekker Inc.

Evans, D. J. 2009. 'Exploitation of plant and archaeal viruses in bionanotechnology.' *Biochem Soc Trans,* 37, 665-670.

Evans, J. S. 2013. '"Liquid-like" biomineralization protein assemblies: a key to the regulation of non-classical nucleation.' *Crystengcomm,* 15, 8388-8394.

Evenson, D. P., Scotto, A., Pla, D. & de Harven, E. 1978. 'The sizes of RNA subunits isolated from high and low leukaemogenic Friend virus.' *J Gen Virol,* 39, 475-486.

Fabritius, H. O., Sachs, C., Triguero, P. R. & Roobe, D. 2009. 'Influence of structural principles on the mechanics of a biological fiber-based composite material with hierarchical organization: the exoskeleton of the lobster *Homarus americanus*.' *Adv Mater,* 21, 391-400.

Filner, B. & Marcus, A. 1974. 'TMV coat protein synthesis *in vivo*: analysis of the N-terminal acetylation.' *Virology,* 61, 537-546.

Finch, J. T. 1972. 'The hand of the helix of tobacco virus.' *J Mol Biol,* 66, 291-294.

Fowler, C. E., Shenton, W., Stubbs, G. & Mann, S. 2001. 'Tobacco mosaic virus liquid crystals as templates for the interior design of silica mesophases and nanoparticles.' *Adv Mater,* 13, 1266-1269.

Fraenkel-Conrat, H. 1957. 'Degradation of tobacco mosaic virus with acetic acid.' *Virology,* 4, 1-4.

Fraenkel-Conrat, H. & Singer, B. 1959. 'Reconstitution of tobacco mosaic virus. III. Improved methods and the use of mixed nucleic acids.' *Biochim Biophys Acta,* 33, 359-370.

Fraenkel-Conrat, H. & Williams, R. C. 1955. 'Reconstitution of active tobacco mosaic virus from its inactive protein and nucleic acid components.' *Proc Natl Acad Sci U S A,* 41, 690-698.

Fujikawa, S. & Kunitake, T. 2003. 'Surface fabrication of hollow nanoarchitectures of ultrathin titania layers from assembled latex particles and tobacco mosaic viruses as templates.' *Langmuir,* 19, 6545-6552.

Fukuda, M. & Okada, Y. 1987. 'Bidirectional assembly of tobacco mosaic virus *in vitro*.' *Proc Natl Acad Sci U S A,* 84, 4035-4038.

Ge, P. & Zhou, Z. H. 2011. 'Hydrogen-bonding networks and RNA bases revealed by cryo electron microscopy suggest a triggering mechanism for calcium switches.' *Proc Natl Acad Sci U S A,* 108, 9637-9642.

Gebauer, D., Kellermeier, M., Gale, J. D., Bergstrom, L. & Colfen, H. 2014. 'Pre-nucleation clusters as solute precursors in crystallisation.' *Chem Soc Rev,* 43, 2348-2371.

Geiger, F. C., Eber, F. J., Eiben, S., Müller, A., Jeske, H., Spatz, J. P. & Wege, C. 2013. 'TMV nanorods with programmed longitudinal domains of differently addressable coat proteins.' *Nanoscale,* 5, 3808-3816.

Gerling, T., Wagenbauer, K. F., Neuner, A. M. & Dietz, H. 2015. 'Dynamic DNA devices and assemblies formed by shape-complementary, non-base pairing 3D components.' *Science,* 347, 1446-1452.

Gierak, J., Madouri, A., Biance, A. L., Bourhis, E., Patriarche, G., Ulysse, C., Lucot, D., Lafosse, X., Auvray, L., Bruchhaus, L. & Jede, R. 2007. 'Sub-5 nm FIB direct patterning of nanodevices.' *Microelectron Eng,* 84, 779-783.

Glass, J. & Wertz, G. W. 1980. 'Different base per unit length ratios exist in single-stranded RNA and single-stranded DNA.' *Nucleic Acids Res,* 8, 5739-5751.

Goelet, P., Lomonossoff, G. P., Butler, P. J., Akam, M. E., Gait, M. J. & Karn, J. 1982. 'Nucleotide sequence of tobacco mosaic virus RNA.' *Proc Natl Acad Sci U S A,* 79, 5818-5822.

Gooding, G. V., Jr. & Hebert, T. T. 1967. 'A simple technique for purification of tobacco mosaic virus in large quantities.' *Phytopathology,* 57, 1285.

Goudouri, O. M., Kontonasaki, E., Lohbauer, U. & Boccaccini, A. R. 2014. 'Antibacterial properties of metal and metalloid ions in chronic periodontitis and peri-implantitis therapy.' *Acta Biomater,* 10, 3795-3810.

Graham, L. M., Nguyen, T. M. & Lee, S. B. 2011. 'Nanodetoxification: emerging role of nanomaterials in drug intoxication treatment.' *Nanomedicine (Lond),* 6, 921-928.

Green, M. R. & Sambrook, J. 2012. *Molecular cloning: a laboratory manual.* New York, NY, U.S.A.: Cold Spring Harbor Laboratory Press.

Griffith, J. D. & Christiansen, G. 1978. 'Electron microscope visualization of chromatin and other DNA-protein complexes.' *Annu Rev Biophys Bio,* 7, 19-35.

Haase, N. R., Shian, S., Sandhage, K. H. & Kröger, N. 2011. 'Biocatalytic nanoscale coatings through biomimetic layer-by-layer mineralization.' *Adv Funct Mater,* 21, 4243-4251.

Hagn, F., Thamm, C., Scheibel, T. & Kessler, H. 2011. 'pH-dependent dimerization and salt-dependent stabilization of the N-terminal domain of spider dragline silk-implications for fiber formation.' *Angew Chem Int Edit,* 50, 310-313.

Hall, A. R., Scott, A., Rotem, D., Mehta, K. K., Bayley, H. & Dekker, C. 2010. 'Hybrid pore formation by directed insertion of alpha-haemolysin into solid-state nanopores.' *Nat Nanotechnol,* 5, 874-877.

Harrington, M. J., Masic, A., Holten-Andersen, N., Waite, J. H. & Fratzl, P. 2010. 'Iron-clad fibers: a metal-based biological strategy for hard flexible coatings.' *Science,* 328, 216-220.

Harrington, W. F. & Schachman, H. K. 1956. 'Studies on the alkaline degradation of tobacco mosaic virus. I. Ultracentrifugal analysis.' *Arch Biochem Biophys,* 65, 278-295.

Heldmaier, G., Neuweiler, G. & Rössler, W. 2013. *Vergleichende Tierphysiologie.* Berlin, Heidelberg: Springer Spektrum.

Henstock, J. R., Canham, L. T. & Anderson, S. I. 2015. 'Silicon: the evolution of its use in biomaterials.' *Acta Biomater,* 11, 17-26.

Hernandez-Ainsa, S. & Keyser, U. F. 2014. 'DNA origami nanopores: developments, challenges and perspectives.' *Nanoscale,* 6, 14121-14132.

Hernandez-Ainsa, S., Misiunas, K., Thacker, V. V., Hemmig, E. A. & Keyser, U. F. 2014. 'Voltage-dependent properties of DNA origami nanopores.' *Nano Lett,* 14, 1270-1274.

Hong, J. H., Duncan, S. E. & Dietrich, A. M. 2010. 'Effect of copper speciation at different pH on temporal sensory attributes of copper.' *Food Qual Prefer,* 21, 132-139.

Howes, P. D., Chandrawati, R. & Stevens, M. M. 2014. 'Bionanotechnology. Colloidal nanoparticles as advanced biological sensors.' *Science,* 346, 1247390.

Hunter, R. J. 1981. *Zeta potential in colloid science: principles and applications.* London, San Diego, New York, Berkeley, Boston, Sydney, Tokoy, Toronto: Academic Press.

Icopini, G. A., Brantley, S. L. & Heaney, P. J. 2005. 'Kinetics of silica oligomerization and nanocolloid formation as a function of pH and ionic strength at 25 °C.' *Geochim Cosmochim Ac,* 69, 293-303.

Jackson, D. J., McDougall, C., Woodcroft, B., Moase, P., Rose, R. A., Kube, M., Reinhardt, R., Rokhsar, D. S., Montagnani, C., Joubert, C., Piquemal, D. &

Degnan, B. M. 2010. 'Parallel evolution of nacre building gene sets in molluscs.' *Mol Biol Evol,* 27, 591-608.

Jain, K. K. 2005. 'The role of nanobiotechnology in drug discovery.' *Drug Discov Today,* 10, 1435-1442.

Joens, M. S., Huynh, C., Kasuboski, J. M., Ferranti, D., Sigal, Y. J., Zeitvogel, F., Obst, M., Burkhardt, C. J., Curran, K. P., Chalasani, S. H., Stern, L. A., Goetze, B. & Fitzpatrick, J. A. 2013. 'Helium Ion Microscopy (HIM) for the imaging of biological samples at sub-nanometer resolution.' *Sci Rep,* 3, 3514.

Jung, S. & Yi, H. 2014. 'An integrated approach for enhanced protein conjugation and capture with viral nanotemplates and hydrogel microparticle platforms *via* rapid bioorthogonal reactions.' *Langmuir,* 30, 7762-7770.

Kadereit, J. W. 2014. 'Strasburger − Lehrbuch der Pflanzenwissenschaften.' *SpringerLink : Bücher*. Berlin, Heidelberg: Springer Spektrum.

Kadri, A., Maiss, E., Amsharov, N., Bittner, A. M., Balci, S., Kern, K., Jeske, H. & Wege, C. 2011. 'Engineered tobacco mosaic virus mutants with distinct physical characteristics in planta and enhanced metallization properties.' *Virus Res,* 157, 35-46.

Kebbekus, P., Draper, D. E. & Hagerman, P. 1995. 'Persistence length of RNA.' *Biochemistry,* 34, 4354-4357.

Kim, Y. J., Hwang, K. H., Park, S. J., Jeon, D. Y., Nam, C. H. & Kim, G. T. 2013. 'Fabrication of a silica nanocable using hydroxyl-group core-engineered filamentous virus.' *J Nanosci Nanotechnol,* 13, 6203-6207.

Kirkham, J., Firth, A., Vernals, D., Boden, N., Robinson, C., Shore, R. C., Brookes, S. J. & Aggeli, A. 2007. 'Self-assembling peptide scaffolds promote enamel remineralization.' *J Dent Res,* 86, 426-430.

Kisailus, D., Najarian, M., Weaver, J. C. & Morse, D. E. 2005. 'Functionalized gold nanoparticles mimic catalytic activity of a polysiloxane-synthesizing enzyme.' *Adv Mater,* 17, 1234-1239.

Kisailus, D., Truong, Q., Amemiya, Y., Weaver, J. C. & Morse, D. E. 2006. 'Self-assembled bifunctional surface mimics an enzymatic and templating protein for the synthesis of a metal oxide semiconductor.' *Proc Natl Acad Sci U S A,* 103, 5652-5657.

Kleefen, A., Pedone, D., Grunwald, C., Wei, R., Firnkes, M., Abstreiter, G., Rant, U. & Tampe, R. 2010. 'Multiplexed parallel single transport recordings on nanopore arrays.' *Nano Lett,* 10, 5080-5087.

Kleinschmidt, A. K., Lang, D., Jacherts, D. & Zahn, R. K. 1962. 'Preparation and length measurements of the total desoxyribonucleic acid content of T2 bacteriophages.' *Biochim Biophys Acta,* 61, 857-864.

Klymov, A., Bronkhorst, E. M., Te Riet, J., Jansen, J. A. & Walboomers, X. F. 2015. 'Bone marrow-derived mesenchymal cells feature selective migration behavior

on submicro- and nano-dimensional multi-patterned substrates.' *Acta Biomater,* 16, 117-125.

Knez, M., Sumser, M., Bittner, A. M., Wege, C., Jeske, H., Martin, T. P. & Kern, K. 2004a. 'Spatially selective nucleation of metal clusters on the tobacco mosaic virus.' *Adv Funct Mater,* 14, 116-124.

Knez, M., Sumser, M. P., Bittner, A. M., Wege, C., Jeske, H., Hoffmann, D. M. P., Kuhnke, K. & Kern, K. 2004b. 'Binding the tobacco mosaic virus to inorganic surfaces.' *Langmuir,* 20, 441-447.

Korlach, J., Marks, P. J., Cicero, R. L., Gray, J. J., Murphy, D. L., Roitman, D. B., Pham, T. T., Otto, G. A., Foquet, M. & Turner, S. W. 2008. 'Selective aluminum passivation for targeted immobilization of single DNA polymerase molecules in zero-mode waveguide nanostructures.' *Proc Natl Acad Sci U S A,* 105, 1176-1181.

Krauskopf, K. B. 1956. 'Dissolution and precipitation of silica at low temperatures.' *Geochim Cosmochim Ac,* 10, 1-26.

Kröger, N. 2007. 'Prescribing diatom morphology: toward genetic engineering of biological nanomaterials.' *Curr Opin Chem Biol,* 11, 662-669.

Kröger, N., Deutzmann, R. & Sumper, M. 1999. 'Polycationic peptides from diatom biosilica that direct silica nanosphere formation.' *Science,* 286, 1129-1132.

Kröger, N. & Poulsen, N. 2008. 'Diatoms-from cell wall biogenesis to nanotechnology.' *Annu Rev Genet,* 42, 83-107.

Kumari, A., Yadav, S. K. & Yadav, S. C. 2010. 'Biodegradable polymeric nanoparticles based drug delivery systems.' *Colloids Surf B Biointerfaces,* 75, 1-18.

Kuno, T., Nonoyama, T., Hirao, K. & Kato, K. 2011. 'Influence of the charge relay effect on the silanol condensation reaction as a model for silica biomineralization.' *Langmuir,* 27, 13154-13158.

Kusters, I., van Oijen, A. M. & Driessen, A. J. 2014. 'Membrane-on-a-chip: microstructured silicon/silicon-dioxide chips for high-throughput screening of membrane transport and viral membrane fusion.' *ACS Nano,* 8, 3380-3392.

Laemmli, U. K. 1970. 'Cleavage of structural proteins during the assembly of the head of bacteriophage T4.' *Nature,* 227, 680-685.

Larkin, J., Foquet, M., Turner, S. W., Korlach, J. & Wanunu, M. 2014. 'Reversible positioning of single molecules inside zero-mode waveguides.' *Nano Lett,* 14, 6023-6029.

Lartey, R. T., Voss, T. C. & Melcher, U. 1996. 'Tobamovirus evolution: gene overlaps, recombination, and taxonomic implications.' *Mol Biol Evol,* 13, 1327-1338.

Leblanc, J. L. 2002. 'Rubber-filler interactions and rheological properties in filled compounds.' *Prog Polym Sci,* 27, 627-687.

Lechner, C. C. & Becker, C. F. 2013. 'Modified silaffin R5 peptides enable encapsulation and release of cargo molecules from biomimetic silica particles.' *Bioorg Med Chem,* 21, 3533-3541.

Lee, S. M., Park, H. & Yoo, K. H. 2010. 'Synergistic cancer therapeutic effects of locally delivered drug and heat using multifunctional nanoparticles.' *Adv Mater,* 22, 4049-4053.

Lee, S. Y., Lim, J. S., Culver, J. N. & Harris, M. T. 2008. 'Coagulation of tobacco mosaic virus in alcohol-water-LiCl solutions.' *J Colloid Interface Sci,* 324, 92-98.

Lee, S. Y., Royston, E., Culver, J. N. & Harris, M. T. 2005. 'Improved metal cluster deposition on a genetically engineered tobacco mosaic virus template.' *Nanotechnology,* 16, S435-S441.

Lee, W. J., Lee, D. H., Han, T. H., Lee, S. H., Moon, H. S., Lee, J. A. & Kim, S. O. 2011. 'Biomimetic mineralization of vertical N-doped carbon nanotubes.' *Chem Commun (Camb),* 47, 535-537.

Lee, Y. J., Yi, H., Kim, W. J., Kang, K., Yun, D. S., Strano, M. S., Ceder, G. & Belcher, A. M. 2009. 'Fabricating genetically engineered high-power lithium-ion batteries using multiple virus genes.' *Science,* 324, 1051-1055.

Lehrach, H., Diamond, D., Wozney, J. M. & Boedtker, H. 1977. 'RNA molecular weight determinations by gel electrophoresis under denaturing conditions, a critical re-examination.' *Biochemistry,* 16, 4743-4751.

Li, D., Qu, X., Newton, S. M., Klebba, P. E. & Mao, C. 2012. 'Morphology-controlled synthesis of silica nanotubes through pH- and sequence-responsive morphological change of bacterial flagellar biotemplates.' *J Mater Chem,* 22, 15702-15709.

Li, F. & Wang, Q. B. 2014. 'Fabrication of nanoarchitectures templated by virus-based nanoparticles: strategies and applications.' *Small,* 10, 230-245.

Li, K. 2007. *Ceramic membranes for separation and reaction.* Chichester [u.a.]: Wiley.

Lieberman, K. R., Cherf, G. M., Doody, M. J., Olasagasti, F., Kolodji, Y. & Akeson, M. 2010. 'Processive replication of single DNA molecules in a nanopore catalyzed by phi29 DNA polymerase.' *J Am Chem Soc,* 132, 17961-17972.

Liu, P., Sehaqui, H., Tingaut, P., Wichser, A., Oksman, K. & Mathew, A. P. 2014. 'Cellulose and chitin nanomaterials for capturing silver ions (Ag^+) from water *via* surface adsorption.' *Cellulose,* 21, 449-461.

Lomonossoff, G. & Evans, D. 2014. 'Applications of plant viruses in bionanotechnology.' In K. Palmer & Y. Gleba (Eds.) *Plant viral vectors:* 61-87. Berlin, Heidelberg: Springer-Verlag.

Love, A. J., Makarov, V., Yaminsky, I., Kalinina, N. O. & Taliansky, M. E. 2014. 'The use of tobacco mosaic virus and cowpea mosaic virus for the production of novel metal nanomaterials.' *Virology,* 449, 133-139.

Lowe, C. R. 2000. 'Nanobiotechnology: the fabrication and applications of chemical and biological nanostructures.' *Curr Opin Struct Biol,* 10, 428-434.

Lu, B., Stubbs, G. & Culver, J. N. 1996. 'Carboxylate interactions involved in the disassembly of tobacco mosaic tobamovirus.' *Virology,* 225, 11-20.

Lu, B., Stubbs, G. & Culver, J. N. 1998. 'Coat protein interactions involved in tobacco mosaic tobamovirus cross-protection.' *Virology,* 248, 188-198.

Luckanagul, J., Lee, L. A., Nguyen, Q. L., Sitasuwan, P., Yang, X. M., Shazly, T. & Wang, Q. 2012. 'Porous alginate hydrogel functionalized with virus as three-dimensional scaffolds for bone differentiation.' *Biomacromolecules,* 13, 3949-3958.

Luckanagul, J. A., Lee, L. A., You, S. J., Yang, X. M. & Wang, Q. 2015. 'Plant virus incorporated hydrogels as scaffolds for tissue engineering possess low immunogenicity *in vivo*.' *J Biomed Mater Res A,* 103, 887-895.

Ma, Y. Z., Miller, R. A., Fleming, G. R. & Francis, M. B. 2008. 'Energy transfer dynamics in light-harvesting assemblies templated by the tobacco mosaic virus coat protein.' *J Phys Chem B,* 112, 6887-6892.

Maglia, G., Heron, A. J., Stoddart, D., Japrung, D. & Bayley, H. 2010. 'Analysis of single nucleic acid molecules with protein nanopores.' *Methods Enzymol,* 475, 591-623.

Mann, S. 1983. 'Mineralization in biological systems.' *Struct Bond,* 54, 125-174.

Mann, S. 2009. 'Self-assembly and transformation of hybrid nano-objects and nanostructures under equilibrium and non-equilibrium conditions.' *Nat Mater,* 8, 781-792.

Manrao, E. A., Derrington, I. M., Laszlo, A. H., Langford, K. W., Hopper, M. K., Gillgren, N., Pavlenok, M., Niederweis, M. & Gundlach, J. H. 2012. 'Reading DNA at single-nucleotide resolution with a mutant MspA nanopore and phi29 DNA polymerase.' *Nat Biotechnol,* 30, 349-353.

Mao, C., Liu, A. & Cao, B. 2009. 'Virus-based chemical and biological sensing.' *Angew Chem Int Ed Engl,* 48, 6790-6810.

Mao, C. B., Solis, D. J., Reiss, B. D., Kottmann, S. T., Sweeney, R. Y., Hayhurst, A., Georgiou, G., Iverson, B. & Belcher, A. M. 2004. 'Virus-based toolkit for the directed synthesis of magnetic and semiconducting nanowires.' *Science,* 303, 213-217.

Marie, B., Joubert, C., Tayale, A., Zanella-Cleon, I., Belliard, C., Piquemal, D., Cochennec-Laureau, N., Marin, F., Gueguen, Y. & Montagnani, C. 2012. 'Different secretory repertoires control the biomineralization processes of

prism and nacre deposition of the pearl oyster shell.' *Proc Natl Acad Sci U S A,* 109, 20986-20991.

Martins-Junior, P. A., Alcantara, C. E., Resende, R. R. & Ferreira, A. J. 2013. 'Carbon nanotubes: directions and perspectives in oral regenerative medicine.' *J Dent Res,* 92, 575-583.

Mayer, M. & Yang, J. 2013. 'Engineered ion channels as emerging tools for chemical biology.' *Acc Chem Res,* 46, 2998-3008.

McCormick, A. A. & Palmer, K. E. 2008. 'Genetically engineered tobacco mosaic virus as nanoparticle vaccines.' *Expert Rev Vaccines,* 7, 33-41.

McNally, B., Singer, A., Yu, Z., Sun, Y., Weng, Z. & Meller, A. 2010. 'Optical recognition of converted DNA nucleotides for single-molecule DNA sequencing using nanopore arrays.' *Nano Lett,* 10, 2237-2244.

Meinkoth, J. & Wahl, G. 1984. 'Hybridization of nucleic-acids immobilized on solid supports.' *Anal Biochem,* 138, 267-284.

Merchant, C. A., Healy, K., Wanunu, M., Ray, V., Peterman, N., Bartel, J., Fischbein, M. D., Venta, K., Luo, Z., Johnson, A. T. & Drndic, M. 2010. 'DNA translocation through graphene nanopores.' *Nano Lett,* 10, 2915-2921.

Miles, B. N., Ivanov, A. P., Wilson, K. A., Dogan, F., Japrung, D. & Edel, J. B. 2013. 'Single molecule sensing with solid-state nanopores: novel materials, methods, and applications.' *Chem Soc Rev,* 42, 15-28.

Miller, R. A., Presley, A. D. & Francis, M. B. 2007. 'Self-assembling light-harvesting systems from synthetically modified tobacco mosaic virus coat proteins.' *J Am Chem Soc,* 129, 3104-3109.

Mirkhalaf, M., Dastjerdi, A. K. & Barthelat, F. 2014. 'Overcoming the brittleness of glass through bio-inspiration and micro-architecture.' *Nat Commun,* 5, 3166.

Morgan, T. T., Muddana, H. S., Altinoglu, E. I., Rouse, S. M., Tabakovic, A., Tabouillot, T., Russin, T. J., Shanmugavelandy, S. S., Butler, P. J., Eklund, P. C., Yun, J. K., Kester, M. & Adair, J. H. 2008. 'Encapsulation of organic molecules in calcium phosphate nanocomposite particles for intracellular imaging and drug delivery.' *Nano Lett,* 8, 4108-4115.

Müller, A., Eber, F. J., Azucena, C., Petershans, A., Bittner, A. M., Gliemann, H., Jeske, H. & Wege, C. 2011. 'Inducible site-selective bottom-up assembly of virus-derived nanotube arrays on RNA-equipped wafers.' *ACS Nano,* 5, 4512-4520.

Müller, R. H. & Hildebrand, G. E. 1996. *Zetapotential und Partikelladung in der Laborpraxis: Einführung in die Theorie - praktische Messdurchführung - Dateninterpretation; Colloidal drug carriers (cdc) 1st expert meeting Berlin 15. - 17. 6. 1995.* Stuttgart: Wissenschaftliche Verlagsgesellschaft.

Müller, W. E. G., Wang, X. H., Jochum, K. P. & Schröder, H. C. 2013. 'Self-healing, an intrinsic property of biomineralization processes.' *IUBMB Life,* 65, 382-396.

Murai, K., Higuchi, M., Kinoshita, T., Nagata, K. & Kato, K. 2013. 'Calcium carbonate biomineralization utilizing a multifunctional beta-sheet peptide template.' *Chem Commun (Camb),* 49, 9947-9949.

Murdock, D. J. E. & Donoghue, P. C. J. 2011. 'Evolutionary origins of animal skeletal biomineralization.' *Cells Tissues Organs,* 194, 98-102.

Nakano, S., Fujimoto, M., Hara, H. & Sugimoto, N. 1999. 'Nucleic acid duplex stability: influence of base composition on cation effects.' *Nucleic Acids Res,* 27, 2957-2965.

Nakatani, K. & Yau, K. W. 1988. 'Calcium and light adaptation in retinal rods and cones.' *Nature,* 334, 69-71.

Nam, Y. S., Magyar, A. P., Lee, D., Kim, J. W., Yun, D. S., Park, H., Pollom, T. S., Jr., Weitz, D. A. & Belcher, A. M. 2010a. 'Biologically templated photocatalytic nanostructures for sustained light-driven water oxidation.' *Nat Nanotechnol,* 5, 340-344.

Nam, Y. S., Shin, T., Park, H., Magyar, A. P., Choi, K., Fantner, G., Nelson, K. A. & Belcher, A. M. 2010b. 'Virus-templated assembly of porphyrins into light-harvesting nanoantennae.' *J Am Chem Soc,* 132, 1462-1463.

Namba, K., Pattanayek, R. & Stubbs, G. 1989. 'Visualization of protein-nucleic acid interactions in a virus. Refined structure of intact tobacco mosaic virus at 2.9 Å resolution by x-ray fiber diffraction.' *J Mol Biol,* 208, 307-325.

Neltner, B., Peddie, B., Xu, A., Doenlen, W., Durand, K., Yun, D. S., Speakman, S., Peterson, A. & Belcher, A. 2010. 'Production of hydrogen using nanocrystalline protein-templated catalysts on M13 phage.' *ACS Nano,* 4, 3227-3235.

Nilsson, J., Lee, J. R. I., Ratto, T. V. & Letant, S. E. 2006. 'Localized functionalization of single nanopores.' *Adv Mater,* 18, 427-431.

Niu, Z., Bruckman, M., Kotakadi, V. S., He, J., Emrick, T., Russell, T. P., Yang, L. & Wang, Q. 2006. 'Study and characterization of tobacco mosaic virus head-to-tail assembly assisted by aniline polymerization.' *Chem Commun (Camb),* 28, 3019-3021.

Niu, Z., Kabisatpathy, S., He, J., Lee, L. A., Rong, J., Yang, L., Sikha, G., Popov, B., Emrick, T., Russell, T. & Wang, Q. 2009. 'Synthesis and characterization of bionanoparticle—Silica composites and mesoporous silica with large pores.' *Nano Res,* 2, 474-483.

Niu, Z., Liu, J., Lee, L. A., Bruckman, M. A., Zhao, D., Koley, G. & Wang, Q. 2007. 'Biological templated synthesis of water-soluble conductive polymeric nanowires.' *Nano Lett,* 7, 3729-3733.

Nivala, J., Marks, D. B. & Akeson, M. 2013. 'Unfoldase-mediated protein translocation through an alpha-hemolysin nanopore.' *Nat Biotechnol,* 31, 247-250.

Oh, H., Kalidindi, S. B., Um, Y., Bureekaew, S., Schmid, R., Fischer, R. A. & Hirscher, M. 2013. 'A cryogenically flexible covalent organic framework for efficient hydrogen isotope separation by quantum sieving.' *Angew Chem Int Ed Engl,* 52, 13219-13222.

Okahata, Y., Kawase, M., Niikura, K., Ohtake, F., Furusawa, H. & Ebara, Y. 1998. 'Kinetic measurements of DNA hybridization on an oligonucleotide-immobilized 27-MHz quartz crystal microbalance.' *Anal Chem,* 70, 1288-1296.

Oldenbourg, R., Wen, X., Meyer, R. B. & Caspar, D. L. 1988. 'Orientational distribution function in nematic tobacco-mosaic-virus liquid crystals measured by x-ray diffraction.' *Phys Rev Lett,* 61, 1851-1854.

Paglini, S. & Lauffer, M. A. 1968. 'Polymerization-depolymerization of tobacco mosaic virus protein. XI. Osmotic pressure studies of solutions in water and in deuterium.' *Biochemistry,* 7, 1827-1835.

Palmer, L. C., Newcomb, C. J., Kaltz, S. R., Spoerke, E. D. & Stupp, S. I. 2008. 'Biomimetic systems for hydroxyapatite mineralization inspired by bone and enamel.' *Chem Rev,* 108, 4754-4783.

Panayotatos, N. & Wells, R. D. 1979. 'Recognition and initiation site for four late promoters of phage T7 is a 22-base pair DNA sequence.' *Nature,* 280, 35-39.

Paris, O., Burgert, I. & Fratzl, P. 2010. 'Biomimetics and biotemplating of natural materials.' *Mrs Bulletin,* 35, 219-225.

Patwardhan, S. V., Emami, F. S., Berry, R. J., Jones, S. E., Naik, R. R., Deschaume, O., Heinz, H. & Perry, C. C. 2012. 'Chemistry of aqueous silica nanoparticle surfaces and the mechanism of selective peptide adsorption.' *J Am Chem Soc,* 134, 6244-6256.

Patwardhan, S. V., Tilburey, G. E. & Perry, C. C. 2011. 'Interactions of amines with silicon species in undersaturated solutions leads to dissolution and/or precipitation of silica.' *Langmuir,* 27, 15135-15145.

Peckham, T. J. & Holdcroft, S. 2010. 'Structure-morphology-property relationships of non-perfluorinated proton-conducting membranes.' *Adv Mater,* 22, 4667-4690.

Pelcher, L. E. & Halasa, M. C. 1979. 'Factors influencing the production of intermediate particles during alkaline degradation of tobacco mosaic virus: time, pH, salt concentration, and temperature.' *J Virol,* 29, 431-437.

Perham, R. N. & Wilson, T. M. A. 1978. 'Characterization of intermediates formed during disassembly of tobacco mosaic-virus at alkaline pH.' *Virology,* 84, 293-302.

Phillip, W. A., O'Neill, B., Rodwogin, M., Hillmyer, M. A. & Cussler, E. L. 2010. 'Self-assembled block copolymer thin films as water filtration membranes.' *ACS Appl Mater Interfaces,* 2, 847-853.

Polini, A., Pagliara, S., Camposeo, A., Cingolani, R., Wang, X., Schröder, H. C., Müller, W. E. & Pisignano, D. 2012. 'Optical properties of *in vitro* biomineralised silica.' *Sci Rep,* 2, 607.

Pouget, E., Dujardin, E., Cavalier, A., Moreac, A., Valery, C., Marchi-Artzner, V., Weiss, T., Renault, A., Paternostre, M. & Artzner, F. 2007. 'Hierarchical architectures by synergy between dynamical template self-assembly and biomineralization.' *Nat Mater,* 6, 434-439.

Pouget, E. & Grelet, E. 2013. 'Dispersions of monodisperse hybrid rod-like particles by mineralization of filamentous viruses.' *Langmuir,* 29, 8010-8016.

Poulsen, N. & Kröger, N. 2004. 'Silica morphogenesis by alternative processing of silaffins in the diatom *Thalassiosira pseudonana*.' *J Biol Chem,* 279, 42993-42999.

Putnam, C. accessed 2015. 'Protein Calculator v3.4 ' *The Scripps Research Institute, La Jolla, California, U.S.A.,* http://protcalc.sourceforge.net.

Raghavendra, K., Adams, M. L. & Schuster, T. M. 1985. 'Tobacco mosaic virus protein aggregates in solution: structural comparison of 20S aggregates with those near conditions for disk crystallization.' *Biochemistry,* 24, 3298-3304.

Raghavendra, K., Kelly, J. A., Khairallah, L. & Schuster, T. M. 1988. 'Structure and function of disk aggregates of the coat protein of tobacco mosaic virus.' *Biochemistry,* 27, 7583-7588.

Reed, J. S. 1995. *Principles of ceramics processing.* New York, NY, U.S.A.: John Wiley & Sons, Inc.

Rego, J. M., Lee, J. H., Lee, D. H. & Yi, H. 2013. 'Biologically inspired strategy for programmed assembly of viral building blocks with controlled dimensions.' *Biotechnol J,* 8, 237-246.

Ren, Z., Guo, Y., Liu, C. H. & Gao, P. X. 2013. 'Hierarchically nanostructured materials for sustainable environmental applications.' *Front Chem,* 1, 1-22.

Rhee, M. & Burns, M. A. 2006. 'Nanopore sequencing technology: research trends and applications.' *Trends Biotechnol,* 24, 580-586.

Richthammer, P., Bormel, M., Brunner, E. & van Pee, K. H. 2011. 'Biomineralization in diatoms: the role of silacidins.' *Chembiochem,* 12, 1362-1366.

Riou, G. & Delain, E. 1969. 'Electron microscopy of the circular kinetoplastic DNA from *Trypanosoma cruzi*: ocurrence of catenated forms ' *Proc Natl Acad Sci U S A,* 62, 210-217.

Rong, J. H., Oberbeck, F., Wang, X. N., Li, X. D., Oxsher, J., Niu, Z. W. & Wang, Q. 2009. 'Tobacco mosaic virus templated synthesis of one dimensional inorganic-polymer hybrid fibres.' *J Mater Chem,* 19, 2841-2845.

Rosa, M. D. 1979. 'Four T7 RNA polymerase promoters contain an identical 23 bp sequence.' *Cell,* 16, 815-825.

Rothenstein, D., Claasen, B., Omiecienski, B., Lammel, P. & Bill, J. 2012. 'Isolation of ZnO-binding 12-mer peptides and determination of their binding epitopes by NMR spectroscopy.' *J Am Chem Soc,* 134, 12547-12556.

Rothenstein, D., Facey, S. J., Ploss, M., Hans, P., Melcher, M., Srot, V., van Aken, P. A., Hauer, B. & Bill, J. 2013. 'Mineralization of gold nanoparticles using tailored M13 phages.' *Bioinspir Biomim Nan,* 2, 173-185.

Royston, E., Ghosh, A., Kofinas, P., Harris, M. T. & Culver, J. N. 2008. 'Self-assembly of virus-structured high surface area nanomaterials and their application as battery electrodes.' *Langmuir,* 24, 906-912.

Royston, E., Lee, S. Y., Culver, J. N. & Harris, M. T. 2006. 'Characterization of silica-coated tobacco mosaic virus.' *J Colloid Interface Sci,* 298, 706-712.

Royston, E. S., Brown, A. D., Harris, M. T. & Culver, J. N. 2009. 'Preparation of silica stabilized tobacco mosaic virus templates for the production of metal and layered nanoparticles.' *J Colloid Interface Sci,* 332, 402-407.

Sachse, C., Chen, J. Z., Coureux, P. D., Stroupe, M. E., Fandrich, M. & Grigorieff, N. 2007. 'High-resolution electron microscopy of helical specimens: a fresh look at tobacco mosaic virus.' *J Mol Biol,* 371, 812-835.

Salieri, B., Righi, S., Pasteris, A. & Olsen, S. I. 2015. 'Freshwater ecotoxicity characterisation factor for metal oxide nanoparticles: a case study on titanium dioxide nanoparticle.' *Sci Total Environ,* 505, 494-502.

Sanders, D. E., Smith, Z. P., Guo, R. L., Robeson, L. M., McGrath, J. E., Paul, D. R. & Freeman, B. D. 2013. 'Energy-efficient polymeric gas separation membranes for a sustainable future: A review.' *Polymer,* 54, 4729-4761.

Sarikaya, M., Tamerler, C., Jen, A. K.-Y., Schulten, K. & Baneyx, F. 2003. 'Molecular biomimetics: nanotechnology through biology.' *Nat Mater,* 2, 577-585.

Schlick, T. L., Ding, Z., Kovacs, E. W. & Francis, M. B. 2005. 'Dual-surface modification of the tobacco mosaic virus.' *J Am Chem Soc,* 127, 3718-3723.

Schneider, C. A., Rasband, W. S. & Eliceiri, K. W. 2012. 'NIH Image to ImageJ: 25 years of image analysis.' *Nat Methods,* 9, 671-675.

Schön, A. & Mundry, K. W. 1984. 'Coordinated two-disk nucleation, growth and properties, of virus-like particles assembled from tobacco mosaic virus capsid protein with poly(A) or oligo(A) of different length.' *Eur J Biochem,* 140, 119-127.

Schröder, H. C., Wiens, M., Schlossmacher, U., Brandt, D. & Müller, W. E. G. 2012. 'Silicatein-mediated polycondensation of orthosilicic acid: modeling of a catalytic mechanism involving ring formation.' *Silicon-Neth,* 4, 33-38.

Seidenstücker, A. 2015. 'Physikalische Voraussetzungen für die Realisierung einer bio-anorganischen Hybridmembran mit uniformen Nanoporen.' *Fakultät für Naturwissenschaften*. Universität Ulm.

Semino, C. E. 2008. 'Self-assembling peptides: from bio-inspired materials to bone regeneration.' *J Dent Res,* 87, 606-616.

Shenton, W., Douglas, T., Young, M., Stubbs, G. & Mann, S. 1999. 'Inorganic-organic nanotube composites from template mineralization of tobacco mosaic virus.' *Adv Mater,* 11, 253-256.

Shim, J., Humphreys, G. I., Venkatesan, B. M., Munz, J. M., Zou, X., Sathe, C., Schulten, K., Kosari, F., Nardulli, A. M., Vasmatzis, G. & Bashir, R. 2013. 'Detection and quantification of methylation in DNA using solid-state nanopores.' *Sci Rep,* 3, 1389.

Shimada, K. & Tarutani, T. 1979. 'Gel chromatographic study of the polymerization of silicic acid.' *J Chromatogr,* 168, 401-406.

Shukla, S., Eber, F. J., Nagarajan, A. S., DiFranco, N. A., Schmidt, N., Wen, A. M., Eiben, S., Twyman, R. M., Wege, C. & Steinmetz, N. F. 2015. 'The impact of aspect ratio on the biodistribution and tumor homing of rigid soft-matter nanorods.' *Adv Healthc Mater,* 4, 874-882.

Smith, M. L., Lindbo, J. A., Dillard-Telm, S., Brosio, P. M., Lasnik, A. B., McCormick, A. A., Nguyen, L. V. & Palmer, K. E. 2006. 'Modified tobacco mosaic virus particles as scaffolds for display of protein antigens for vaccine applications.' *Virology,* 348, 475-488.

Song, F., Soh, A. K. & Bai, Y. L. 2003. 'Structural and mechanical properties of the organic matrix layers of nacre.' *Biomaterials,* 24, 3623-3631.

Song, L., Hobaugh, M. R., Shustak, C., Cheley, S., Bayley, H. & Gouaux, J. E. 1996. 'Structure of staphylococcal alpha-hemolysin, a heptameric transmembrane pore.' *Science,* 274, 1859-1866.

Soto, C. M. & Ratna, B. R. 2010. 'Virus hybrids as nanomaterials for biotechnology.' *Curr Opin Biotechnol,* 21, 426-438.

Stark, W. J., Stoessel, P. R., Wohlleben, W. & Hafner, A. 2015. 'Industrial applications of nanoparticles.' *Chem Soc Rev,* 44, 5793-5805.

Stauffer, H., Srinivasan, S. & Lauffer, M. A. 1970. 'Calorimetric studies on polymerization-depolymerization of tobacco mosaic virus protein.' *Biochemistry,* 9, 193-200.

Steinmetz, N. F., Shah, S. N., Barclay, J. E., Rallapalli, G., Lomonossoff, G. P. & Evans, D. J. 2009. 'Virus-templated silica nanoparticles.' *Small,* 5, 813-816.

Stellwagen, N. C., Gelfi, C. & Righetti, P. G. 2000. 'DNA and buffers: the hidden danger of complex formation.' *Biopolymers,* 54, 137-142.

Stingl, K., Bartz-Schmidt, K. U., Besch, D., Braun, A., Bruckmann, A., Gekeler, F., Greppmaier, U., Hipp, S., Hortdorfer, G., Kernstock, C., Koitschev, A., Kusnyerik, A., Sachs, H., Schatz, A., Stingl, K. T., Peters, T., Wilhelm, B. & Zrenner, E. 2013. 'Artificial vision with wirelessly powered subretinal electronic implant alpha-IMS.' *Proc Biol Sci,* 280, 20130077.

Stöber, W., Fink, A. & Bohn, E. 1968. 'Controlled growth of monodisperse silica spheres in micron size range.' *J Colloid Interface Sci,* 26, 62-69.

Storm, A. J., Chen, J. H., Ling, X. S., Zandbergen, H. W. & Dekker, C. 2003. 'Fabrication of solid-state nanopores with single-nanometre precision.' *Nat Mater,* 2, 537-540.

Studart, A. R. 2013. 'Biological and bioinspired composites with spatially tunable heterogeneous architectures.' *Adv Funct Mater,* 23, 4423-4436.

Sumper, M. & Brunner, E. 2008. 'Silica biomineralization in diatoms: the model organism *Thalassiosira pseudonana*.' *Chembiochem,* 9, 1187-1194.

Sumper, M. & Kröger, N. 2004. 'Silica formation in diatoms: the function of long-chain polyamines and silaffins.' *J Mater Chem,* 14, 2059-2065.

Tang, F., Li, L. & Chen, D. 2012. 'Mesoporous silica nanoparticles: synthesis, biocompatibility and drug delivery.' *Adv Mater,* 24, 1504-1534.

Tenenbaum, H. C. & Heersche, J. N. 1982. 'Differentiation of osteoblasts and formation of mineralized bone *in vitro*.' *Calcif Tissue Int,* 34, 76-79.

Tsuruoka, M., Yano, K., Ikebukuro, K., Nakayama, H., Masuda, Y. & Karube, I. 1996. 'Optimization of the rate of DNA hybridization and rapid detection of methicillin resistant *Staphylococcus aureus* DNA using fluorescence polarization.' *J Biotechnol,* 48, 201-208.

Tuoriniemi, J., Cornelis, G. & Hassellov, M. 2012. 'Size discrimination and detection capabilities of single-particle ICPMS for environmental analysis of silver nanoparticles.' *Anal Chem,* 84, 3965-3972.

Turner, D. R. & Butler, P. J. 1986. 'Essential features of the assembly origin of tobacco mosaic virus RNA as studied by directed mutagenesis.' *Nucleic Acids Res,* 14, 9229-9242.

Turner, D. R., Joyce, L. E. & Butler, P. J. 1988. 'The tobacco mosaic virus assembly origin RNA. Functional characteristics defined by directed mutagenesis.' *J Mol Biol,* 203, 531-547.

Turner, D. R., McGuigan, C. J. & Butler, P. J. 1989. 'Assembly of hybrid RNAs with tobacco mosaic virus coat protein. Evidence for incorporation of disks in 5'-elongation along the major RNA tail.' *J Mol Biol,* 209, 407-422.

Urban, M., Kleefen, A., Mukherjee, N., Seelheim, P., Windschiegl, B., Vor der Bruggen, M., Kocer, A. & Tampe, R. 2014. 'Highly parallel transport recordings on a membrane-on-nanopore chip at single molecule resolution.' *Nano Lett,* 14, 1674-1680.

Uriz, M. J. 2006. 'Mineral skeletogenesis in sponges.' *Can J Zool,* 84, 322-356.

Vallet-Regi, M. & Ruiz-Hernandez, E. 2011. 'Bioceramics: from bone regeneration to cancer nanomedicine.' *Adv Mater,* 23, 5177-5218.

van der Zwaag, S., van Dijk, N. H., Jonkers, H. M., Mookhoek, S. D. & Sloof, W. G. 2009. 'Self-healing behaviour in man-made engineering materials: bioinspired but taking into account their intrinsic character.' *Philos Trans A Math Phys Eng Sci,* 367, 1689-1704.

Venkatesan, B. M. & Bashir, R. 2011. 'Nanopore sensors for nucleic acid analysis.' *Nat Nanotechnol,* 6, 615-624.

Vogel, D. 1982. 'Neutral salt effects on the polymorphism of tobacco mosaic virus protein - a contribution to the understanding of its mechanism of aggregation and virus reassembly.' *Biochim Biophys Acta,* 706, 65-79.

Vollenweider, H. J., Sogo, J. M. & Koller, T. 1975. 'A routine method for protein-free spreading of double- and single-stranded nucleic acid molecules.' *Proc Natl Acad Sci U S A,* 72, 83-87.

Wang, X., Hu, S., Gan, L., Wiens, M. & Müller, W. E. 2010. 'Sponges (Porifera) as living metazoan witnesses from the Neoproterozoic: biomineralization and the concept of their evolutionary success.' *Terra Nova,* 22, 1-11.

Weiner, S. & Dove, P. M. 2003. 'An overview of biomineralization processes and the problem of the vital effect.' *Rev Mineral Geochem,* 54, 1-29.

Weiner, S., Mahamid, J., Politi, Y., Ma, Y. & Addadi, L. 2009. 'Overview of the amorphous precursor phase strategy in biomineralization.' *Front Mater Sci China,* 3, 104-108.

Wells, L. A., Furukawa, S. & Sheardown, H. 2011. 'Photoresponsive PEG-anthracene grafted hyaluronan as a controlled-delivery biomaterial.' *Biomacromolecules,* 12, 923-932.

Werner, S., Marillonnet, S., Hause, G., Klimyuk, V. & Gleba, Y. 2006. 'Immunoabsorbent nanoparticles based on a tobamovirus displaying protein A.' *Proc Natl Acad Sci U S A,* 103, 17678-17683.

Wu, Z., Müller, A., Degenhard, S., Ruff, S. E., Geiger, F., Bittner, A. M., Wege, C. & Krill, C. E., 3rd 2010. 'Enhancing the magnetoviscosity of ferrofluids by the addition of biological nanotubes.' *ACS Nano,* 4, 4531-4538.

Wu, Z., Xiang, H., Kim, T., Chun, M. S. & Lee, K. 2006. 'Surface properties of submicrometer silica spheres modified with aminopropyltriethoxysilane and phenyltriethoxysilane.' *J Colloid Interface Sci,* 304, 119-124.

Wyckoff, R. W. G. 1937. 'An ultracentrifugal study of the pH stability of tobacco mosaic virus protein.' *J Biol Chem,* 122, 239-247.

Yamashita, I. 2008. 'Biosupramolecules for nano-devices: biomineralization of nanoparticles and their applications.' *J Mater Chem,* 18, 3813-3820.

Yampolskii, Y. 2012. 'Polymeric gas separation membranes.' *Macromolecules,* 45, 3298-3311.

Yang, C., Choi, C. H., Lee, C. S. & Yi, H. 2013a. 'A facile synthesis-fabrication strategy for integration of catalytically active viral-palladium nanostructures into polymeric hydrogel microparticles *via* replica molding.' *ACS Nano,* 7, 5032-5044.

Yang, F., Moss, L. G. & Phillips, G. N., Jr. 1996. 'The molecular structure of green fluorescent protein.' *Nat Biotechnol,* 14, 1246-1251.

Yang, J., Ferranti, D. C., Stern, L. A., Sanford, C. A., Huang, J., Ren, Z., Qin, L. C. & Hall, A. R. 2011a. 'Rapid and precise scanning helium ion microscope milling of solid-state nanopores for biomolecule detection.' *Nanotechnology,* 22, 1-6.

Yang, S. H., Chung, W. J., McFarland, S. & Lee, S. W. 2013b. 'Assembly of bacteriophage into functional materials.' *Chem Rec,* 13, 43-59.

Yang, S. Y., Ryu, I., Kim, H. Y., Kim, J. K., Jang, S. K. & Russell, T. P. 2006. 'Nanoporous membranes with ultrahigh selectivity and flux for the filtration of viruses.' *Adv Mater,* 18, 709-712.

Yang, S. Y., Yang, J. A., Kim, E. S., Jeon, G., Oh, E. J., Choi, K. Y., Hahn, S. K. & Kim, J. K. 2010. 'Single-file diffusion of protein drugs through cylindrical nanochannels.' *ACS Nano,* 4, 3817-3822.

Yang, X., Tang, H., Cao, K., Song, H., Sheng, W. & Wu, Q. 2011b. 'Templated-assisted one-dimensional silica nanotubes: synthesis and applications.' *J Mater Chem,* 21, 6122-6135.

Yi, H., Nisar, S., Lee, S. Y., Powers, M. A., Bentley, W. E., Payne, G. F., Ghodssi, R., Rubloff, G. W., Harris, M. T. & Culver, J. N. 2005. 'Patterned assembly of genetically modified viral nanotemplates *via* nucleic acid hybridization.' *Nano Lett,* 5, 1931-1936.

Yi, H., Rubloff, G. W. & Culver, J. N. 2007. 'TMV microarrays: hybridization-based assembly of DNA-programmed viral nanotemplates.' *Langmuir,* 23, 2663-2667.

Yildirim, A., Acar, H., Erkal, T. S., Bayindir, M. & Guler, M. O. 2011. 'Template-directed synthesis of silica nanotubes for explosive detection.' *ACS Appl Mater Interfaces,* 3, 4159-4164.

Ying, Y. L., Zhang, J., Meng, F. N., Cao, C., Yao, X., Willner, I., Tian, H. & Long, Y. T. 2013. 'A stimuli-responsive nanopore based on a photoresponsive host-guest system.' *Sci Rep,* 3, 1662.

Yuan-Jen, C. & Yun-Shang, C. 1964. 'Polymerization and depolymerization of virus protein II. Kinetic study of the depolymerization action of formamide and sodium dodecyl sulfate on tobacco mosaic virus.' *Acta Biochim Biophys Sin (Shanghai),* 4, 645-651.

Yuan-Jen, C., Yun-Shang, C. & Tien-Chin, T. 1964. 'The polymerization and depolymerization of virus protein I. The depolymerization of TMV protein and the conformational changes of its subunits.' *Acta Biochim Biophys Sin (Shanghai),* 4, 610-621.

Yusko, E. C., Johnson, J. M., Majd, S., Prangkio, P., Rollings, R. C., Li, J. L., Yang, J. & Mayer, M. 2011. 'Controlling protein translocation through nanopores with bio-inspired fluid walls.' *Nat Nanotechnol,* 6, 253-260.

Yuwono, V. M. & Hartgerink, J. D. 2007. 'Peptide amphiphile nanofibers template and catalyze silica nanotube formation.' *Langmuir,* 23, 5033-5038.

Zahr, O. K. & Blum, A. S. 2012. 'Solution phase gold nanorings on a viral protein template.' *Nano Lett,* 12, 629-633.

Zaitlin, M. 2000. 'Tobacco mosaic virus.' *AAB Descr. Plant Viruses,* 370, 1-13.

Zaitlin, M. & Palukaitis, P. 2000. 'Advances in understanding plant viruses and virus diseases.' *Annu Rev Phytopathol,* 38, 117-143.

Zane, A. C., Michelet, C., Roehrich, A., Emani, P. S. & Drobny, G. P. 2014. 'Silica morphogenesis by lysine-leucine peptides with hydrophobic periodicity.' *Langmuir,* 30, 7152-7161.

Zavala-Rivera, P., Channon, K., Nguyen, V., Sivaniah, E., Kabra, D., Friend, R. H., Nataraj, S. K., Al-Muhtaseb, S. A., Hexemer, A., Calvo, M. E. & Miguez, H. 2012. 'Collective osmotic shock in ordered materials.' *Nat Mater,* 11, 53-57.

Zhou, K., Li, F., Dai, G., Meng, C. & Wang, Q. 2013. 'Disulfide bond: dramatically enhanced assembly capability and structural stability of tobacco mosaic virus nanorods.' *Biomacromolecules,* 14, 2593-2600.

Zimmern, D. 1977. 'The nucleotide sequence at the origin for assembly on tobacco mosaic virus RNA.' *Cell,* 11, 463-482.

Zimmern, D. 1983. 'An extended secondary structure model for the TMV assembly origin, and its correlation with protection studies and an assembly defective mutant.' *EMBO J,* 2, 1901-1907.

Zollfrank, C., Scheibel, T., Seitz, H. & Travitzky, N. 2014. 'Bioinspired materials engineering.' *Ullmann's Encyclopedia of Industrial Chemistry*. Wiley-VCH Verlag GmbH & Co. KGaA.

Zuker, M. 2003. 'Mfold web server for nucleic acid folding and hybridization prediction.' *Nucleic Acids Res,* 31, 3406-3415.

Anhang

Chemische Strukturen der verwendeten Linker, Farbstoffe und Peptide

Fluoreszenzfarbstoff: Atto488-Maleimid

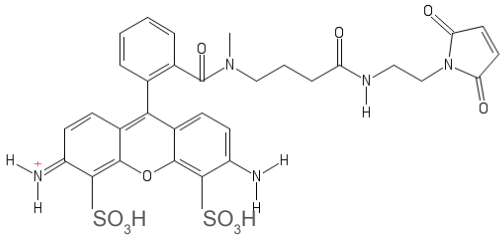

Heterobifunktionaler Linker: (Succinimidyl-[(N-Maleimidopropionamido)-Tetraethylenglykol] Ester ($SM(PEG)_4$)

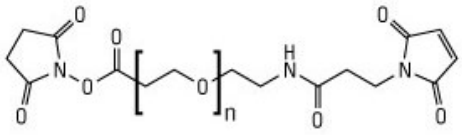

Quelle: http://www.piercenet.com/images/structures/22102-SM(PEG)n-stc.jpg

SiO_2-Abscheidung induzierendes Peptid: $(KD)_5C$ (Kuno et al. 2011)

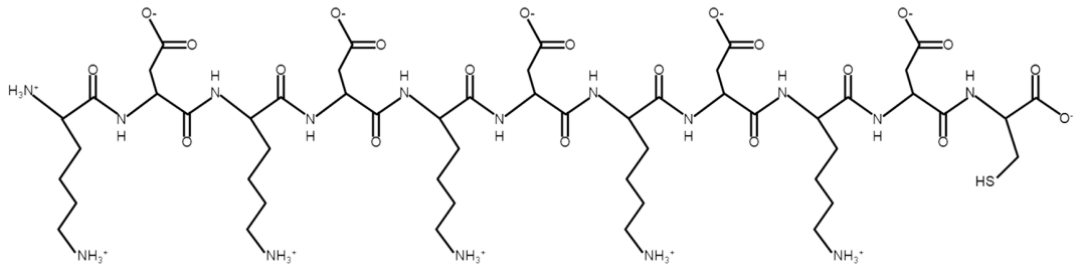

SiO_2-Abscheidung induzierendes Peptid: CA_4H_4 (Yuwono & Hartgerink 2007)

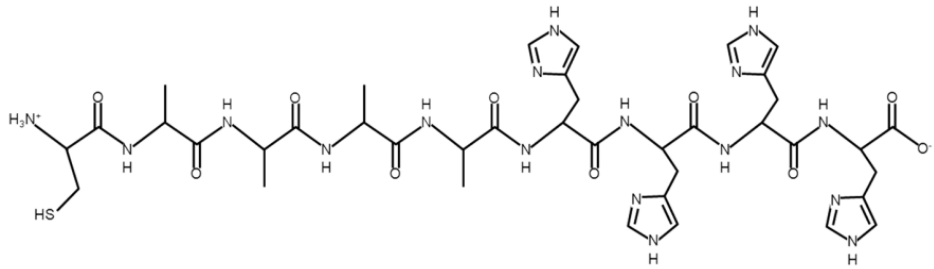

ZnO-affines Peptid: 31C (Rothenstein et al. 2012)

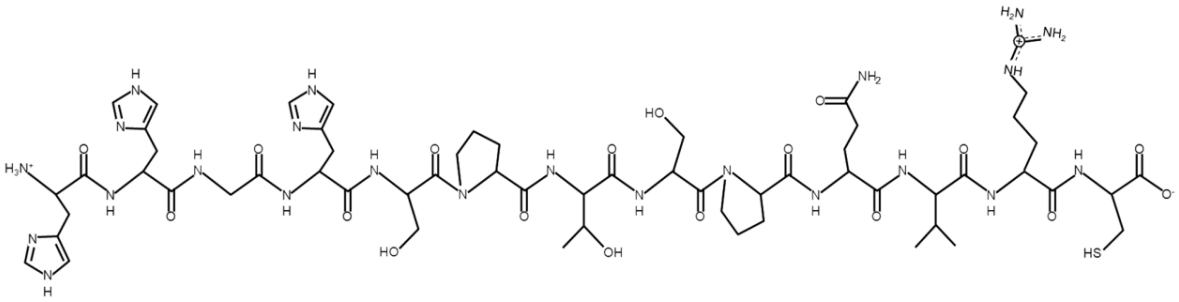

ZnO-affines Peptid: 44C (Rothenstein et al. 2012)

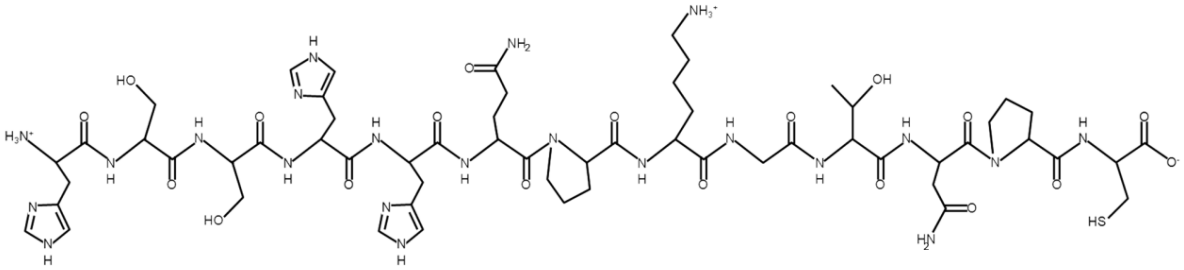

Reaktionsmechanismen

- Der Reaktionsmechanismus zur Fluoreszenzmarkierung und Immobilisierung der RNA-stabilisierten TMV-„Disks“ auf einem ITC-funktionalisierten Substrat ist im Manuskript I in der **Figure 6** (Seite 64) dargestellt.
- Die Reaktionsmechanismen zur peptidvermittelten SiO_2-Abscheidung mit Kieselsäure als Substrat sind in der deutschen Einleitung in den **Abbildungen 2** (Seite 25) und **3** (Seite 27) sowie in Manuskript III in **Figure 6** (Seite 124) gezeigt.
- Die Reaktionsmechanismen zur SiO_2-Bildung mit Tetraethylorthosilikat als Substrat sind in Manuskript III (**Figure 1**, Seite 110) und Manuskript IV (**Figure 1**, Seite 139) gezeigt.

Danksagung

Ein großer Dank geht an **Prof. Dr. Christina Wege** dafür, dass sie mir ein außergewöhnlich spannendes Projekt angeboten, mir sehr viel Freiheit bei dessen Umsetzung gelassen und mir viele Tipps für die Präsention von Daten und Verfassen von Manuskripten gegeben hat.

Bei **Prof. Dr. Sabine Laschat** möchte ich mich für die Zusage zum Erstellen des Zweitgutachtens bedanken.

Bei **Prof. Dr. Bernhard Hauer** bedanke ich mich zum einen dafür, den Vorsitz der Doktorprüfung zu leiten, zum anderen dafür, Peptide von **Dr. Martin Ploß** für die Entwicklung eines Protokolls zur Modifikation von TMV zur Verfügung zu stellen.

Prof. Dr. Holger Jeske danke ich für die Diskussionen während der Arbeitssitzung, die äußerst kritischen Anmerkungen zu meinen experimentellen Arbeiten und natürlich für die Idee, die TMV-Disks mit RNA zu stabilisieren. Ohne diesen Hinweis wären vermutlich die meisten Experimente nicht möglich gewesen.

Für die durchgehend gute Zusammenarbeit und zahlreichen Gespräche, die erheblich zur praktische Umsetzung des Projekts beigetragen haben, bedanke ich mich bei **Dr. Axel Seidenstücker**.

Dr. Alfred Plettl, **Prof. Dr. Othmar Marti**, **Dr. Hartmuth Gliemann** und **Dr. Carlos Azucena**, die mit zahlreichen, teilweise ausgefallenen, Beiträgen aus der Sichtweise von Physikern und Chemikern dem Projekt immer wieder eine neue Richtung gegeben haben, danke ich. Durch diese interdisziplinäre Zusammenarbeit hatte ich die Möglichkeit verschiedene Methoden aus der Physik und Chemie theoretisch und teils auch praktisch kennenzulernen.

Ganz herzlich bedanken möchte ich mich bei allen **Mitarbeitern der Abteilung der Molekularbiologie und Virologie der Pflanzen** für die unglaubliche Hilfsbereitschaft, die mir dabei geholfen hat mich im Labor einzuleben, und spontan bei vielen Fragestellungen nach Antworten zu suchen.

Bei **Dr. Sabine Eiben**, **Dr. Fabian Eber** und **Dr. Sven Degenhard** möchte ich mich bedanken, dass sie mir die zahlreichen Arbeitsschritte und Protokolle gezeigt haben, die notwendig sind, um das TMV als Nanobaustein einzusetzen.

Besonders möchte ich mich bei **Sigrid Kober** und **Rebecca Hummel** für die TMV-Präparation aus Tabakpflanzen bedanken, bei **Gabriele Kepp** für die Unterstützung

bei der Fluoreszenz-Mikroskopie und bei **Cornelia Kocher** für die Vermittlung der Methoden zur Probenpräparation für die TEM-Analyse und die Bedienung des TEMs.

Bei **Prof. Dr. Stephan Nussberger** und **PD Dr. Michael Schweikert** möchte ich mich für den Zugang zu den TEMs bedanken.

Bei **Dr. Sabine Eiben**, **Claudia Koch** und **Nana Wenz** bedanke ich mich von ganzem Herzen für die erste Korrekturrunde der Manuskripte meiner Dissertation.

Diether Gotthardt, **Cornelia Roesler** und **Marvin Müller** danke ich für die Anzucht der Tabakpflanzen im Gewächshaus.

Erklärung

Hiermit erkläre ich, dass ich die vorliegende Arbeit selbstständig und nur mit den Hilfsmitteln durchgeführt habe, die im Text angegeben sind.

Auf Arbeiten, die durch oder mit Kooperationspartnern durchgeführt wurden, ist an der entsprechenden Stelle im Text eindeutig hingewiesen.

Stuttgart, den 23. November 2015

Klara Altintoprak